Minnesota Department of Transportation

RESEARCH SERVICES

Office of Policy Analysis, Research & Innovation

Validation of Prestressed Concrete I-Beam Deflection and Camber Estimates

Catherine E. French, Principal Investigator
Department of Civil Engineering
University of Minnesota

June 2012

Research Project
Final Report 2012-16

Your Destination...Our Priority

Technical Report Documentation Page

1. Report No. MN/RC 2012-16	2.	3. Recipients Accession No.	
4. Title and Subtitle Validation of Prestressed Concrete I-Beam Deflection and Camber Estimates		5. Report Date June 2012 6.	
7. Author(s) Cullen R. O'Neill, Catherine E. French		8. Performing Organization Report No.	
9. Performing Organization Name and Address Department of Civil Engineering University of Minnesota 500 Pillsbury Drive SE Minneapolis, MN 55455		10. Project/Task/Work Unit No. CTS #2010093 11. Contract (C) or Grant (G) No. (c) 89261 (wo) 200	
12. Sponsoring Organization Name and Address Minnesota Department of Transportation Research Services 395 John Ireland Blvd., MS 330 St. Paul, MN 55155		13. Type of Report and Period Covered Final Report 14. Sponsoring Agency Code	
15. Supplementary Notes http://www.lrrb.org/pdf/201216.pdf			

16. Abstract (Limit: 250 words)

The camber at the time of bridge erection of prestressed concrete bridge girders predicted by the Minnesota Department of Transportation (MnDOT) was observed to often overestimate the measured cambers of girders erected at bridge sites in Minnesota, which, in some cases, was causing significant problems related to the formation of the bridge deck profile, the composite behavior of the girders and bridge deck, delays in construction and increased costs.

Extensive historical data was collected from two precasting plants and MN counties and it was found that, on average, the measured cambers at release and erection were only 74% and 83.5%, respectively, of the design values. Through data collection, analysis, and material testing, it was found that the primary causes of the low camber at release were concrete release strengths that exceeded the design values, the use of an equation for concrete elastic modulus that greatly under-predicted the measured values, and thermal prestress losses not accounted for in design.

Fourteen girders were instrumented and their camber measured and the program PBEAM was used to evaluate the influence of various time-dependent effects (i.e., solar radiation, relative humidity, concrete creep and shrinkage, length of cure and bunking/storage conditions) on long-term camber. Once investigated, these effects were included in long-term camber predictions that were used to create sets of both time-dependent and single-value camber multipliers. The use of these multipliers, along with modifications made to the elastic release camber calculations, greatly reduced the observed discrepancy between measured and design release and erection cambers.

17. Document Analysis/Descriptors Camber, Deflection, Prestressed concrete bridges, Camber multipliers, Compressive strength, Modulus of elasticity, Thermal prestress losses, Creep, Shrinkage, Curvature, I beams, Girders, Erection (Building), Mathematical prediction		18. Availability Statement No restrictions. Document available from: National Technical Information Services, Alexandria, Virginia 22312	
19. Security Class (this report) Unclassified	20. Security Class (this page) Unclassified	21. No. of Pages 205	22. Price

Validation of Prestressed Concrete I-Beam Deflection and Camber Estimates

Final Report

Prepared by:

Cullen O'Neill
Catherine E. French

Department of Civil Engineering
University of Minnesota

June 2012

Published by:

Minnesota Department of Transportation
Research Services
395 John Ireland Boulevard, Mail Stop 330
St. Paul, Minnesota 55155

ACKNOWLEDGMENTS

I would first like to thank the Department of Civil Engineering at the University of Minnesota and the Minnesota Department of Transportation for granting me the opportunity to pursue a Master's degree and conduct a research project. I would also like to sincerely thank my advisor, Dr. Catherine French, for providing me with her expertise, invaluable guidance and for treating me as an equal partner in this research endeavor.

Second, I would like to thank the two precasting plants, Cretex in Elk River, MN, and County Materials in Roberts, WI, for their participation in this project. I would like to especially thank John Link, Pat Gapinski and Joel Mich of Cretex and Brandon Boleen of County Materials, who were incredibly helpful and were so willing to assist me on all facets of my field work, including data collection, concrete sampling and girder instrumentation. Without the assistance of these individuals, this project would simply not have been possible.

Third, I would like to thank all of the researchers, graduate and undergraduate students who helped me with all phases of this project. I deeply appreciate the work done by Marsha Swatosh, who conducted the majority of the equipment calibration and concrete material testing. I would also like to specifically thank Ben Dymond for assisting with girder instrumentation, Mounir Najm for braving the cold Minnesota winter to help with camber measurements, and Ryan Melhouse and Rachel Gaulke for assisting with concrete sampling and material testing.

Finally, I would like to graciously thank my family for all of their love and support over the years, and my wife, Breanna, who made even the most frustrating days an absolute joy. I am so grateful for all her unconditional love, encouragement, patience and support, which always inspires me to work harder and do my best.

TABLE OF CONTENTS

LIST OF FIGURES

LIST OF TABLES

EXECUTIVE SUMMARY

The camber, or total net upward deflection, of prestressed concrete bridge girders is the result of the eccentric axial compression force provided by prestressing strands which counteract the deflections due to gravity loads. At the time of strand release, the deflection behavior of prestressed concrete girders is considered to be elastic, and it is common for bridge designers to use elastic camber calculations to predict the camber at release. To estimate the girder camber at bridge erection, a multiplier method is typically used, which amplifies the camber at release to roughly account for the time-dependent effects (e.g., creep and shrinkage) that occur between release and erection. Additionally, there are numerous factors that affect the camber at erection and are not known at the time of design, including the girder storage condition in the precasting yard (i.e., bunking) and the age of the girder at erection, which further lead to potential errors in the estimates of the girder camber at erection. The Minnesota Department of Transportation (MnDOT) uses the release camber calculations, based on gross section properties and elastic shortening losses, and a multiplier method to predict the camber at release and erection, respectively.

An accurate estimate of camber at erection is important; if the girders that arrive at a bridge site have cambers that are much lower or much higher than the expected design erection camber, it causes significant problems related to the formation of the bridge deck profile, the composite behavior of the girders and bridge deck, negative or very high stool height requirements, delays in construction and increased costs. It was recently observed that girders were being erected at bridge sites in Minnesota with cambers that were often much lower than predicted. The main side effect of this problem is required stool heights that are too high, especially at midspan. If the required stool heights approach the height of the protruding top flange shear reinforcement, the composite action needed between the girders and the bridge deck cannot be achieved, thus requiring the use of additional reinforcement or changing the entire bridge deck profile, which adds cost and creates delays. To account for this issue, MnDOT switched in late 2007 from the multiplier method recommended by Leslie A. Martin (1977) and PCI (2010), to a universal multiplier of 1.5. However, the problem persisted and camber of girders continued to be overestimated.

The primary objective of this study was to investigate and determine the cause of low girder camber at both release and bridge erection, which was observed by MnDOT, and to create an improved method for camber prediction through modified calculations (if necessary) and a new set of multipliers. This objective was achieved through examination of extensive camber records from precasting plants and from in-situ measurements during erection of Minnesota I-girders, instrumentation and camber monitoring of fourteen girders from release to erection, concrete material testing, an analysis of prestress losses due to thermal effects, and PBEAM time-dependent camber modeling to investigate various effects including creep and shrinkage, girder support conditions during storage and age at erection.

Extensive historical fabrication data was collected from two precasting plants (referred to as Plant A and B) for 1067 girders produced between 2006 and 2010. Camber at erection data was collected from the counties for 768 of those girders. On average, it was found that the measured camber at release for those 1067 girders was only 74% of the design value. Furthermore, it was found that the measured camber at erection for the 768 girders was only 83.5%, on average, of the design value; and that girders erected at early ages almost always had cambers that were significantly lower than the design value. Because the predicted camber at

erection is obtained by amplifying the elastic camber at release, inaccurate estimates of the camber at release can compound the problems of estimating the camber at erection.

Various factors that affect the release camber were investigated, including concrete strength and modulus of elasticity, and variation in the strand prestress force. It was found that the increased concrete strengths achieved at the precasting plants (15.5% over the specified design value, on average) decrease camber due to the increased elastic modulus. Multiple concrete cylinder samples from both precasting plants were tested to investigate the concrete strength and elastic modulus over time. It was found that the ACI363R-10 expression used by MnDOT to estimate the concrete modulus of elasticity from the specified concrete compressive strength greatly underestimates the elastic modulus of concrete produced at both precasting plants. The Pauw (ACI 318-08, AASHTO LRFD 2010) equation was determined to be the best predictor of the concrete elastic modulus, and when used to recalculate the release camber predictions for the 1067 historical girders, yielded significantly more accurate results.

A thermal effects analysis was conducted to determine the effect of concrete and ambient temperatures on the strand stress at release. It was found that the combined thermal effects (and strand relaxation) cause a reduction in strand stress at release of approximately 3%, on average. The position of each girder in the bed was also found to cause variations in prestress force through the redistribution of draped strand stress due to the harping sequence (at Plant A) and friction losses (at Plant B). Thus, it was determined that the major causes for the discrepancy in release camber predictions and observed cambers were the increased concrete release strengths, the fact that the ACI 363 equation for concrete elastic modulus underestimated the measured elastic moduli, and strand prestress losses due to thermal effects.

The effects of these primary factors were considered in re-predicting the cambers of a select data set for which detailed fabrication data, including curing and temperature records, were known. The girders included in this data set were those from which the concrete material samples were obtained, the instrumented girders, and selected girders from the historical data set. It was found that the accuracy of the re-predicted cambers was much greater than the original design cambers, and that the amount of variability in the results was reduced. Recommendations for modified camber calculations were made based on average effects (i.e., 15.5% release concrete strength increase, the Pauw equation for estimating concrete elastic modulus, and thermal prestress losses of 3%). These recommendations were then tested against the entire historical girder database, and it was found that the discrepancy between measured and design camber values improved from approximately 74% to 99%, on average. This result confirmed that the revised release camber calculations provided much more accurate camber predictions than the original design equations. It should be noted that the overall scatter was not reduced because the recommendations were implemented in an average sense to all 1067 girders in the historical database.

Once the discrepancy between measured and design release camber values was determined, various factors that affect long-term (erection) camber were investigated, including solar radiation, relative humidity, concrete creep and shrinkage, length of cure and bunking/storage conditions. The program PBEAM was also validated for use in release and long-term camber modeling. It was found that solar radiation affects the measurement of camber by as much as 15% during the course of a day, emphasizing that camber is a constantly fluctuating value. Relative humidity was found to cause changes in concrete creep and shrinkage and induce camber variability. High relative humidity during the winter months was also observed to cause slight increases in camber. Through PBEAM validation, it was found that the

ACI 209R-92 concrete creep and shrinkage models provided the best results for long-term camber predictions and that the Mokhtarzadeh ACI 209 variation models provided a consistent lower bound. As such, the ACI 209R-92 creep and shrinkage models were used in the time-dependent camber modeling predictions. Weekend curing was found to cause lower erection cambers than weekday-cured girders, even though the camber discrepancy at release was less evident, due to additional stress recovery from cooler curing conditions. Finally, it was found that bunking/storage conditions led to increased cambers, additional camber variability, and possible exceedance of codified stress limits. Bunking limitations were recommended to limit these undesirable effects.

These observations and results were used to create PBEAM inputs and ensuing long-term (erection) camber predictions for girders of varying depth and length. From these results, four "sets" of multipliers were created by comparing the long-term (erection) camber predictions to the current MnDOT and improved release camber predictions. Two of the sets of multipliers were developed to be applied to the MnDOT approach to predict release camber, and the other two were developed to be applied to the improved release camber predictions. For each approach, one set was based on a single multiplier to best predict erection camber and the other set recommended four different multipliers that reflected approximate age ranges for the girders at erection. These four different sets of multipliers were then applied to the historical girder data set and compared to the measured erection camber data. It was found that all four sets of multipliers greatly improved the erection camber predictions, with average measured vs. adjusted design erection camber percent values of 95.6%-97.1%. However, only the "time-dependent" multipliers, which accounted for four potential ranges in girder age at erection, reduced the amount of scatter in the results. In particular, these multipliers alleviated the problem of over-predicted erection cambers for girders erected at early ages. Both the improved release camber predictions and the "Improved Time-Dependent" multipliers are recommended to be used by MnDOT for future camber predictions.

In addition to the recommendations for the modified camber calculations at release and the new set of multipliers, recommendations for girder fabrication were also created to reduce camber variability and improve girder production at the precasting plants. Included in these recommendations are limitations for bunking/storage conditions and alternative methods designed to produce more accurate temperature corrections (for Plants A and B). It was found that the amount of camber variability that can be expected using the recommended calculations and multipliers is approximately ±15%, or even lower if the girder fabrication recommendations are put into practice.

CHAPTER 1. INTRODUCTION

1.1 Background

Camber describes the upward deflection of a girder induced to offset downward deflection due to self-weight and superimposed loads. In prestressed concrete I-girder applications, camber is achieved by placing high-strength steel strands toward the bottom of the girder, primarily in the bottom flange of the section. The strands are pretensioned to high stresses (usually 0.75*f_{pu}=202.5 ksi as specified by the AASHTO LRFD 2010 Bridge Design Specifications). Then, the concrete is cast and allowed to cure until it reaches the design release strength, f'_{ci}. The side-forms are then removed and the steel strands are cut. The shortening of the strands, when released, induces compression in the girder. Due to the eccentricity of the strands, the axial compression force in the girder causes it to deflect upwards, and thus, have camber. In this report, the term "camber" will be used to describe the total net deflection of a girder, that is, the upward deflection due to strand eccentricity minus the downward deflection due to self-weight.

In prestressed concrete applications, there are stress limits that must not be exceeded and are defined by the AASHTO LRFD 2010 Bridge Design Specifications. In order to keep the tension stress in the top flange toward the girder ends to within the specified limits, some of the strands (within the web) are commonly draped to reduce the strand eccentricity near the ends of the girder. The "harp" or "hold-down" points are usually located symmetrically at approximately 40% of the total girder length.

1.2 Current Methods for Camber Prediction

The current method for camber prediction used by the Minnesota Department of Transportation (MnDOT) consists of calculating the expected camber at release and using a multiplier to estimate the camber at the time of bridge erection. At the time of strand release, the deflection behavior of prestressed concrete girders is considered to be elastic, as creep and shrinkage have yet to take effect. However, the elastic camber calculations depend highly on the stress in the strands and the concrete modulus of elasticity at release, which are values not known precisely at the time of design. The camber calculations are based on gross section properties and include elastic shortening losses. (The alternative is to use transformed section properties for which losses due to elastic shortening are directly considered.) The calculations for the camber at release used by MnDOT are as follows:

Prestress loss due to elastic shortening:

$$\Delta f_{ES} = \frac{\left(A_{ps} f_j (I_c + (e_{mid})^2 A_c)\right) - e_{mid} A_c M_{sw}}{\left(A_{ps}(I_c + (e_{mid})^2 A_c)\right) + \frac{I_c A_c E_{ci}}{E_{ps}}} \quad \textbf{(1-1)}$$

Total prestress force at release:

$$P_{re} = A_{ps}(f_j - \Delta f_{ES}) \quad \textbf{(1-2)}$$

Upward deflection due to prestressing:

$$\Delta_{ps} = \frac{P_{re}}{E_{ci} I_c} \left(\frac{e_{mid} {L_{des}}^2}{8} - \frac{(e_{mid} - e_{end}) {x_{hold}}^2}{6} \right) \quad \textbf{(1-3)}$$

Downward deflection due to self-weight:

$$\Delta_{sw} = \frac{5 * w_{sw} {L_{des}}^4}{384 * E_{ci} I_c} \quad \textbf{(1-4)}$$

Total camber at release:

$$Camber = \Delta_{ps} - \Delta_{sw} \quad \textbf{(1-5)}$$

where:

- A_{ps}: Total area of prestressing strands
- f_j: Jacking stress in each strand
- I_c: Gross concrete moment of inertia
- A_c: Gross concrete area
- E_{ci}: Concrete modulus of elasticity at release
- E_{ps}: Strand modulus of elasticity
- e_{mid}: Strand eccentricity at midspan
- e_{end}: Strand eccentricity at girder end
- M_{sw}: Self-weight moment
- w_{sw}: Concrete self-weight
- L_{des}: Girder design length
- x_{hold}: Distance from girder end to hold-down point for draped strands

Once the camber at release is estimated using the above calculations, a multiplier, or set of multipliers is used to estimate the camber at the time of bridge erection. In 1977, Leslie A. Martin published an article that produced a table of multipliers based on rough estimations of prestress losses, creep and shrinkage effects and the girder age at erection. For estimating the camber at erection, Martin suggested multiplying the self-weight deflection by 1.85 and the upward prestress deflection by 1.80 (Martin 1977). His table of multipliers was published as the "PCI multiplier method" in the PCI Design Handbook and is still being used by designers today. Refer to Section 2.2 for further discussion of this article. For years, MnDOT used Martin's multipliers to estimate the expected camber at erection. However, in late 2007, MnDOT and other Minnesota bridge designers switched to using a single multiplier of 1.5, which when multiplied by the total camber at release, is used to estimate the camber at erection. The switch to the 1.5 multiplier was made because it was found that a significant number of girders were arriving at the bridge site with cambers that were much lower than what was predicted.

1.3 Research Motivation and Problem Statement

As previously mentioned, prior to the multiplier switch in late 2007, MnDOT had noticed that many girders were arriving at their respective bridge sites with cambers that were much lower than predicted. However, even after the 1.5 multiplier was implemented, the problem persisted. Girders that arrive at the bridge site with cambers much lower or much higher than the

expected design erection camber can cause significant problems related to the bridge deck profile or composite behavior of the bridge that require adjustments in the field creating delays in construction and resulting in increased costs. Because the girder seats are prepared prior to the arrival of the girders and are based on the design erection camber, the stool heights (i.e., formed region between the top flange and the bottom of the deck that is the width of the flange) must accommodate the girder cambers that are too high or too low. If the girder camber is too high, it can result in required stool heights that are too low or even negative (i.e., the girder top flange may protrude into the deck), which causes the need for the bridge deck profile to be re-done. If the girder camber is too low, it can result in required stool heights that are too high, especially at midspan. The horizontal shear reinforcement that protrudes from the top flange of the girder to create composite action between the girders and the bridge deck typically extends approximately 6 in above the top of the girder. If the stool height requirement is too high, there is insufficient anchorage of the horizontal shear reinforcement in the deck, requiring the use of additional reinforcement (i.e., splices) that add cost and create delays.

The objective of this investigation was to determine the cause of low girder camber that has been observed in the field and to improve the method for camber calculation, including the creation of new multipliers that better predict the camber at erection.

1.4 Research Objectives and Methodology

The primary objective of this study was to determine the cause of low girder camber at both release and bridge erection, which has been observed by MnDOT, and to create an improved method for camber prediction, through modified calculations (if necessary) and a new set of multipliers. The methodology and tasks used to achieve this objective were as follows:

1. Obtain extensive historical camber data using records from precasting plants and from in-situ measurements recorded during erection of Minnesota I-girders, as well as similar information from the literature.
2. Instrument and monitor the cambers of fourteen girders from release to erection, including lift-set measurements at release and periodic measurements while bunked in storage at the precasting yard.
3. Measure the compressive strengths and elastic moduli over time of concrete cylinder samples collected from two precasting plants.
4. Investigate the effects of potential sources for variations in camber, including girder material properties, support conditions, thermal and environmental effects, and concrete creep and shrinkage, to identify trends and potential causes for observed behaviors, specifically the cause of the low girder cambers observed at release and erection.
5. Conduct a parametric study to investigate time-dependent effects using the program PBEAM (Suttikan 1978) to determine the potential range of camber variability and to develop recommendations for a new set of long-term camber multipliers for erection camber predictions.
6. Develop recommendations for girder fabrication to reduce camber variability and facilitate improved camber predictions.

1.5 Organization of Report

The detailed results of the investigation are summarized in the following chapters. Chapter 2 summarizes previous research regarding camber and related effects. Chapter 3 describes the collected historical girder data and observations from that data. Chapter 4 details the purpose and process of girder instrumentation and the recorded long-term camber behavior measurements. Chapter 5 describes the issues and effects related to release camber, as well as the investigation of these effects, including concrete strength, concrete elastic modulus, concrete material testing, variation in prestress force, and the cross section moment of inertia. Chapter 6 details the release camber predictions that were conducted, using the collected historical data, instrumented girder data and the results from concrete material testing and the thermal effects analysis, to determine the cause of low girder camber at release. Chapter 7 describes the issues and effects related to long-term (erection) camber as well as the investigation of these effects; including concrete creep and shrinkage, solar radiation, relative humidity, length of cure and bunking/storage conditions. Chapter 7 also describes the validation of the camber modeling program PBEAM. Chapter 8 details the long-term camber predictions that were conducted using the results of the erection camber effects investigation, describes the development of the new multipliers created to improve the predictions of erection camber, and examines the amount of camber variability anticipated in the field. Finally, Chapter 9 summarizes the results of the study and describes the recommendations for girder fabrication and improved release and long-term (erection) camber predictions, as well as the possible implementation of the new multipliers.

Appendices are included at the end of the report that show additional figures from the historical data (APPENDIX A), details of the thermal effects analysis (APPENDIX B), a description of the material testing equipment calibration (APPENDIX C), a description of the input procedure for PBEAM (APPENDIX D), fabrication records for the instrumented girders (APPENDIX E), additional PBEAM modeling results (APPENDIX F), creep and shrinkage inputs used in PBEAM modeling (APPENDIX G) and a detailed review of the Tadros et al. (2011) proposed method for camber prediction (APPENDIX H).

CHAPTER 2. PREVIOUS CAMBER RESEARCH

2.1 Introduction

A literature review of previous camber research is summarized in this chapter. While some studies specifically examined camber, other studies included camber as part of a much broader investigation. Findings from studies that examined other topics that relate to camber, such as high strength concrete material properties, are described in the appropriate chapter or section later in the report.

2.2 *Martin, Leslie A.* (PCI Journal, Jan-Feb 1977)

"A Rational Method for Estimating Camber and Deflection of Precast Prestressed Members"

In 1977, Leslie A. Martin developed a set of multipliers for estimating camber at various time intervals that are still widely used by prestressed concrete designers today. Table 3 from this paper, shown below as Table 2-1, is included in the PCI (2010) Design Handbook and is the suggested method for estimating long-term camber and deflection. Martin made some very general assumptions when developing the multipliers, which makes them very approximate. For example, Martin assumed that the concrete release strength is 70% of the 28-day strength, making E_{ci} approximately 85% of the final E_c. Martin also used an "average value" of 15% for the long-term part of the prestress losses. In determining the erection camber multiplier, the assumption was made that girders are between 30 and 60 days old at the time of bridge erection and that one-half of the long-term camber, prestress losses and creep and shrinkage effects occur in that initial time interval (Martin 1977). With these assumptions, the recommended multipliers to be used for estimating the erection camber are 1.80 for the deflection due to the effects of prestress and 1.85 for the self-weight deflection.

Table 2-1. Long-term camber multipliers (Martin 1978, PCI 2010)

	Without Composite Topping	With Composite Topping
At erection:		
(1) Deflection (downward) component – apply to the elastic deflection due to the member weight at release of prestress.	1.85	1.85
(2) Camber (upward) component – apply to the elastic camber due to prestress at the time of release of prestress.	1.80	1.80
Final:		
(3) Deflection (downward) component – apply to deflection calculated in (1) above.	2.7	2.4
(4) Camber (upward) component – apply to camber calculated in (2) above.	2.45	2.2
(5) Deflection (downward) – apply to elastic deflection due to super-imposed dead loads only.	3.0	3.0
(6) Deflection (downward) – apply to elastic deflection caused by the composite topping.	--	2.30

2.3 *Saiidi, M. Saiid et al.* (PCI Journal, Sep-Oct 1996)

"Variation of Prestress Force in a Prestressed Concrete Bridge During the First 30 Months"

Saiidi et al. (1996) conducted a study in the early 1990s on a prestressed box girder bridge in Reno, Nevada. Prestress losses and beam deflection data were collected over a 30-month period. During this time, the climate was a key factor in the results. The temperature and relative humidity (RH) in the area showed opposite trends, as expected, with the RH ranging from approximately 30% in the summer months to 60-70% in the winter months. For the midspan deflection, data showed that "when the tendon force was nearly constant or on the rise, the bridge moved upward." It was also observed that when the RH exceeded 50%, the bridge cambered up. "This trend was repeated consistently three times during Nov 1988-Mar 1989, Oct 1989-Mar1990 and Nov 1990-Mar 1991." In other words, during the winter months, the camber of the bridge increased associated with an increase in RH.

2.4 *Tadros, Maher et al.* (PCI Journal, Winter 2011)

"Precast, Prestressed Girder Camber Variability"

In this PCI Journal article, Tadros et al. (2011) proposed a method for incorporating new AASHTO prediction formulas into a spreadsheet to predict initial and long-term camber, as well as an investigation of camber variability. The proposed equations follow the design approach of applying the prestress force just before release to the transformed section properties, as well as

taking into account strand debonding (shielding). The authors explained that a common alternative to this approach is applying the prestress force just after release (initial prestress force minus elastic shortening losses) to the gross section properties. These two methods of camber calculation were found to be equivalent to within 2%. The proposed equation for self-weight deflection also takes into account the effect of storage support conditions, that is, the effect of the overhanging ends of the beam during bunking.

The authors also examined the effect of using two different equations (AASHTO LRFD 2007 and ACI 363 2010) for the concrete modulus of elasticity and reported a large variance in camber (±22%) between the results using these two equations. Thus, they recommended that historical records be kept of elastic moduli for concrete produced at precasting plants that supply prestressed girders. The authors recognized the effect of higher concrete release strengths, weekend curing, and temperature gradients in the concrete, but did not examine these effects in detail. They also made reference to using lift/set cambers for accurate measurements to cancel the effect of friction in the bed.

For long-term camber prediction, the authors summarized Martin's multipliers and referred to a "variable multiplier method" originally published by Tadros et al. in 1985 and later adopted by the PCI Bridge Manual, NCHRP 496 and AASHTO LRFD 2005. Their newly-proposed method for long-term camber prediction involves using the AASHTO method for prestress losses, an aging factor of 0.7 for prestress loss and the calculation of a creep coefficient (multiplier) based on various factors (i.e., volume-to-surface ratio, relative humidity, f'_{ci}, loading age and age at erection). This multiplier is then used to adjust the deflection due to prestress plus self-weight and prestress loss. The authors acknowledged the effect of variable storage time, prestress losses, concrete creep and support conditions on long-term camber but did not examine these effects in much detail.

Finally, the authors recommended that girders be designed for a minimum haunch of 2.5 in (63.5 mm) to account for camber variability and to avoid the issue of large or negative stool heights, although this could still lead to problems if the girder cambers are much lower than expected, resulting in high stool height requirements. The authors also recommended that girder seats not be finalized until near the time of installation to allow for camber measurements to be taken before shipping, if possible. This proposed method was evaluated using data collected in this study. A detailed description of the method and the results of the evaluation are shown in APPENDIX H.

2.5 *Rosa, Michael A. et al.* (2007 Concrete Bridge Conference)

"Improving Predictions for Camber in Precast, Prestressed Concrete Bridge Girders"

Rosa et al. (2007), a research group from the University of Washington, studied camber using field measurements, material testing and various predictive models. The ultimate goal of the research was to produce a new or modified camber prediction method that reduced the observed error found in previous predictions. Ultimately, a program was developed that allowed the user to input the desired parameters in order to create better camber predictions.

The authors first evaluated the current camber prediction method used by the Washington Department of Transportation (WSDOT), which uses models and expressions for concrete aging, elastic modulus, concrete creep, shrinkage, prestress losses and camber that are consistent with the 2007 AASHTO LRFD Bridge Design Specifications. In order to analyze the camber prediction method, the authors monitored the camber of eight girders for the first two months

after fabrication, and compared the behavior to the predicted camber based on the results of material tests that examined concrete strength, elastic modulus, and concrete creep and shrinkage. Fabricator data was also collected for 146 girders of varying length, shape, and strand pattern from the two main fabricators in Washington. Finally, the authors monitored the camber of 91 additional girders during various stages of construction to study the effects of varying support and loading conditions.

The authors found that, on average, the measured release concrete strength exceeded the design value by 10% and the concrete elastic modulus exceeded the value predicted by the AASHTO LRFD equation by 15%. This result for the concrete elastic modulus was used to minimize the error in the predictions for release camber. Based on these release camber predictions and the long-term camber measurements, the optimization of the results led to the modification of the creep coefficient from 1.9 to 1.4. Once these provisions were included in the long-term camber prediction method, the error was greatly reduced. The authors did not examine the effects of bunking conditions, support restraints or environmental conditions such as ambient temperature, relative humidity and thermal gradients, which also affect camber.

2.6 *Barr, P.J. et al.* (Journal of Performance of Constructed Facilities, Nov-Dec 2010)

"Differences between Calculated and Measured Long-Term Deflections in a Prestressed Concrete Girder Bridge"

Barr et al. (2010) conducted a study that closely examined the effects that influence camber and evaluated various methods for camber prediction. Five girders (137 ft long and 72 in deep) were monitored during fabrication and service and were instrumented with vibrating-wire strain gauges (VWSG) to record strains and temperatures. The measured camber values were compared with predictions from the multiplier method (PCI 2004), improved multiplier method (Tadros et al. 1985) and a detailed time-step method (NCHRP Report 496 in 2003). Various effects, such as thermal gradients, were also closely studied.

The authors focused largely on the effect of elevated curing temperatures and thermal gradients because it was found that material properties (e.g., elastic modulus) differed by no more than 5% from the design values. In an earlier paper by Barr et al. (2005), which assumed constant values for the girder and bed lengths and ranges of values for the curing and ambient temperatures, the following results were reported. It was found that the concrete and strand temperatures increase during curing and before bond, which causes a reduction in strand stress, and a loss of camber of 0.2 to 0.4 in (5.7 to 10.0 mm). However, there is a small gain in stress as the concrete and strands cool down due to the differing coefficients of thermal expansion, which caused a gain of 0.2 to 0.3 in (4.7 to 7.8 mm) of camber. Finally, because these girders were fabricated in the winter, the ground acted as a heat sink, which cooled down the bottom of the girder and induced a significant thermal gradient through the cross section, which caused a reduction in camber of 1.0 to 1.5 in (25.1 to 37.8 mm).

In total, there was a reduction in strand prestress of 5.5 to 12.1 ksi (or approximately 3% to 7% of the initial prestress including elastic shortening losses) and a corresponding reduction in release camber of 1.0 to 1.6 in (26 to 40 mm) (or approximately 26% to 40% of the design release camber), caused by these combined temperature effects.

The camber of the five girders was then monitored for three years while the girders were in service. It was found that the time-step method using material properties recommended by NCHRP Report 496 predicted cambers that were within 10% of the long-term measured

cambers, whereas the multiplier method (PCI 2004) and improved multiplier method (Tadros et al. 1985) produced camber predictions that were 22% lower and 27% higher, respectively, than the measured cambers.

2.7 *Jayaseelan, Hema et al.* (Oklahoma State University Final Report, August 2007)

"Prestress Losses and the Estimation of Long-Term Deflections and Camber for Prestressed Concrete Bridges"

Jayaseelan et al. (2007), from Oklahoma State University, conducted a literature review of prestress loss prediction methods and related research and a parametric study of related effects on camber. The investigated parameters included the addition of top prestressing strands, the addition of mild steel in the bottom flange at midspan and varying the creep coefficient and concrete elastic modulus by +/- 20%. The results were analyzed using the PCI (2010) Design Handbook method, the AASHTO LRFD Refined Losses method, the NCHRP 496 Detailed Prestress Losses method and the AASHTO LRFD Time Step method.

It was found that decreasing the creep coefficient by 20% led to a total net long-term camber reduction of 6.8% and a 20% increase in the concrete elastic modulus resulted in a long-term camber reduction of 12%. Additionally, it was recommended that the AASHTO LRFD Time Step method be used for more accurate prestress loss and camber/deflection predictions. It was also recommended that the addition of top prestressing strands and/or mild steel in the bottom flange at midspan is an effective way to avoid excessive long-term camber in prestressed bridge girders.

2.8 *Woolf, Douglass et al.* (MnDOT Report 1998-08)

"A Camber Study of MnDOT Prestressed Concrete I-Girders"

Woolf et al. (1998), from the University of Minnesota., conducted a study which investigated the relationship between predicted and measured cambers and analyzed the parameters that affect camber and the methods used for long-term camber predictions. Data was collected over a three-year period on girders of varying depths and lengths from the time of release to shipping. A parametric study was conducted that evaluated certain effects, including concrete modulus of elasticity, gross and transformed moment of inertia, concrete density, initial strand stress, girder length and harp point locations. Finally, three camber prediction methods; the PCI method, Branson's time-step approach and the "CRACK" analysis program by Ghali et al., were analyzed and compared to measured values.

The collected girder data revealed that there were variations in camber of up to 10%, even for girders cast together on the same bed, and that the ratio of predicted to measured initial cambers differed by up to 20%. Additionally, it was found that the initial camber decreased by 12%, on average, due to friction between the girder and the prestressing bed. A field study was conducted to examine the effect of solar radiation. The 128 ft 72M girders examined during the field study increased in camber by 1.5 in (38.1 mm) as the temperature on the top flange increased from 80 to 110 °F during the day. It was concluded that camber could increase by as much as 10% during any given day due to the effect of solar radiation.

Conclusions from the parametric study and camber prediction method analysis were that variations in prestress force, concrete modulus of elasticity, moment of inertia (transformed vs.

gross) independent of elastic shortening losses, and ultimate creep coefficient had the largest influence on camber and that the Branson time-step approach yielded the most accurate camber predictions. However, the simpler PCI Method gave reasonable long-term camber results. It was recommended that the material properties of the concrete being produced in Minnesota be examined to ensure that the equations being used in the predictions were good representations of those properties.

Limitations with regard to this study included the fact that the support (or bunking) conditions during girder storage, 28-day concrete compressive strengths, and actual prestress forces applied to the girders, were not recorded. Even though appropriate approximations were used to account for these limitations, some loss of accuracy in the predictions can be assumed.

2.9 *Ahlborn, Theresa et al.* (MnDOT Report 2000-32)

"High-Strength Concrete Prestressed Bridge Girders: Long Term and Flexural Behavior"

Ahlborn et al. (2000), from the University of Minnesota, studied the behavior of high strength concrete (HSC) prestressed girders in conjunction with Mokhtarzadeh et al. (1998), who studied the HSC material properties. In the Ahlborn et al. (2000) study, two high-strength concrete prestressed bridge girders were designed, monitored, tested and analyzed. As part of the long-term behavior investigation, the camber was monitored from the time of release until the girders were loaded to failure at ages of 860 and 840 days, respectively.

The early-age camber was measured by making a simple centerline measurement with a ruler between the precasting bed and the bottom flange of the girders, whereas a surveying level and rod were used after the girders were moved to the storage yard and test facility. When measuring the camber at release, the assumed true initial camber was calculated by averaging the "on-bed" camber taken immediately after release and the lift/set camber taken the next day.

Three camber predictions methods, the PCI Multiplier Method, the Moment-Area Method and the program PBEAM, were used and compared to the measured cambers at various time intervals. Both nominal and measured material properties and gross geometric design properties were used in all but the PBEAM prediction method, in which just the measured material properties were used.

With regard to the initial camber, the PCI Method predicted the cambers of both girders reasonably well, however, the camber of Girder I was most accurately predicted using measured properties and lower bound elastic shortening and relaxation losses, whereas the camber of Girder II was most accurately predicted using measured properties and upper bound losses. This difference was attributed to the pre-release cracking observed in Girder II, which was believed to cause a significant reduction in camber. The Moment-Area Method was found to produce reasonable predictions for the initial camber of both girders using measured properties, and the program PBEAM predicted initial cambers that were slightly higher than the measured cambers.

At the time of deck casting, both the PCI Multiplier Method and the program PBEAM were used to make camber predictions. Both prediction methods only slightly underestimated the measured camber change due to deck casting, resulting in the conclusion that the measured material properties and other assumptions were accurate. It should be noted that the predicted and measured cambers were compared three days prior and five days after deck casting to avoid the effect of thermal gradients that were present in the girders due to the heat of hydration of the curing deck. Before the girders were taken to flexural failure, PBEAM predictions significantly underestimated the measured cambers.

CHAPTER 3. HISTORIC GIRDER DATA

3.1 Introduction

Historical data were obtained to evaluate the trends that have occurred with respect to precast girder camber at release and at erection. Records and associated data were obtained for girders that were used in bridges throughout Minnesota. Fabrication data pertaining to girder production was obtained from precasting plants and girder elevations at erection were obtained from the counties in which the girders were installed in bridges. The data were evaluated to identify trends and potential causes for observed behaviors.

3.2 Background

Information was gathered on a large and broad set of girders cast over a five-year period from 2006 to 2010, with the bulk of them from 2009 and 2010. This time period was chosen because it dates back to when MnDOT began noticing the low camber problem and because records from precasting plants were more readily available for those years. A conscious effort was made to obtain data for a full range of lengths (short-span to long-span) for girders of each shape. These data were chosen to provide reasonable "bounds" with respect to the maximum and minimum lengths typically used for each shape. Data was extracted from a variety of sources, including MnDOT bridge plans, fabricator shop drawings, pour records and tensioning sheets, as well as beam survey shots taken in the field at the time of bridge erection.

Data from the fabricators was obtained from two plants (hence referred to as Plant A and Plant B) which have produced the majority of prestressed concrete bridge girders for the State of Minnesota. Even though the I-girder shapes produced by each plant were identical, the procedures and materials used at each plant were very different.

At Plant A, the girder concrete mix incorporates a round or partially crushed river rock aggregate, Type III cement and a high range water reducer admixture. The bed lengths at Plant A vary from 316 ft (96.3 m) to 386 ft (117.7 m). The tensioning procedure consists of pulling the straight strands from the "live end" abutment to the specified force and then pulling the draped strands to a *lower* force, depending on the number of harp points along the bed. After the draped strands are tensioned, they are lifted off the bed at the harp points and secured in place by a steel horse that straddles the bed. This procedure, which is referred to as the "harping sequence," stretches the strand and brings it to the desired tension.

At Plant B, the girder concrete mix incorporates a limestone aggregate with a water absorption percent of 1.8, Type I cement and fly ash. For the tensioning procedure, Plant B has the option of using a 150, 350 or 500 ft bed due to a moveable live end abutment. Unlike at Plant A, Plant B harps the draped strands *before* tensioning. This means that the draped strands must be pulled to a higher force than the straight strands because of stress loss due to friction in the drape and hold-down rollers. Plant B also has the option of pulling the draped strands from both ends of the bed, which is used when the maximum allowable pull force is done at one end and the required elongation has not been met.

At both plants, temperature corrections are made to account for the elongation or shortening that will occur when the concrete is poured onto the strands. The rule of thumb commonly used by the precasters is to make a correction to the strand pull force of plus/minus one percent (of the initial pull force) for every ten degrees the strand temperature at the time of

tensioning is lower/higher than the typical girder concrete mix temperature. For example, if the concrete mix for the past few days had been running at 80 °F and if the strand temperature when tensioned was 60 °F, the strand pull force would be increased by 2% to compensate for the expected difference in temperature. Because the anchored strand in the bed is of fixed length, the change in total strain (sum of mechanical and thermal strain) must sum to zero. As a consequence, any change in temperature of the strands will affect the mechanical strain so that the changes in strain sum to zero in the fixed bed. Adjustments to the strand pull force to account for potential changes in temperature are intended to compensate for this phenomenon. Thus, if the strand temperature increases, the mechanical strain (and stress) decreases, and vice versa. Timing of the concrete-steel bonding is critical to this assumption and is very difficult to determine. In addition, the temperature of the free length of strand also impacts the resulting mechanical strain in the girders. Further discussion of the effect of temperature changes on the variation in prestress force is provided in Section 5.3 and in greater detail in APPENDIX B.

3.3 Methodology

The historical girder data was obtained from a variety of sources, as previously stated. MnDOT bridge plans were obtained from the MnDOT Bridge Office as well as from their online database. Information taken from the plans included the beam shape, span and beam number, full and clear beam lengths, the size, number and pattern of the prestressing strands, the design release and shipping strengths and design erection camber for every girder in the historical data set. Additionally, the cross-sectional properties for each girder shape were taken from a MnDOT database.

Fabricator data was obtained by visiting each plant and through email correspondence to acquire shop drawings, pour records and tensioning sheets. Information included the bed length, design and recorded tensioning forces and any temperature corrections, the location of the harp points and lift hooks, number of girders and the position of each girder on the bed, pour date and time, ambient and concrete temperatures during the pour, release and 28-day concrete strengths and the release camber for every girder. Notes were taken if anything differed from the corresponding bridge plans.

Finally, the beam survey shots were obtained from MnDOT and county bridge inspectors for most of the bridges in the study. The inspector typically recorded the elevation of the top or bottom of the girder at five foot intervals along the entire length of the girder at erection. The camber at erection of the girder was calculated using the elevations at the beam ends and near midspan. The date when the survey shots were taken was also obtained, making it possible to determine the age of each girder at erection. However, it should be noted that the weather conditions, specifically the amount of solar radiation, may have had a significant effect on camber, and was rarely recorded during the surveys. The effect of solar radiation on the camber of girders at erection is discussed in Section 7.3.1.

3.4 Summary and Results of Collected Data

Historical data was obtained for a total of 1067 girders from 47 different bridges, including 804 girders from Plant A and 263 girders from Plant B. Data was collected for girders of seven commonly-used MnDOT shapes (i.e., 27M, 36M, MN45, MN54, MN63, 72M and 81M). However, data was obtained for more girders of certain shapes simply because they were more commonly used. Table 3-1 gives the number of girders for which data was collected from

each plant, for each shape. The historical data collected represents approximately 40% and 30%, respectively, of the total numbers of girders produced at each plant from 2006-2010.

Table 3-1. Breakdown of collected camber records from each precasting plant

	27M	36M	MN45	MN54	MN63	72M	81M
# Plant A	88	164	149	146	116	28	113
# Plant B	30	43	53	0	131	6	0

Girder elevation data, which made it possible to find the camber at erection, was also obtained for 768 of the 1067 girders in the study. Table 3-2 gives the number of girders for which data was collected from each plant, for each shape.

Table 3-2. Breakdown of collected girder elevation records

	27M	36M	MN45	MN54	MN63	72M	81M
# Plant A	46	102	91	122	88	28	97
# Plant B	0	30	33	0	131	0	0

3.4.1 Release Camber

Bridge plans do not explicitly give the design release camber for each girder in a bridge. The "initial camber," which refers to the camber at erection before deck placement, is the value given in the plans. However, knowing the multipliers used to calculate this deflection makes it possible to back-calculate the design release camber. On average, the measured release camber for the 1067 girders was approximately 74% of the design release camber. There were many possible reasons for this discrepancy, including higher release strengths, higher elastic moduli, thermal effects, and friction in the bed, which were some of the factors explored in this study.

3.4.2 Lift and Set Camber

When the strands are released in a precasting bed, the girder undergoes elastic shortening as the tension in the steel is equilibrated by compression in the girder. It is likely that friction between the bottom of the girders and the bed restrains some of the movement of the ends of the girders as the strands are released. Any restraint of the girder ends at release would lead to a lower observed camber.

To observe the significance of this effect, the girders could be lifted on one end, releasing built-up friction, and set back down on the bed. Lifting the girder on one end was chosen to facilitate replacing the girder on the bed without damaging the chamfered edges. Fabricators at both plants measured the camber at release and again after lifting and setting the girders. This was done for a few bridge projects at each plant in the summer of 2010. The time between measurements was minimized such that the effects of temperature, creep and shrinkage could be ruled out as possible causes for any observed differences between the initial on-bed and lift/set

cambers. This procedure was conducted on approximately 100 girders. On average, the camber in the girders increased by anywhere from a negligible change to 0.30 in (7.6 mm). In general, it was observed that larger and longer girders had higher camber changes after lifting and setting. As the girder end is lifted by the lift hooks, the weight of the girder causes downward deflection of the girder end. As the girder end is set on the bed, friction acts in the opposite direction to resist the weight of the girder pushing the girder end back outward. Thus, the lift/set cambers represent an upper bound for the effect of friction on camber. The release cambers that might be obtained from a frictionless bed would be expected to lie somewhere between the initial on-bed release camber reading and the lift/set camber reading. Ahlborn et al. (2000) used the average of the measured release camber and the lift/set camber as the assumed "true" release camber, as is discussed in Section 2.9. Table 3-3 gives the average changes in camber for girders categorized by shape and length.

Table 3-3. Camber differences measured between initial on bed and lift/set at release

Shape/ Length	27M	36M	MN45	MN54	MN63	72M	81M
40-60 ft	-	~0.090"[1] (9.43%)[2] S=23[3]	N/A[4]	N/A	N/A	N/A	N/A
60-80 ft	~0.075" (2.95%) S=12	~0.125" (7.70%) S=10	-[5]	N/A	N/A	N/A	N/A
80-100 ft	N/A	-	-	~0.112" (9.15%) S=3	-	N/A	N/A
100-120 ft	N/A	N/A	~0.100" (2.85%) S=9	~0.125" (3.95%) S=12	-	-	-
120-150 ft	N/A	N/A	N/A	~0.180" (5.90%) S=4	~0.285" (13.0%) S=19	-	-

[1]Positive values indicate lift/set cambers were larger than initial on bed cambers
[2]Parenthetical numbers indicate the percent increase in lift/set camber over the measured release camber (i.e., $((\Delta_{lift/set}-\Delta_{initial})/\Delta_{initial})*100$)
[3]Denotes the number of girders in the sample
[4]N/A denotes girder lengths that are outside the range of lengths typically used for each shape
[5](-) denotes girder shape/lengths that were fabricated during the course of the study for which lift/set data were not measured

Based on these results, it can be concluded that friction in the bed contributed to the lower than predicted release cambers. Given the fact that the "true" release camber can be approximated as the average of the on-bed and lift/set cambers, this contribution was not very large (i.e., less than 5%). Thus, this effect was not considered to be a primary factor contributing to the discrepancy between design and measured release cambers.

3.4.3 Design vs. Measured Concrete Release Strength

In bridge plans, it is common practice to specify the concrete release strength, f'_{ci}, and shipping strength, f'_c, for each girder or set of girders. The fabricators are required to meet the specified release strength before cutting the strands. Bridge designers use this release strength in their calculations for the modulus of elasticity at release and hence, camber predictions, as illustrated in Section 1.2. In order to efficiently "turn-over" the precasting beds, fabricators often use higher strength concretes to ensure that there will be no problems achieving the required strengths at release. From the historical database, measured release strengths have been observed to be as much as 35% higher than the design strength. But, on average for the 1067 girders in the study, the measured release strengths were approximately 15.5% higher than the specified required release strengths. In recent years, fabricators at both plants have worked to perfect their mix designs so that the high strengths required can be achieved at earlier ages. Table 3-4 gives the average percent (in bold) by which the design release strengths were exceeded by plant and year, along with the minimum-maximum range (in parenthesis). The wider range shown for concrete strengths from Plant A are likely due to the larger sample sizes (i.e., 804 for Plant A vs. 263 for Plant B), as both plants often achieve a wide range of strengths because of varying curing and environmental conditions. As noted earlier, the 804 girders from Plant A and the 263 girders from Plant B included in the historical database represent approximately 40% and 30%, respectively, of the total numbers of girders produced at each plant from 2006-2010.

Table 3-4. Percent increase in measured versus design concrete strength at release

Year(s)	Plant A	Plant B
2006-2008	**14.4%**[1] (4.8%-24%)[2]	**2.80%** (0%-4.3%)
2009	**14.1%** (6.5%-23.7%	**18.2%** (16%-19.6%)
2010	**17.8%** (4%-36%)	**24.2%** (15.2%-31.9%)

[1]Percent increase determined as $((f'_{ci,meas} - f'_{ci,design})/ f'_{ci,design})*100$
[2]Parenthetical numbers represent the range in results

Because the concrete modulus of elasticity is related to the concrete compressive strength (typically assumed to be a function of the square root of the concrete compressive strength), higher release strengths result in higher material stiffnesses, and thus lower cambers. The significance of this effect is discussed further in Section 5.2.1.

3.4.4 Erection Camber

As previously stated in Section 3.3, the camber at erection can be determined from the girder elevations (or beam survey shots) taken by bridge surveyors at the time of bridge erection. For the 768 girders for which data was available, the camber at erection was, on average, approximately 83.5% of the design erection camber. For the girders designed using the original 1.80/1.85 multipliers, the camber at erection was approximately 78% of the design camber. For girders designed using the 1.5 multiplier, the camber at erection was approximately 86% of the

design camber. Because the time of erection can vary so greatly, it is beneficial to express these values in greater detail.

Figure 3-1 shows the measured erection cambers as a percentage of the design erection camber, plotted against the average girder age at erection. Each data point represents a unique set of girders, separated by bridge, girder design and age. Because it is not realistic to plot each individual girder, the data points represent the average of the erection cambers for anywhere from two to forty-plus girders. The error bars in the figure represent the highest and lowest camber values for each girder set. The girders are also separated by the multiplier used in the design, as the multiplier was changed in late 2007, as discussed in Section 1.2.

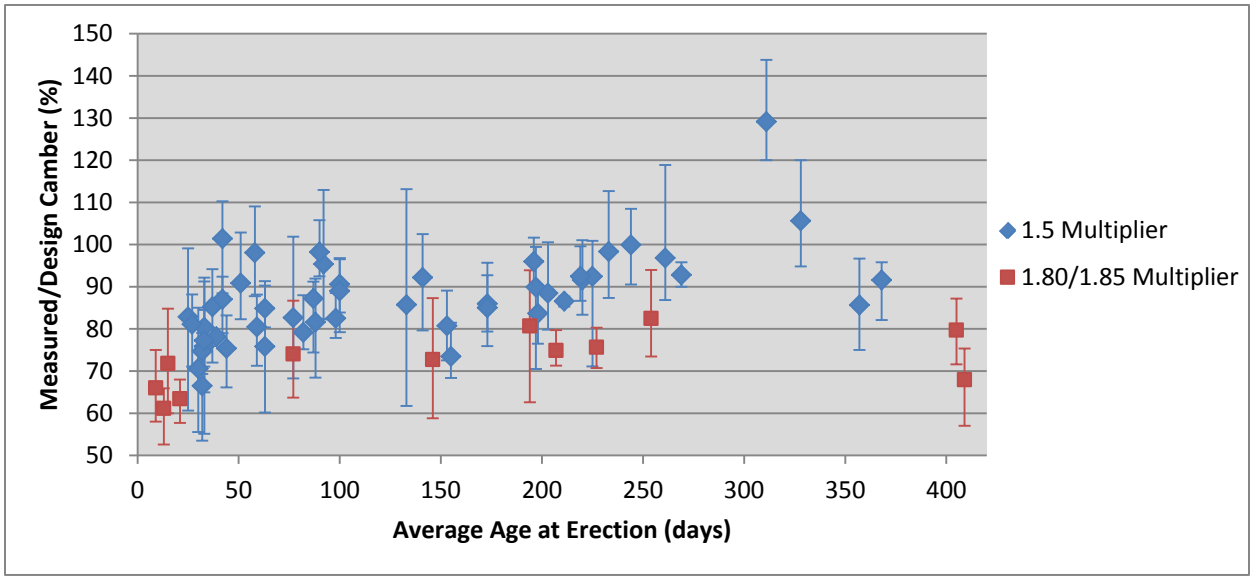

Figure 3-1. Measured/design erection cambers over time

A few key observations can be made from examining the data in this manner. First, the majority of girders in the study were erected at early ages (less than 100 days) and had cambers that were much lower than the design values. Second, the switch from the Martin (PCI) 1.80/1.85 multipliers to the 1.5 multiplier slightly improved the erection camber results, but not to the point where there were no longer any problems. Third, only a handful of girder sets had cambers that, on average, exceeded the design erection cambers (>100% on the above plot). For a few sets of girders that exceeded the design camber, it was noted in the girder elevation survey sheets provided by the counties, that the girder elevations were recorded during hot summer days. For example, the set of girders that were erected at ~40 days that had erection cambers that exceeded the predicted cambers (data point at ~101% on the above figure), had survey shots taken on two sunny August afternoons where recorded temperatures in the area were 85-90 °F and 70-75 °F on each day. Thus, it is very likely that the girder cambers were affected by solar radiation. It should be noted, however, that there were other girders with girder elevations recorded on warm and sunny summer days that had measured cambers below the design erection cambers. For example, the set of girders that was erected at ~77 days, and had erection cambers that were just 74% of the design values, were shot on a sunny 70 °F day in June. Even though many of the girders in the historical data set likely had elevations recorded on summer days, the

effect of solar radiation does account for the upper outliers. Further investigation of the effect of solar radiation is discussed in Section 7.3.1.

Plotting the measured vs. design erection cambers as a percent, as shown in Figure 3-1, may lead to misleading results for girders that have small cambers (i.e., negligible differences in nominal camber can result in large percent differences). In these cases, large percent differences might be associated with mere tenths of an inch, and would not cause significant problems at erection. To better illustrate the differences between the measured and design erection cambers, Figure 3-2 shows the same data that is shown in Figure 3-1, except that the measured erection cambers are plotted against the design camber values. The solid line, at a slope of unity, represents the situation where the design camber would have predicted the measured camber.

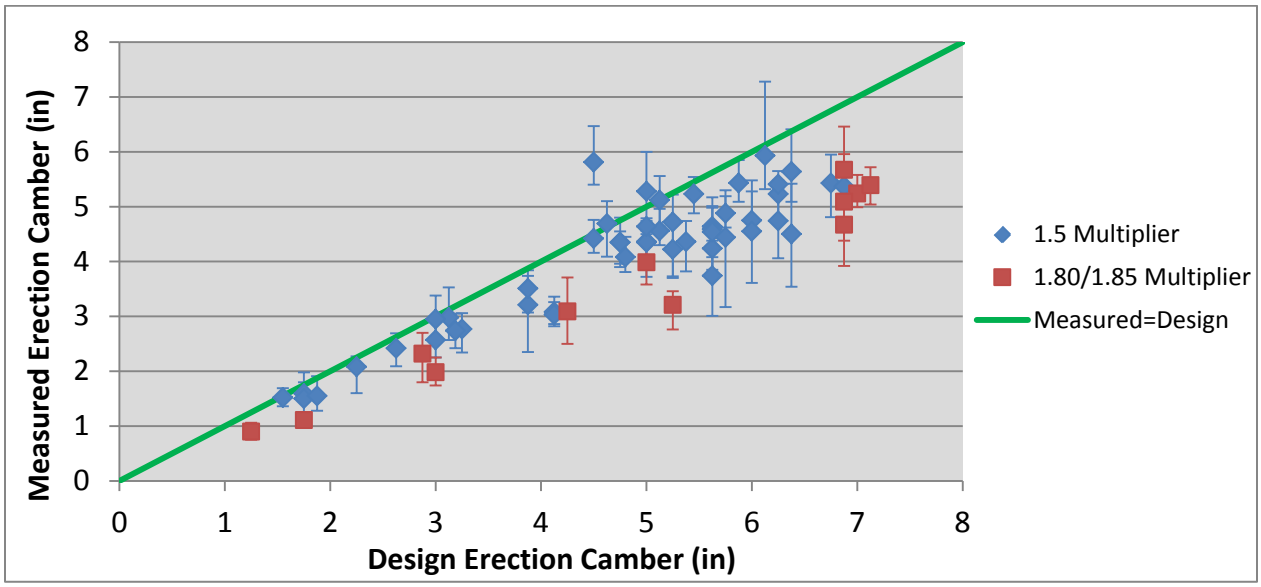

Figure 3-2. Measured vs. design erection cambers

These results indicate that, for some girders, the nominal difference between the measured and design camber values was significant and that for girders with higher nominal design values, this discrepancy was even larger. Furthermore, the results show that there were very few girders with measured erection cambers that exceeded the design values. Because some of the girders had measured erection cambers that were as much as 2 in or more below the design values, the large percent differences shown in Figure 3-1 were significant.

These erection camber results are examined further in Section 8.5, as part of the optimization of the new multipliers.

3.5 Sources of Error

There were inherent sources of error in the data collected from fabricators that were unavoidable, and it was nearly impossible to distinguish the extent of the error on an overall basis. The first source of error involved the recorded release and 28-day concrete strengths. It was common practice for the fabricators to break three or more cylinders early in the morning to ensure that the strength of the concrete in the girders being produced had exceeded the specified design value. Because the cylinder strengths were recorded before the tarps and side-forms were

removed, the actual release strengths of the girders could have exceeded the recorded values due to the extra curing time. With regard to the 28-day concrete strengths, it was common practice for the fabricators to take the cylinders well past the specified design value, but not necessarily to failure. This was done to limit the stress on the cylinder-testing machine. Therefore, the actual 28-day concrete strengths often had to be approximated, which was done by examining cylinders from other pours in the same bridge project that were taken to failure.

Another source of error involved the recorded release cambers. Fabricators obtained the release camber by measuring the vertical distance from the chamfer on the side of the precasting bed to the edge of the bottom flange at midspan. This form of measurement is not as precise as a stretch-wire system, which was used for girder instrumentation (described in Section 4.3). In fact, it was common for the camber measurements obtained from the stretch-wire system to differ, by as much as 0.25 in, from those recorded by the fabricators. Additionally, the fabricators did not always record the release camber *immediately* at the time of strand release.

Finally, there were additional effects (e.g., the uncertainty in the temperature at which the strand-concrete bond formed and potential pre-release cracking due to cooling while the girder was restrained prior to strand release) that led to sources of error discussed in Sections 5.3.1, 7.4.3.2 and APPENDIX B.

3.6 Summary

Fabrication data was collected for 1067 girders cast at two precasting plants over a five-year period from 2006 to 2010, and camber at erection data was collected from the counties for 768 girders of that group. On average, it was found that the observed camber at release for the 1067 girders was only 74% of the design value. Furthermore, it was found that the observed camber at erection for the 768 girders was only 83.5%, on average, of the design value; and that girders erected at early ages almost always had cambers that were significantly lower than the design value. Additionally, the fabricator records indicated that the concrete release strengths were, on average, 15.5% over the specified design value. Finally, lift/set camber data was recorded at both precasting plants for approximately 100 girders during the summer of 2010. It was found that friction in the bed caused the recorded initial on-bed release cambers to be slightly lower than the “true” release camber value. The historical data was used to investigate potential trends in camber behavior and served as a database for which modifications to camber predictions could be tested.

CHAPTER 4. GIRDER INSTRUMENTATION

4.1 Introduction

To investigate changes in camber due to time-dependent effects, fourteen Plant A girders of varying length and shape were instrumented with a stretch-wire system that was monitored periodically from strand release to girder shipment. The measurements were used to validate the numerical analysis program, PBEAM, which was subsequently used in a parametric study to investigate factors that influenced the time-dependent camber (e.g., solar radiation, relative humidity, and bunking conditions during storage).

4.2 Methodology

The girders were selected based on a few key criteria. First, it was desired that girders of varying shape and length be instrumented in groups of two or three to provide some measure of statistical variation. It was also important that the selected girders would remain in the storage yard for a considerable length of time prior to shipment to provide sufficient time-dependent data. Finally, it was preferred that a set, or sets, of girders be selected such that the effects of both weekday and weekend cures could be investigated.

Fortunately, there were a few bridge projects at Plant A that met all of the above criteria. Four sets of girders, including I-girder shapes MN45, MN54 and MN63, were selected for instrumentation. Table 4-1 contains information regarding the shape, length, pour date and shipping date for each set of girders.

Table 4-1. Description of selected instrumented girders

Set	# of girders	Shape	Length	Bridge #	Cast Date	Ship Date
1[1]	2	MN54	122’ 4.75”	73037	Fri 9/3/10	Dec 2010
1	2	MN54	122’ 4.75”	73038	Wed 9/8/10	Dec 2010
2	3	MN54	92’ 9.25”	73038	Mon 10/4/10	Dec 2010
3	3	MN45	119’ 3”	27B58	Wed 10/20/10-Thu 10/21/10	July 2011
4	2	MN63	131’ 6”	73044	Thu 11/4/10	June 2011
4	2	MN63	131’ 6”	73044	Fri 11/5/10	June 2011

[1]Each girder set is separated by shading.

As can be seen in Table 4-1, each set of girders sat in the storage yard for at least 2.5 months. Sets 1 and 4 each contained girders that were cast over a weekend. It should also be noted that Sets 1, 3 and 4 contained girders that were on the long end of typical lengths obtained with those I-girder shapes.

4.3 Materials and Instrumentation Setup

A simple, yet effective, stretch-wire system was used for the girder instrumentation, which was modeled after the system used by Erkmen et al (2008). The system consisted of a line strung along the full length of each girder. The line was strung over two near-frictionless pulleys, which were placed on steel rods anchored to the side of the top flange at each end of the girders. On one end, the line was anchored (i.e., tied off to a bolt anchored in the concrete). On the other end, the line was fitted with an S-hook so that a weight could be hung to provide constant tension in the line. A ruler and mirror were epoxied to the top flange of each girder at midspan to measure the girder camber. By lining up the "stretch-wire" with its reflection in the mirror, the camber could be measured to an accuracy of 0.5 mm.

The materials used in this instrumentation setup included the following:

- Stainless steel 3 in (76.2 mm) bolts
- Corrosion-resistant black-oxide finished double-threaded 3 in (76.2 mm) steel rods
- High-strength 3 in (76.2 mm) diameter nylon pulleys with near-frictionless bearings
- Standard aluminum 12 in (304.8 mm) ruler and simple 4x6 in (101.6x152.4 mm) mirror
- A 20-lb weight
- 80-lb test braided fishing line

The instrumentation setup is shown in Figure 4-1, Figure 4-2 and Figure 4-3.

Figure 4-1. Free end of stretch-wire system with weight and pulley

Figure 4-2. Anchored end of stretch-wire

Figure 4-3. Ruler and mirror located at midspan

The material used for the stretch-wire system was important because the line was required to hold the weight, have minimal self-weight and elongation under tension, and be easy to handle. Other stretch-wire systems used in similar applications used thin metal piano wire,

which was originally used to instrument the first set of girders. However, because of its tendency to snag and tangle, its significant self-weight and its difficulty to handle and tie, the piano wire was replaced with 80-lb test braided fishing line. The fishing line proved to be strong, durable and easy to work with and unwind.

It was also important that the entire system be resistant to adverse weather conditions. Since the girders sat in the storage yard during the cold Minnesota winter, it was important that the pulleys remained near-frictionless and that the fishing line could keep its strength in cold temperatures. It was also important that the fishing line did not absorb too much water or get crusted with ice, which would result in added self-weight.

The winter of 2010 proved to be very cold, with many measurements being taken in temperatures below 0 °F. There were also several instances where the fishing line was frozen to the side of the girder and had to be literally pulled out of the ice. During these times, special care was taken to ensure that the line was completely free of ice and that the pulleys were moving freely on the rods. When the cambers began to increase during the winter, there was concern that there were still issues with the system in cold weather. So, a "dummy" check was created by placing heavy weights on the ground below the girder at midspan. A tape measure was used to measure the distance between the weight and the bottom flange of the girder. This "dummy" check proved that the stretch-wire camber readings were reasonable. The reason for the increase in camber during the winter is explained in Section 7.3.2.

4.4 Camber Measurements

The instrumentation was installed onto each girder just after the side-forms were removed and just before the strands were cut. It was important to be as efficient as possible with the installation in order to minimize the time that the girders were exposed before strand release. Once the instrumentation was in place and secure, an initial flat-line camber reading was taken on each girder which would serve as the "zero" reading. Thus, the camber could be calculated as the difference between any subsequent measurement and this "zero" reading.

To determine the initial on-bed camber at release, a measurement was taken on each instrumented girder immediately after the strands were cut. One of the possible effects that could result in lower release cambers is friction build-up between the girder and the precasting bed. As the strands are released and the girders begin to camber up, the girder ends must slide inward. However, the friction between the girders and the bed resists this sliding. Thus, a lift/set camber measurement was taken soon after the release camber reading. The lift/set camber involved the fabricators lifting one end of each girder to release the friction and then setting it back down so that the measurement could be taken. This process and the results are discussed further in Section 3.4.2.

After the lift/set camber readings were taken, the girders were transported to the prep area where they could be cleaned and prepared for eventual shipping. Then, the girders were placed in the storage yard where they remained bunked until shipment. Camber measurements were taken approximately once a week following fabrication through the first 60 days and then were taken bi-weekly after that. Each camber measurement involved checking the pulleys to make sure they were rotating freely, checking the line to make sure that it was positioned correctly and then hanging the weight and recording the camber. Each camber measurement after fabrication was to be taken at dawn in order to avoid the effect of solar radiation on camber and to provide consistency from one reading to the next. Unfortunately, the first few readings on the first set of girders were taken around mid-day (rather than at dawn) and the effect of solar radiation is

clearly visible in the results shown in Figure 4-4. The effect of solar radiation is further discussed in Section 7.3.1, and the camber results for the remaining sets of instrumented girders are shown in Figure 4-5, Figure 4-6 and Figure 4-7. In these figures, the "design camber" refers to the camber at erection predicted by MnDOT and included in the bridge plans for these girders.

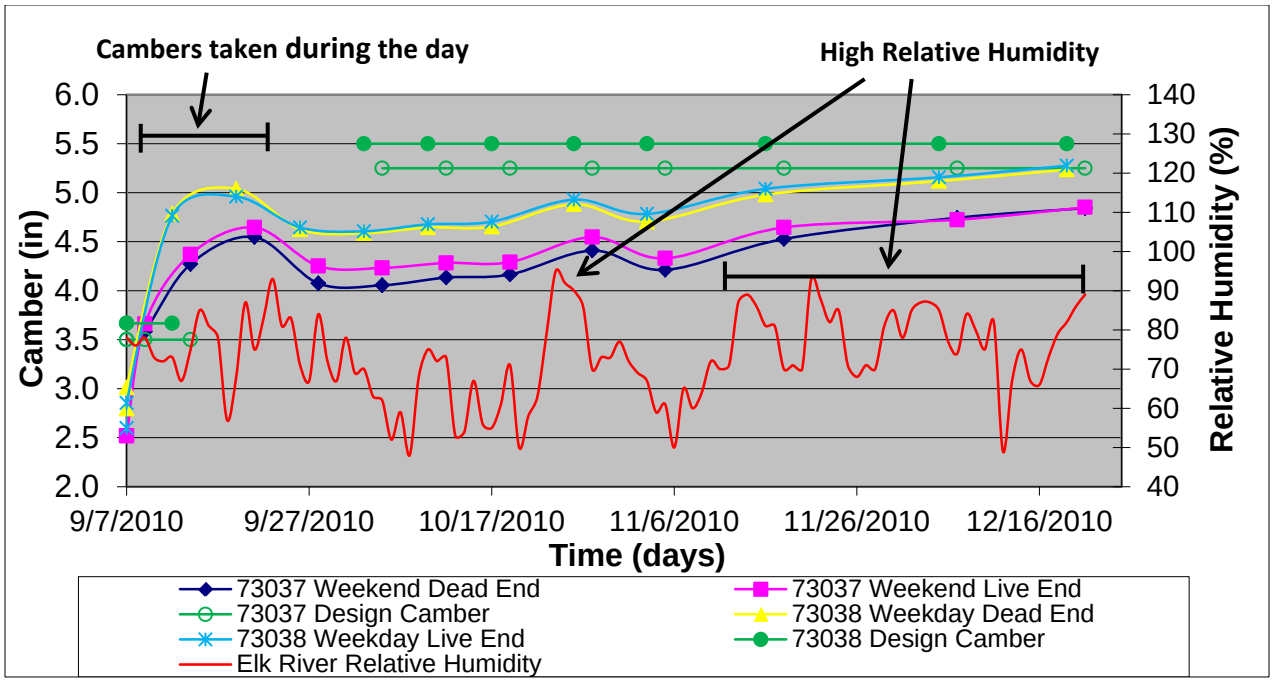

Figure 4-4. Camber measurements for instrumented girders set 1 (MN54, L=122 ft)

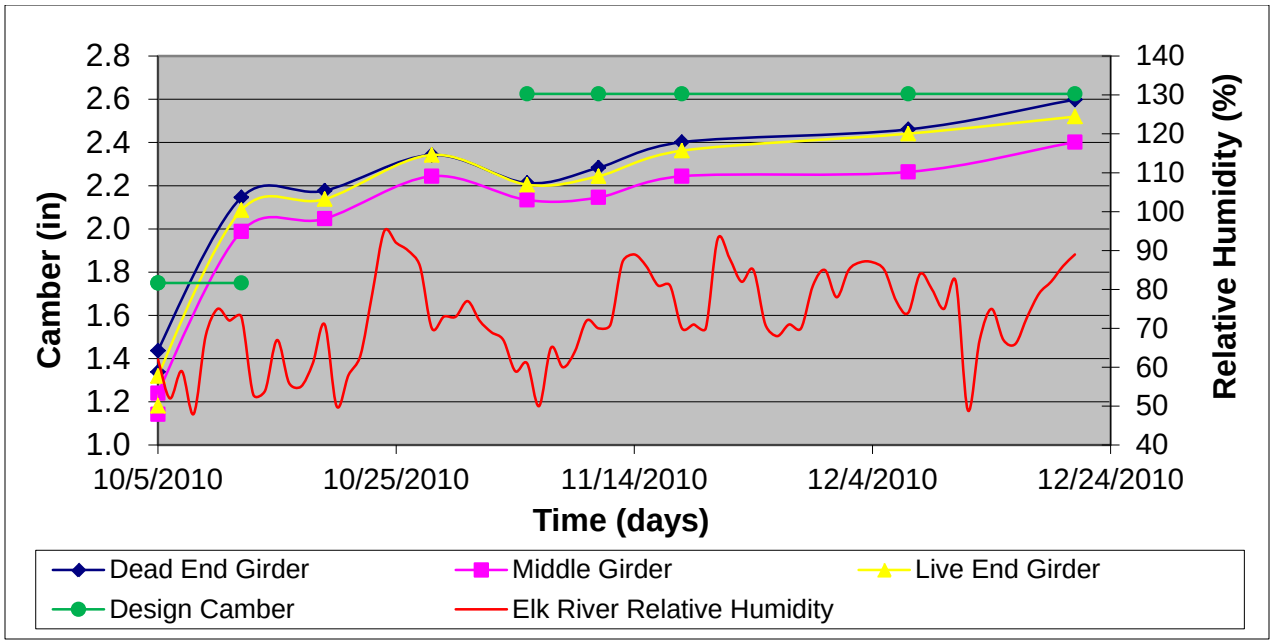

Figure 4-5. Camber measurements for instrumented girders set 2 (MN54, L=93 ft)

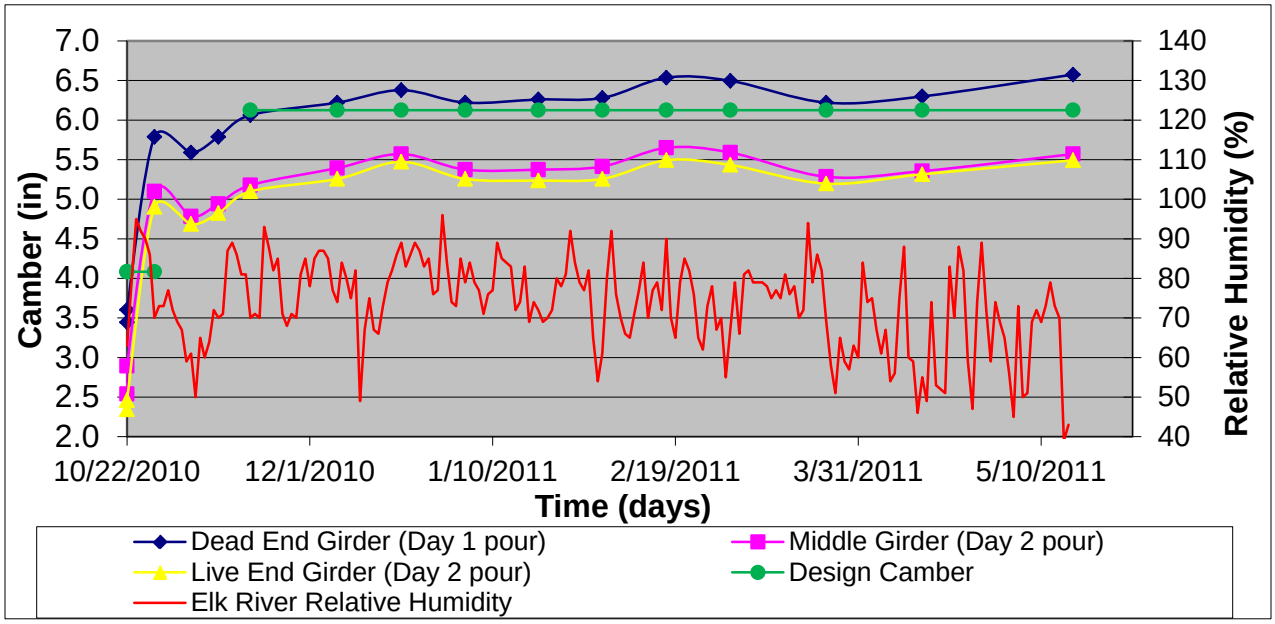

Figure 4-6. Camber measurements for instrumented girders set 3 (MN45, L=119 ft)

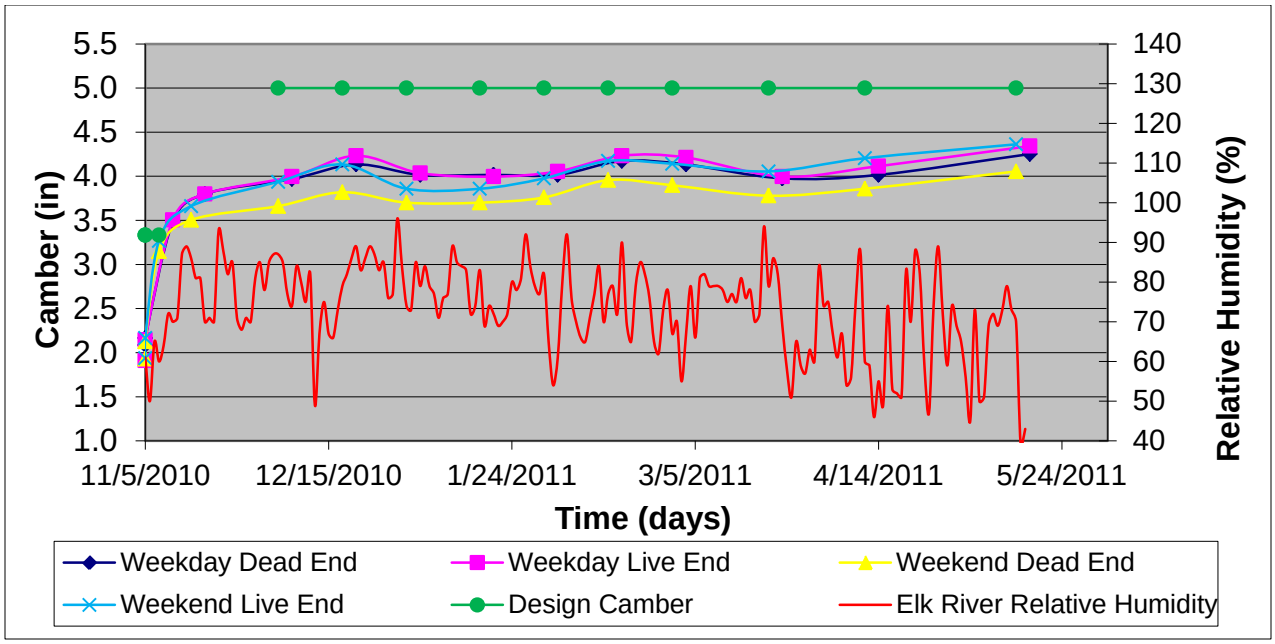

Figure 4-7. Camber measurements for instrumented girders set 4 (MN63, L=131.5 ft)

4.5 Summary

Fourteen girders were instrumented and their camber monitored from the time of strand release until the girders were shipped. The camber measurements were used to correlate potential effects with observed camber behaviors and to provide a suitable database for PBEAM program validation, which is discussed in Section 7.4. All of the collected data for these girders, including fabrication records, camber measurements and thermal curing data are given in APPENDIX E.

CHAPTER 5. RELEASE CAMBER: ISSUES AND INVESTIGATED EFFECTS

5.1 Introduction

The large amount of collected data from the plant records and instrumented girders facilitated investigation of a number of possible effects on camber with increased statistical significance. Comparisons were made and observations verified for numerous effects. In Section 1.2, the calculations for camber are shown, based on elastic analysis. Because the details of the girders (e.g., cross-sectional properties, strand eccentricities, girder lengths, and concrete compressive strengths) were recorded, the observed discrepancy between the predicted and measured release cambers (as reported in Section 3.4.1) could be attributed to inaccurate assumptions about the remaining values; namely the prestress force at release, the concrete modulus of elasticity, and the cross-sectional moment of inertia. In the following sections, the impact of potential inaccuracies in each of these assumptions on the predicted cambers is investigated.

5.2 Concrete Strength and Modulus of Elasticity

5.2.1 Concrete Strength

As mentioned in Section 3.4.3, the concrete compressive strengths at release, $f'_{ci,meas}$, measured at the two plants over the period of time when the historical data was collected (2006-2010) exceeded the specified design release strengths, $f'_{ci,design}$, by 15.5%, on average, and in some cases by as much as 35%. Because camber is inversely related to elastic modulus, as is shown in Section 1.2, and because elastic modulus is a function of the concrete compressive strength, higher concrete compressive strengths will lead to lower cambers. A number of equations for the concrete modulus of elasticity, including the ACI 363R-10 equation used by MnDOT (described in Section 5.2.2.3), are related to the concrete compressive strength by the square root. As an example, if the design release strength is 7000 psi and the measured strength is 8000 psi (~14% increase in concrete strength), the calculated elastic moduli using the ACI 363 equation are 4347 ksi and 4578 ksi, respectively, resulting in an expected camber that is 95.8% of the design release camber. Table 5-1 gives the expected cambers as a percentage of the design release cambers resulting from increased concrete strengths at 5% intervals. It should be noted that a starting f'_{ci} of 7500 psi was used to calculate the values shown in Table 5-1. However, the values would not change significantly if a different starting f'_{ci} were used.

Table 5-1. Impact of high concrete release strengths on camber

% Increase in Concrete Strength	% of Design Release Camber[1]
5%	98.4%
10%	97.0%
15%	95.5%
20%	94.2%
25%	92.9%
30%	91.7%
35%	90.6%

[1]Where the modulus of elasticity is assumed to be the ACI 363 equation used by MnDOT, which is a function of the square root of f'_{ci} (assumed to be 7500 psi)

There is no question that higher release strengths result in lower cambers; however, because the modulus is assumed to vary as the square root of the compressive strength, large changes in concrete strength have a lesser impact on the stiffness.

Another potential source of error associated with the elastic modulus is the model or equation used to predict it. The relationship between the elastic modulus and concrete strength changes over time as the concrete compressive strength increases. Other variables, such as aggregate and cement type, can also affect the concrete elastic modulus.

The quality of the aggregates in the region used by Plants A and B may be associated with stronger and stiffer concrete mixes than what might be predicted by the ACI 363 equation. In other words, 10 ksi concrete produced at these plants might be stiffer than 10 ksi concrete produced elsewhere.

Because of the significance of the effect of elastic modulus on camber and the possibility of stiffer girder concrete, material tests were conducted at the University of Minnesota to investigate the concrete compressive strength and modulus of elasticity with respect to time. A literature review was also conducted to compare commonly-used models to the material test data.

5.2.2 Modulus of Elasticity: Reviewed Models

There are many models and expressions that attempt to predict the concrete modulus of elasticity based on concrete strength and, possibly, other parameters. Mokhtarzadeh et al. (1998) conducted a broad literature review to find commonly-used models and compared them to extensive experimental results. Because the models in the Mokhtarzadeh study were compared to material tests on concrete obtained from Plant A, those models were investigated in this study. Updated versions of these models, if applicable, were used, along with additional models found in the literature review. It should be noted that many of the following models are specified to be applicable for high strength concrete and are thus appropriate for use in this study.

The models for concrete elastic modulus chosen for this study were the following:

- Pauw 1960 (ACI 318-08, AASHTO LRFD 2010)
- Carrasquillo et al.1981
- MnDOT LRFD Bridge Manual 2009 (ACI 363 2010)
- CEB-FIP 1990
- GL2000 (Gardner and Lockman 2001)
- Ahmad and Shah 1985
- Tomosawa and Noguchi 1993
- Radain et al. 1993
- NS 3473 1992

The following is a brief description of each model.

5.2.2.1 Pauw 1960 (ACI 318-08, AASHTO LRFD 2010)

Based on experimental results of lightweight and normal weight concretes, Pauw (1960) developed a model which is used by ACI 318-08 (prov. 8.5.1) and by the AASHTO LRFD 2010 Bridge Design Specification (prov. 5.4.2.4).

The expression for the concrete modulus of elasticity is given as:

$$E_c = 33w^{1.5}\sqrt{f'_c} \qquad \textbf{(5-1)}$$

where

E_c = concrete modulus of elasticity, in psi
w = unit weight of concrete at time of test, in pcf
f'_c = concrete compressive strength at time of test, in psi

In this equation, the effect of the concrete density is represented by the unit weight of concrete (w), and is specified for values between 90 and 155 pcf. In ACI 318-08, there is no restriction given to the applicable concrete compressive strength range for this expression. In AASHTO LRFD 2010, it is specified to be applicable for concrete strengths up to 15.0 ksi; however, the MnDOT LRFD Bridge Manual (2009) specifies that this expression is to be used only for concrete strengths up to and including 6.0 ksi.

5.2.2.2 Carrasquillo et al. 1981

An experimental investigation by Carrasquillo et al. (1981) found that the Pauw 1960 (ACI 318-08, AASHTO LRFD 2010) equation overestimated the elastic modulus of concrete with strengths greater than 6,000 psi. Thus, the following recommendation was made for the expression for concrete modulus of elasticity:

$$E_c = \left(1265\sqrt{f'_c} + 1000\right)(w/145)^{1.5} \qquad \textbf{(5-2)}$$

where

E_c = concrete modulus of elasticity, in ksi
w = unit weight of concrete at time of test, in pcf
f'_c = concrete compressive strength at time of test, in ksi

This equation was specified for concrete strengths between 3,000 and 12,000 psi. In the ACI Committee 363 State-of-the-Art Report on High Strength Concrete (ACI 363R-10), the Carrasquillo equation was recommended for use with high strength concrete. It was specified for use with normal density concretes and the term with the unit weight of concrete, *w*, was dropped (as is shown in Section 5.2.2.3). It was noted that this equation has been proven to be a "relatively reliable lower bound expression" and that other studies (Myers and Carrasquillo (1999), Gross and Burns (1999)) have raised concerns that this equation may significantly underestimate the modulus of elasticity for high strength concretes (ACI 363R-10).

5.2.2.3 MnDOT LRFD Bridge Manual 2009 (ACI 363 2010)

The MnDOT LRFD Bridge Manual 2009 recommends using the ACI 363 (ACI 363R-10) equation for normal density concretes with strengths exceeding 6,000 psi. The expression for the concrete modulus of elasticity is given as:

$$E_c = 1265\sqrt{f'_c} + 1000 \qquad \textbf{(5-3)}$$

where

E_c = concrete modulus of elasticity, in ksi
f'_c = concrete compressive strength at time of test, in ksi

As previously mentioned, the ACI 363R-10 equation does not contain a term for the unit weight of concrete. In the case of the Pauw equation in ACI 318-08, a simplification is given for normal weight concrete which implicitly indicates the unit weight of normal weight concrete is 144 pcf. Considering that the ACI 363 equation has been found to be a lower bound expression for elastic modulus, the absence of the unit weight of concrete term may make this expression an even *lower* bound estimation of concrete elastic modulus in cases where the unit weight of concrete is on the high end. In the calculation of deflection due to self-weight, MnDOT assumes the unit weight of concrete to be 155 pcf (which includes the effect of the reinforcement). It should be noted that while the value of 155 pcf was used for the reinforced concrete, the self-weight of the cylinder samples obtained during material testing (discussed in Section 5.2.3), were 155 pcf, on average, even after taking out the reduction in weight due to water loss.

5.2.2.4 CEB-FIP1990

The CEB-FIP Model Code 1990 recommends using the following expression for concrete modulus of elasticity for concrete with strengths up to 11,600 psi.

$$E_c = 593{,}400\alpha_\beta\left((f'_c + 1160)/10\right)^{1/3} \qquad \textbf{(5-4)}$$

where

E_c = concrete modulus of elasticity, in psi
f'_c = concrete compressive strength at time of test, in psi
α_β = 1.2 for basalt, dense limestone aggregates; = 1.0 for quartzitic aggregates; = 0.9 for limestone aggregates; = 0.7 for sandstone aggregates

Because of the mix designs at the two precasting plants, the values used for α_β were 1.0 and 1.2 for Plant A and B, respectively.

5.2.2.5 GL2000 (Gardner and Lockman 2001)

Gardner and Lockman (2001) recommended using the following expression for concrete modulus of elasticity in the absence of experimental data.

$$E_c = 3500 + 4300\sqrt{f'_c} \quad \textbf{(5-5)}$$

where

E_c = concrete modulus of elasticity, in MPa
f'_c = concrete compressive strength at time of test, in MPa

This equation comes from the same ACI Materials Journal paper by these authors that emphasized the GL2000 creep and shrinkage models for normal strength concrete. As was the case with these creep and shrinkage models, the above expression for concrete modulus of elasticity is likely applicable for concrete strengths only up to 70 MPa (~10 ksi), but was still compared in this study.

5.2.2.6 Ahmad and Shah 1985

Ahmad and Shah 1985 conducted a study that investigated properties of medium and high strength concrete. They recommend using the following expression for concrete modulus of elasticity for concrete with strengths up to 12,000 psi.

$$E_c = w^{2.5}(f'_c)^{0.325} \quad \textbf{(5-6)}$$

where

E_c = concrete modulus of elasticity, in psi
w = unit weight of concrete at time of test, in pcf
f'_c = concrete compressive strength at time of test, in psi

5.2.2.7 Tomosawa and Noguchi 1993

Tomosawa and Noguchi 1993 recommended using the following expression for concrete modulus of elasticity for high strength concrete. The data investigated to derive this expression were obtained from concrete with compressive strengths of 2,900 to 23,200 psi.

$$E_c = 4.86 \times 10^6 k_1 k_2 (w/150)^2 \left(f'_c/8{,}700\right)^{1/3} \quad \textbf{(5-7)}$$

where

E_c = concrete modulus of elasticity, in psi
w = unit weight of concrete at time of test, in pcf
f'_c = concrete compressive strength at time of test, in psi
k_1 = 1.2 for crushed limestone aggregates; = 1.0 for river gravel and similar aggregates; = 0.95 for crushed quartzitic and other crushed aggregates.
k_2 = 1.10 for addition of fly ash; = 0.95 for addition of silica fume, ground granulated blast-furnace slag and fly ash fume; = 1.00 for any other kind of addition

The correction factors in the expression are designed to take into account the type of coarse aggregate and the presence of mineral additives, such as silica fume and fly ash, in the concrete mix. Because of the mix designs at the two precasting plants, the values used for k_1 and k_2 were 1.0 and 1.0 for Plant A, and 1.2 and 1.1 for Plant B, respectively.

5.2.2.8 Radain et al. 1993

Radain et al. (1993) recommended using the following expression for concrete modulus of elasticity for concrete with strengths up to 13,000 psi.

$$E_c = 2{,}101{,}775 + 26{,}200\sqrt{f'_c} \quad \textbf{(5-8)}$$

where

E_c = concrete modulus of elasticity, in psi
f'_c = concrete compressive strength at time of test, in psi

5.2.2.9 NS 3473 1992

The Norwegian Concrete Code NS 3473 (1992) recommends using the following expression for concrete modulus of elasticity for high strength concrete.

$$E_c = 309{,}500(f'_c)^{0.30} \quad \textbf{(5-9)}$$

where

E_c = concrete modulus of elasticity, in psi
f'_c = concrete compressive strength at time of test, in psi

5.2.3 Modulus of Elasticity: Concrete Material Testing

5.2.3.1 Introduction

Numerous studies have been conducted to investigate the relationship between concrete compressive strength and modulus of elasticity and how those quantities change over time. The result of most of these studies is an equation for the modulus of elasticity that has some

dependence on the concrete strength, f'c, at any given time (usually a square root dependence), as has been shown in the previous section. Accurate knowledge of the relationship between concrete strength and modulus of elasticity and how it changes over time is vital to the prediction of camber. Given that there are many proposed equations for modulus of elasticity and that concrete mixes vary considerably from plant to plant and region to region, it is important to examine the properties of the concrete being made at Plants A and B.

5.2.3.2 Methodology

A material testing study was conducted by Marsha Swatosh at the University of Minnesota through an Undergraduate Research Opportunity Program (UROP) project. The goal of the study was to investigate the relationship between the concrete modulus of elasticity and compressive strength, determine proper aging coefficients and determine the equation for elastic modulus that best represented the data for concrete samples obtained from both Plants A and B. To accomplish this goal, 4x8 in (101.6x203.2 mm) concrete cylinders were taken from the girder mix concrete at Plants A and B and were tested for compressive strength and elastic modulus at various ages. Tests were conducted often at early ages because of their importance to the investigation of the modulus of elasticity at release.

A concerted effort was made to mimic the curing conditions of the girders as closely as possible by placing the curing cylinders on the girder side-forms and under the tarps. Additionally, the equipment and apparatus used to test the cylinders for strength and to measure the elastic modulus were calibrated to reduce the possibility of any errors associated with the testing procedure. ASTM testing standards were followed for all facets of testing, including cylinder capping (ASTM C617), and compressive strength (ASTM C39/C39M) and elastic modulus (ASTM C469) testing.

All of the testing was done in the University of Minnesota Structures Laboratory (UMN Lab), except for the 1-day tests done at Plants A and B that provided the release strength and elastic modulus data. Both a Forney Compression Machine and a 200 kip MTS hydraulic testing system were used in the study. A compressometer fitted with an LVDT was used to determine the axial strain characteristics while the cylinders were subjected to compression. Information regarding the material testing equipment calibration and initial testing is given in APPENDIX C.

5.2.3.3 Concrete Cylinder Testing

The concrete cylinder samples obtained from Plants A and B were taken directly from a mix being used to make girders. The 4x8 in (101.6x203.2 mm) plastic cylinder molds were filled with concrete and prepared according to the ASTM C31/C31M standard. The cylinders were made adjacent to the girder bed line using concrete from the same batch, and were subsequently placed on the outside of the girder side-forms and under the tarps to subject the cylinders to similar curing conditions as the girders. In total, 42 cylinders were made at Plant A and 36 cylinders were made at Plant B.

The following day, the cylinders were removed from the outside of the side-forms just before the girders were stripped and the strands were cut. Because it was desired to obtain the concrete compressive strength and modulus of elasticity at the time of release, the cylinders were first tested at the plant at the same time the strands were being cut. Both Plants A and B use a Forney testing machine identical to the one used in the University of Minnesota laboratory. Neoprene caps were used in these tests. The first cylinder was tested to failure to determine the

initial concrete compressive strength (this was needed because the tests for modulus of elasticity are taken to ~0.40$f'_{c,}$ as specified by ASTM C469). Three more cylinders were then tested to determine the modulus of elasticity according to ASTM C469. After removing the compressometer, these cylinders were then tested to failure in compression to determine their strengths. The concrete compressive strength testing was done according to ASTM C39/C39M. In addition to obtaining this material data, information from the tensioning and pour records as well as curing and ambient temperature data were also collected for the girders from which the cylinders were taken. This data was required to post-calculate the release camber and compare it to the measured values, which is discussed further in Section 6.3.1.

The remaining cylinders were brought back to the UMN Lab for further testing. Because of the high strengths achieved by the concrete in later ages, the Neoprene pads could no longer be used as the cylinder caps. Instead, a sulfur mortar capping compound was used to ensure that the ends of the cylinders remained plane and that imperfections would not cause stress concentrations during testing. The capping was done according to the procedure in ASTM C617.

The concrete compressive strength and modulus of elasticity tests for the first set of concrete samples, taken from Plant A, were conducted at release, 2, 3, 4, 7, 14, 28 and 61 days. Cylinders from the second set of samples, taken from Plant B, were tested at release, 2, 3, 7, 14 and 28 days. To achieve better accuracy in the elastic modulus testing, the 200 kip automated MTS hydraulic testing system was used for both the Plant A and B cylinders. However, the concrete compressive strengths were still determined using the Forney testing machine. The procedure for testing the cylinders was as follows: one cylinder was tested to failure to obtain the concrete compressive strength and then three to five more cylinders were tested to determine the modulus of elasticity, the compressometer was then removed, and these cylinders were subsequently tested to failure to determine the concrete compressive strengths. Additionally, the cylinders were also weighed after being removed from the molds, before and after capping and before being tested to determine the water content lost over time. It was found that the concrete cylinders had an average density of approximately 155 pcf at the time of the 28-day tests, at which point most of the water loss had been completed. Because water is an incompressible fluid, it was believed that the amount of water in the cylinder may have an impact on both the compressive strength and modulus of elasticity, which would vary with time as the moisture was lost to the environment.

5.2.3.4 Test Results

The results for the concrete compressive strength and modulus of elasticity for the cylinder samples taken from Plants A and B are shown in Figure 5-1 and Figure 5-2.

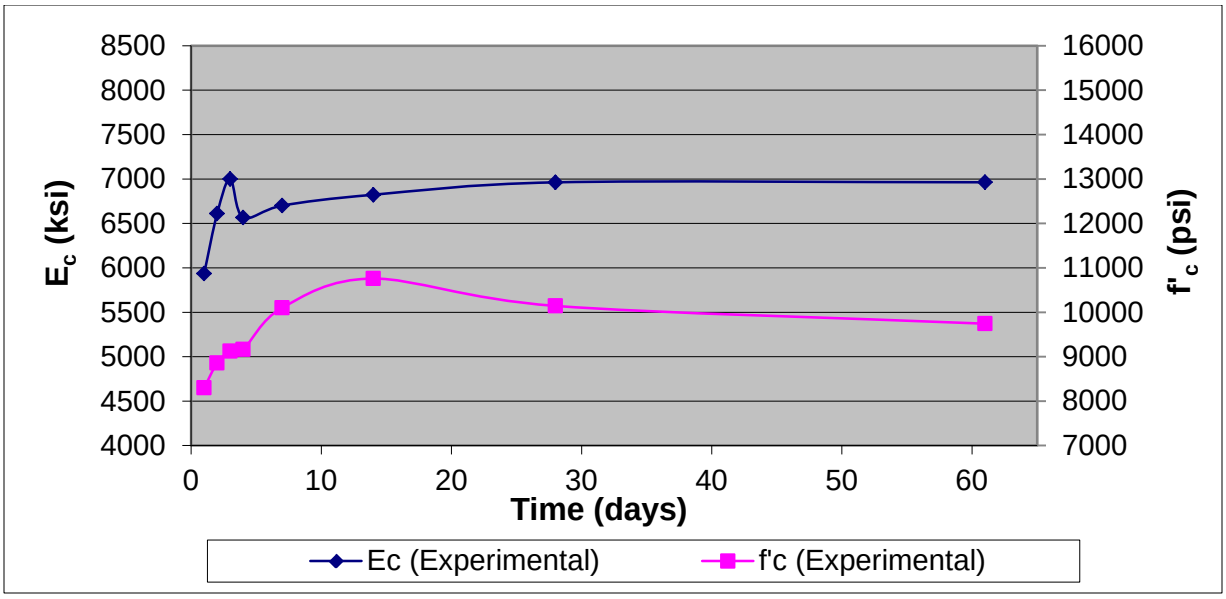

Figure 5-1. Plant A elastic modulus and concrete strength over time

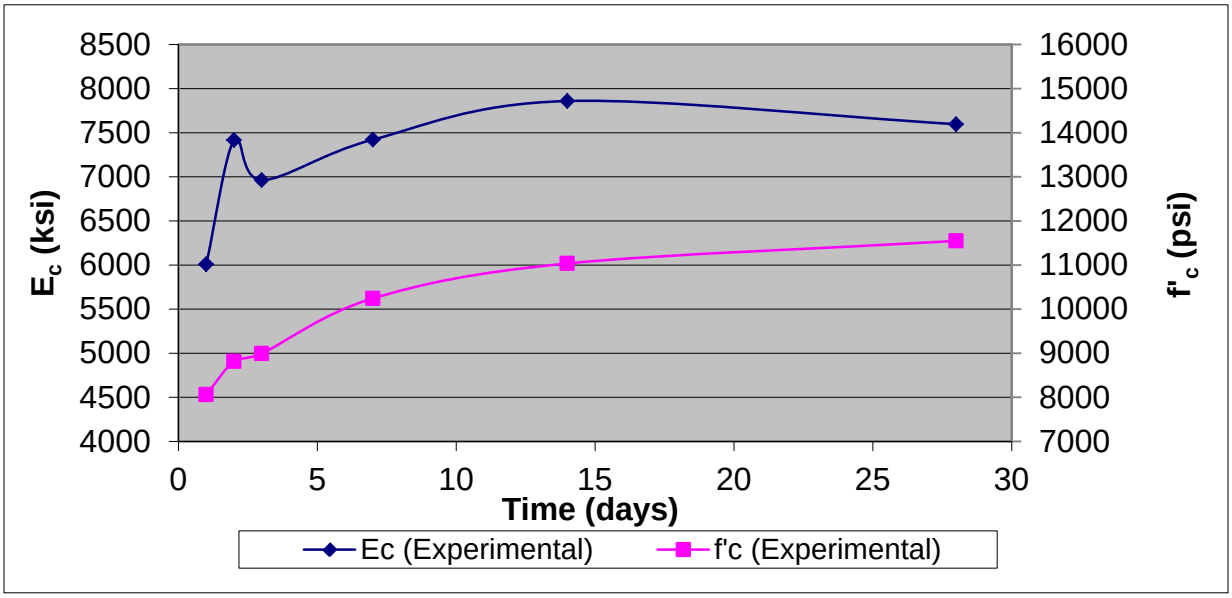

Figure 5-2. Plant B elastic modulus and concrete strength with time

A few comments should be made about the results. On Day 2 of the Plant B testing, it was noticed that there were some problems with the loading in the 200 kip MTS system. The bearing pad was not properly greased which led to some incomplete failures and inaccurate elastic modulus results. On Day 14 of the Plant B testing, it was noticed that the compressometer hinge was sticking. As a result, the data from these testing days were neglected when determining the aging coefficients for the concrete, as discussed in Section 5.2.5. Additionally, on Days 2 and 3 of the Plant A testing and Day 3 of the Plant B testing, it was found that there was minimal drying of the concrete; it is plausible that the water within the cylinders led to higher elastic moduli results (i.e., the "jumps" at early ages visible in the

figures). The data from these testing days was not neglected when determining the aging coefficients.

Another important observation is that the relationship between the concrete strength and elastic modulus does not stay consistent over time. So, it is difficult to predict the elastic modulus of concrete at any given time with just one expression based on f'_c. Given that MnDOT and other designers use the ACI 363 equation for the elastic modulus, it is insightful to plot the experimental elastic modulus versus the elastic modulus calculated using the ACI 363 equation and the experimental concrete strengths, which is shown in Figure 5-3 and Figure 5-4. Note that in the figures, the line marked as "E_c (ACI 363)" represents the elastic modulus calculated from the experimental f'_c results and the ACI 363 equation used by MnDOT. Also note that the vertical axis starts at a value of 4000 psi. The scale was expanded to more clearly show the differences in the results.

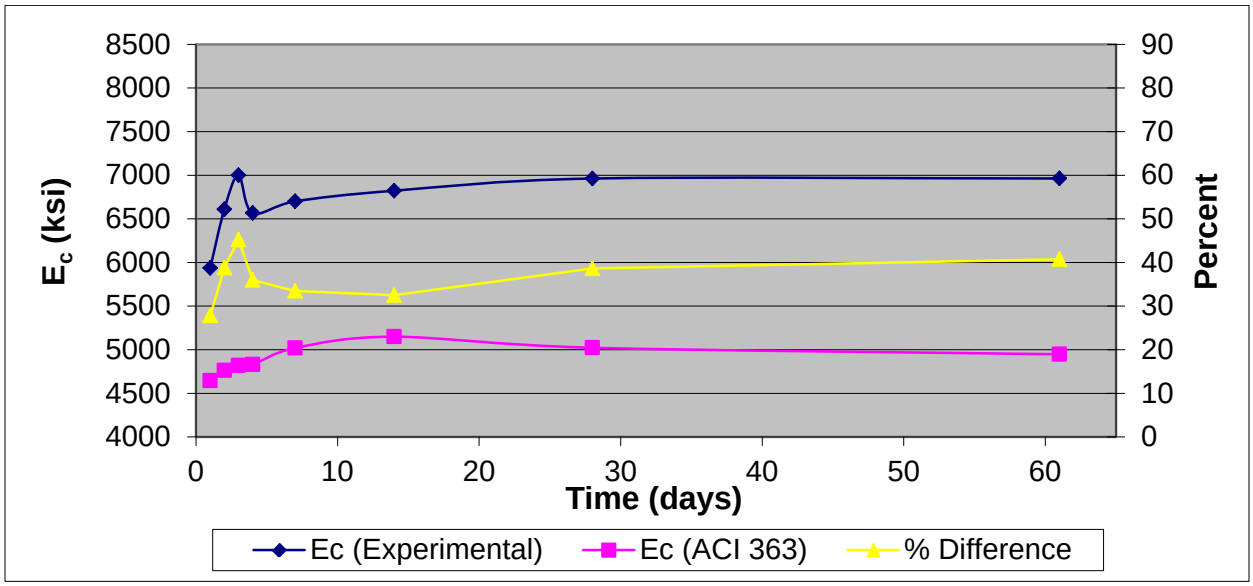

Figure 5-3. Concrete elastic modulus comparison for Plant A

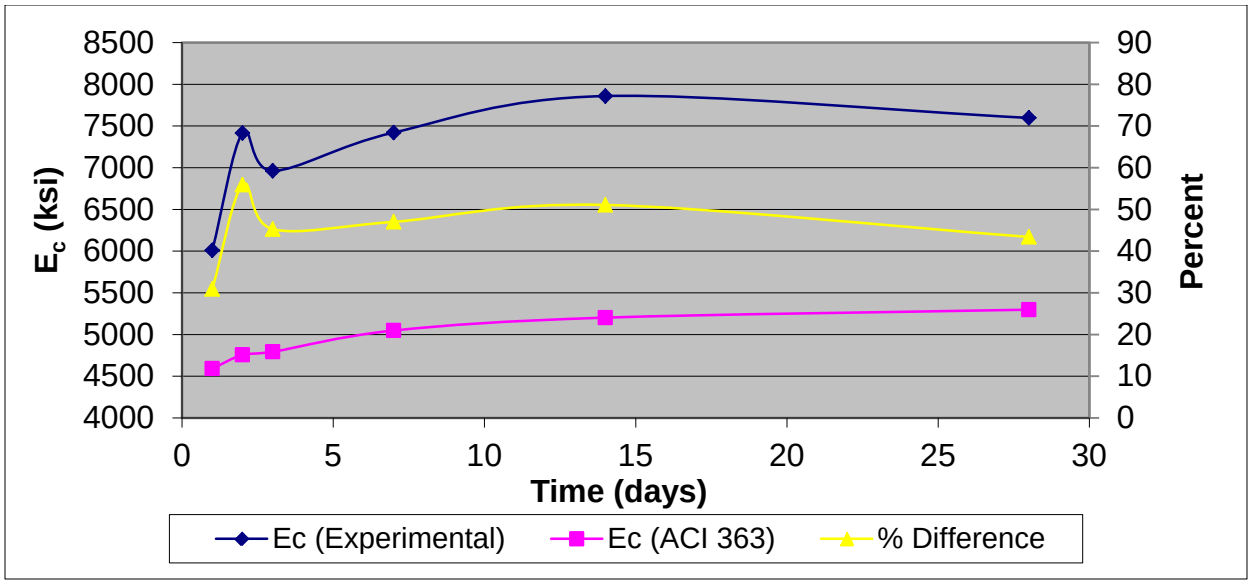

Figure 5-4. Concrete elastic modulus comparison for Plant B

These results show that the ACI 363 equation for modulus of elasticity under-predicted the measured elastic moduli achieved in the sampled concrete at both plants by approximately 35% and 45% for the samples from Plants A and B, respectively. This finding was believed to be a significant factor regarding why MnDOT release camber predictions typically overestimated the on-bed camber measurements. In Section 5.2.4, the other equations for modulus of elasticity reviewed in the literature (Section 5.2.2) were compared to the experimental results to determine if MnDOT should consider a different expression for E_c in their design calculations for camber.

5.2.4 Comparison of E_c Models to Material Testing Results

The measured concrete compressive strengths, f'_c, from the tests were used in the expressions for E_c obtained from the literature (see Section 5.2.2) to "predict" the modulus of elasticity of the specimens with time. It should be noted that for equations that include the unit weight of concrete, *w*, a value of 155 pcf was used. By comparing the predicted results to the measured modulus of elasticity at each time, it could be determined which model(s) best predicted the properties of the concrete from both plants. Figure 5-5 and Figure 5-6, show the results for Plants A and B, respectively.

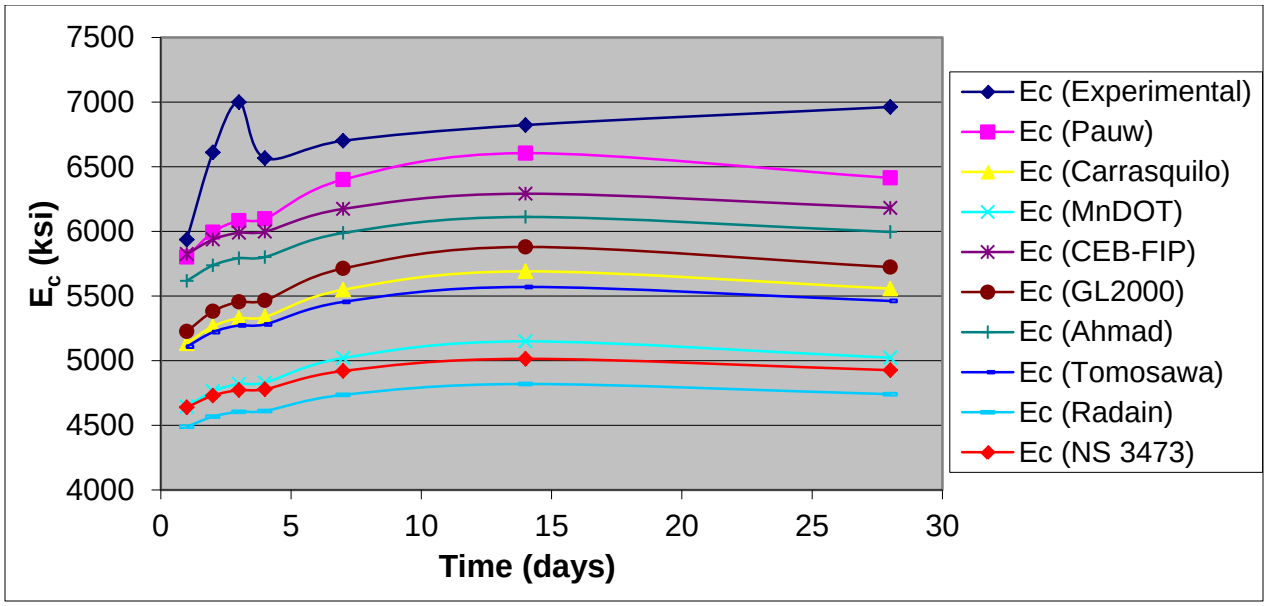

Figure 5-5. Comparison of elastic modulus models for Plant A

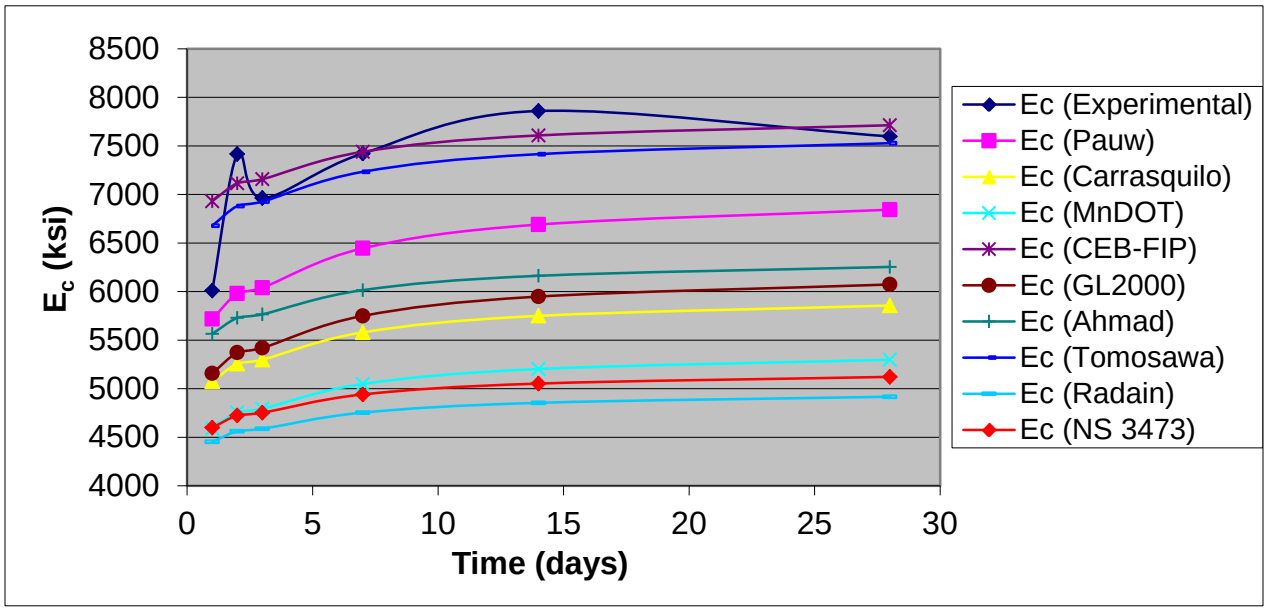

Figure 5-6. Comparison of elastic modulus models for Plant B

Figure 5-5 shows that all of the examined models underestimated the measured modulus of elasticity for concrete obtained from Plant A. Figure 5-6 shows that, for concrete obtained from Plant B, the CEB-FIP 1990 and Tomosawa et al. (1993) models for modulus of elasticity best predicted the measured results. However, these two models underestimated the measured results when the correction factor α_β for the CEB-FIP model and the factors k_1 and k_2 for the Tomosawa et al. (1993) model were assumed to be 1, instead of using those specified in Sections 5.2.2.4 and 5.2.2.7. A possible explanation for this result is that the concrete used at both Plants A and B was stiffer than the concrete from which these expressions were derived. After

speaking with fabricators at both plants, a possible cause of the high stiffness was the quality of the aggregates used in the concrete.

Because the MnDOT designers do not know the plant at which girders for a particular bridge will be fabricated, it was desired to select one model for modulus of elasticity that most closely predicted the measured E_c results. Based on the results of the material testing, it was determined that the Pauw (ACI 318-08, AASHTO LRFD 2010) equation most closely predicted the modulus of elasticity in comparison with the other models. Substituting the Pauw equation for E_c into the camber calculations (and using the design f'_{ci}) in place of the ACI 363 equation increased the ratio of observed camber at release to predicted camber from 74% on average, in Section 3.4.1, to approximately 88% for the 1067 girders included in the historical girder database. Thus, the conclusion can be made that the high stiffness of the concrete produced at these plants was a significant cause of the lower-than-predicted observed cambers.

It should be noted that based on the original study conducted by Mokhtarzadeh et al. (1998), the report recommended that the ACI 363 equation should be used in the design of high-strength prestressed bridge girders because it represented a better lower-bound estimate of the elastic modulus for high-strength concrete. The results were found to vary with cylinder size and the aggregate type, being higher for 4x8 in (101.6x203.2 mm) cylinders and glacial gravel concrete than for 6x12 in (152.4x304.8mm) cylinders and limestone aggregate concrete investigated in their study. Since that study was conducted, the mix designs at both Plants A and B have changed significantly, and for camber, it is more meaningful to use an expression that is the most accurate, rather than a lower bound estimate. The results shown in Figure 5-5 and Figure 5-6 indicate that the ACI 363 equation significantly underestimated the elastic modulus of the concrete sampled at the precasting plants during the course of this study. It should be noted that the findings shown in Figure 5-5 and Figure 5-6 are based on tests of 4x8 in (101.6x203.2 mm) cylinders only and also represent a limited body of data in comparison with the more extensive tests conducted by Mokhtarzadeh et al. (1998).

MnDOT also estimates an E_c (or 28-day elastic modulus) using the specified design f'_c (or shipping strength). Because the design shipping strength is based on the strength required to be within the stress limits at service, it can vary considerably and may not provide an adequate value for the estimation of E_c. By examination of the material testing results, it was found that the 28-day elastic moduli for the concrete from Plant A and B was approximately 1.17 and 1.26 times the elastic moduli at release, respectively. Thus, it was determined that a reasonable estimation of E_c would be 1.15 times the E_{ci} calculated using the Pauw (ACI318-08, AASHTO LRFD 2010) equation for elastic modulus. The implication of this recommendation is discussed further in Section 9.3.2.

5.2.5 Concrete Strengthening: Aging Coefficients

Concrete gains strength over time due to further hydration of the cement. This increase in strength is also known as aging. The ACI 209 Committee (2008) proposed the following strength-age relationship, which gives the concrete strength at any time given the 28-day strength.

$$f'_t = f_{28}(t/(a + bt)) \qquad \textbf{(5-10)}$$

The ACI 209 Committee proposed the following relationship to define the strains corresponding to the peak strengths at any age.

$$\varepsilon'_t = \varepsilon_{28}\sqrt{(t/(a+bt))} \quad \textbf{(5-11)}$$

where f'_t, f_{28}, ε'_t and ε_{28} are concrete strengths and corresponding strains at age t and 28 days, and a and b are the aging coefficients, in the preceding relationships.

Using Hooke's law, the aging curve that expresses the change in elastic modulus with time can be calculated.
The modulus-age curve is given as:

$$E'_t = E_{28}\sqrt{(t/(a+bt))} \quad \textbf{(5-12)}$$

where E'_t and E_{28} are concrete moduli at age t and 28 days.

The aging coefficients, a and b, are functions of cement type and method of curing but have recommended values (by ACI 209) in the absence of experimental data (ACI 209 (2008)). However, Mokhtarzadeh et al. (1998) recommended values for a and b, using a nonlinear least square fit analysis of data he obtained from extensive material tests that included both steam (heat) and moist curing conditions and samples with different cement admixtures. Using the elastic modulus data collected during the material testing in this study, a similar analysis was conducted to determine aging coefficients for both Plants A and B. It should be noted that both plants use steam and/or heat curing, but Plant A uses Type III cement and Plant B uses Type I cement with fly ash.

The results of the nonlinear least square fit analysis, along with the recommendations by ACI 209 and Mokhtarzadeh et al. (1998), are given in Table 5-2.

Table 5-2. Aging coefficients

Curing/Mix Conditions	Heat curing, Type III cement (Plant A)		Heat curing, Type I cement (Plant B)	
Aging Coefficients	a	b	a	b
ACI 209	0.70	0.98	1.00	0.95
Mokhtarzadeh	0.28	0.99	0.24	0.98
O'Neill	0.31	0.99	0.63	0.97

It is interesting to note that the aging coefficients determined by Mokhtarzadeh et al. (1998) were similar for both types of cement. This study found similar results to those obtained

by Mokhtarzadeh for Type III cement, but the results were very different and trended more with the ACI 209 recommendations for Type I cement (i.e., larger coefficient "a" for Type I cement compared to Type III cement). This could have been due to the fact that concrete from Plant A was used in the study by Mokhtarzadeh et al. (1998) and concrete from Plant B was not. Additionally, the girder mix design at Plant B had changed considerably since the study by Mokhtarzadeh et al. (1998) was completed.

Figure **5-7** and Figure 5-8 show how closely these aging coefficients relate to the experimental results for modulus of elasticity.

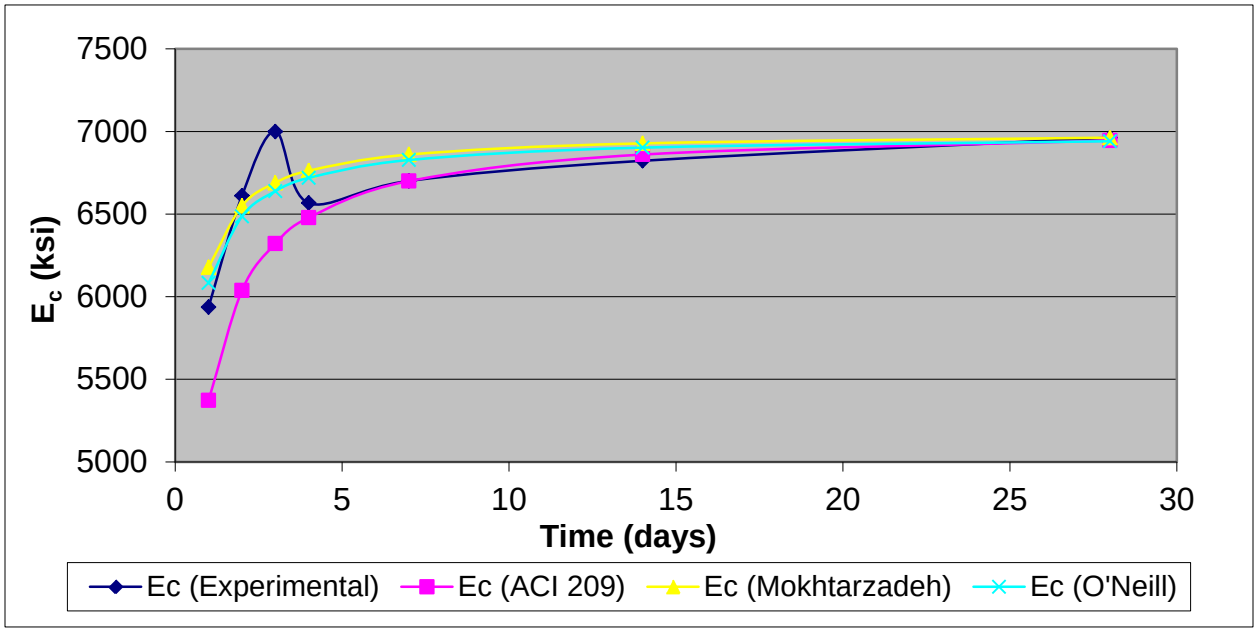

Figure 5-7. Aging coefficients for Plant A

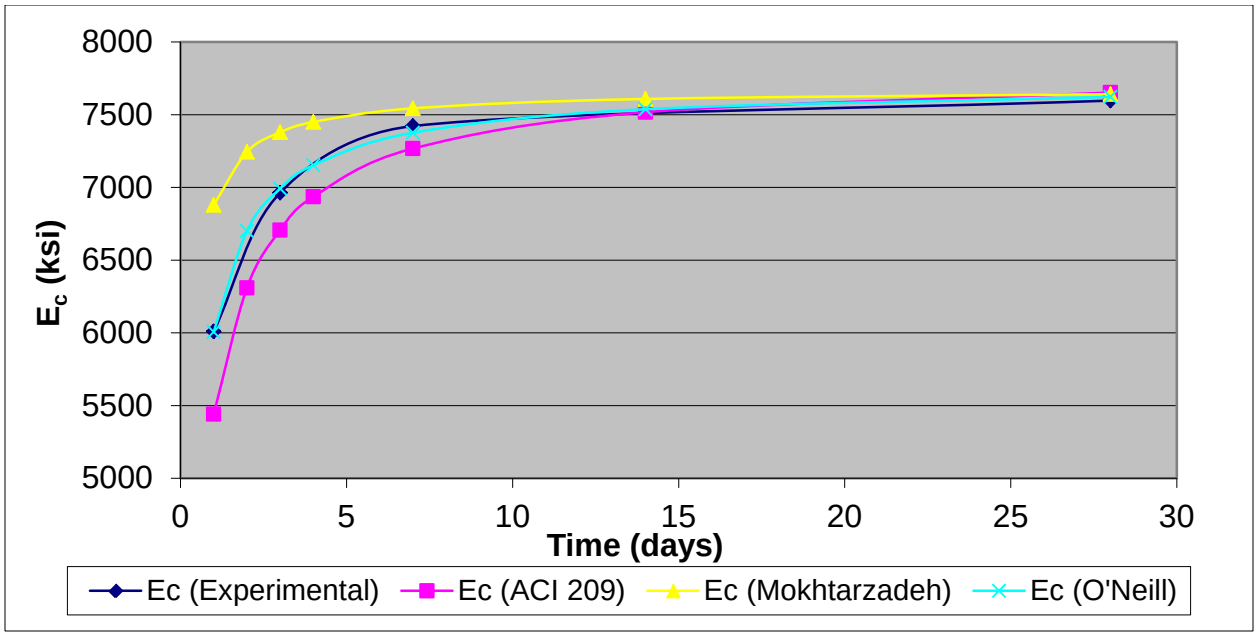

Figure 5-8. Aging coefficients for Plant B

From these figures, the aging coefficients were selected for the PBEAM modeling. For the modeling of girders fabricated at Plant A, the Mokhtarzadeh aging coefficients matched very closely to those determined in this study. Given the fact that the sample size in the Mokhtarzadeh study was much larger (Mokhtarzadeh et al. 1998), the Mokhtarzadeh aging coefficients were used in the PBEAM modeling. For the modeling of girders fabricated at Plant B, the best option was determined to be the aging coefficients determined in this study.

Thus, for Plants A and B, the modulus-age expressions were taken as:

$$E'_t = E_{28}\sqrt{(t/(0.28+0.99t))} \qquad \text{(Plant A)} \qquad \textbf{(5-13)}$$

$$E'_t = E_{28}\sqrt{(t/(0.63+0.97t))} \qquad \text{(Plant B)} \qquad \textbf{(5-14)}$$

5.3 Variation in Prestress Force

By far the most commonly used strand in MnDOT prestressed girders is 0.6 in (15.2 mm) dia. 270-ksi low-relaxation seven-wire strand. The design pull force specified by MnDOT (and specified by AASHTO LRFD 2010 and ACI 318-08) is 0.75*f_{pu}=202.5 ksi for each strand. Fabricators pull each strand to this specified force using hydraulic jacks and a pressure gauge reading. The designers account for elastic shortening losses to determine the strand stress just after release, and use this stress to calculate the expected release camber. However, due to thermal effects, strand relaxation, redistribution of strand stress through harping or friction losses, and varying curing conditions, it is likely that the stress in each strand does not match the expected strand stress just after release.

5.3.1 Thermal Effects

Even though steps are taken by the precasters to account for strand temperature changes, as described in Section 3.2, the current temperature correction procedures only account for the differences in strand temperature at tensioning relative to the temperature assumed at concrete placement (i.e., the concrete mix temperature). These corrections do not take into account the effect of ambient temperature changes on the uncovered free length of strand in the bed or the effect of temperature on the strand within the freshly cast concrete, which experience elevated temperatures prior to bonding due to the concrete heat of hydration.

Because the strands are anchored to the precasting bed, which has a fixed length, the changes in the mechanical and thermal strains must sum to zero. As a consequence, the temperature changes along the length of strand in the bed will impact the amount of mechanical stress at the time of concrete-steel bond and strand release. Between strand pull and concrete-steel bond, strands within the freshly cast concrete heat up as a result of the concrete heat of hydration while curing, and undergo a loss in mechanical strain to balance the increase in thermal strain. Additionally, any uncovered free length of strand on the bed must be taken into consideration when determining the effect of temperature on the strand stress, because the ambient air temperature at the time of concrete-steel bond is likely to have changed since the strands were initially stressed. However, these changes in strand stress due to thermal effects prior to concrete-steel bond are partially recoverable, as long as the concrete temperature decreases between bond and strand release.

Because the coefficients of thermal expansion of the steel and concrete differ, additional prestress changes occur as the system changes temperature between concrete-steel bond and strand release. Because the concrete temperature at strand release is typically lower than it is at the time of concrete-steel bond, this effect usually results in the recovery of some prior prestress losses that occur between strand pull and concrete-steel bond. In other words, some of the stress loss that occurs prior to concrete-steel bond will be recovered due to the cooling of the concrete and strand during the curing process. Finally, after strand release, additional prestress changes occur as the system undergoes further thermal changes to match the ambient temperature. As such, a thermal datum point should be selected such that the desired level of prestress in the section can be referenced relative to that temperature (e.g., 70 ^{o}F).

Barr et al. (2005) examined thermal effects in their study and developed a simple expression to calculate the stress loss in the strand between strand pull and concrete-steel bond, due to high fabrication temperatures. Erkmen et al. (2008) also examined the effect of high fabrication temperatures, but included an extensive analysis of the effect due to the cooling of the concrete and strand prior to strand release. Erkmen et al. (2008) did not, however, investigate the effect of varying ambient temperatures on the stress in the free length of strand. Using expressions from both research groups, and accounting for the effect of varying ambient temperatures on the free length of strand, a parametric study was conducted to determine the possible range of strand stress losses that might be expected to occur due to thermal effects.

The following conceptual assumptions were made for the thermal effects analysis conducted in the parametric study.

1. Bending stresses/strains due to thermal effects can be neglected.
2. Concrete coefficient of thermal expansion remains constant.
3. Concrete modulus of elasticity remains constant from time of bond to strand release.
4. No thermal gradient along the girders or through the girder depth.
5. No thermal gradient along the free length of strand.
6. The ambient temperature between concrete-steel bond and strand release remains constant. In other words, once bond is achieved, any stress changes in the free length of strand due to thermal effects are assumed to have a negligible effect on the prestress in the girder(s).

The parametric study was conducted on a 129 ft-9 in (39.55 m) MN54 girder with 50 0.6 in (15.2 mm) diameter 270 ksi low relaxation prestressing strands, pulled to an initial stress of 202.5 ksi. To take into account the temperature corrections used at the precasting plants, the initial strand stress was raised or lowered by 1% for each 10 °F difference in temperature between the ambient conditions at strand pull and the assumed concrete mix temperature, which was the typical procedure used. For the parametric study, the concrete mix temperature was assumed to be 70 °F (21 °C). The length of the bed was taken to be 365 ft (111.3 m). The coefficient of thermal expansion and the elastic modulus of the prestressing strand were assumed to be 6.8 με/°F (12 με/°C) and 28,500 ksi, respectively. The coefficient of thermal expansion and the elastic modulus of the concrete were assumed to be 5.8 με/°F (10.4 με/°C) and 4464 ksi, respectively. The temperature in the concrete at the time of concrete-steel bond and strand release were assumed to be 140 °F (60 °C) and 97 °F (36 °C), respectively. These concrete temperature values were consistent with those used by Barr et al. (2005) and Erkmen et al. (2008), respectively, and with observations from thermal curing data obtained from the precasting plants. It should be noted that the time at which concrete-steel bond occurs was assumed to be 6-10 hours after concrete pouring, which was consistent with the assumption made by Barr et al. (2005).

The parameters varied in the study were the amount of free length of strand in the bed, L_{free}, the ambient air temperature at the time of strand pull, $T_{air,pull}$, and the ambient air temperature at the time of concrete-steel bond, $T_{air,bond}$. A minimum, average and maximum free (uncovered) length of strand was found by examining the historical girder data. These values were taken as 6 ft (1.83 m), 62 ft (18.9 m) and 260 ft (79.2 m), respectively, for the parametric study. The ambient air temperatures used at both the time of strand pull and concrete-steel bond were 70 °F (21 °C), 36 °F (2.2 °C) and 104 °F (40 °C). These temperatures represented a realistic average value and lower and upper bounds for possible ambient temperatures experienced in a pouring season. There were 27 separate cases in the parametric study, resulting from three possible values for the three varied parameters. Finally, it should be noted that because the fabricators measure the camber immediately (or soon after) strand release, the parametric study only examined changes in prestress due to thermal effects that occur between strand pull and strand release. Table 5-3 shows the results of the parametric study that represent the most realistic cases (of the total 27) likely observed in the field. Further explanation of the assumptions and the expressions used in the parametric study are given in APPENDIX B, along with an example problem and a more extensive parametric study investigating the effect of variations in other parameters (i.e., girder size, total strand area and temperatures at the time of concrete-steel bond and strand release).

Table 5-3. Thermal effects analysis and parametric study results

Case	L_{free} (ft)	$T_{air,pull}$ (°F)	$T_{air,bond}$ (°F)	Initial Strand Stress (ksi)	Final Strand Stress (ksi)	Prestress change (ksi)	Prestress change (%)	Camber change (%)
1	62	70	36	202.5	195.63	-6.87	-3.39[1]	-6.20[2]
2	62	70	70	202.5	194.54	-7.96	-3.93	-7.19
3	62	70	104	202.5	193.43	-9.07	-4.48	-8.18
4	6	70	36	202.5	196.51	-6.00	-2.96	-5.41
5	6	70	70	202.5	196.40	-6.10	-3.01	-5.51
6	6	70	104	202.5	196.29	-6.21	-3.07	-5.60
7	260	70	36	202.5	204.48	+1.98	+0.98	+1.78
8	260	70	70	202.5	199.90	-2.60	-1.28	-2.35
9	260	70	104	202.5	195.27	-7.23	-3.57	-6.52
10	62	36	36	210.6	197.30	-13.30	-6.32	-4.70
11	62	36	70	210.6	196.21	-14.39	-6.83	-5.68
12	6	36	36	210.6	198.18	-12.42	-5.90	-3.91
13	6	36	70	210.6	198.07	-12.53	-5.95	-4.00
14	260	36	36	210.6	206.15	-4.45	-2.11	+3.28
15	260	36	70	210.6	201.57	-9.03	-4.29	-0.84
16	62	104	70	194.4	192.94	-1.46	-0.75	-8.63
17	62	104	104	194.4	191.84	-2.56	-1.32	-9.62
18	6	104	70	194.4	194.80	+0.40	+0.21	-6.95
19	6	104	104	194.4	194.69	+0.29	+0.15	-7.05
20	260	104	70	194.4	198.30	+3.90	+2.01	-3.79
21	260	104	104	194.4	193.67	-0.73	-0.38	-7.96

[1]Percent change determined as (prestress change/initial strand stress)*100
[2]Percent change determined as the change in release camber associated with the use of the final strand stress in place of 202.5 ksi, in the camber calculations described in Section 1.2

The results of the parametric study show that, in most cases, there could be considerable camber loss due to thermal effects. Comparing Cases 1, 2 and 3 to Cases 4 through 9, the results indicate that the prestress and camber loss is more significant for the case(s) where the *average* amount of free length of strand is uncovered, which is clearly the most common situation. This is due to the fact that the net stress loss is a two-step process. The amount of stress loss between strand pull and concrete-steel bond is maximized when the free length of strand goes to zero. However, the stress recovery that occurs between bond and strand release is also maximized when the free length of strand goes to zero. Thus, there is an amount of free length of strand that maximizes the total *net* stress loss. The amount of prestress and camber loss also increases with increased ambient air temperature at the time of bond, as can be seen by comparing Case 3 to Cases 1 and 2. This is because the warmer ambient temperatures cause the strand to experience a reduction in mechanical strain. Therefore, the "worst-case" scenario is when the average amount of free length of strand (approximately) is on the bed and the ambient air temperature when the bond is formed is very high, relative to the temperature when the strands were pulled. In the parametric study, this case leads to decreases in release cambers of 6-10%. Finally, the average

reduction in strand prestress is approximately 5.5 ksi, (approximately 2.7% of the initial pull stress and 2.0% of f_{pu}), and the average reduction in release camber is approximately 5.0% considering the 21 cases shown.

5.3.2 Strand Relaxation

Strand relaxation begins as soon as the strands are tensioned and anchored in place and continues throughout the entire life of the girder. As such, there will be a reduction in prestress that occurs between strand pull and strand release, which MnDOT does not take into account in the release camber calculations. The expression for calculating the magnitude of relaxation over time was recommended by the PCI Committee on Prestress Losses (1975) and is given as:

$$(f_{st})_{i+1} = (f_{st})_i + (f_{st})_i \frac{\log(24t_{i+1}) - \log(24t_i)}{C_2}\left(\frac{(f_{st})_i}{C_1} - C_3\right) \quad if \quad \frac{(f_{st})_i}{f_{sy}} \geq C_4 \qquad \textbf{(5-15)}$$

where

f_{st} = steel stress at any time t (days) after strand pull
f_{sy} = specified yield strength of steel strand
f_{pu} = specified ultimate strength of steel strand
$C_1 = f_{sy} = 0.90 f_{pu}$
$C_2 = 45$
$C_3 = 0.55$
$C_4 = 0.6$

for low-relaxation strands (PCI 1975)

From this expression, the amount of relaxation that occurs between strand pull and strand release was calculated to determine the effect of strand relaxation on the expected strand stress at release. By examining the collected data from the precasting plants, it was found that the amount of time between strand pull and strand release varied from ~1 to 6 days. Thus, different relaxation stress losses were determined for times between pull and release of 1, 2, 3, 4, 5 and 6 days. Table 5-4 gives the results of this analysis, assuming an initial pull force of $0.75 f_{pu}$.

Table 5-4. Strand stress losses due to relaxation

Time between pull and release	1 Day	2 Days	3 Days	4 Days	5 Days	6 Days
Stress loss (ksi)	1.76	2.13	2.35	2.50	2.62	2.71

Because it was most common for the fabricators to tension the strands two to three days prior to strand release, it was assumed that the typical strand stress loss due to relaxation was approximately 2.2 ksi, or approximately 1.1% of the initial pull stress and 0.8% of fpu.

5.3.3 Bed Position

The bed position of a particular girder refers to its location along the precasting bed. Fabricators generally begin by placing the first girder next to the "dead end" abutment. Then, subsequent girders are poured down the length of the bed. Depending on the length of the bed and the lengths of the girders, one to six girders can typically be fabricated on a bed at one time.

The procedure used to tension the draped strands can affect the amount of prestress in each girder. At Plant A, where the draped strands are harped after tensioning all of the strands, the "harping sequence" can affect the distribution of the draped strand stress along the bed. It should be noted that at Plant A, the draped strand are harped at each end of the girder line *prior* to tensioning, which would result in some friction losses as well. At Plant B, where the draped strands are pulled through the drape and hold-down rollers during the tensioning process, the friction losses that occur affect the distribution of draped strand stress. The draped strands at Plant B are also harped at each end. In some cases, fabricators at Plant B pull the strands from both ends of the bed because of this effect. As a consequence, it is possible that "identical" girders poured on the same bed (at both plants) will have different release cambers due to the variation in the draped strand prestress.

This effect was examined by carefully selecting girders that were identical in shape, length, strand pattern and design cambers. Additionally, only pours that had the exact same number of girders on the bed were compared. In other words, the only differences between them were their curing conditions and their position on the bed. It should be noted, however, that there are other possible factors that could lead to variable release cambers on the same bed, such as differences in concrete elastic modulus. In order to minimize the potential effect of varying strength and associated elastic modulus, the cambers were normalized relative to their measured release concrete strengths. This was implemented by altering the predicted release cambers by using the measured release compressive strengths in the ACI 363 equation for elastic modulus.

For this study, the release and erection cambers of approximately 300 girders from eight different bridges were examined, which included girders of every MnDOT shape included in the historical database. The results for three of the eight bridges are shown in Figure 5-9 through Figure 5-11, which compare the "normalized cambers" (i.e., the ratio of the measured initial on-bed release camber to the adjusted predicted release camber, which is based on an improved estimation of E_{ci}). Figures for the remaining sets of girders are shown in APPENDIX A.

Figure 5-9 is an example of a girder set (fabricated at Plant A) with pours containing only two girders on the bed. In the case shown below, there is very little difference between the cambers of the dead end and live end girders at both release and erection. Of the four sets of girders in the study that have just two girders on the bed, the cambers at release differed by less than 1%. This is likely due to the fact that there was only one harp point on the bed with the two girders. Therefore, the stress in the strand should distribute rather evenly across the bed (for Plant A) and the friction losses should be minimal (for Plant B).

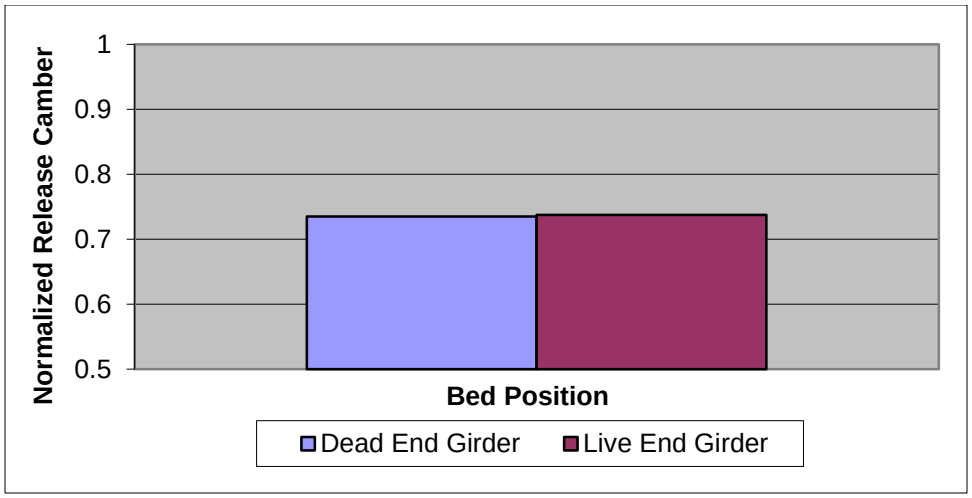

Figure 5-9. Camber of girders in different bed positions for Br. 14549 (Plant A)

Figure 5-10 and Figure 5-11 are examples of girder sets containing pours with four girders on the bed. It should be noted that both of the bridges represented in these figures were fabricated at Plant A. Unlike the case with just two girders on the bed, these results have more variation in the release cambers and are not as consistent with one another. As can be seen in the two figures, almost opposite trends are shown. In Figure 5-10, the middle two girders had higher release cambers, whereas in Figure 5-11, the dead and live end girders had higher cambers. Because there are more harp points (three) for these cases, the harping sequence may not be the same for each pour and, thus, the stress redistribution may differ. Because the harping sequence is not recorded, it is recommended that this procedure be documented and kept consistent from pour to pour and bridge to bridge. Additionally, it is recommended that in situations where there are three or more harp points (four or more girders), the strands located at harp points nearer the center of the girder line should be harped first, in order to re-distribute the strand stress as evenly as possible through the girders.

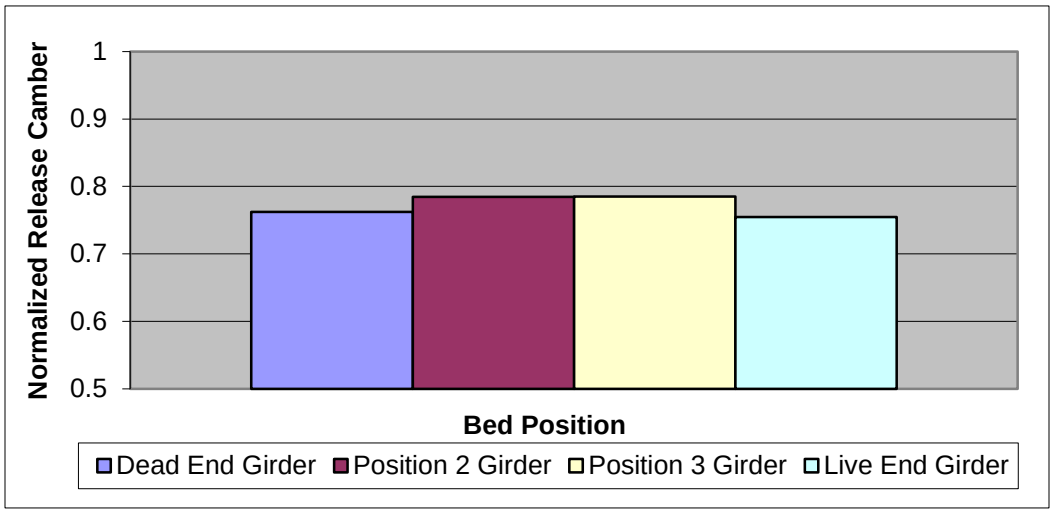

Figure 5-10. Camber of girders in different bed positions for Br. 03009 (Plant A)

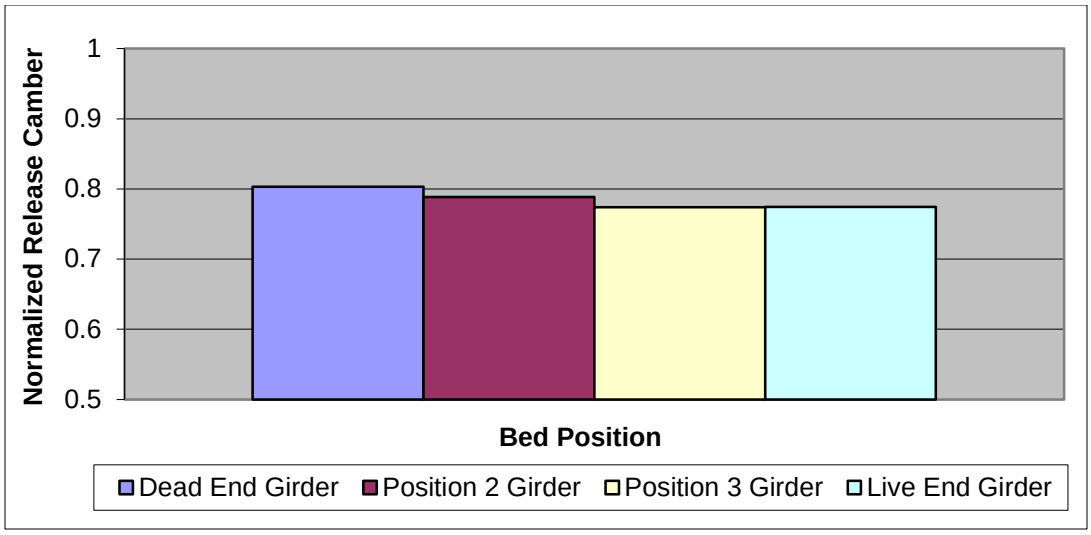

Figure 5-11. Camber of girders in different bed positions for Br. 19561 (Plant A)

5.4 Moment of Inertia: Strand Density

In 2006, MnDOT introduced three new I-girder shapes: MN45, MN54 and MN63, which made up approximately 56% of the girders in the historical database. The MN-shapes feature top and bottom flanges that are 4 in (101.6 mm) wider than the M-shapes. The MN-shapes also feature curved transition regions between the flanges and web. These shapes are able to span greater lengths and can hold more prestressing strands. Figure 5-12 shows a comparison of the M-shape and MN-shape girder cross sections.

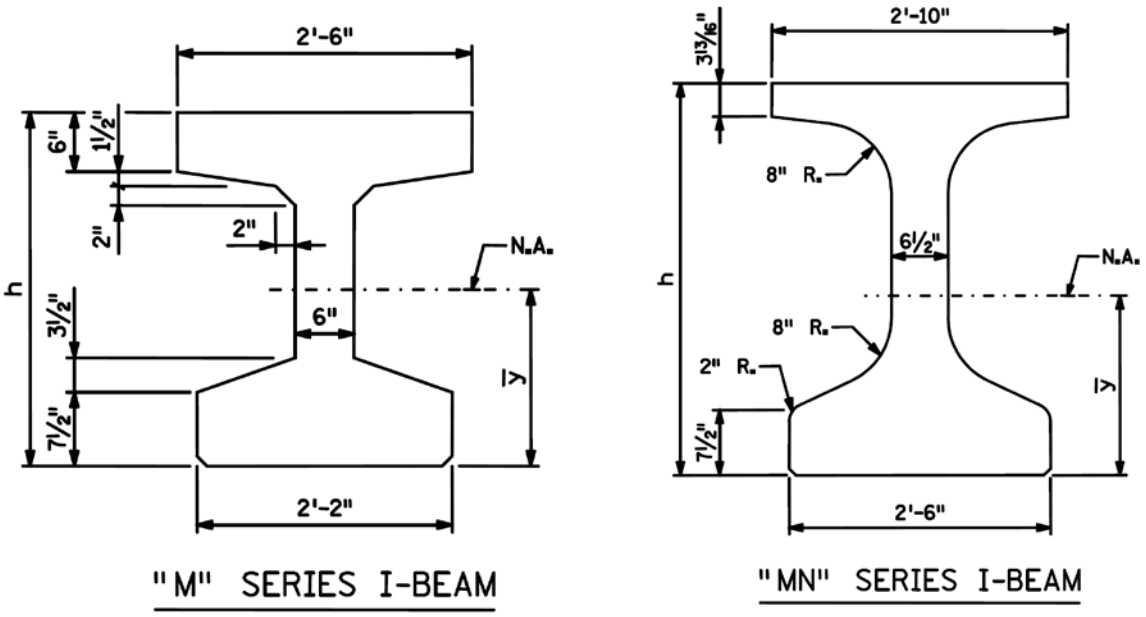

Figure 5-12. M-shape and MN-shape girder cross sections

Because the MN-shapes are able to hold more prestressing strands, it was possible that this increase in strand density (A_{ps}/A_g) could have had an effect on camber not accounted for in design. Increasing the number of strands in a girder cross section increases both its transformed moment of inertia and its prestress. The increase in prestress increases the camber, whereas the increased transformed moment of inertia decreases the camber. Even though transformed properties are not used in the camber calculations described in Section 1.2, calculating camber using gross properties and elastic shortening prestress losses is equivalent to using transformed properties, for which losses due to elastic shortening are directly considered (as discussed in Section 2.4). Thus, the effect on camber of changing the number of strands in a girder cross section is accounted for in design, regardless of the camber calculation method used.

Even though changing the number of strands in a girder cross section is accounted for in the camber calculations, it was possible that a particular cross section may be more *sensitive* to changes in strand density than another. To investigate this possibility, the old-shape 45M, 54M and 63M girders were compared to the new-shape MN45, MN54 and MN63 girders, using the method of calculating camber described in Section 1.2. The old and new girder shapes were paired up by cross section depth (i.e., 45M's and MN45's) and identical "short" and "long" girder lengths were used for each pair. It was found that the MN-shape girders were more sensitive to changes in strand density than the M-shapes. In other words, the exact same percent change in strand density caused a larger change in camber for the MN-shape girders. This discrepancy was more substantial for the longer MN-shape girders. It was also found that it takes a higher strand density to achieve the same nominal camber for the MN-shapes.

However, because camber was accurately calculated (elastically) at release by the method described in Section 1.2 regardless of the number of strands in a girder cross section or the dimensions of the cross section, any increase in strand density was not considered to be a cause of the observed discrepancy between measured and predicted release cambers.

5.5 Conclusion

Various factors that affect the release camber were investigated, including concrete compressive strength and associated concrete modulus of elasticity, variation in the strand prestress force, and the cross section moment of inertia. It was found that the increased concrete strengths achieved at the precasting plants decrease camber via increasing the elastic modulus. The concrete modulus of elasticity was examined through material tests and through review of the literature. Multiple concrete cylinder samples from both precasting plants were tested for concrete strength and elastic modulus over time, in order to determine the relationship between these two quantities. It was found that the ACI 363 equation for the concrete modulus of elasticity used by MnDOT and other Minnesota bridge designers under-predicts the elastic modulus of concrete produced at both precasting plants by approximately 35%-45%. The Pauw (ACI 318-08, AASHTO LRFD 2010) equation was determined to be the best predictor of the concrete elastic modulus, and when plugged back into the release camber predictions for the historical girders, improved the discrepancy between measured and design release cambers from approximately 74% to 88%. A thermal effects analysis was conducted to determine the effect of concrete and ambient temperatures at the time of concrete-steel bond and concrete temperatures at strand release relative to ambient temperatures at strand pull. It was found that thermal effects and strand relaxation cause an average reduction in strand stress at release of approximately 2.7% and 1.1%, respectively. The position of each girder in the bed was also found to cause variations in prestress force through the redistribution of draped strand stress due to the harping

sequence (at Plant A) and friction losses (at Plant B). Finally, it was found that high strand density, though often found in long MN-shape girders, was not a major cause of reduced release camber. Thus, it was determined that the major causes for the discrepancy in release camber predictions and observed cambers were the increased concrete release strengths associated with higher elastic moduli, the underestimation in elastic moduli predicted by the ACI 363 equation used by MnDOT, and the strand prestress losses due to thermal effects. These conclusions will be further examined in the following chapter, by using these results to re-predict the release camber of the material test girders, the instrumented girders and selected historical girders.

CHAPTER 6. RELEASE CAMBER PREDICTION

6.1 Introduction

In order to better predict long-term girder camber, it is important to be able to better predict the camber at release. Because the girder is assumed to be elastic and uncracked at release, and because time-dependent factors such as creep and shrinkage are not issues at release (the only time-dependent issue is the relaxation of the steel strand that occurs between strand tensioning and release), the prediction of release camber seems to be a relatively straightforward task. MnDOT uses basic deflection equations to predict the release camber, as discussed in Section 1.2. However, as previously mentioned in Section 3.4.1, the measured release cambers of the 1067 historical girders were, on average, 74% of the design release cambers.

The potential causes for this discrepancy have been discussed previously in this report. Girder precasters achieve higher release strengths than those specified in design to ensure they can efficiently "turn-over" their precasting beds, as discussed in Section 3.4.3. This causes an increase in girder stiffness and a reduction in release camber due to the dependence of concrete modulus of elasticity on concrete strength, as detailed in Section 5.2.1. Additionally, the material testing conducted on concrete cylinder samples taken at Plants A and B, and discussed in Section 5.2.3, revealed that the equation for concrete elastic modulus (ACI 363) used by MnDOT underestimated the measured concrete elastic modulus produced at the two plants by approximately 35%-45%. The results of the testing indicated that the Pauw (ACI 318-08, AASHTO LRFD 2010) equation was the best predictor of the concrete elastic modulus at release.

The potential reduction in strand prestress due to the effect of concrete and ambient temperatures at the time of concrete-steel bond and concrete temperatures at strand release relative to ambient temperatures at strand pull was found to be another significant factor that can lead to a reduction in camber, as described in Section 5.3.1 and APPENDIX B. The variation in strand prestress caused by harping or friction losses (for Plant A and B, respectively), discussed in Section 5.3.3, can lead to a variation in camber dependent upon bed position. Strand relaxation that occurs between the time of strand pull and release is another effect that leads to lower cambers. However, this effect is rather small (i.e., prestress losses on the order of approximately 1%) and is neglected by MnDOT and by the precasters. Finally, the effect of friction of the girders on the bed, discussed in Section 3.4.2, can lead to reported release cambers that are less than the "true" camber values, which can only be found after relieving the built-up friction in the bed through girder lifting and setting.

6.2 Methodology

In order to determine whether the potential sources of error in release camber predictions had been correctly identified, revised release camber predictions were developed that considered each of these effects and the results were compared with the cambers measured at release. The group of girders that was used in this study included the girders from which the material samples were taken (Section 5.2.3), the instrumented girders (Chapter 4), and selected historical girders. A group of these selected girders were also chosen for validation of the PBEAM program used to investigate time-dependent effects, which is described in Section 7.4.

In order to develop the revised release camber predictions for these girders, the girder cross section, concrete and steel material properties, precasting bed dimensions, amount of free length of strand in the bed, strand pull forces, assumed concrete temperature at concrete-steel bond, and ambient temperatures all had to be known or approximated. Much of this data was collected for each girder from the tensioning sheets and pour records available at the precasting plants. This data consisted of the bed and girder lengths, cross section dimensions, strand material properties and initial pull force, curing temperatures, ambient temperature at the time of strand pull, time between strand pull and concrete pour, length of cure, and concrete strengths at release. The ambient temperature at the time of concrete-steel bond was approximated based on recorded weather histories. The concrete temperature at the time of strand release was approximated by examining the thermal curing data obtained from the fabricators. For the girders from which cylinder samples were taken, the measured concrete modulus of elasticity at the time of release, recorded during material testing, was used in the camber predictions. However, for the instrumented and historical girders, the Pauw (ACI 318-08, AASHTO LRFD 2010) equation was used to determine the concrete modulus of elasticity at release, based on the recorded concrete release strengths.

It should be noted that there was some uncertainty in some of the data, specifically the curing temperature at the time of concrete-steel bond and ambient temperatures at the plant. However, given that there were already some assumptions made in the thermal effects analysis (as discussed in Section 5.3.1 and APPENDIX B), it was appropriate to make some reasonable approximations in the case of imprecise or non-existent data. The most significant source of error in this analysis was the concrete temperature at the time of strand release. Thermal curing data was kept for the cylinders being cured for testing, which were programmed to match the curing temperatures experienced by the girders. However, because the girders continued to cool as the tarps and side-forms were removed and after the thermal data was no longer being recorded, the concrete temperature at the time of strand release was approximated. As such, an approximate release concrete temperature of 97 °F was used for girders cured over a weekday, and a temperature of 70 °F was used for girders cured over a weekend due to the additional time for cooling, as is discussed in Section 7.5.1 and APPENDIX B.

To produce the revised release camber predictions, the following procedure was used for each girder. The stress in the strands at the time of concrete pouring was determined by reducing the recorded pull stress due to strand relaxation. Then, the thermal effects analysis was conducted using the recorded or approximated data to calculate the change in strand stress between strand pull and strand release due to temperature effects. The concrete modulus of elasticity at release was measured for the girders from which material samples were taken and was calculated from the recorded release concrete strengths and the Pauw (ACI 318-08, AASHTO LRFD 2010) E_c equation for the instrumented and selected historical girders. Finally, the calculated prestress force just after release and the measured/calculated concrete modulus of elasticity were inserted into the camber calculations described in Section 1.2 (including elastic shortening losses) to determine a new prediction for the release camber that could be compared to the measured values.

6.3 Release Camber Predictions

6.3.1 Material Test Girders

All of the data needed to perform the thermal effects analysis for the girders from which cylinder samples were taken were readily available. The concrete modulus of elasticity determined from testing at the time of strand release was used in the analysis. The cylinders from Plant A were taken from a pour consisting of four 66 ft-6.5 in (20.28 m) 27M girders with a design release camber of 2.61 in (66.3 mm). The average measured release camber was 1.84 in (46.7 mm). Unfortunately, no lift/set cambers were recorded for these girders, but based on the data in Section 3.4.2, a reasonable estimate for the lift/set camber was 1.92 in (48.8 mm). Assuming that the "true" release camber could be approximated as the average of the measured release and lift/set cambers, as discussed in Section 2.9, the "true" release camber would be estimated to be on the order of 1.88 in (47.8 mm). The concrete modulus of elasticity at release was determined to be 5940 ksi from the material testing.

The cylinders from Plant B were taken from a pour consisting of two 129 ft-3 in (39.4 m) MN63 girders with a design release camber of 3.84 in (97.5 mm). The average measured release camber was 2.50 in (63.5 mm). Unfortunately, no lift/set cambers were recorded for these girders either, but based on the data in Section 3.4.2, a lift/set camber of approximately 2.78 in (70.6 mm) was assumed. The "true" release camber, approximated as the average of the measured release and estimated lift/set cambers, was estimated to be 2.64 in (67.1 mm). The concrete modulus of elasticity at release was determined to be 6010 ksi from the material testing. The results of the analysis for the girders from both plants are shown in Table 6-1.

Table 6-1. Design vs. revised release camber predictions for material test girders

	Plant A 27M girders	Plant B MN63 girders
Measured Release Camber	1.84"[1]	2.50"[2]
Approx. Lift/Set Camber	1.92"	2.78"
"True" Release Camber	1.88"	2.64"
Design Release Camber	2.61"	3.84"
% Difference	38.7	45.5
Design E_c (ksi)	4464	4464
Measured E_c (ksi)	5937	6009
Initial Pull Stress (ksi)	203.2	204.8
Strand Stress after Thermal and Relaxation Effects (ksi)	192.53[3]	192.93[3]
Release Camber Prediction	1.89"	2.78"
% Difference	0.40	5.30

[1]Average release camber of four girders (range: 1.75" to 1.875")
[2]Average release camber of two girders (both 2.50")
[3]Strand stress calculated as the initial pull stress minus prestress losses due to thermal and relaxation effects (does not include elastic shortening losses)

The results of this analysis indicate that the higher concrete modulus of elasticity and the strand stress loss due to thermal and relaxation effects causes a significant reduction and improvement in the release camber prediction. In fact, the results show that the design release cambers over-predicted the measured release cambers by 38.7% and 45.5% for the two girder sets, whereas the revised release camber predictions only over-predicted the cambers by 0.40% and 5.30%. Not only is this a significant improvement in the camber predictions, it also indicates that the release camber can be accurately predicted if the necessary data is available for each pour and each set of girders and that this analysis gives important insight into the discrepancy between design and measured release cambers.

6.3.2 Instrumented Girders

A similar procedure to the one conducted for the material test girders detailed above was performed on each set of instrumented girders. The only differences in the above procedure were that lift/set cambers were measured and the concrete modulus of elasticity was calculated using the Pauw (ACI 318-08, AASHTO LRFD 2010) equation, because material tests were not conducted on these girders. Initial on-bed and lift/set cambers recorded at release using the camber measuring instrumentation, described in Chapter 4, were used in the analysis. Table 6-2

shows the results of the revised release camber predictions for the instrumented girders. All of the collected data for these girders, including fabrication records, camber measurements and thermal curing data are given in APPENDIX E.

Table 6-2. Release camber predictions for instrumented girders

Girder Set	Measured Camber	Lift/Set Camber	"True" Camber	Design Camber	% Diff	Camber Prediction	% Diff
73037 122' MN54's (weekend cure)	2.44"[1]	2.67"[1]	2.56"[1]	3.47"	35.8[2]	2.44"	4.50[3]
73038 122' MN54's (weekday cure)	2.70"	2.93"	2.82"	3.70"	31.4	2.86"	1.60
73038 93' MN54's (weekday cure)	1.22"	1.33"	1.28"	1.75"	37.3	1.23"	3.53
27B58 119' MN45 (2-day cure)	3.44"	3.60"	3.52"	4.09"	16.2	3.44"	2.27
27B58 119' MN45's (1-day cure)	2.44"	2.68"	2.56"	4.09"	59.8	2.89"	12.9
73044 131'6" MN63's (weekday cure)	2.00"	2.16"	2.08"	3.28"	57.7	2.37"	13.9
73044 131'6" MN63's (weekend cure)	1.94"	2.15"	2.04"	3.28"	60.6	2.32"	13.6

[1]Values shown represent average camber values for the girders in each "girder set" (or pour)
[2]Percent difference determined as ((design camber-true camber)/true camber) *100
[3]Percent difference determined as |((camber prediction-true camber)/true camber) *100|

The discrepancy between the design and measured release cambers is once again evident in these results, as the design cambers for the instrumented girders over-predicted the measured cambers by an average of approximately 44%. However, the revised release camber predictions for these girders were much closer to the measured cambers. The percent difference for the camber prediction values shown in Table 6-2 represents an absolute value. Thus, the release camber predictions differ from the measured cambers by an absolute average of approximately 7.6%, which is a significant improvement. However, even though this is an improvement, there is still some discrepancy in the predictions. This is likely due to some uncertainty in the data (i.e., actual E_{ci} in the girders and actual temperatures at concrete-steel bond and strand release) and possible effects that are not accounted for in the analysis (i.e., pre-release cracking due to extended time between side-form removal and strand release, which was observed for the 73044 MN63 weekday cure girders).

Because the revised release camber predictions used known data regarding the concrete material properties and thermal prestress losses, there should be a reduction in the scatter. A normalized camber (observed camber divided by design or predicted camber) was used to analyze these results. The average and the coefficient of variation (COV) for the normalized

(original design) cambers of the six girders from which cylinder samples were taken and the fourteen instrumented girders was 70.4% and 9.59, respectively. The average and COV for the normalized (revised) cambers of these girders was 96.8% and 7.81, respectively. This result shows that the revised camber predictions made with the use of available data greatly improved prediction accuracy and reduced the scatter, or amount of variability, in the results. It should be noted that the rather high COV values were likely due to the small sample size of just twenty girders.

6.3.3 Historical Girders

Release camber predictions could also be made for the 1067 girders in the historical database. However, the detailed analysis was only conducted on a selected group of these girders because of the amount of data required to conduct the thermal effects analysis on each individual girder. The longest and shortest girders of each shape from the historical girder database were used in order to ensure that the full potential range of length-depth ratios was examined. It should be noted that for the historical girders, there was more imprecise or missing data and the material properties may not have been as well known. The thermal effects analysis and the revised release camber predictions were conducted for the following historical girders:

Table 6-3. Selected historical girders for release camber re-predictions

Girder Shape	27M	36M	MN45	MN54	MN63	72M	81M
Short Length	43’ 0”	51’ 0”	75’ 9”	85’ 1.5”	95’ 2”	110’ 6”	124’ 3”
Bridge #	03009	17532	19561	07589	14816	07581	72013
Long Length	72’ 6.5”	93’ 0”	111’ 3”	130’ 6”	145’ 6”	139’ 9”	156’ 9”
Bridge #	25025	17532	27B65	14549	27302	07581	86820

It should also be noted that because of the amount of data required to make revised release camber predictions for each girder, the revised predictions were made for the girders from just *one* pour from each girder set described above. For these girders, the average normalized camber (observed vs. design value) and the COV was 71.6% and 16.4, respectively. Just like with the instrumented and material test girders, the COV for these girders was high because the sample size was rather small. The average normalized camber for the re-predicted cambers (observed vs. predicted value) and the COV was 98.6% and 15.5, respectively. This result confirms that the revised predictions made from the available data greatly improved the accuracy of the camber predictions and reduced the scatter in the results.

6.4 Recommendations for Revised Release Camber Calculations

Three primary factors were found to cause the discrepancy between the design and observed girder release cambers. The observed cambers were lower than predicted primarily because: (1) higher concrete elastic moduli associated with the higher concrete compressive strengths at release, (2) higher concrete elastic moduli than predicted due to the use of an equation for E_c (ACI 363) which under-predicted the modulus, and (3) lower strand prestress

forces at release due to thermal effects and strand relaxation. In order to take each of these effects into account in the elastic release camber calculations, the following revisions to those calculations are recommended:

1. The concrete release strength used in the camber calculations should be the design concrete release strength, f'_{ci}, multiplied by a factor of 1.15. This modification accounts for the higher release strengths produced at the fabrication plants because of the need to exceed the design strength at release and efficiently turn over the precasting beds.
2. The Pauw (ACI 318-08, AASHTO LRFD 2010) equation for the concrete modulus of elasticity should be used instead of the ACI 363 equation currently used in the camber calculations. This modification accounts for the stiffer concrete produced at the fabrication plants.
3. ***The stress in the strands at release should be reduced by 3%, from $0.75*f_{pu}$ to $0.72*f_{pu}$, in the camber calculations. This modification accounts for the strand prestress losses due to strand relaxation and thermal effects. Note: This recommendation should be removed if the fabricators are allowed to use the provided spreadsheet for temperature corrections.

Two spreadsheets were created, one for each precasting plant, which use the thermal effects analysis, discussed in Section 5.3.1 and APPENDIX B, to output a temperature correction for each pour. This spreadsheet was designed to improve upon the rule-of-thumb procedure currently used by the precasters by incorporating the thermal analysis to reduce camber variability and to ensure the desired prestress is achieved. If the precasters are given permission to use the spreadsheet, Recommendation #3 no longer applies. Prior to implementation, it is recommended that a short field study be conducted to further quantify the effect of temperature and girder setting on the strand stress.

A description of the spreadsheets can be found in APPENDIX B and a more detailed description of the temperature correction recommendations to precasters can be found in Section 9.2.2. Further description of the recommended revisions to the release camber calculations can also be found in Section 9.3.1.

6.4.1 Impact of Revised Camber Calculations on Historical Girder Camber Predictions

These recommendations for the release camber calculations were examined using the entire 1067 girders in the historical database. Because the recommendations can be applied to any girder without the need for recorded data, revised release camber predictions were made in a much more general, or average, sense for all of the 1067 girders. As mentioned in Section 5.2.4, if the Pauw (ACI 318-08, AASHTO LRFD 2010) equation is inserted into the design calculations for camber, the discrepancy between the design cambers and measured cambers of the historical girders improved from 74% to nearly 88%, which is essentially just implementing Recommendation #2. When all three recommendations were applied in the revised release camber predictions, the discrepancy between the measured and design (predicted) cambers improved to approximately 99%. This result confirms that the discrepancy between design and measured release cambers was nearly eliminated when the major effects of higher concrete elastic moduli (due to higher concrete strengths and more appropriate expression for E_c) and strand prestress losses due to thermal effects (and strand relaxation) were included in the predictions. It should be noted that even though the revised release camber predictions using

these recommendations greatly reduced the discrepancy between measured and design cambers, it did not reduce the scatter because the recommendations were applied to the camber calculations in a general, or average, sense.

6.5 Conclusion

The issues and investigated effects related to release camber discussed in Chapter 5, specifically higher concrete elastic moduli due to higher release strengths and a more accurate expression to predict the concrete elastic modulus, and thermal effects, were used to develop revised release camber predictions for the material-test girders, instrumented girders and selected historical girders. It was found that the accuracy of the revised release camber predictions was much greater than the original design cambers, and that the amount of variability in the results was reduced. A set of revised camber calculation recommendations was made based on the discussed analysis. These recommendations were then applied to the entire historical girder database, and it was found that the discrepancy between observed and design camber values improved from approximately 74% to 99%, on average. This result confirmed that the revised release camber calculations can provide much more accurate camber predictions than the original design equations.

CHAPTER 7. ERECTION CAMBER: ISSUES AND INVESTIGATED EFFECTS

7.1 Introduction

As described in Section 1.2, MnDOT determines the release camber through elastic analysis and then uses multipliers to estimate the camber at the time of bridge erection. These erection camber estimates have led to observed discrepancies between the measured and predicted cambers of 83.5%, on average, for the girders in the historical girder database. The effects that influence time-dependent camber, such as concrete creep and shrinkage, solar radiation, and bunking, are examined in this chapter. The program PBEAM was used to investigate these time-dependent effects. PBEAM was first validated using the camber measurements from the instrumented girders and the recorded cambers from selected historical girders. Once validated, PBEAM was used to conduct a parametric study and long-term camber modeling.

It should be noted that the girder age at erection is the most influential effect, because the longer a girder sits in storage, the more it is affected by time-dependent effects such as creep, shrinkage, bunking, etc. It has been observed that camber increases with time, but the rate of increase is highly variable, and depends on the influence of these effects. In Section 3.4.4, it was shown that girders erected at early ages had cambers that were much lower, in general, than what was predicted, and that the discrepancy between measured and predicted cambers improved with increased girder ages. The nature of this discrepancy between measured and predicted cambers at erection is due to the fact that the release cambers were not accurately predicted and that both the Martin (PCI) multipliers (detailed in Section 2.2) and the current MnDOT multiplier are used for all girder ages at erection.

7.2 Concrete Creep and Shrinkage

Concrete creep and shrinkage are time-dependent effects that play a significant role in the increase of camber over time. Creep represents dimensional change in a concrete specimen under sustained loading, and thus, begins to take effect as soon as the prestress force is released into a girder. Shrinkage represents a dimensional decrease in a concrete specimen as moisture is lost over time. Various commonly-used creep and shrinkage models were examined and compared in order to select a few of these models for PBEAM program validation, and eventually, long-term camber prediction modeling.

A literature review was conducted to find various current and commonly-used concrete creep and shrinkage models for analysis and comparison in this study. Special consideration was given to models that were determined from or validated with testing of high-strength concrete. PBEAM accounts for the time-dependent effects of creep and shrinkage; however, its input format uses the ACI 209 Committee (1992) form of these expressions. As a result, some of the creep and shrinkage models considered in the study were modified for use in PBEAM.

The creep coefficient, defined as the ratio of creep strains to the initial elastic strains, and the shrinkage strain, were compared for each model. Because PBEAM uses the ACI 209 expressions for these quantities, a nonlinear least square fit analysis was done to create PBEAM-ready inputs for the other models. The chosen models were then implemented into the long-term camber modeling of the instrumented and selected historical girders in PBEAM to validate the program and to determine the creep and shrinkage model that best predicted the measured

camber results. This model was then used for a time-dependent parametric study and long-term camber prediction modeling.

The creep and shrinkage models chosen for this study included the following:

- ACI 209R-92
- Mokhtarzadeh et al. (1998) ACI 209 variation
- CEB-FIP 1990
- Muller et al. (1999) (CEB-FIP 1999)
- AASHTO LRFD 2010
- Mazloom (2008)
- GL2000 (Gardner and Lockman 2001)
- B3 (Short-form) (Bažant et al. 1996)

These models represent the most recent and commonly-used models and are based on extensive research and experimental studies. However, not all of these models examined the creep and shrinkage of high-strength concrete, which is used in prestressed girder applications. As such, the strengths achieved at both Plants A and B approached or exceeded the applicable strengths associated with these models. Each of these models are affected by some or all of the following factors; loading age, concrete strength, concrete modulus of elasticity, ambient relative humidity, volume-to-surface ratio, cement type, etc. One important difference among the models is that the ACI 209, CEB-FIP 1990, Muller, AASHTO LRFD 2010 and Mazloom creep models are hyperbolic in nature, whereas the GL2000 and B3 creep models are logarithmic. Descriptions of these models are included in the following sections.

7.2.1 Creep and Shrinkage: Reviewed Models

7.2.1.1 ACI 209R-92

The American Concrete Institute (ACI) recommended the following procedure for the prediction of creep and shrinkage in ACI 209R-92. The procedure is applicable to all strength concretes, with both moist and steam curing and Types I and III cement.
The expression for shrinkage strain is given as:

$$(\varepsilon_{sh})_t = \frac{t}{f+t}(\varepsilon_{sh})_u \gamma_{sh} \qquad \textbf{(7-1)}$$

where

$(\varepsilon_{sh})_t$ = shrinkage strain at time t
$(\varepsilon_{sh})_u$ = ultimate shrinkage strain; 780×10^{-6} in/in (given by ACI 209)
f = constant; 55 (given by ACI 209)
γ_{sh} : Represents the product of applicable correction factors for conditions other than the standard conditions defined by ACI 209 (i.e., volume-surface ratio (V/S) of 1.5 in, 1-3 days steam cured, 40% ambient relative humidity, etc.)

The expression for the creep coefficient is given as:

$$v_t = \frac{t^{\psi}}{d + t^{\psi}} v_u \gamma_{cr} \quad \textbf{(7-2)}$$

where

v_t = creep coefficient at time t (ratio of creep strain to initial elastic strain)
ψ = constant; 0.6 (given by ACI 209)
d = constant; 10 (given by ACI 209)
v_u = ultimate creep coefficient; 2.35 (given by ACI 209)
γ_{cr} : Represents the product of applicable correction factors for conditions other than the standard conditions defined by ACI 209 (i.e., volume-surface ratio (V/S) of 1.5 in, 1 to 3 days steam cured, 40% ambient relative humidity, etc.)

The suggested values for the constants given above are specified by ACI 209 (2008) to be used in the absence of experimental data. In the case of prestressed girders fabricated using steam or heat curing, correction factors are needed for loading ages >3 days, ambient relative humidity >40% and volume-surface ratio other than 1.5 in (38.1 mm). It should be noted that there are also correction factors for concrete composition conditions (i.e., slump, cement content, air content, etc.) that are other than standard (ACI 209R-92). However, because the exact concrete composition can vary considerably from pour to pour and plant to plant and because specific mix data was not collected, these correction factors were neglected.

The expressions for the applicable correction factors related to creep and shrinkage are given as:

Loading Age: $Creep\ \gamma_{la} = 1.13(t_{la})^{-0.094}$ **(7-3)**

for steam-cured concrete where the loading age in days, t_{la}, is other than 1-3 days.

Ambient RH: $Creep\ \gamma_{RH} = 1.27 - 0.0067RH \ \ for\ RH > 40$ **(7-4)**

$$Shrinkage\ \gamma_{RH} = 1.4 - 0.0102RH \ \ for\ 40 \leq RH \leq 80 \quad \textbf{(7-5)}$$

$$Shrinkage\ \gamma_{RH} = 3.0 - 0.03RH \ \ for\ 80 < RH \leq 100 \quad \textbf{(7-6)}$$

where *RH* is the ambient relative humidity as a percent.

V/S Ratio: $Creep\ \gamma_{VS} = \frac{2}{3}(1 + 1.13e^{(-0.54\frac{v}{s})})$ **(7-7)**

$$Shrinkage\ \gamma_{VS} = 1.2e^{(-0.12\frac{v}{s})} \quad \textbf{(7-8)}$$

where *v/s* is the volume-surface ratio of the member in inches.

7.2.1.2 Mokhtarzadeh et al. (1998) ACI 209 variation

Even though creep and shrinkage data were not collected in the present study, Mokhtarzadeh et al. (1998) had gathered extensive experimental data on concrete samples taken from Plant A. After analyzing the creep and shrinkage data of the many samples, Mokhtarzadeh et al. (1998) proposed modifications to the ACI 209 model. Aside from the following modifications, the model proposed by Mokhtarzadeh et al. (1998) is identical to the ACI 209 model. The modifications to the shrinkage model are as follows:

f = constant; 65
$(\varepsilon_{sh})_u$ = ultimate shrinkage strain; 530×10^{-6} in/in

Mokhtarzadeh et al. (1998) also proposed modifications to the creep model by adjusting the ultimate creep coefficient, v_u, depending on aggregate type. Experimental creep data was collected for round and crushed river rock, crushed granite and two types of limestone aggregates. Mokhtarzadeh et al. (1998) made the following recommendations for the ultimate creep coefficient using these aggregates:

Aggregate Type	v_u
Round river rock	2.45
Crushed granite	1.83
Partially crushed river rock	1.31
High-absorption limestone	1.03
Low-absorption limestone	0.94

It was not known whether the river rock aggregates used at Plant A would be considered round or partially crushed by the standards used by Mokhtarzadeh et al. (1998). Either of the ultimate creep coefficients for river rock (i.e., 2.45 for round and 1.31 for partially crushed) might have been representative of concrete produced at Plant A. However, because the purpose of investigating various creep and shrinkage models was to determine the best predictor of the observed long-term camber behavior of the instrumented girders (and bound these results), the ultimate creep coefficient of 1.31 was selected to be used for concrete produced at Plant A. Selecting the ultimate creep coefficient of 2.45 would not substantially differentiate the Mokhtarzadeh model from the ACI 209 model for creep. The limestone aggregate used at Plant B had a water absorption percent of 1.8, which fell between the standards indicated by Mokhtarzadeh et al. (1998) for high and low absorption limestone. Thus, an ultimate creep coefficient of 0.98 was used when modeling the selected historical girders that were manufactured at Plant B.

7.2.1.3 CEB-FIP 1990

The CEB-FIP Model Code 1990 prediction for creep and shrinkage was restricted to concretes having a 28-day mean cylinder strength of less than 80 MPa, or approximately 11.5 ksi. Considering that typical 28-day cylinder strengths of concrete used at Plants A and B range from approximately 10 to 13 ksi, the girder concrete in this study was on the upper end of this model's applicability range.
The expression for the shrinkage strain is given as:

$$(\varepsilon_{sh})_t = [160 + 10\beta_{sc}(9 - 0.1f_{cm})] \times 10^{-6}\beta_{RH}\sqrt{\frac{t}{(350(\frac{v/s}{1.97})^2 + t)}} \quad \textbf{(7-9)}$$

where

β_{sc} = 4 for slow hardening cements; = 5 for normal or rapid hardening cements; = 8 for rapid hardening high strength cements
f_{cm} = 28-day mean concrete compressive strength in MPa
v/s = volume-surface ratio of the member in inches
$\beta_{RH} = 1.55(1 - h^3)$ where h is the ambient relative humidity as a decimal

The expression for the creep coefficient is given as:

$$\Phi(t, t_0) = \left[1 + \frac{1 - h}{0.46(\frac{v/s}{1.97})^{1/3}}\right]\left[\frac{5.3}{\sqrt{0.1f_{cm}}}\right]\left[\frac{1}{0.1 + {t_0}^{0.2}}\right]\left[\frac{(t - t_0)^{0.3}}{[\beta_H + (t - t_0)]^{0.3}}\right] \quad \textbf{(7-10)}$$

where

$\beta_H = 150[1 + (1.2h)^{18}]\left(\frac{v/s}{1.97}\right) + 250 \leq 1500$
f_{cm} = 28-day mean concrete compressive strength in MPa
v/s = volume-surface ratio of the member in inches
h = ambient relative humidity as a decimal
t_0 = loading age in days

7.2.1.4 Muller et al. (1999) (CEB-FIP 1999)

Muller et al. (1999) developed a model for predicting creep that closely resembled the CEB-FIP 1990 model. In fact, it was adopted by CEB-FIP and is commonly known as the CEB-FIP MC90-99 model. However, the Muller model is applicable to high strength concretes having a 28-day mean cylinder strength of up to 120 MPa, or approximately 17 ksi. Even though this would seem to be more suitable for the concretes in this study, the Muller model is also specified for moist curing conditions and loading ages of at least one day. At Plants A and B, loading ages can be as short as 18 hours and moist curing is never used.
The expression for the shrinkage strain is given as:

$$(\varepsilon_{sh})_t = \alpha_{as}(\frac{0.1f_{cm}}{6 + f_{cm}})^{2.5}[1 - \exp(-0.2t^{0.5})] \times 10^{-6} + (220 + 110\alpha_{ds1})\exp(-0.1\alpha_{ds2}f_{cm}) \times 10^{-6} \times \beta_{RHm}\sqrt{\frac{t}{(350(\frac{v/s}{1.97})^2 + t)}} \quad \textbf{(7-11)}$$

where

f_{cm} = 28-day mean concrete compressive strength in MPa
v/s = volume-surface ratio of the member in inches
$\beta_{RHm} = 1.55(1 - h^3)$ where h is the ambient relative humidity as a decimal
α_{as}, α_{ds1}, α_{ds2} = 800, 3, 0.13 for slow hardening cements; = 700, 4, 0.12 for normal or rapid hardening cements; = 600, 6, 0.12 for rapid hardening high strength cements

The expression for the creep coefficient is given as:

$$\Phi(t,t_0) = \left[1 + \left(\frac{1-h}{0.46(\frac{v/s}{1.97})^{1/3}}\right)\alpha_{m1}\right]\alpha_{m2}\left[\frac{5.3}{\sqrt{0.1f_{cm}}}\right]\left[\frac{1}{0.1+{t_0}^{0.2}}\right]\left[\frac{(t-t_0)^{0.3}}{[\beta_H+(t-t_0)]^{0.3}}\right] \quad \textbf{(7-12)}$$

where

$\beta_H = 150[1+(1.2h)^{18}]\left(\frac{v/s}{1.97}\right) + 250\alpha_{m3} \leq 1500\alpha_{m3}$
f_{cm} = 28-day mean concrete compressive strength in MPa
v/s = volume-surface ratio of the member in inches
h = ambient relative humidity as a decimal
t_0 = loading age in days
$\alpha_{m1} = (35/f_{cm})^{0.7}, \quad \alpha_{m2} = (35/f_{cm})^{0.2}, \quad \alpha_{m3} = (35/f_{cm})^{0.5}$

7.2.1.5 AASHTO LRFD 2010

The AASHTO LRFD 2010 Bridge Design Specifications manual specifies that a bridge designer may use the CEB-FIP 1990 model code, the ACI 209 (2008) model or the expressions found in Articles 5.4.2.3.2 and 5.4.2.3.3 of the AASHTO LRFD 2010 manual for the predictions of creep and shrinkage. These provisions are specified to be applicable for concrete strengths up to 15.0 ksi. Even though the manual gives the option of using the CEB-FIP model or the ACI 209 model, the model provided by AASHTO closely resembles the ACI 209 model, where the expressions for the creep coefficient and shrinkage strain contain a time-dependent function multiplied by a set of correction factors. The main significant difference between the AASHTO LRFD 2010 model and the ACI 209 model is that the AASHTO LRFD model is very dependent on the concrete strength at release.
The expression for the shrinkage strain is given as:

$$(\varepsilon_{sh})_t = k_s k_{hs} k_f k_{td}(0.48) \times 10^{-3} \quad \textbf{(7-13)}$$

The expression for the creep coefficient is given as:

$$\Phi(t,t_0) = 1.9 k_s k_{hc} k_f k_{td} {t_0}^{-0.118} \quad \textbf{(7-14)}$$

where

$k_s = 1.45 - 0.13(V/S) \geq 1.0$
$k_{hs} = 2.00 - 0.014H$
$k_{kc} = 1.56 - 0.008H$
$k_f = \frac{5}{1+f'_{ci}}$
$k_{td} = \left(\frac{t}{61-4f'_{ci}+t}\right)$
V/S = volume-surface ratio of the member in inches
H = ambient relative humidity as a percent
t_0 = loading age in days
f'_{ci} = concrete compressive strength at release in ksi

7.2.1.6 Mazloom (2008)

Mazloom (2008) developed a model for predicting creep that closely resembled the ACI 209R-92 model, but was specifically designed for high strength concrete applications. This model was developed using granite sand and gravel aggregate with ordinary Portland cement and different levels of silica fume. The 28-day concrete compressive strengths achieved by their specimens were 65 to 70 MPa (9.4 to 10.2 ksi) (Mazloom 2008). Because the concrete used at Plant A and Plant B does not use granite aggregate and contains no silica fume, this model may not be as applicable. However, its specific application to high strength concrete is advantageous. The expression for the shrinkage strain is given as:

$$(\varepsilon_{sh})_t = \frac{t}{(0.3SF + 12.6) + t}(1.14 - 0.007v/s)(\varepsilon_{sh})_u \qquad \textbf{(7-15)}$$

where

SF = silica fume content as a percent of the total cementitious material by weight
v/s = volume-surface ratio in mm
$(\varepsilon_{sh})_u$ = ultimate shrinkage strain; 516×10^{-6} mm/mm

The expression for the creep coefficient is given as:

$$\Phi(t, t_0) = \frac{t^{0.6}}{(26.5 - SF) + t^{0.6}}(103 - 3.65SF)(1.08 - 0.0114t_0)E_c(t_0) \times 10^{-6} \qquad \textbf{(7-16)}$$

where

SF = silica fume content as a percent of the total cementitious material by weight
t_0 = loading age in days
$E_c(t_0)$ = concrete modulus of elasticity at t_0 (release)

7.2.1.7 GL2000 (Gardner and Lockman 2001)

The GL2000 model for predicting creep was developed by Gardner and Lockman (2001) and represents a modified form of the earlier model developed by Gardner and Zhao (1993). Unlike other models, the GL2000 model uses the information available at the time of design (specified concrete strengths, etc.) instead of the actual experimental data. However, for the sake of comparison, the measured data from the obtained historical records for the instrumented and selected historical girders were used in the model. This model was created more for cast-in-place (CIP) and post-tensioning (PT) applications with loading ages greater than 7 days and is also restricted to concrete with 28-day mean cylinder strengths up to just 70 MPa (~10 ksi) and water-cement ratios of 0.40 to 0.60 (Gardner et al. 2001). Girders fabricated at Plants A and B had loading ages of 1 to 4 days and typical girder concrete used at these plants almost always exceeded strengths of 10 ksi and usually had w/c ratios lower than 0.40. Thus, this model was not considered applicable to this study.

The expression for the shrinkage strain is given as:

$$(\varepsilon_{sh})_t = (\varepsilon_{sh})_u(1 - 1.18h^4)\sqrt{\frac{t}{0.15(V/S)^2 + t}} \quad \textbf{(7-17)}$$

where

$(\varepsilon_{sh})_u = 1000K\sqrt{30/f_{cm}} \times 10^{-6}$
V/S = volume-surface ratio in mm
h = ambient relative humidity as a decimal
K = 1.0 for Type I cement; = 0.75 for Type II cement; = 1.15 for Type III cement
f_{cm} = 28-day mean concrete compressive strength in MPa

The expression for the creep coefficient is given as:

$$\Phi(t, t_0) = \left(\frac{2.0t^{0.3}}{t^{0.3} + 14}\right) + \sqrt{\frac{7t}{t_0(t + 7)}} + 2.5(1 - 1.086h^2)\sqrt{\frac{t}{0.15(V/S)^2 + t}} \quad \textbf{(7-18)}$$

where

V/S = volume-surface ratio in mm
h = ambient relative humidity as a decimal
t_0 = loading age in days

7.2.1.8 B3 (Short-form)

The original B3 model was developed by Bažant and Baweja and was recommended by RILEM TC-107-GCS in 1995, reported in ACI 209R-96 and referenced in ACI 209R-08. However, a simplified short-form was developed by Bažant and Baweja in 1996 and is considered sufficient for structures of medium sensitivity (i.e., reinforced concrete beams, frames and slabs, plain concrete footings, prestressed beams and slabs). Like the GL2000 model, this model was created more for cast-in-place (CIP) and post-tensioning (PT) applications with loading ages greater than 7 days and is restricted to concrete with 28-day mean cylinder strengths of up to just 70 MPa (~10 ksi) (Bažant et al. 1996). Additionally, even though this is the short-form B3 model, it is still more complex than the others. Considering that many different modeling situations were required for this study (i.e., different loading ages, concrete strengths, *v/s* ratios and relative humidities) and that applicable loading ages were 1 to 4 days and concrete strengths usually exceeded 10 ksi, this model was not considered applicable to this study.
The expression for the shrinkage strain is given as:

$$(\varepsilon_{sh})_t = (\varepsilon_{sh})_u(1 - h^3)S(t) \quad \textbf{(7-19)}$$

$$S(t) = \tanh\sqrt{\frac{t}{\tau_{sh}}} \qquad \tau_{sh} = 128(v/s)^2 \quad \textbf{(7-20)}$$

$$(\varepsilon_{sh})_u = \alpha_1 \alpha_2 \left[26w^{2.1} {f_{cm}}^{-0.28} + 270\right] \times 10^{-6} \quad \textbf{(7-21)}$$

where

f_{cm} = 28-day mean concrete compressive strength in psi
v/s = volume-surface ratio of the member in inches
h = ambient relative humidity as a decimal (≤0.98)
α_1 = 1.00 for Type I cement; = 0.85 for Type II cement; = 1.10 for Type III cement
α_2 = 0.75 for steam curing; = 1.00 for curing in water or at 100% relative humidity; = 1.20 for sealed curing or normal curing in air with initial protection against drying

The expression for the creep coefficient is given as:

$$\Phi(t, t_0) = E(t_0) J(t, t_0) - 1 \quad \textbf{(7-22)}$$

$$\mathrm{J}(t, t_0) = [q_1 + C_0(t, t_0) + C_d(t, t_0)] \times 10^{-6} \quad \textbf{(7-23)}$$

$$C_0(t, t_0) = q_0 \ln[1 + 0.3[{t_0}^{-0.5} + 0.001](t - t_0)^{0.1}] \quad \textbf{(7-24)}$$

$$C_d(t, t_0) = q_5 \sqrt{[e^{-3H(t)} - e^{-3H(t_0)}]} \qquad H(t) = 1 - (1 - h)S(t) \quad \textbf{(7-25)}$$

where

$q_0 = 200(f_{cm})^{-0.5}$, $q_1 = 60{,}000/E_{28}$, $q_5 = 6{,}000/f_{cm}$
f_{cm} = 28-day mean concrete compressive strength in psi
$E(t_0)$ = concrete modulus of elasticity at release
E_{28} = 28-day concrete modulus of elasticity in psi (equation given but can be changed)
h = ambient relative humidity as a decimal
$S(t)$ = same as for shrinkage (above)
t_0 = loading age in days

7.2.2 Creep and Shrinkage Model Comparison

Before utilizing the chosen creep and shrinkage models in the time-dependent camber modeling, the shrinkage strain and creep coefficient of each model were compared, given some appropriate arbitrary conditions. These conditions were as follows:

Ambient relative humidity = 70%
Loading age = 1 day
Volume-surface ratio = 3.55 in. (average V/S of the seven I-girder shapes in the study)
28-day mean concrete compressive strength = 10,000 psi
Release concrete compressive strength = 7,500 psi

Pauw (ACI 318-08, AASHTO LRFD 2010) equation used for concrete modulus of elasticity
Type III cement, no silica fume and partially crushed river rock aggregate

The shrinkage strain and creep coefficient of each model were plotted for 500 days. Given the above conditions, the creep coefficient comparison is shown in Figure 7-1.

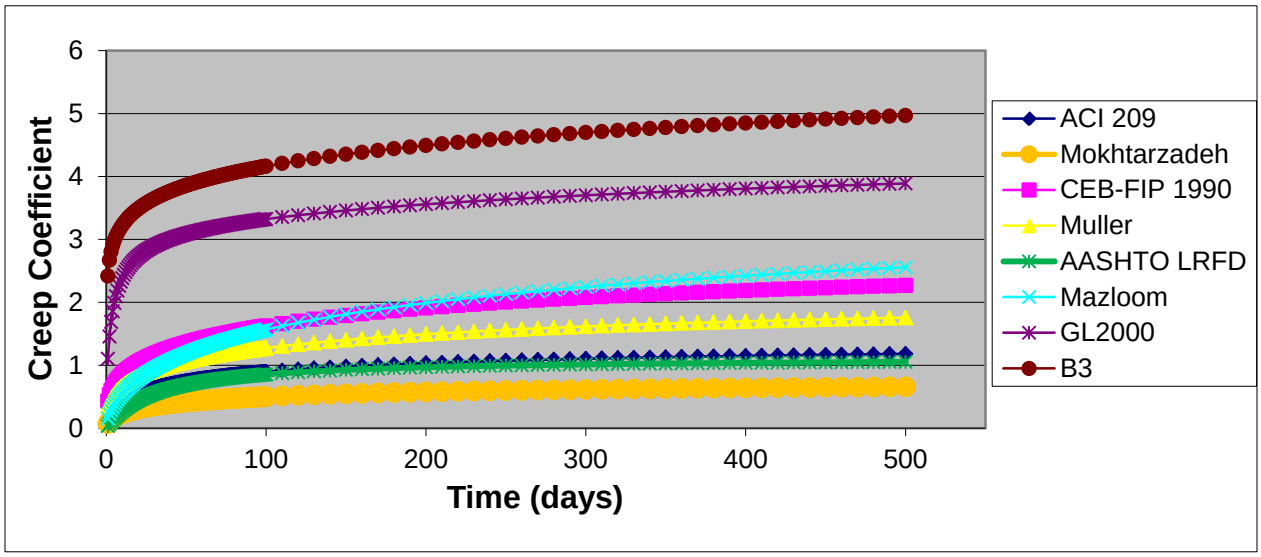

Figure 7-1. Comparison of reviewed creep models

Clearly, the GL2000 and B3 models have a different form than the rest. These two models are highly dependent on loading age and are not well suited to model precast, prestressed concrete applications with short loading ages, as discussed in Sections 7.2.1.7 and 7.2.1.8. Additionally, given that these models are also specified to be applicable for 28-day strengths of only up to approximately 10 ksi, the GL 2000 and B3 models were not used further in this study. Additionally, as previously predicted in Section 7.2.1.5, the AASHTO LRFD 2010 model provided results similar to those of the ACI 209R-92 model.
The shrinkage strain for the remaining models is shown in Figure 7-2.

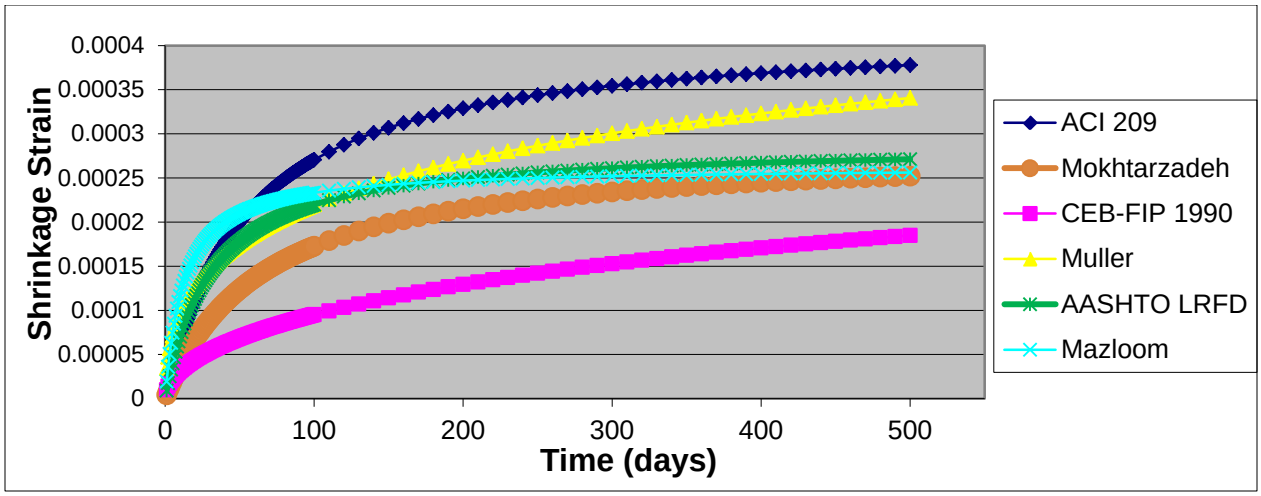

Figure 7-2. Comparison of selected shrinkage models

The chosen models; ACI 209, Mokhtarzadeh variation, CEB-FIP 1990, Muller, AASHTO LRFD and Mazloom, do not all use the same parameters and are affected differently by changes in these parameters. Thus, it is important to compare these models with changes made to the original arbitrary conditions detailed above. To examine variation in these models, the creep coefficient for each model was compared over time. The parameter that is of most importance is the relative humidity, given that it can change by the widest margin from pour to pour and girder to girder. As such, Figure 7-3 shows a comparison of the creep coefficient of each model for relative humidities of 55% and 85%, which are reasonable lower and upper bounds for short time interval relative humidities in Minnesota, discussed further in Section 7.5.2.

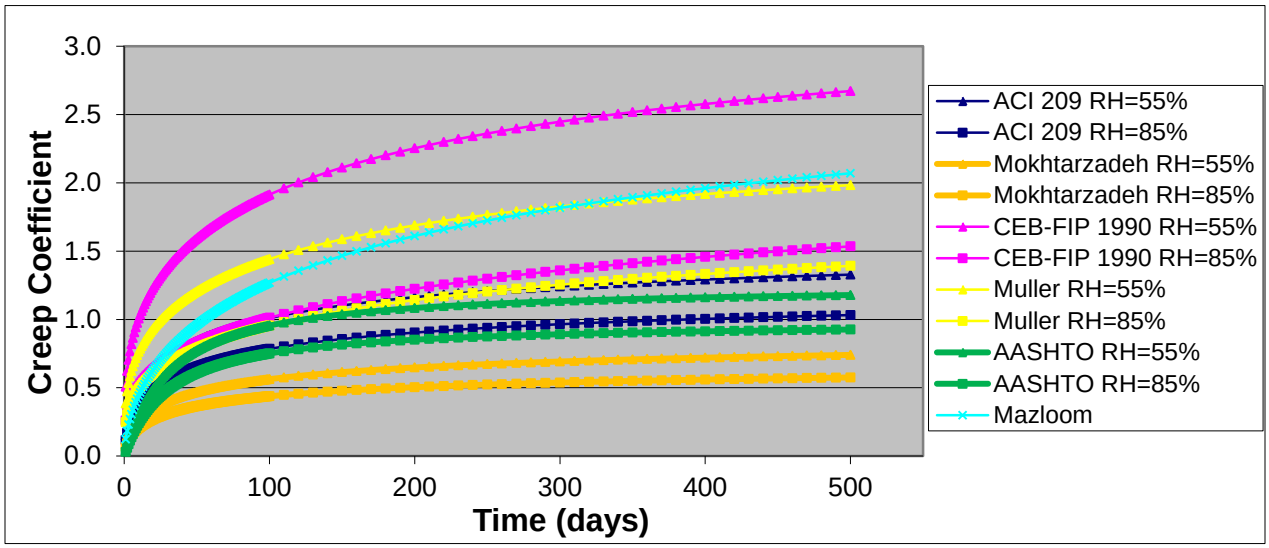

Figure 7-3. Comparison of the effect of relative humidity on selected creep models

The ACI 209, Mokhtarzadeh ACI 209 variation and AASHTO LRFD models are clearly less affected by changes in relative humidity than are the CEB-FIP 1990 and Muller models.

Additionally, the Mazloom model does not include relative humidity as a parameter (Mazloom 2008), which is clearly a weakness of the model, as creep is well-known to vary with relative humidity. It should also be noted that the creep coefficient for the CEB-FIP 1990 and Muller models for a relative humidity of 85% are greater than the creep coefficient for the ACI 209, Mokhtarzadeh and AASHTO LRFD models with a relative humidity of 55%.

7.2.3 Conversion to PBEAM Inputs

As part of the PBEAM model validation, the chosen creep and shrinkage models (i.e., ACI 209, Mokhtarzadeh variation, CEB-FIP 1990, Muller, AASHTO LRFD and Mazloom) were modeled separately to investigate which model most closely followed the actual behavior of the girders. However, as previously mentioned in Section 7.2, PBEAM assumes the ACI 209 form of the creep coefficient and shrinkage strain expressions. Thus, a nonlinear least square fit analysis was conducted to convert the CEB-FIP 1990 and Muller models into PBEAM-ready inputs by using the following general form of the ACI 209 expressions. (The AASHTO LRFD and Mazloom models take the general form of the ACI 209 expressions, with different, but easy-to-calculate input coefficients).

Shrinkage strain:

$$(\varepsilon_{sh})_t = \frac{t}{f + t}\Phi \qquad \textbf{(7-26)}$$

Creep coefficient:

$$v_t = \frac{t^{\Psi}}{d + t^{\Psi}}\Omega \qquad \textbf{(7-27)}$$

The CEB-FIP 1990 and Muller models were plotted for 500 days, which was selected as a reasonable upper bound for the age of a girder at bridge erection. Table 7-1 contains the results of this analysis.

Table 7-1. Modified creep and shrinkage inputs for PBEAM

	CEB-FIP 1990	Muller
Shrinkage coefficient, f	108	38*
Shrinkage coefficient, Φ	150*	318*
Creep coefficient, d	9.27	8.83
Creep coefficient, ψ	0.56	0.57
Creep coefficient, Ω	**	**

* Approximate, varies depending on values used for relative humidity, loading age, volume-to-surface ratio, concrete strength and applicable coefficients

** Varies considerably depending on values used for relative humidity, loading age, volume-to-surface ratio and concrete strength

It should be noted that changes in certain parameters cause slight changes in the time-dependent part of the model expressions that would lead to small changes in the nonlinear least square fit coefficients. However, given the large quantity of different modeling conditions, the coefficients not marked by an (*) or (**) were kept as average constants. The creep and shrinkage inputs used for each model in Phase 1 of the PBEAM validation (discussed in Section 7.4.3.1) are given in APPENDIX G.

7.3 Environmental Effects

7.3.1 Solar Radiation

Woolf et al. (1998) reported that cambers were observed to increase by as much as 10% during the course of a day as a result of solar radiation. The instrumented girders provided an opportunity to study this effect further. Camber readings were recorded throughout the course of a day on three separate occasions.

The first was on September 28, 2010, when only the first set of girders had been instrumented. The weather at dawn was partly cloudy and 48 °F and by 3:15pm it was only 58 °F and had gotten completely cloudy. However, even though the temperature increased by just 10 °F and it was a cloudy day, it was observed that the camber of the four 122 ft-4.75 in (37.3 m) MN54 girders increased by an average of 0.3 in (7.6 mm), or approximately 7.1%. These camber results are shown in Figure 7-4.

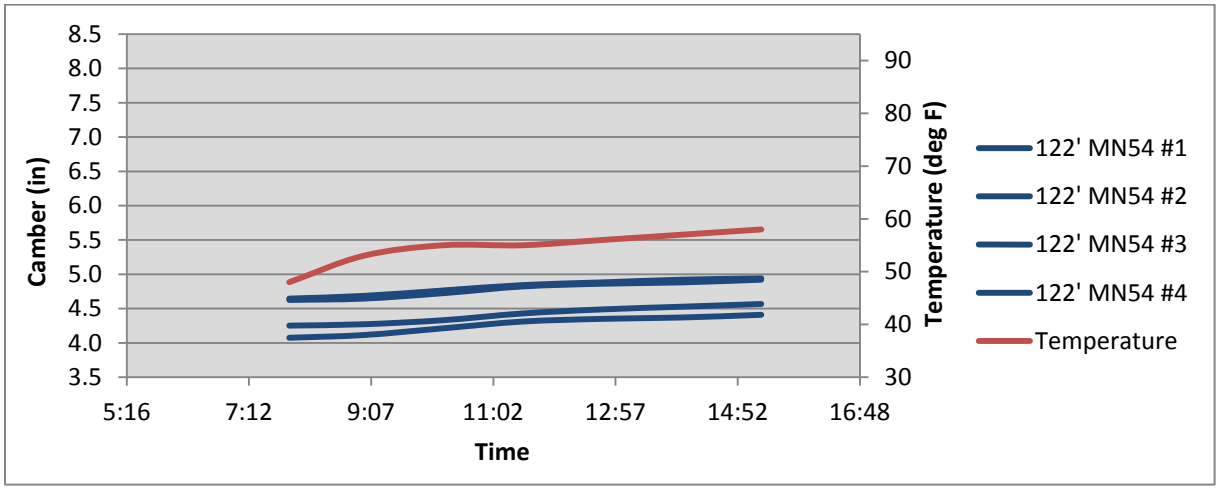

Figure 7-4. Solar radiation camber results for day 1 (Sep. 28, 2010)

The second full day of camber recording was done on May 17, 2011, when Sets 3 and 4 were still present in the storage yard. The weather at dawn was sunny and 42 °F and by 4:00pm it was still sunny and 66 °F. On this day the temperature increased by 24 °F and it was sunny all day, which resulted in larger camber changes. It was observed that the camber of the three 119 ft-3 in (36.35 m) MN45 girders increased by an average of 0.95 in (24.1 mm)and the four 131 ft-6 in (40.08 m) MN63 girders increased by an average of 0.7 in (17.8 mm), which resulted in an overall percent increase of 16.1% for both sets of girders. These camber results are shown in Figure 7-5.

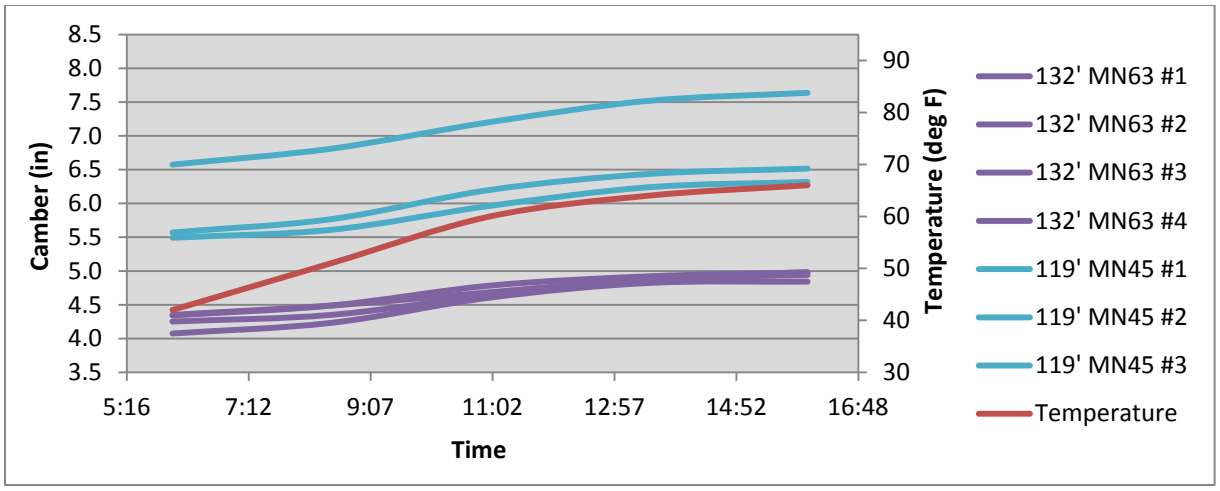

Figure 7-5. Solar radiation camber results for day 2 (May 17, 2011)

The third and final full day of camber recording was done on June 30, 2011, when only Set 3 was left in the storage yard. The weather at dawn was sunny and 71 °F and by 4:00pm it was hazy and sunny and 91 °F. The average camber increase for the three 119 ft-3 in (36.35 m) MN45 girders was 0.85 in (21.6 mm), or approximately 13.3%. Given that June 30 is typically when solar radiation is near its peak for the year, it is interesting that the camber increases for the Set 3 girders were slightly less than on May 17. The most likely explanation is that there had been three hot and sunny days leading up to June 30 and it is plausible that the cambers never fully "recovered" from the previous days' solar radiation effects, even by dawn. These camber results are shown in Figure 7-6. It should be noted that the 119' MN45 girder with higher camber (as shown in Figure 7-5 and Figure 7-6) was poured one day before the other two, on the same precasting bed. Its measured camber was consistently higher than the other two, as was reported in Figure 4-6, which was attributed to its lower compressive strength and corresponding elastic modulus.

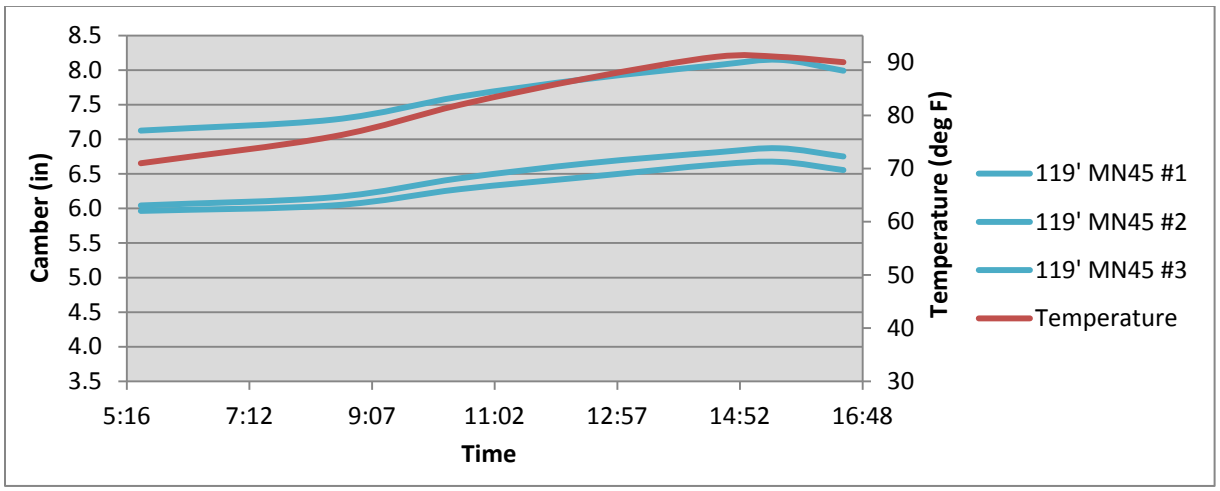

Figure 7-6. Solar radiation camber results for day 3 (June 30, 2011)

Solar radiation is a significant and unavoidable daily effect on camber as confirmed by this study. This result has two significant implications. The first is that solar radiation results in a source of error in the erection camber results recorded for the 1067 girders in the historical data set. Because the time of day and weather conditions were rarely recorded along with the girder elevation survey shots, it was impossible to determine the magnitude of this effect on each girder. It is likely that the erection camber results were larger than the values that would have been obtained if the cambers were recorded at dawn.

The second significant implication relates to the actual process of bridge construction. It is common practice for the survey shots to be used to determine the necessary stool heights along the length of each girder. So, if for example, the survey shots are taken one day and the stools placed the next, it is possible and even likely that the girders would have a different camber than that from which the stool heights were determined. Additionally, it was observed that the increase in camber due to solar radiation depended on the concrete elastic modulus, such that the camber increase for girders with lower elastic moduli was comparatively higher. This is shown in Figure 7-6, where the girder with the higher camber had a lower elastic modulus and a greater increase in camber due to solar radiation. Thus, if there is variability among the cambers of girders being erected, the effect of solar radiation will likely cause this variability to be exacerbated. Thus, it is recommended that the survey shots be taken before mid-afternoon to reduce the effect of solar radiation.

7.3.2 Ambient Relative Humidity

As previously mentioned in Section 4.4, during the winter of 2010 when the camber of the instrumented girders was being regularly recorded, a noticeable increase in camber was observed in all of those girders during periods of high relative humidity. Even though the relative humidity can fluctuate considerably from day-to-day, it is common for the relative humidity to be higher, on average, during the winter months.

Saiidi et al. (1996) found that the camber of a closely-studied concrete box girder bridge in Reno, Nevada experienced an increase in camber every winter for three consecutive years, as described in Section 2.3. During the winter months in Nevada, the average relative humidity increased considerably to around 60-70%, up from around 30-40% during the summer months. The authors credited the increase in camber to this environmental change (Saiidi et al. 1996). Erkmen et al. (2008) also observed and recorded this effect on concrete I-girders fabricated in Minnesota. Erkmen reported that during the winter months, the prestress force in the strands ceased to decrease. In other words, the gradual decrease in prestress force that is usually experienced by prestressing strands “paused” when the relative humidity increased. Erkmen observed that this effect coincided with an increase in camber (Erkmen et al. 2008).

Because of the results from these studies, the daily average relative humidity was recorded from data available at the Princeton, MN weather station (just 19 miles north of Plant A in Elk River, MN). In September and October, the average relative humidity was 72.0% and in November-February (when the increase in camber was observed) it was 76.2%. Even though this may seem like a negligible difference, there was often a spike in relative humidity leading up to the days where the increased cambers were recorded. Additionally, during the winter, the girders were constantly surrounded by snow and ice. The top of the girders was always covered with snow and ice and the bottom of the girders was often sitting in or around snow. It is likely that the relative humidity actually experienced by the girders was even higher than 76.2% during the winter months, although the relative humidity was never recorded at the Plant A storage yard.

Figure 7-7 shows the environment that the girders in the storage yard usually experienced during the winter months.

Figure 7-7. Winter environment for girders at Plant A

The effects of solar radiation and relative humidity can be seen in Figure 7-8, which is the measured camber over time for the girders in Set 1 along with the daily average relative humidity.

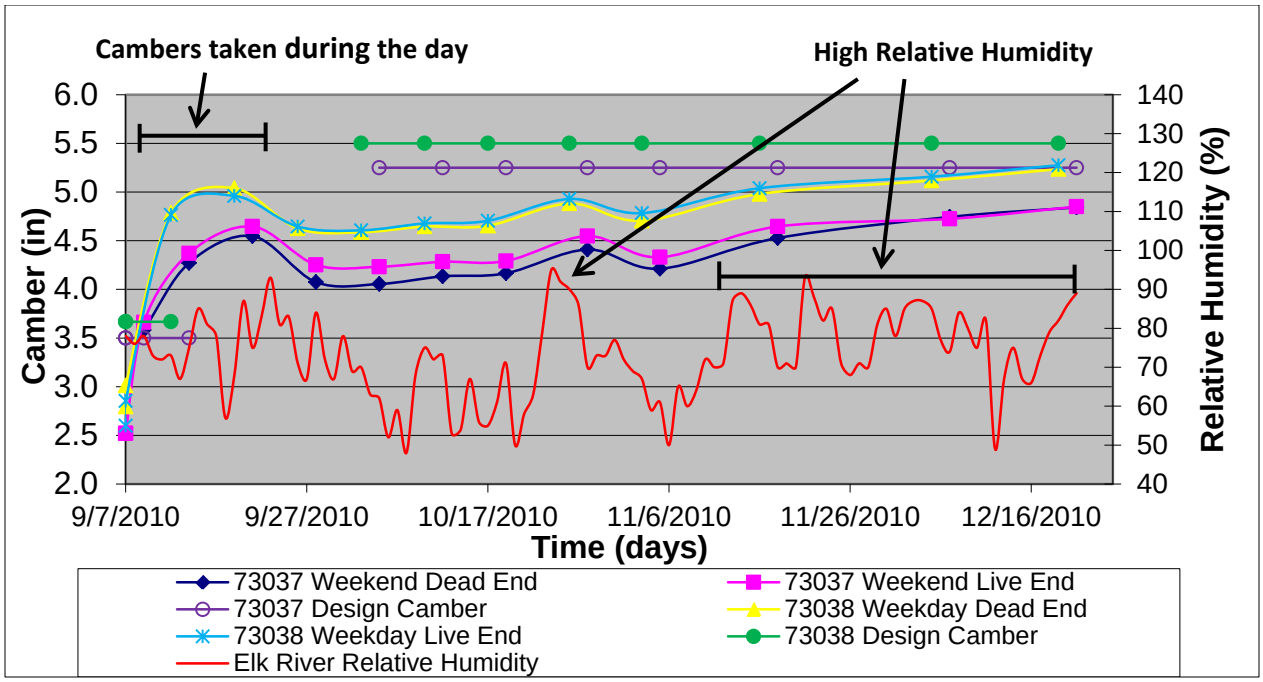

Figure 7-8. Camber measurements for instrumented girders set 1

As can be seen in Figure 7-8, the high camber recorded at early ages was due to solar radiation (early camber readings were recorded during the day) and the increase in camber at later ages corresponded with an increase in relative humidity during the winter months.

7.4 PBEAM Model Validation

Before the program PBEAM was used to conduct a parametric study and develop long-term camber predictions, it was first validated using data from the instrumented girders and select girders from the historical data set. From the selected group of historical girders, the "long" girders of each shape used to make release camber predictions (detailed in Section 6.3.3) were also used for PBEAM validation. Table 7-2 contains the list of these selected girders. By modeling the instrumented girders and selected historical girders in PBEAM, the results could be validated against the known camber measurements. For the instrumented girders, all of the necessary data needed to make release and long-term camber predictions was provided by the fabrication records and weather histories, and through the use of the thermal effects analysis, material testing results and chosen creep and shrinkage models. Because the historical girders were not instrumented and consistently monitored, only the release and erection cambers were recorded and the bunking conditions and solar radiation effects had to be approximated.

Table 7-2. Selected girders from historical database used for PBEAM modeling

Girder Shape	27M	36M	MN45	MN54	MN63	72M	81M
Long Length	72’ 6.5”	93’ 0”	111’ 3”	130’ 6”	145’ 6”	139’ 9”	156’ 9”
Bridge #	25025	17532	27B65	14549	27302	07581	86820

Before validating PBEAM with respect to long-term time-dependent effects, it first had to produce reasonable release camber values. The release cambers were validated by comparing the PBEAM results to the predictions from Section 6.3, where the program inputs were created to match the conditions on which the predictions were made. For further program validation, PBEAM was used to generate long-term camber predictions using the chosen creep and shrinkage models from Section 7.2.2. These long-term camber models were then compared to the long-term camber behavior of the instrumented girders and selected historical girders, and based on these results, a few creep and shrinkage models were then selected to be used for the parametric study and long-term camber predictions, discussed in Section 7.5 and Chapter 8, respectively.

7.4.1 Methodology

The PBEAM program validation was conducted in two modeling phases. Phase 1 consisted of modeling the instrumented girders and used all of the creep and shrinkage models discussed in Section 7.2.2 that were determined to be appropriate for this study. Phase 2 consisted of modeling the “long” girders from the group of selected historical girders and used the chosen creep and shrinkage models that provided the best results from Phase 1.

Before the modeling began, the PBEAM input files were prepared using the information known about each girder and the results of the analysis used to make the revised release camber predictions. The creep and shrinkage model coefficients were prepared for input in PBEAM, as described in Section 7.2.3, by inputting the loading age, *V/S* ratio, relative humidity and concrete properties (if necessary) into the creep and shrinkage models to determine the corresponding coefficients for each set of girders.

Because the concrete stress-strain curve in PBEAM is generated by the 28-day concrete compressive strength and modulus of elasticity, the program uses the input aging coefficients to determine the strength and modulus at any time. However, PBEAM also internally calculates an initial tangent modulus, E_{ci}, given as:

$$E_{ci} = E_c\left(1 + \left(\frac{f'_c}{E_c \varepsilon_0} - 1\right)^2\right) \qquad \textbf{(7-28)}$$

Depending on the stresses and strains in the member at any given time, PBEAM will use a value for the elastic modulus that is somewhere between E'_t and E_{ci}. Therefore, a simple algorithm was developed to calculate the appropriate input E_c to give the desired release and 28-day modulus in PBEAM. The algorithm can best be described as the following two-step process, which is described further in APPENDIX D:

1. Calculate the 28-day modulus that gives the desired release modulus based on the chosen aging coefficients.
2. Calculate the input E_c that yields this previously-calculated 28-day modulus in PBEAM.

The strain in the strands at release (input in PBEAM as the initial prestrain) was determined from the strand stress at release calculated after taking into account the thermal and strand relaxation effects, as described in Section 6.2. Additionally, the appropriate strand relaxation and concrete aging coefficients were used based on the discussions in APPENDIX D and Section 5.2.5, respectively. For Phase 1, the support/bunking locations used in the modeling matched the bunking conditions experienced by the instrumented girders in the storage yard. For Phase 2, the bunking locations were approximated for the historical girders by assuming a realistic upper bound based on observations made at the precasting plants. In each Phase, the girders were first modeled as end-supported to determine the on-bed camber at release. Then, the girders were modeled on the measured or approximated bunks to determine the camber over time. (The effect of bunking is discussed in detail in Section 0.) The PBEAM model inputs and the results of the modeling are included in the following sections.

It should be noted that the average daily relative humidity data collected from the Princeton, MN and New Richmond, WI weather stations (near Plants A and B, respectively) were used to find the average relative humidity experienced by each set of girders during the time from fabrication to shipping. For the instrumented girders, it was found that the average relative humidity experienced by each set was approximately 73%. However, the average relative humidity for the selected historical girders varied.

7.4.2 PBEAM Modeling Inputs

The important PBEAM inputs for Phase 1 of the validation modeling are given in Table 7-3. Not included in Table 7-3 are the creep and shrinkage coefficients, which varied according to each model used, and are given in APPENDIX G. The ACI 209, Mokhtarzadeh variation, CEB-FIP 1990, Muller, AASHTO LRFD and Mazloom creep and shrinkage models were used in Phase 1. Also, the aging coefficients used for each set of girders below were the same, because all of the instrumented girders were produced at Plant A.

Table 7-3. PBEAM input parameters for instrumented girders

Girder Set (Pour)	Loading Age	*V/S* Ratio	Avg *RH* (%)	f'_c (psi)	E_c (ksi)	Prestrain (x10^-3)
73037 122’ MN54’s (weekend cure)	4	3.67	73	11280	6280	6.943
73038 122’ MN54’s (weekday cure)	1	3.67	73	11180	6310	6.970
73038 93’ MN54’s (weekday cure)	1	3.67	73	11700	6390	6.879
27B58 119’ MN45 (2-day cure)	2	3.63	73	10700	5700	7.046
27B58 119’ MN45’s (1-day cure)	1	3.63	73	10700	6380	6.651
73044 131’6” MN63’s (weekday cure)	1	3.7	73	10700	6130	6.743
73044 131’6” MN63’s (weekend cure)	3	3.7	73	10400	6030	6.791

The important PBEAM inputs for Phase 2 of the validation modeling are given in Table 7-4. Not included in Table 7-4 are the creep and shrinkage coefficients, which varied according to each model used. The ACI 209, Mokhtarzadeh variation and Muller creep and shrinkage models were used in Phase 2.

Table 7-4. PBEAM input parameters for selected historical girders

Girder Label	Aging coeff. 1	Aging coeff. 2	Loading Age	*V/S* Ratio	Avg *RH* (%)	f'_c (psi)	E_c (ksi)	Prestrain (x10^-3)
27M 72'6.5" 25025	0.28	0.99	1	3.61	72.5	11400	6370	6.848
36M 93'0" 17532	0.28	0.99	1	3.54	73.9	10500	6420	6.703
MN45 111'3" 27B65	0.63	0.97	1	3.7	66.3	12300	7380	6.789
MN54 130'6" 14549	0.28	0.99	1	3.67	72.8	10300	6300	6.687
MN63 145'6" 27302	0.63	0.97	1	3.63	75.0	13000	7220	6.778
72M 139'9" 07581	0.28	0.99	1	3.37	68.4	10500	6310	6.746
81M 156'9" 86820	0.28	0.99	1	3.35	70.7	10500	6110	6.724

7.4.3 Modeling Results

7.4.3.1 Phase 1: Instrumented Girders

As previously mentioned, the validation of PBEAM began with verifying the release camber outputs. After conducting Phase 1 of the modeling, it was evident that PBEAM was accurately outputting the release camber of the instrumented girders, when compared to the calculated release camber predictions accounted for in the analysis. Table 7-5 contains the release camber predictions for the instrumented girders, which can also be found in Section 6.3.2, and the PBEAM release camber outputs. It should be noted that the instrumented girders were initially modeled in PBEAM as end-supported to determine the on-bed camber at release.

It should be noted that the PBEAM release camber outputs were always slightly higher than the release camber predictions, as can be seen in Table 7-5, by as much as 0.10 in (2.54 mm). This was due to the fact that the moments of inertia for the MN girder shapes in PBEAM were lower than the real values (by no more than 1.0%), which resulted in a corresponding slight increase in camber. Another cause for discrepancy between the release camber predictions and PBEAM camber outputs was the inherent error in the input procedure for the concrete material properties. Because PBEAM internally calculates the elastic modulus at release based on the input 28-day E_c and the aging coefficients, the algorithm for inputting these values was designed so that the E_{ci} calculated by PBEAM was as close as possible to the E_{ci} determined by the measured f'_{ci} values and the Pauw equation for E_c, as described in Section 7.4.1. However, this algorithm did not produce E_{ci} values in PBEAM that *exactly* matched the calculated values.

Both of these issues are discussed in further detail in APPENDIX D. Based on the results below including the known reasons for discrepancies, it was determined that PBEAM produced sufficiently accurate and reliable release camber outputs.

Table 7-5. PBEAM release camber validation

Girder Set	Release Camber Prediction	PBEAM Output
73037 122’ MN54’s (weekend cure)	2.44”	2.45”
73038 122’ MN54’s (weekday cure)	2.86”	2.93”
73038 93’ MN54’s (weekday cure)	1.23”	1.28”
27B58 119’ MN45 (2-day cure)	3.44”	3.45”
27B58 119’ MN45’s (1-day cure)	2.89”	3.00”
73044 131’6” MN63’s (weekday cure)	2.37”	2.46”
73044 131’6” MN63’s (weekend cure)	2.32”	2.33”

In order to further validate PBEAM, the long-term camber PBEAM outputs were compared to the actual measured cambers for the instrumented girders. Because the girders were moved to the storage yard after strand release and because the camber measurements were recorded while they sat on the storage bunks, the girders were modeled as bunk-supported in PBEAM so that the long-term camber outputs could be compared to the measured camber values. The bunk locations for each girder were measured so that the supports in PBEAM accurately represented the real support conditions. As previously mentioned, various creep and shrinkage models were chosen for use in this comparison. Figure 7-9 and Figure 7-10 show the measured cambers recorded for two of the seven distinct sets (from Table 7-3) of instrumented girders (73038 93 ft MN54 and 73044 131 ft-6 in MN63 (weekday cure)); along with the long-term PBEAM camber outputs using each of the creep and shrinkage models. It should be noted that in Figure 7-9, the measured cambers at erection are included as the last data point in the measured camber results. Because the girders were end-supported at the time of erection, the elastic difference due to bunking was subtracted from the last PBEAM output data point to represent the girders being moved from bunked to end supports. Figures for the remaining five sets of instrumented girders can be found in APPENDIX F.

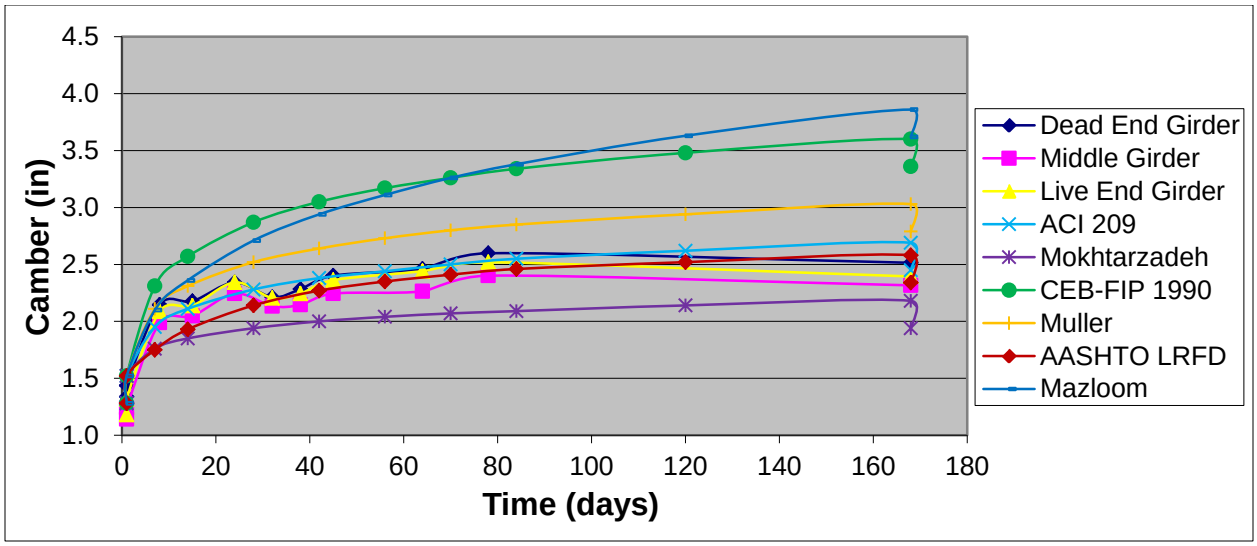

Figure 7-9. Long-term camber comparison for Br. 73038 93' MN54 (weekday cure) girders

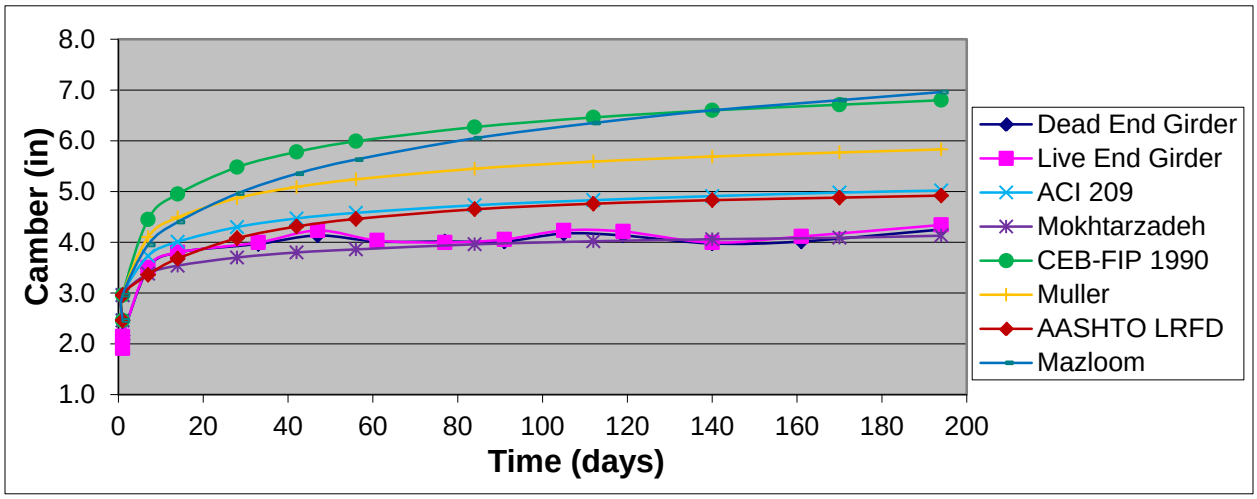

Figure 7-10. Long-term camber comparison for Br. 73044 131'6" MN63 (weekday cure) girders

The results from the above figures, and those of the other girder sets in APPENDIX F, indicate that the Mokhtarzadeh, AASHTO LRFD and ACI 209 creep and shrinkage models most accurately predicted the measured camber behavior. Additionally, the Mokhtarzadeh and ACI 209 models seemed to provide adequate lower and upper bounds, respectively. Thus, these two models were used for further PBEAM validation and modeling. The AASHTO LRFD model also predicted the camber behavior relatively well, but given that it did not predict the camber behavior as well at early ages and that it always lay between the Mokhtarzadeh and ACI 209 models, it was not used for further PBEAM modeling. The CEB-FIP 1990, Muller and Mazloom models consistently overestimated the camber behavior of the instrumented girders, with the Muller model being the best of that group. Therefore, the CEB-FIP 1990 and Mazloom models were no longer used and the Muller model was used as an upper bound only when the ACI 209 model underpredicted the camber behavior of further investigated girders.

7.4.3.2 Phase 2: Selected Historical Girders

The selected historical girders, detailed in Section 7.4, served as another valuable database for further validation of the PBEAM program. The major difference between Phase 2 and Phase 1 of the PBEAM validation modeling was that the camber of the historical girders was only recorded at the time of release and erection. This meant that the lift/set camber, the bunking conditions during storage, and the environmental conditions at the time of erection were never recorded and had to be approximated in the camber comparison.

The lift/set camber of each girder was estimated using the data from Section 3.4.2. The bunking conditions were approximated by using an assumed bunk location of L/20, which was determined to be a reasonable upper bound for long girders stored at Plants A and B. Similar to Phase 1, each girder was initially modeled as end-supported to determine the on-bed camber at release. Then, the girders were modeled on the L/20 bunked supports to determine the long-term camber after release. However, because measured cambers were recorded when the girders were end-supported at the time of release and erection, the line shown in the following figures represents the end-supported case and the bunk-supported case is represented as a "jump" at the time of erection. This "jump" at the time of erection represents the camber that would be present if the girders had sat on the L/20 bunks and then were moved to end supports at bridge erection (i.e., the elastic difference due to bunking was subtracted from the bunked PBEAM output).

The effect of solar radiation was taken into account by comparing the environmental conditions present at the time of erection to the observed results of the solar radiation effects discussed in Section 7.3.1. Camber increases of 15% and 10% were used for May-August and September-April erection dates, respectively. These values were determined from the observations discussed in Section 7.3.1 and represent reasonable upper bounds for the effect of solar radiation on camber for those months of the year. The effect of solar radiation is shown as the second "jump" at the time of erection.

If the actual recorded erection camber fell within the upper bound determined from the effects of bunking and solar radiation, the PBEAM model was considered validated. It should be noted that this is clearly a much less precise form of model validation, but it is still appropriate given that the goal is to predict camber behavior with even less information than is known with these historical girders. Additionally, because all of the instrumented girders were produced at Plant A, this phase of modeling provided an opportunity to validate PBEAM for girders produced at Plant B.

Figure 7-11, Figure 7-12 and Figure 7-13 contain the measured release, lift/set (approximate) and measured erection cambers for three of the seven selected historical girders; along with the PBEAM modeling results with the upper bound due to bunking and solar radiation effects included as "jumps" at the time of erection. These figures are representative of the others and highlight an important topic for discussion. Because of the amount of data required to make revised release camber predictions for each girder, this modeling procedure was conducted for girders from just one pour from each bridge. Figures for the remaining four selected historical girders can be found in APPENDIX F.

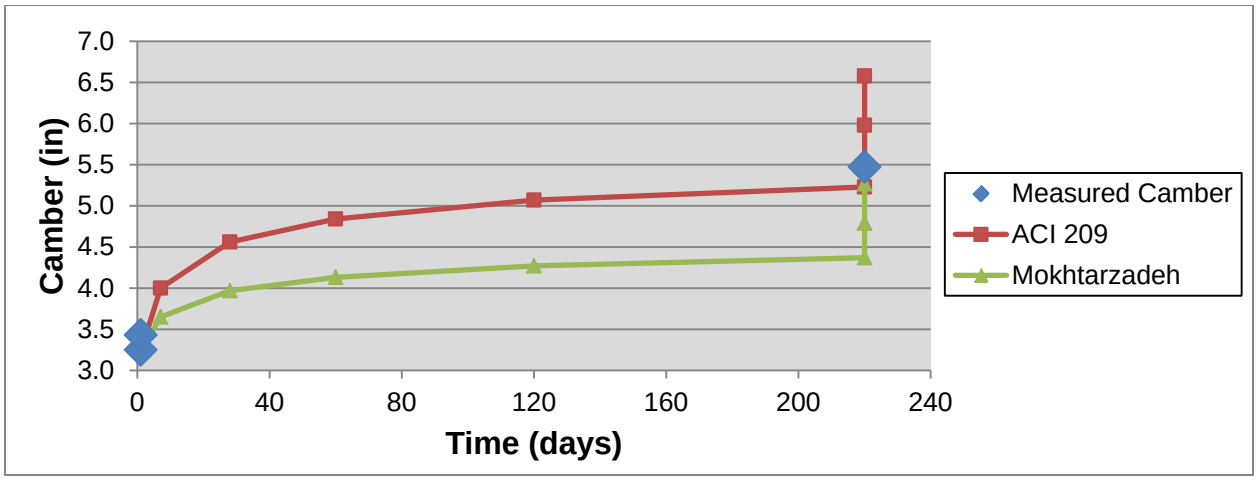

Figure 7-11. Camber comparison for Br. 14549 MN54 130'6" girder

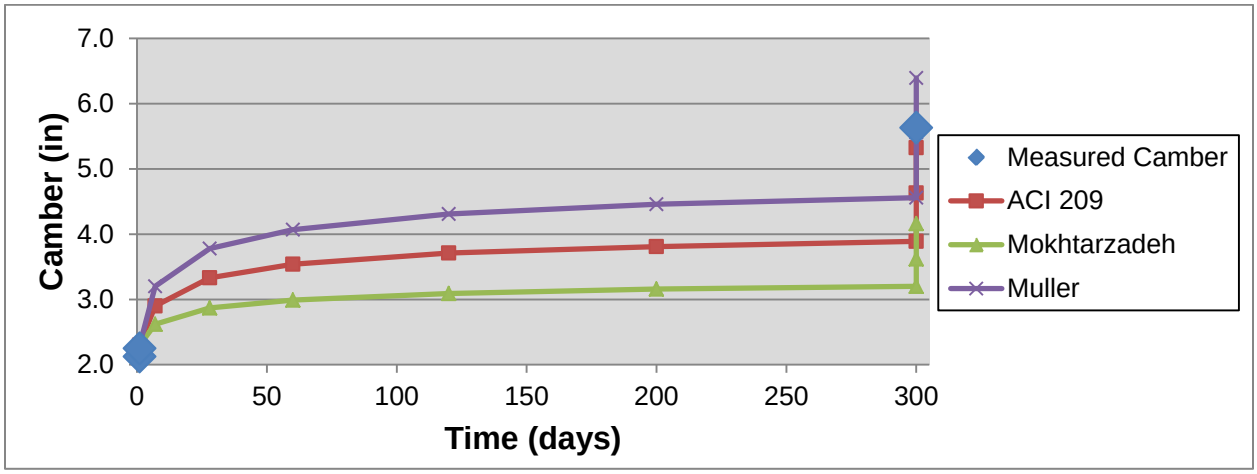

Figure 7-12. Camber comparison for Br. 86820 81M 156' 9" girder

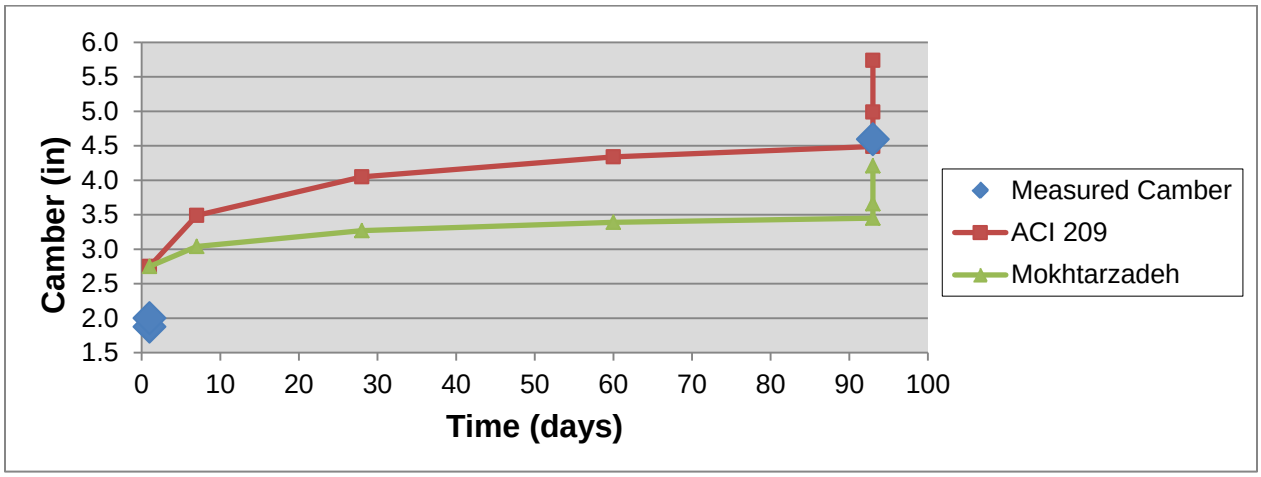

Figure 7-13. Camber comparison for Br. 27B65 MN45 111' 3" girder

The results from the above plots give insight into some interesting observations. The first is with regard to release camber. Figure 7-11 and Figure 7-12 indicate that PBEAM was able to predict the measured release camber very accurately. However, the PBEAM release camber output shown in Figure 7-13 overestimated the measured release camber. The MN45 111 ft-3 in girder shown in Figure 7-13 and the MN63 145 ft-6 in girder shown in APPENDIX F were both fabricated at Plant B and both had release cambers that were well below the PBEAM and revised release camber predictions. Given that the release camber of the material-test girders from Plant B matched the revised predictions, as discussed in Section 6.3.1, the inaccuracy shown in Figure 7-13 must be the result of inaccurate assumptions made about the recorded data (i.e., ambient temperatures at strand pull and concrete-steel bond, and concrete temperatures at bond and release) or other effects that are not included in the predictions (i.e., thermal gradients, unknown procedures during strand release, and pre-release cracking). For example, the formation of pre-release cracks was occasionally observed at both plants when the time between side-form removal and strand cutting was too long. It was reported by Ahlborn, et al. (2000) that this caused a significant reduction in release camber, as discussed in Section 2.9. These results emphasize the importance of having accurate historical data and, if possible, full knowledge of pull, pour and release procedures, when making camber predictions.

The second important observation is with regard to the long-term camber comparisons. Figure 7-11 and Figure 7-13 indicate that the actual erection cambers fell within bounds created by the ACI 209 and Mokhtarzadeh variation creep and shrinkage models, which matches the results from Phase 1. However, Figure 7-12 shows that the ACI 209 and Mokhtarzadeh variation models both under-predicted the erection camber, even with the inclusion of the expected bunking and solar radiation effects. This high erection camber may be the result of bunking locations greater than L/20 or extreme solar radiation effects. However, it is also possible that the ACI 209 model does not always provide an upper bound for the long-term camber behavior. As such, the Muller model provided an upper bound for these results.

7.4.4 Discussion of Results

The release camber results from Phase 1, discussed in Section 7.4.3.1, showed that PBEAM matched the release camber predictions on which the PBEAM inputs were based to within 0.10 in (2.54mm). This small discrepancy was due to inherent sources of error in the concrete moduli of elasticity and cross-sectional dimensions, which all had to be modified for input in PBEAM and are explained in Section 7.4.3.1 and APPENDIX D.

Furthermore, the Phase 1 and Phase 2 PBEAM validations for long-term camber indicated that the ACI 209 creep and shrinkage models provided the best predictions. Even though these models usually slightly overestimated the camber behavior, they were by far the most consistently accurate models. The results also showed that the Mokhtarzadeh variation and Muller models provided appropriate lower and upper bounds, respectively, of the long-term camber behavior. These three models were used in the parametric study discussed in Section 7.5, and the camber prediction modeling discussed in Section 8.4.

7.5 Additional Effects: PBEAM Parametric Study

After validating PBEAM for camber modeling, it provided a valuable tool for examining the influence of additional time-dependent effects on camber behavior. Effects of special interest were those that were variable, and thus could lead to inconsistencies in camber among girders of

the same design. These effects included ambient relative humidity, ambient and concrete temperatures during the curing process, length of cure, concrete strength and associated elastic modulus, and bunking conditions. The effects that needed further investigation in PBEAM were the length of cure, ambient relative humidity, and bunking conditions.

These effects were uniquely analyzed in PBEAM to determine how each of these parameters might influence the long-term camber behavior. The logic employed, the inputs used for the investigation of each parameter, and the results of the modeling are described in the following sections.

7.5.1 Length of Cure

Generally, girders are poured around mid-day and released the following morning, provided that they have achieved the required release strength. This means that on weekdays, girders are cured in approximately 18-24 hours. However, it is not uncommon for girders to be poured on Fridays and released on Monday morning, resulting in a cure time of almost three days. The most obvious consequence of this situation, according to the historical data, is that weekend-cured girders had higher concrete release strengths and elastic moduli, as a result of the long curing time, which could result in lower release and erection cambers. However, it was found that the discrepancy in camber between weekend- and weekday-cured girders was not nearly as evident at release as it was at erection.

To examine the effect of weekend curing, girders from the historic database were carefully selected so that their shape, length, strand pattern and design cambers were identical. Furthermore, only girders that were poured within 2-3 weeks of each other were compared, so that their ages at bridge erection were similar. Because the effect of weekend-curing was more noticeable at erection, the following figure(s) compare "normalized erection cambers." Unlike in the bed position study described in Section 5.3.3, the normalized erection cambers represent the ratio of the measured to design cambers at erection. Adjustments were not made for release strength because that was essentially the variable studied (i.e., longer cure times mean higher release strengths). For this study, the erection cambers of approximately 210 girders from ten different bridges were examined.

Figure 7-14 shows an example of a typical trend for this study, where on average, the weekend-cured girders had lower erection cambers than those cured on weekdays. In fact, of the ten bridges examined, nine had weekend-cured girders with lower cambers than the weekday-cured girders in the same bridge, and the remaining one had cambers that were nearly identical. Figures for the remaining nine bridges are included in APPENDIX A.

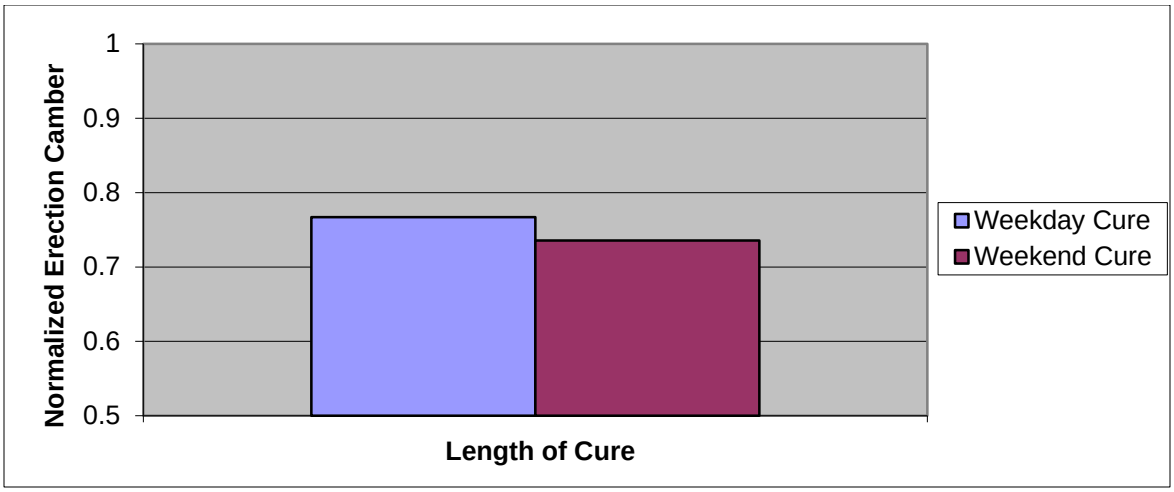

Figure 7-14. Normalized camber of weekend vs. weekday cured girders for Br. 19850

Table 7-6 summarizes the average normalized erection cambers of both weekday- and weekend-cured girders for all ten bridges. On average, the weekend-cured girders had normalized erection cambers that were approximately 6% lower than those cured on weekdays.

Table 7-6. Weekday vs. weekend cure normalized camber results

Bridge #	Weekday Cure	Weekend Cure	% Difference[1]
17532	.967	.859	12.7
01531	.914	.846	8.11
19561	.905	.888	1.89
27R20,21	.930	.872	6.63
19850	.767	.736	4.28
14816	.755	.759	-0.50
07581	.735	.720	2.21
72013	.712	.680	4.78
69844	.810	.700	15.8
14549	.857	.809	5.96
Total			6.18

[1]Percent difference determined as ((weekday cure value – weekend cure value)/weekend cure value)

An important observation that can be made from the historical data regarding the practice of weekend curing is that even if the difference in *release* cambers seemed negligible, the girders cured on weekends did not camber up as much over time as those cured on weekdays. It was not clear why the effect of weekday versus weekend cure did not manifest itself at release through the higher concrete release strengths (and thus the elastic moduli) that were realized for the weekend-cured girders. One of the reasons for the negligible difference at release was that the actual nominal difference in camber was less at release and fabricator measurements were often simply rounded to the nearest 1/8 in (3.18 mm). Another reason was that the extended curing time resulted in cooler girder temperatures at release and, thus, a greater recovery in strand stress at release. Additionally, when fabricators use steam curing, they often keep it on low or turn it off completely for girders cast on Fridays, because there is no concern about achieving the required release strength, which results in a lower temperature at the time of concrete-steel bond. It should also be noted that because the weekend-cured girders have higher elastic moduli at release, they will experience less elastic shortening losses.

To appropriately analyze these effects, the girder design from the 73044 MN63 instrumented girders was used because it had fairly average release and erection design cambers. In order to study the possible effect of the cooler curing temperatures, one weekday-cured girder and two separate weekend-cured girders were examined using the thermal effects analysis and modeling in PBEAM. The weekday-cured girder served as the control for comparison, and was assumed to have a f'_{ci} and E_{ci} of 7500 psi and 5515 ksi, respectively. Both weekend-cured girders were modeled with a higher f'_{ci} and E_{ci} of 8800 psi and 5974 ksi, respectively, which was consistent with the values calculated from the concrete strength-aging curve.

As discussed in Section 5.3.1, using thermal curing data obtained from the fabricators, the concrete temperature at the time of strand release was approximated as 97 °F and 70 °F for the weekday- and weekend-cured girders, respectively. It was also approximated using this thermal curing data, that the average concrete temperature at the time of concrete-steel bond was 140 °F. However, for curing situations where no steam was used or it was kept on low, the average temperature at the time of concrete-steel bond was approximated as 122 °F. An example of thermal curing data obtained from Plant A for steam and heat-of-hydration cures are shown in Figure 7-15 and Figure 7-16, respectively.

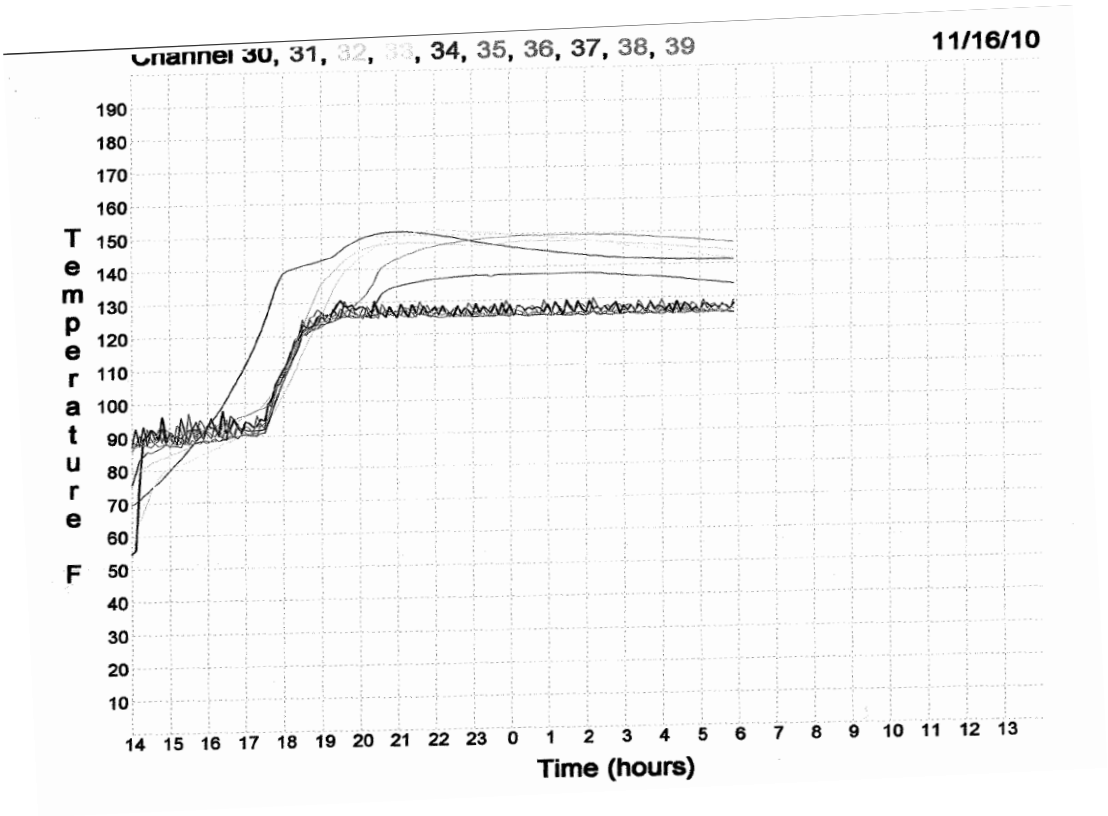

Figure 7-15. Thermal curing data for a steam cure

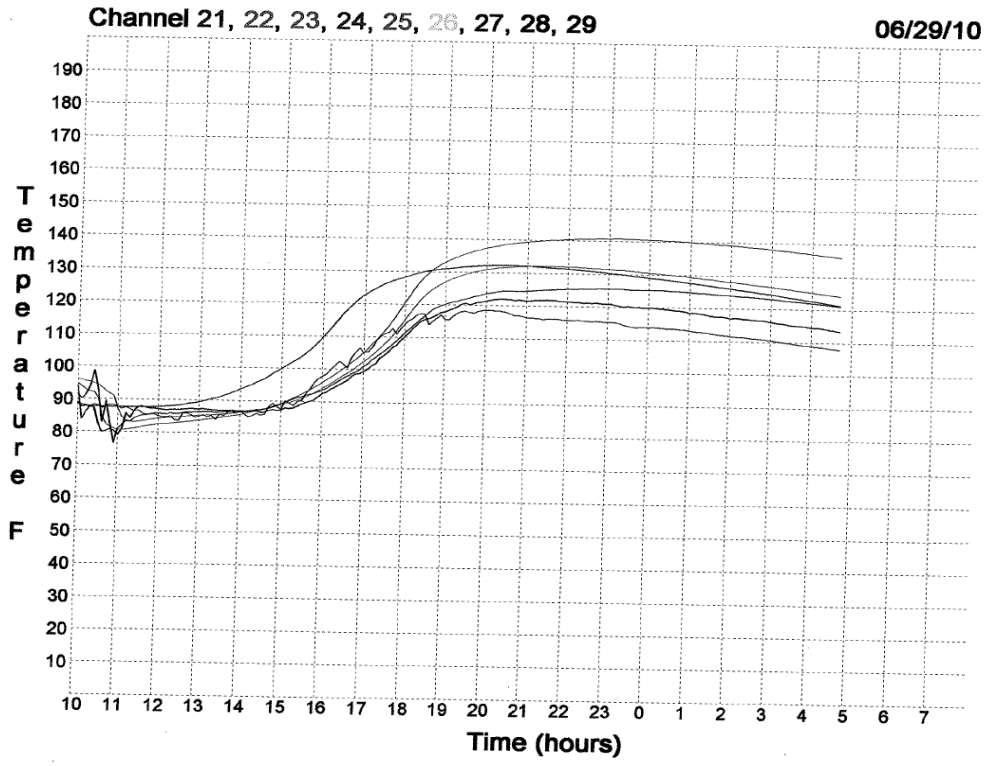

Figure 7-16. Thermal curing data for a heat-of-hydration cure

To isolate the effect of higher concrete strength and elastic modulus, both the weekday and weekend 1 girders were assumed to have concrete temperatures at concrete-steel bond and strand release of 140 °F and 97 °F, respectively. Using the thermal effects analysis, it was found that these girders had a reduction in strand stress at release of approximately 8.0 ksi and 8.1 ksi, respectively, due to thermal effects. The 0.1 ksi difference in these two results was due to the difference in the concrete elastic modulus of the two girders. The weekend 2 girder, however, was assumed to have concrete temperatures at concrete-steel bond and strand release of 122 °F and 70 °F, respectively, resulting in a reduction in strand stress at release of 5.1 ksi due to thermal effects. It was also found that the weekday- and weekend-cured girders had reductions in strand stress of 15.8 ksi and 14.8 ksi, respectively, due to elastic shortening. Thus, total stress losses at release for the weekday, weekend 1 and weekend 2 girders were 23.8 ksi, 22.9 ksi and 19.9 ksi, respectively. Therefore, it was determined that the cooler concrete temperatures often experienced during weekend curing (i.e., weekend 2 girder) resulted in less stress loss due to thermal effects. This analysis is discussed in more detail in APPENDIX B. It should be noted that all other parameters (i.e., relaxation (2 days), aging, creep and shrinkage, initial strand stress (202.5 ksi) and ambient temperatures at the time of strand pull and concrete-steel bond (70 °F)) were kept constant for the weekday and weekend-cured girders.

To investigate the possible effect that length of cure might have on the camber at erection, these three separate girders were modeled in PBEAM for a period of one year. The concrete material properties were kept consistent with those described above, and the resulting strand stress at release was converted to an initial strain at release for input in PBEAM. The varied parameters and important PBEAM modeling inputs are given in Table 7-7.

Table 7-7. Length of cure varied parameters and PBEAM model inputs

Girder Label	Length of Cure	Temp at Bond (°F)	Temp at Release (°F)	f'_{ci} (psi)	E_{ci} (ksi)	Strain just prior to release (x10^-3)
73044 MN63 weekday	1 day	140	97	7500	5515	6.75
73044 MN63 weekend 1	3 days	140	97	8800	5974	6.74
73044 MN63 weekend 2	3 days	122	70	8800	5974	6.85

The camber comparison for the camber after one year for the three girders is shown in Figure 7-17. The results indicate that the nominal difference in release cambers was smaller than the difference in long-term cambers, which was expected. It was also found that the nominal difference in release camber between the weekday and weekend 1 girders was 0.200 in (5.08 mm) and only 0.125 in (3.18 mm) between the weekday and weekend 2 girders. This result was expected given that the cooler concrete temperatures at concrete-steel bond and strand release resulted in less strand stress loss due to thermal effects. Additionally, considering that this latter camber difference was only 1/8 in (3.18 mm), it is very possible that measurement rounding was part of the cause of the camber discrepancy not being as significant at release. The nominal (and percent) camber difference at one year was 0.35 in (8.9 mm) (8.25%) for the weekday and weekend 1 girders and 0.22 in (5.6 mm) (5.19%) for the weekday and weekend 2 girders. Both of these results are within the range of erection camber discrepancies observed in the historical data (and shown in Table 7-6). Because of these results, it was determined that the discrepancy in camber between weekend- and weekday-cured girders was not as significant at release due to the effect of cooler concrete temperatures at concrete-steel bond and strand release. However, because of the effect of higher concrete strengths and associated elastic moduli at release for the weekend-cured girders, there is still a considerable discrepancy in the cambers at erection.

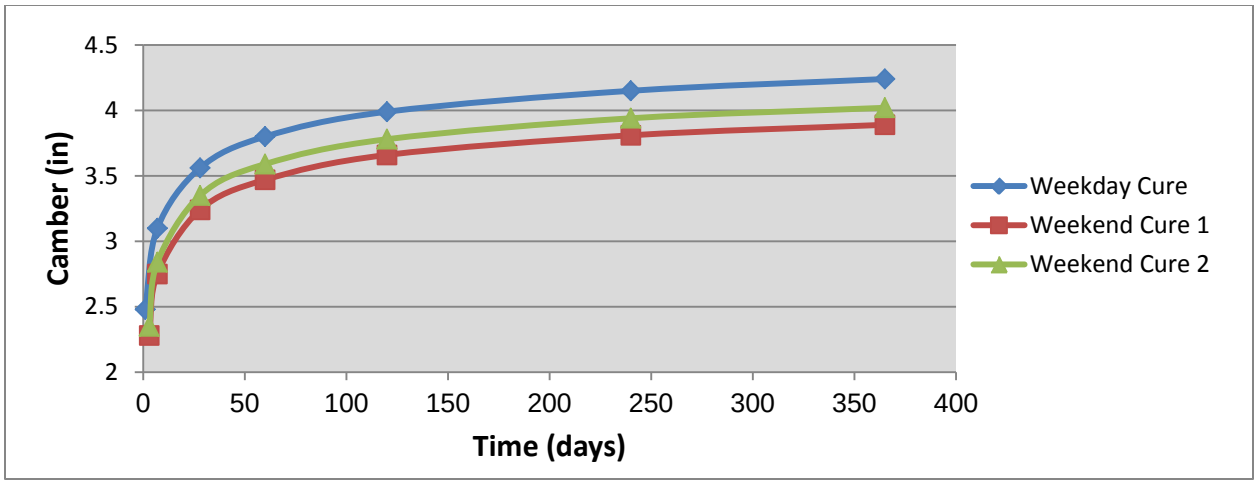

Figure 7-17. Length of cure PBEAM modeling results

7.5.2 Relative Humidity Revisited

It was observed, and discussed in Section 7.3.2, that ambient relative humidity affects the daily measurement of camber through the "pausing" of prestress losses. This is associated with the effect of relative humidity on the creep and shrinkage of concrete. Considering that concrete creep and shrinkage have a large influence on long-term camber behavior and that the relative humidity in Minnesota can change dramatically from day to day and season to season, it was important to investigate this effect. To determine the possible range of this effect, realistic upper and lower bounds were used for the relative humidity. As previously mentioned in Section 7.3.2, daily average relative humidity data was collected from the Princeton, MN and New Richmond, WI weather stations (near Plant A and B, respectively). Because girders typically sit in storage for at least one week, it was found that 55% and 85% were appropriate lower and upper bound average relative humidities for any given 7-day period. These two bounds were used in the PBEAM modeling to determine the realistic range of the relative humidity effect on camber.

To study the effect of relative humidity on camber, Sets 2 and 4 of the instrumented girders (three 73038 93 ft MN54's and four 73044 131 ft MN63's) were modeled in PBEAM. Even though each creep and shrinkage model has differing sensitivity to changes in relative humidity, only the ACI 209 and Mokhtarzadeh variation models were used in this study because those were the ones primarily used for the PBEAM validation. The girders were modeled for approximately 60 days, representing an extended period of very high or very low relative humidity. Figure 7-18, Figure 7-19 and Figure 7-20 show the results of the relative humidity modeling and the measured cambers for each girder set.

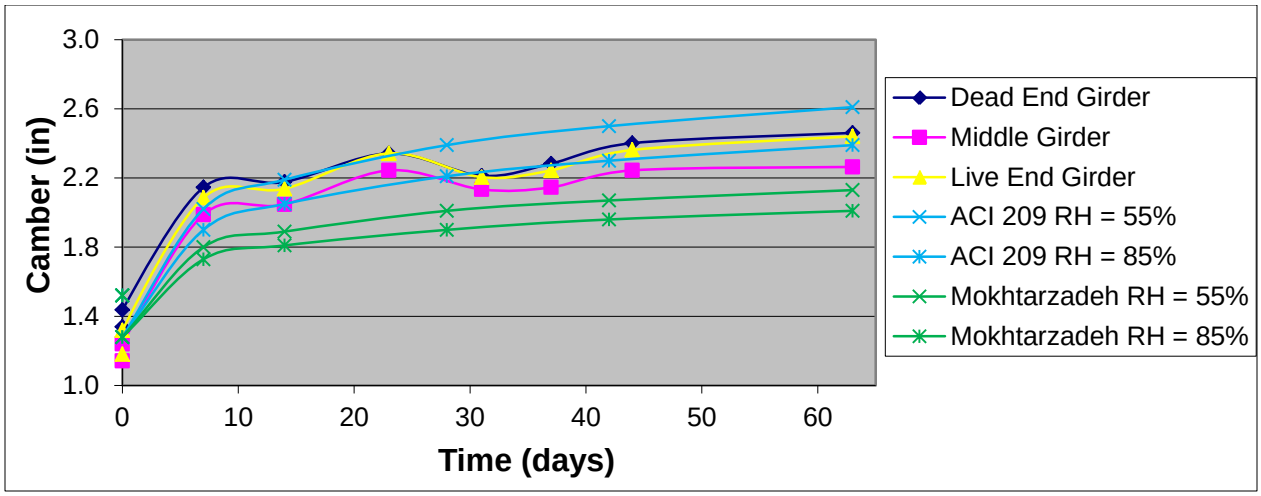

Figure 7-18. Effect of relative humidity on camber (Set 2 modeling results)

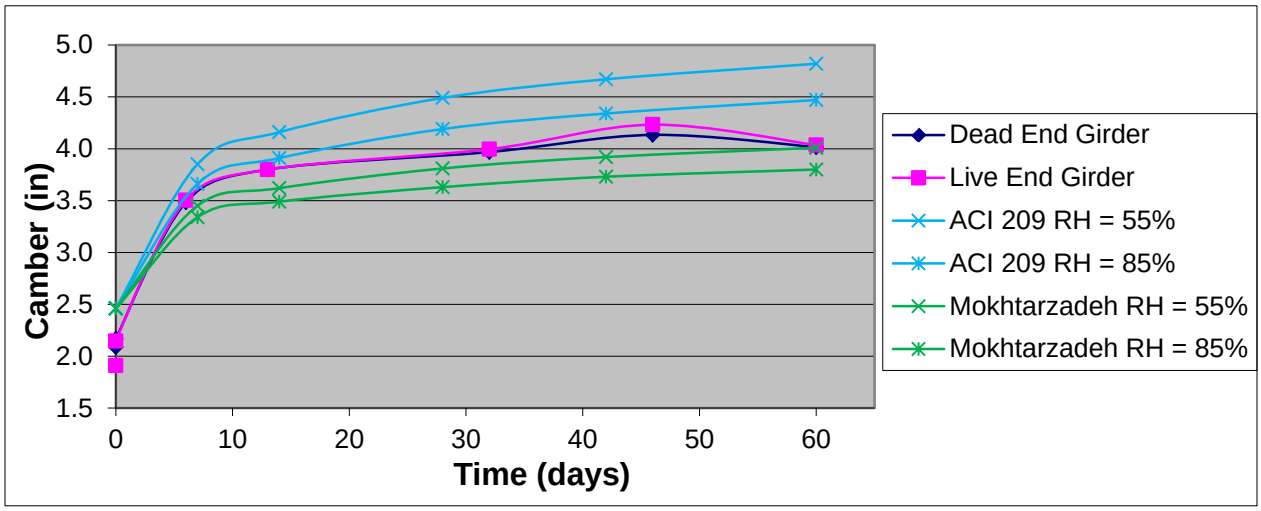

Figure 7-19. Effect of relative humidity on camber (Set 4 (weekday cure) modeling results)

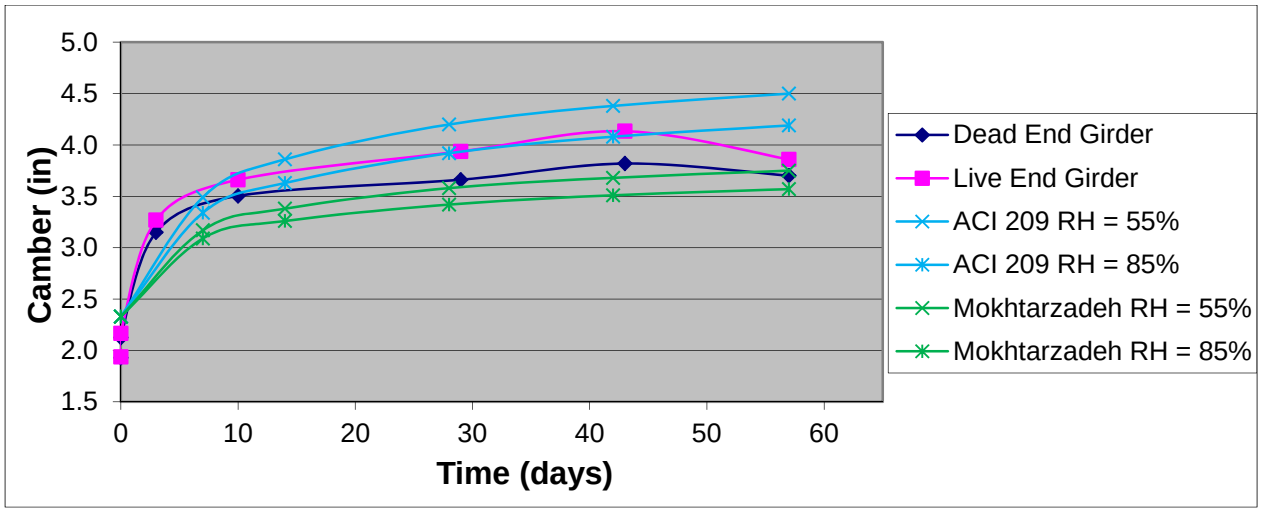

Figure 7-20. Effect of relative humidity on camber (Set 4 (weekend cure) modeling results)

The results indicated that the camber variability range due to a ±15% change in relative humidity was approximately ±4.0% for the ACI 209 model and ±2.8% for the Mokhtarzadeh variation model at 60 days, given an assumed average relative humidity of 70%. This means that even if a girder had experienced an extended period of very low (e.g., 55%) or high (e.g., 85%) relative humidity, its camber should not have been significantly affected. It should be noted, however, that these results contradicted those from Section 7.3.2, in that an increase in relative humidity caused *lower* cambers. This was likely due to the fact that there are competing effects taking place; an increase in relative humidity causes lower creep and shrinkage *and* less prestress losses.

7.5.3 Bunking/Storage Conditions

The locations of the bunks (girder supports) in the storage yards at Plant A and B are highly variable and have no required limitations. Fabricators typically place girders on bunks that happen to be available and that are not *too* far in from the girder ends. Fabricators at Plant A use a rule-of-thumb method that places bunks at a distance from the girder ends that is equal to the girder depth (no rule-of-thumb was mentioned at Plant B). However, it was observed at both plants that bunking was, at times, inconsistent for girders of similar lengths and design, which could lead to additional camber variability.

The support/bunking conditions experienced by girders in the storage yard can have a significant impact on camber. As discussed further in APPENDIX D, the cantilever effect caused by the overhanging girder ends causes an elastic increase in camber. As the bunks are moved in from the ends of the girder, the added overhanging weight increases this cantilever effect, and thus, leads to an elastic increase in camber. More importantly, bunking has an impact on the long-term camber due to concrete creep, which causes this increase in camber to grow over time. This camber growth associated with bunking conditions can cause significant camber variability, if the girders are not bunked similarly, which would be undesirable at the time of bridge erection. Tadros et al. (2011) discussed the effect of bunking (as described in Section 2.4) and recommended including it in the erection camber design predictions. However, neither the

amount of bunking nor the girder age at erection is known at the time of design. Thus, PBEAM modeling was used to investigate the potential influence of bunking on long-term camber.

In order to properly study the effect of bunking conditions, it was desired to examine the effect on girders with varying length-to-depth ratios using a realistic range of bunking locations. As such, "short" and "long" girders of the shapes 27M, MN54 and 81M and bunking locations of L/20, L/10 and end supported, were chosen for this study. All of the input parameters except shape, length, strand pattern, and support locations were kept identical for each girder. Each girder cross section was designed to meet, but not exceed, the maximum stress limits at the time of release according to the ACI 318-08 design code specifications. However, it should be noted that these stress limits are identical to those specified by AASHTO LRFD 2010, with the exception of the midspan top tension stress at release, which in AASHTO LRFD 2010, is limited to 200 psi. This is a typical practice for bridge designers, and as such, the current MnDOT design calculations were used. A design release concrete strength of 7500 psi was used for this study, resulting in allowable stresses at release of 260 psi, 520 psi and -4500 psi for the midspan tension, end tension and compression stresses, respectively. For the "short" girders, the top tension stress at midspan controlled the design and for the "long" girders, the bottom compression stress at the girder ends (and at midspan) controlled. The girders were also designed using standard (average) release and shipping concrete strengths, aging, relative humidity, strand stress, etc. and were modeled for one year using the ACI 209 creep and shrinkage model. Table 7-8 contains the important parameters that were varied in the study.

Table 7-8. PBEAM inputs for bunking conditions study

Girder Label	Shape	Length (ft)	L/D ratio	# straight strands	# draped strands	Design release camber (in)
27M short	27M	40	17.8	16	8	0.71[1]
27M long	27M	80	35.6	20	8	2.64
MN54 short	MN54	80	17.8	22	6	1.14
MN54 long	MN54	120	26.7	34	8	2.79
81M short	81M	120	17.8	30	8	2.12
81M long	81M	160	23.7	34	8	2.96

[1]Release camber prediction using an f'_{ci} of 7500 psi, the Pauw equation for E_c and no strand stress losses due to relaxation and thermal effects (i.e., stress at pull = 202.5 ksi)

Figure 7-21 shows the potential "erection" camber over the course of one year for the 120 ft MN54 girder. Because it is most appropriate to compare the "erection" cambers, the cambers shown in the plot are those that would be expected when the girder is moved from the bunks to end supports at any age. This was determined by subtracting from the time-dependent camber the difference in the elastic deflection at release of the end-supported and bunked-supported results (to recover the elastic component of deflection due to bunking). The base case represents

the end-supported girder over the course of the entire year. As can be seen in Figure 7-21, the camber increases as the bunks are moved further from the girder ends.

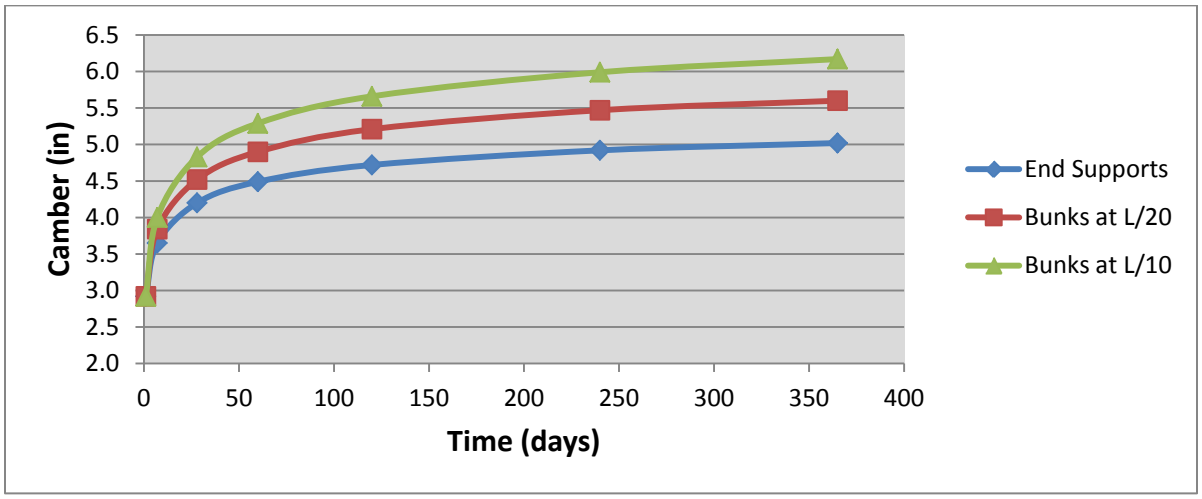

Figure 7-21. "Erection" camber comparison for 120' MN54 girder on bunked supports

To compare the effect that the bunked supports had on each modeled girder, Figure 7-22, Figure 7-23 and Figure 7-24 show the percent increase in camber after one month, four months and one year for the L/20 and L/10 bunk locations over the base case (end supports). Once again, the percent increases shown in the figures are for the "erection" cambers (i.e., the cambers present after the girders are moved from bunks to end supports).

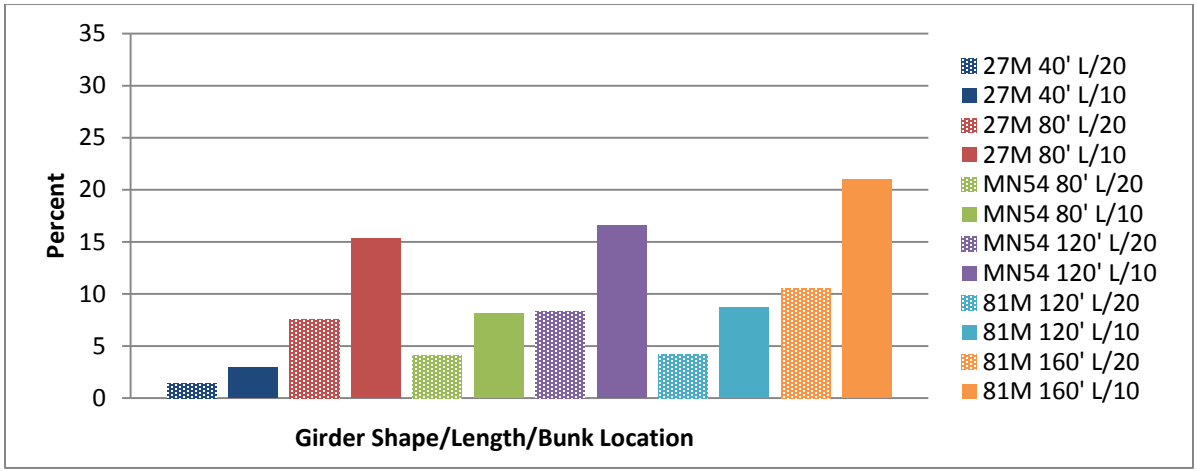

Figure 7-22. Percent increase in camber for bunked girders after one month

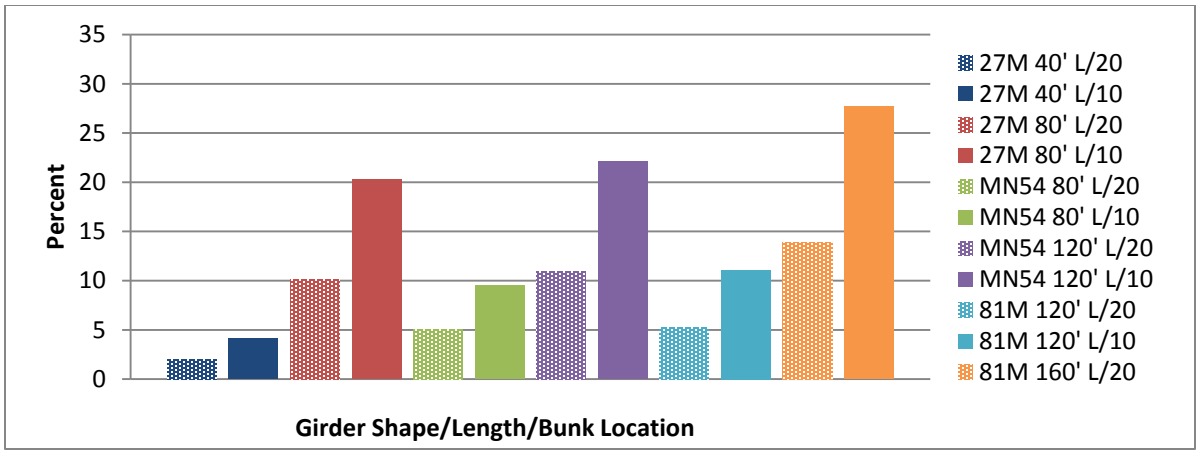

Figure 7-23. Percent increase in camber for bunked girders after four months

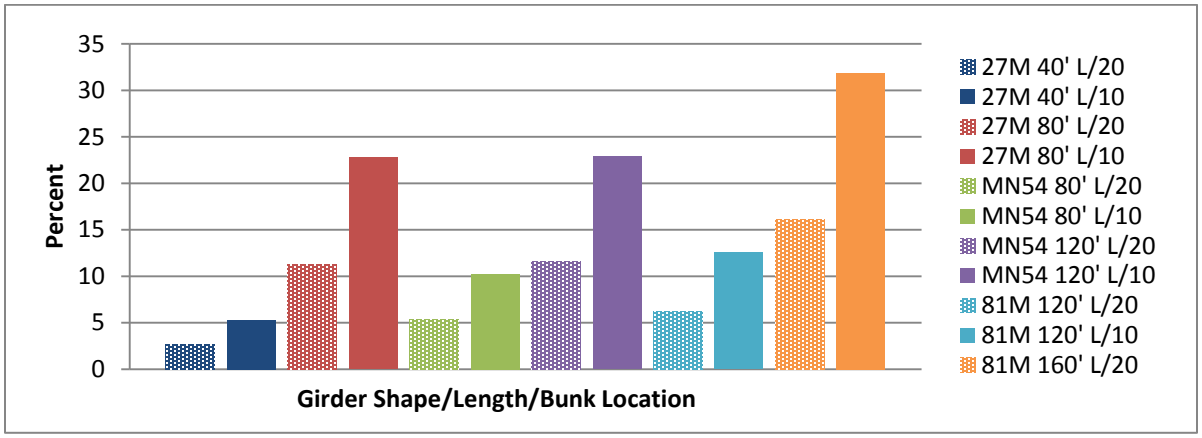

Figure 7-24. Percent increase in camber for bunked girders after one year

It is clear that for the "short" girders of each shape, the bunked supports do not have a large effect on camber. However, the nominal bunk locations are smaller for the "short" girders, so it is useful to examine these results with the nominal bunk locations for each modeled girder. Table 7-9 contains these results.

Table 7-9. Percent increase in camber for bunked girders

Girder Shape	Girder Length (ft)	Bunk Locations (ft)	% Increase (1 month)	% Increase (4 months)	% Increase (1 year)
27M	40	2	1.4	2.0	2.6
27M	40	4	3.0	4.1	5.3
27M	80	4	7.5	10.2	11.3
27M	80	8	15.3	20.3	22.8
MN54	80	4	4.0	5.0	6.1
MN54	80	8	8.1	9.6	11.7
MN54	120	6	8.3	10.9	12.4
MN54	120	12	16.5	22.1	25.0
81M	120	6	4.2	5.3	6.2
81M	120	12	8.7	11.1	12.6
81M	160	8	10.5	13.9	16.1
81M	160	16	20.9	27.7	31.8

These results reveal that the “long” girders of each shape see the most significant increase in camber, especially for bunks located at L/10. This is consistent with the fact that the longer girders of the same shape are more slender (larger L/d ratio) and would be more affected by the cantilever effect of the overhanging girder ends. Additionally, the results indicate that the effect of the bunking conditions is nonlinear. Even though the effect gets worse over time, a significant portion of the effect (percentage-wise) occurs in the first month. Thus, it is not an effect that can be avoided by short storage times.

To establish some limitation on the bunking locations, practicality and camber variability are the most important factors. In other words, if the fabricators establish a regular practice of limiting the bunking to a nominal range, the camber variability could be reduced. Given the results above, it was determined that the camber increase should be kept to less than approximately 10% at one month, 15% at four months and 20% at one year. Thus, for practicality, it is recommended that girders of shapes 27M, 36M and MN45 be bunked at no more than six feet and that girders of shapes MN54, MN63, 72M and 81M be bunked at no more than eight feet. The two separate recommendations are due to the fact that girders with larger depths have typically longer lengths and can handle more *nominal* girder overhang. Finally, it is also recommended that girders from the same bridge be stored with bunk locations that vary by no more than two feet in order to reduce camber variability. Further, more detailed, recommendations can be found in Section 9.2.3.

It should be noted that the preceding recommendations are limitations designed to keep the camber increase due to bunking and the camber variability to a minimum. There may be

situations, however, where the fabricators or designers are concerned that some girders will not reach the desired camber at the time of bridge erection. In these situations, it should be allowed to store those girders on bunks that exceed the above limitations. In any case, the bunks for girders of shapes 27M, 36M and MN45 should never exceed ten feet, and the bunks for girders of shapes MN54, MN63, 72M and 81M should never exceed twelve feet.

Another side-effect caused by storing the girders on bunked supports, especially at early ages, is that the allowable stresses specified by ACI 318-08 (and AASHTO LRFD 2010) may be exceeded. In other words, because the girders are typically designed to nearly reach the allowable stresses at release, when the girders are moved to bunked supports soon after strand release, the allowable stresses could be exceeded due to the additional weight of the overhanging girder ends. According to the modeling results, this was the case for the "short" girders of each shape. Originally, the "short" girders of each shape were designed to nearly reach the midspan top tension stress limit at release (the "long" girders of each shape were designed to nearly reach the bottom compression stress at the girder ends (or at midspan)). This means that the additional tensile stresses created in the girder due to the additional bending caused by the overhanging girder ends resulted in exceedance of the tensile stress limits at midspan. However, it should be noted that the stress limit checks did not account for the effect of mild reinforcement in the top flange that could be used to resist tensile stresses. A summary of those results is shown in Table 7-10.

Table 7-10. Tension stress limit exceedance for bunked girders

Girder Label	Bunk Locations	Midspan Top Tension Stress (psi)
27M short	L/20	OK[1]
27M short	L/10	326
27M long	L/20	OK
27M long	L/10	OK
MN54 short	L/20	322
MN54 short	L/10	491
MN54long	L/20	OK
MN54 long	L/10	OK
81M short	L/20	300
81M short	L/10	520
81M long	L/20	OK
81M long	L/10	OK

[1]Denotes a midspan top tension stress that did not exceed the allowable stress of 260 psi

These results indicate that the effect is worse for more extreme bunking conditions, providing more reason to adhere to the specified limitations discussed above. Even though it is common for the actual concrete strength at release (or shortly after release) to be, on average, approximately 15% higher than the specified design strength, the stresses given above would still exceed the adjusted allowable stresses. Given that this is a side-effect that would need to be calculated by the designer on a case-by-case basis with no knowledge of the actual bunking conditions, it is advised that the designer by aware of this problem and take precautions when designing a girder in which the midspan top tension stress at release is the controlling stress in the design. In those cases, it is recommended that the designer require a stricter limit for the bunking conditions.

7.6 Conclusion

Various factors that affect long-term and erection camber were investigated, including solar radiation, relative humidity, concrete creep and shrinkage, length of cure and bunking/storage conditions. The program PBEAM was first validated for use in release and long-term camber modeling using the instrumented girders and select historical data. It was found that solar radiation affects the measurement of camber by as much as 15% during the course of a day, demonstrating that there is a potential high degree of variability in measured camber. Relative humidity was found to cause changes in concrete creep and shrinkage and induce camber variability. High relative humidity during the winter months was also observed to cause slight increases in camber. Through PBEAM validation, it was found that the ACI 209 creep and shrinkage model provided the best results for long-term camber predictions and that the Mokhtarzadeh ACI 209 variation model provided a consistent lower bound. As such, the ACI 209 creep and shrinkage model was used in the long-term camber modeling and the creation of camber multipliers, as is discussed in the following chapter. Weekend curing was found to cause lower erection cambers than weekday-cured girders, even though the camber discrepancy at release was less evident, because of less thermal prestress losses due to cooler concrete temperatures at concrete-steel bond and strand release. Finally, it was found that bunking/storage conditions can lead to increased cambers, additional camber variability, and possible exceedance of specified stress limits. Bunking limitations were recommended to limit these undesired effects.

These observations and results were used during long-term camber modeling and the creation of camber multipliers; and the influence of each effect was examined further in the following chapter.

CHAPTER 8. LONG-TERM CAMBER PREDICTION

8.1 Introduction

As discussed in Section 1.2, MnDOT uses elastic analysis to predict the camber at release and uses multipliers to estimate the camber at erection. However, as outlined in the previous chapter, effects such as concrete creep and shrinkage and bunking are highly time-dependent, making erection camber predictions difficult, especially when the girder age at erection is highly variable. Therefore, there is motivation to create a set or sets of long-term time-dependent camber multipliers to estimate the girder camber at erection. In order to determine these multipliers, PBEAM was used to conduct camber prediction modeling for a range of girder designs. By comparing the release camber predictions to the long-term camber outputs at various ages, multipliers were created that account for the time-dependent effects that influence camber. PBEAM was also used to determine upper and lower bounds for these effects to investigate the level of camber variability that is possible in realistic situations.

8.2 Methodology

Similar to the bunking conditions parametric study, the girder cross sections used for the prediction modeling were designed to reach, but not exceed, the allowable stress limits at release, according to the ACI 318-08 code provisions (these girder designs were identical to those used in Section 0). It should be noted that these stress limits are identical to those specified by AASHTO LRFD 2010, with the exception of the midspan top tension stress at release, which in AASHTO LRFD 2010, is limited to 200 psi. Additionally, "short" and "long" girders of each most commonly-used Minnesota girder shapes (27M, 36M, MN45, MN54, MN63 and 81M) were used in the modeling. (The 72M shape has been largely replaced by the MN63 shape, which overlaps its length range). The "short" and "long" lengths were determined from minimum and maximum lengths typically used for each shape, according to the designers and fabricators and verified with the historical girder database. Finally, design release and shipping concrete strengths of 7500 and 9000 psi, respectively, were chosen for this study, as they were typical strengths observed in recent bridge designs. In order to appropriately determine the expected camber prediction and lower and upper bounds, it was necessary to choose initial design strengths and use realistic modifications based off of that design (e.g., use an f'_{ci} that is equal to 1.15*7500 to account for the higher strengths at release achieved at the precasting plants). Because PBEAM had already been validated, it was assumed that the predictions could be reproduced for any girder design or cross section. Table 8-1 contains the dimensions and strand patterns for the girders in this study.

Table 8-1. Prediction modeling girder dimensions and strand patterns

Girder Label	Shape	Length (ft)	# straight strands	# draped strands	Design release camber (in)
27M short	27M	40	16	8	0.86[1]
27M long	27M	80	20	8	3.15
36M short	36M	50	16	10	0.95
36M long	36M	95	22	8	3.10
MN45 short	MN45	75	22	6	1.56
MN45 long	MN45	120	30	10	3.12
MN54 short	MN54	85	24	8	1.68
MN54 long	MN54	130	34	8	3.34
MN63 short	MN63	100	32	6	2.26
MN63 long	MN63	145	36	10	3.40
81M short	81M	120	30	8	2.54
81M long	81M	160	34	8	3.52

[1]Calculated using an f'_{ci} of 7500 psi and the Pauw equation for E_c

As discussed in Section 1.2, the current MnDOT design procedure was to use one multiplier (1.5) for all girders in all situations. However, because it was observed that camber increases with time and that erection cambers got closer to the design values as the girders aged, as discussed in Section 3.4.4, it was desired to create different multipliers to be used at various time intervals. The observations made in Section 3.4.4 indicated that, on average, erection cambers were more likely to be significantly less than the design camber at early ages.

To investigate the potential effectiveness of time-dependent multipliers, it was insightful to first examine the erection camber results, as a function of age, from the historical girder database. The dates for which the survey shots, or girder elevations, were taken was recorded for most of the 768 girders for which erection camber data was available. Because the pour dates were also known, an average girder age at bridge erection was calculated. Figure 8-1 shows the measured erection cambers as a percentage of the design camber, plotted against the girder age. Each data point represents a unique set of girders, separated by bridge, girder design and age. However, because it was not realistic to plot each individual girder, the data points are the average of the erection cambers for anywhere from two to forty-plus girders. The girders are also separated by the multiplier used in the original design, as the multiplier was changed in late 2007, as discussed in Section 1.2.

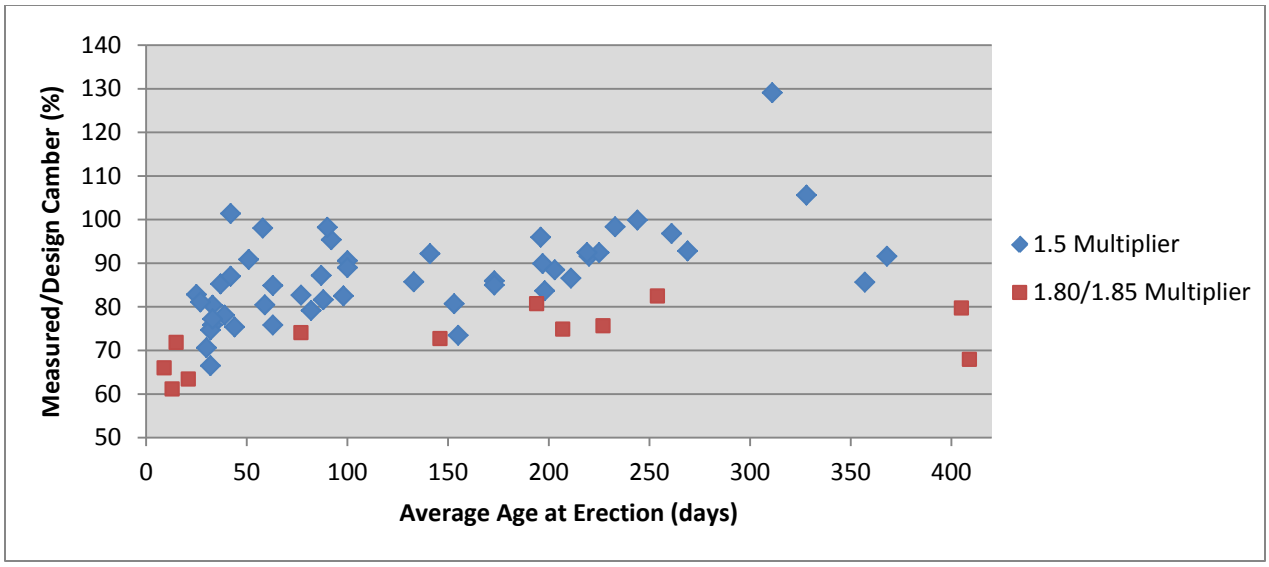

Figure 8-1. Measured/design erection cambers over time

There are a few important observations that can be made from these results. First, only a handful of girders actually matched or exceeded the design erection camber (100% on the above plot). In fact, it is known that for the few sets of girders that did exceed the design camber, the girder elevations were recorded during hot summer days. Even though these were not the only girders to have elevations recorded on summer days, the effect of solar radiation does account for the upper outliers. For the girder set with measured cambers that greatly exceeded the design value (129% and ~310 days on the above plot), the girder elevations were recorded on a hot August day. Additionally, it was believed by the researchers of this study that the girders had large overhangs when bunked, which after 300+ days of storage, led to an unusual increase in camber. However, the actual bunking conditions were not recorded.

Second, the girders that were erected at early ages (less than 100 days) had cambers that were much lower than the design values, as was previously discussed. Third, the switch from the Martin (PCI) 1.80/1.85 multipliers to the 1.5 multiplier did slightly improve the erection camber results, but not to the point where there were no longer any problems. Finally, based on the above results, it appears that the majority of the girders actually shipped in the first 100 days, supporting the method of using more than one multiplier to reflect the increase in camber over time. Figure 8-2 shows the same results as those above, except with the lower and upper bound erection cambers included. These bounds were determined from the lowest and highest cambers recorded for each set of girders.

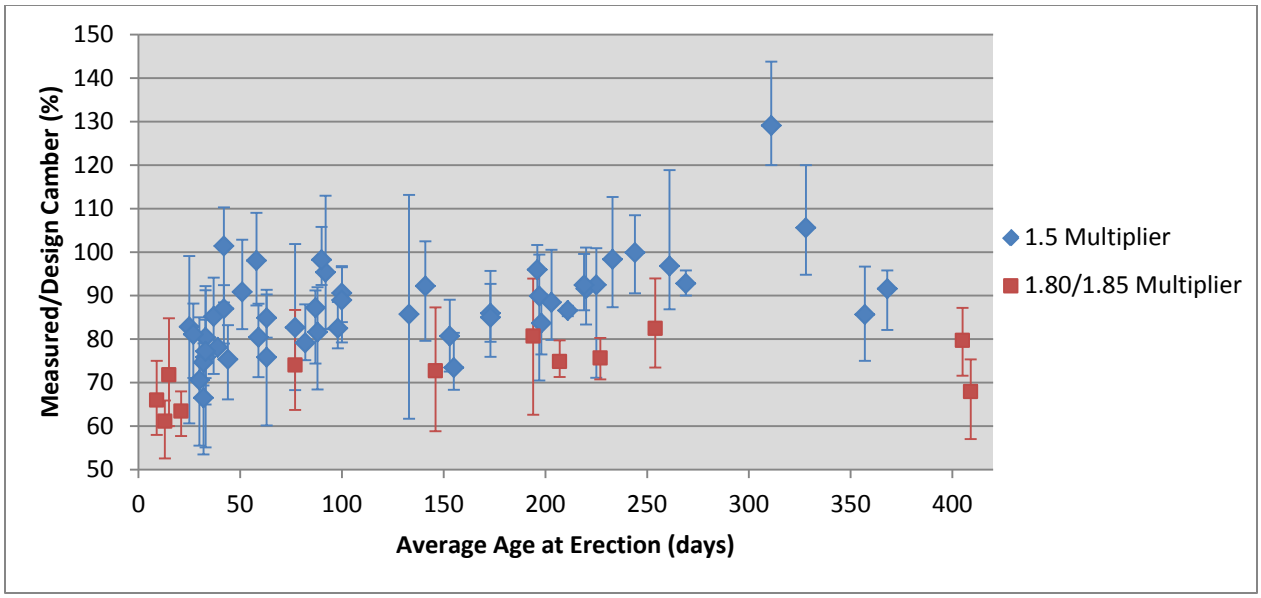

Figure 8-2. Measured/design erection cambers over time (with bounds)

These results indicate that camber variability was, at times, very high. Additionally, the data in the above figure is separated by average girder age at erection, within each bridge project. Thus, if a bridge project was poured or constructed in two stages, camber variability could be increased. The recommendations discussed in Section 9.2 are designed to reduce the amount of camber variability observed at the time of bridge erection.

Finally, as previously discussed in Section 3.4.4, it is also worthwhile to show these results by plotting the nominal measured erection cambers vs. the nominal design values. These results, shown in Figure 8-3, indicate that the nominal discrepancy between the measured and design erection camber values was, for some girders, on the order of 2 in or more.

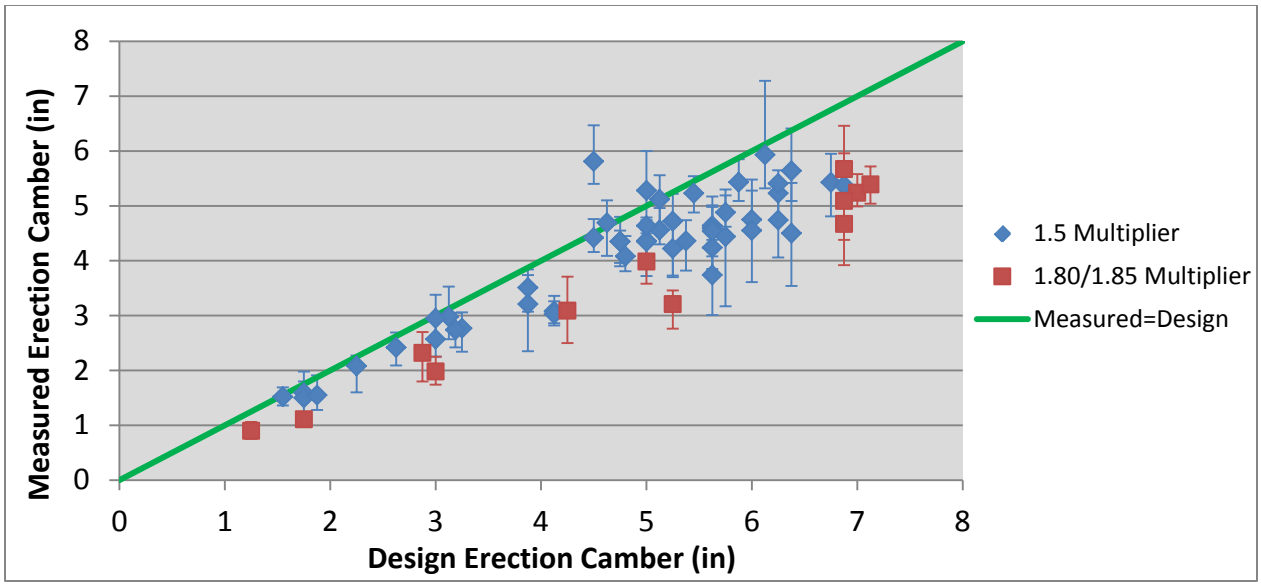

Figure 8-3. Measured vs. design erection cambers

Because it is rare for girders to be stored for more than about one year, as can be seen in Figure 8-1 and Figure 8-2, the girders in this study were modeled for one year, so that multipliers could be determined from the camber results at time intervals of 0-60 days, 61-180 days, 181-365 days, and 366+ days. These time intervals were chosen based on practicality and on the erection camber results shown in the above figures. The release camber for each girder in this study was designed using the current MnDOT design procedure and an improved design procedure based on the recommendations detailed in Section 6.4. Four sets of multipliers were created from the prediction modeling camber results; two sets of recommended multipliers were developed to accompany the current MnDOT design release camber calculations if kept unchanged and the other two sets were developed to accompany the improved design release camber calculations described in Section 6.4. The two sets of multipliers developed for each camber calculation method included a single value multiplier and a set of time-dependent multipliers.

8.3 PBEAM Modeling Inputs

To prepare for the prediction modeling, each important input parameter (i.e., strand relaxation, thermal prestress losses, expected concrete strength and elastic modulus, concrete creep and shrinkage, etc.) was examined to create a lower and upper bound and a "best prediction" value. A realistic minimum, average and maximum value was carefully selected for each parameter based on information gathered in the historical girder database, results of the material testing, thermal effects analysis, PBEAM model validation and parametric study. In order to produce the most "extreme" results, parameter values were grouped together based on whether they would increase or decrease camber. Certain parameters were kept constant. The design initial strand pull force was set at $0.75*f_{pu}$, as was always specified in the bridge designs. The concrete aging coefficients of 0.28 and 0.99 were kept constant, which were the coefficients determined to be used for girders produced at Plant A based on the material testing. Although, it should be noted that the use of the aging coefficients determined for girders produced at Plant B

did not significantly alter the results. Finally, the ACI 209 creep and shrinkage model was used throughout, as it was determined to be the best fit model for camber prediction, as discussed in Section 7.4.4. It should be noted that the Mokhtarzadeh variation and Muller creep and shrinkage models were examined separately and the results are discussed later in this section. The values that would lead to a lower and upper bound and "best prediction" camber for each remaining parameter are given in Table 8-2.

Table 8-2. Prediction modeling input parameters

Parameter	"Low Camber" Value	"Best Prediction" Value	"High Camber" Value
f'_{ci} (psi)	9375	8625	7875
E_{ci} (ksi)	6166	5914	5651
f'_c (psi)	11500	10500	9500
E_c (ksi)	6510	6450	6110
RH	85%	73%	55%
Thermal Losses	5% stress loss	2.5% stress loss	None
Relaxation	6 days	2 days	1 day
Length of Cure	3 days	1 day	1 day
Bunking	L/30	L/24	L/16
Solar Radiation	None	5% camber increase	10% camber increase

Some of these input choices require further explanation. The relative humidity, thermal losses, relaxation, bunking and solar radiation values (shown above) were realistic minimum, average and maximum values, as discussed in previous chapters. The relative humidity values came from the collected weather history data, the thermal losses values from the results of the thermal effects analysis, and the bunking and solar radiation values from field observations.

Regarding the concrete strengths and elastic moduli, the "low camber" values shown in the table above were associated with a 3-day weekend cure situation. It was discussed in Section 7.5.1 that weekend-cured girders typically have higher release concrete strengths and associated elastic moduli, which lead to lower cambers. The "high camber" and "best prediction" values were associated with standard 1-day cures. The release strengths, f'_{ci}, were chosen based on a 5%, 15% and 25% release strength increase over the design strength (7500 psi) for the minimum, average and maximum values, respectively. These percentages were consistent with the results from the historical girder database. The 28-day concrete strengths, f'_c, were also chosen based on examining historical girder data and determining realistic minimum, average and maximum values for f'_c. The elastic moduli at release, E_{ci}, were calculated using the Pauw (ACI 318-08, AASHTO LRFD 2010) equation, as was recommended and discussed in Section 5.2.4. Finally, the elastic moduli at 28 days, E_c, were calculated using the algorithm described in Section 7.4.1

and APPENDIX D, which creates the desired elastic modulus values in PBEAM using the built-in strength-age curve.

8.4 Modeling Results and Discussion

The following figures illustrate representative modeling results for a few of the twelve girders modeled in this study. Figures containing the modeling results of the remaining girders can be found in APPENDIX F. As can be seen in these figures, the "low" camber, "high" camber and "best prediction" camber for each girder were modeled for one year. These modeled cambers represent the cambers that would be present at the time of erection. In other words, the cambers shown in the figures are those that would be present after the girders were moved from bunks to end supports, at any given time. Additionally, the design erection camber that would be calculated using the current MnDOT procedure is shown as a straight-line value in these figures.

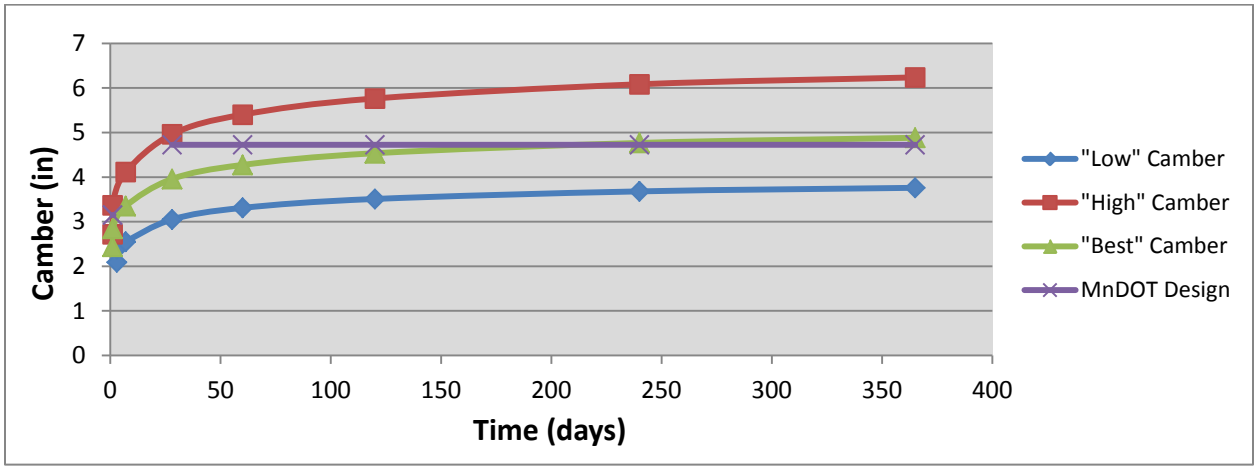

Figure 8-4. Long-term (erection) camber predictions for 80' 27M girder

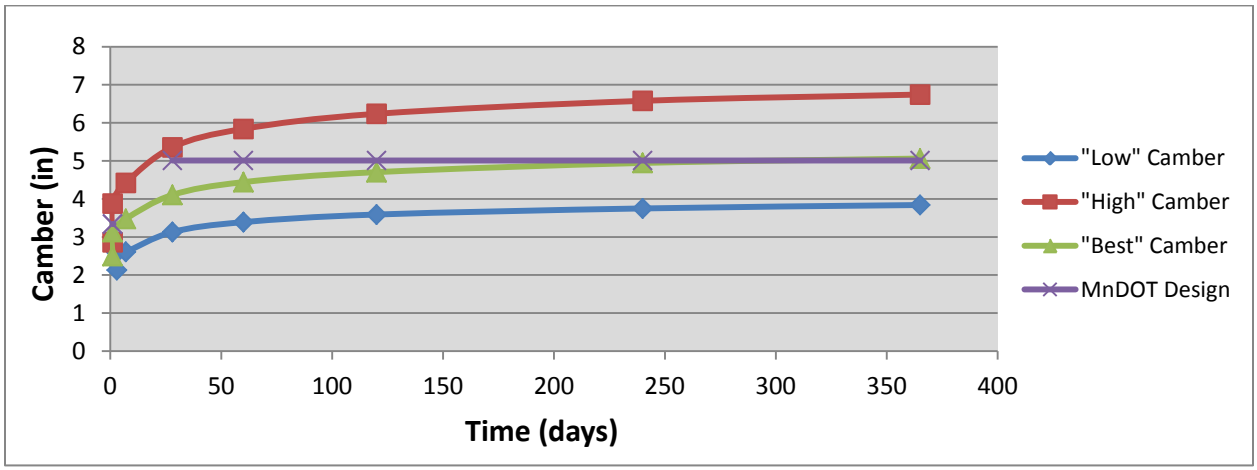

Figure 8-5. Long-term (erection) camber predictions for 130' MN54 girder

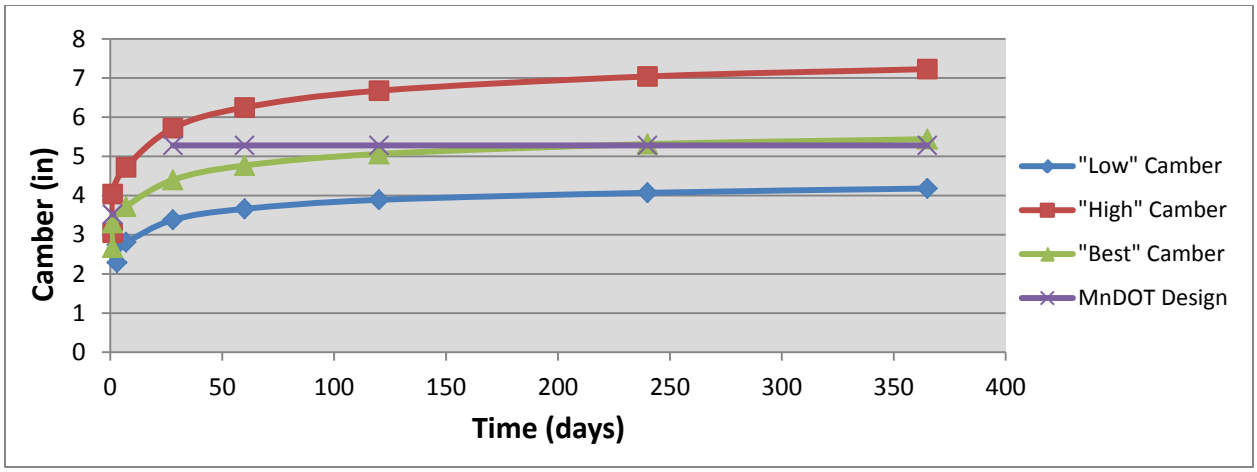

Figure 8-6. Long-term (erection) camber predictions for 160' 81M girder

These results indicate that the current MnDOT design procedure, including the 1.5 universal multiplier, should produce good erection camber results for girders with ages over about 180 days (or about 6 months) at the time of bridge erection. This is fairly consistent with the historical erection camber results shown in Figure 8-1 and Figure 8-2. The problem, of course, is that girders are usually not stored that long before shipping. These prediction modeling results provided expected erection cambers with respect to time that were used to create sets of multipliers that correspond to the erection camber prediction values at selected time intervals.

Additionally, the possible range of camber, at any girder age, is approximately +25%/-20% for the "short" girders of each shape and approximately +30%/-25% for the "long" girders of each shape. The difference is likely due to the larger effect of bunking on the longer girders. Even though these values seem high, they represent a "perfect storm" of combined parameter values that all lead to lower or higher cambers. Given that these are very unlikely scenarios and that girders of the same bridge project are likely to experience similar conditions, these results indicate that the created multipliers should produce camber predictions that are likely to be off by no more than ±15%. This result will be investigated further in Section 8.6, along with a more detailed look at camber variability.

As previously mentioned, the ACI 209 creep and shrinkage model was the only model used in the camber prediction modeling study. Because of the results of the PBEAM model validation process, discussed in Section 7.4.3, it was important to examine the extreme lower and upper bound models, which were the Mokhtarzadeh variation and Muller models, respectively. Figure 8-7 shows the "best prediction" camber results for one of the girders in the study, where the only parameter changed was the creep and shrinkage model.

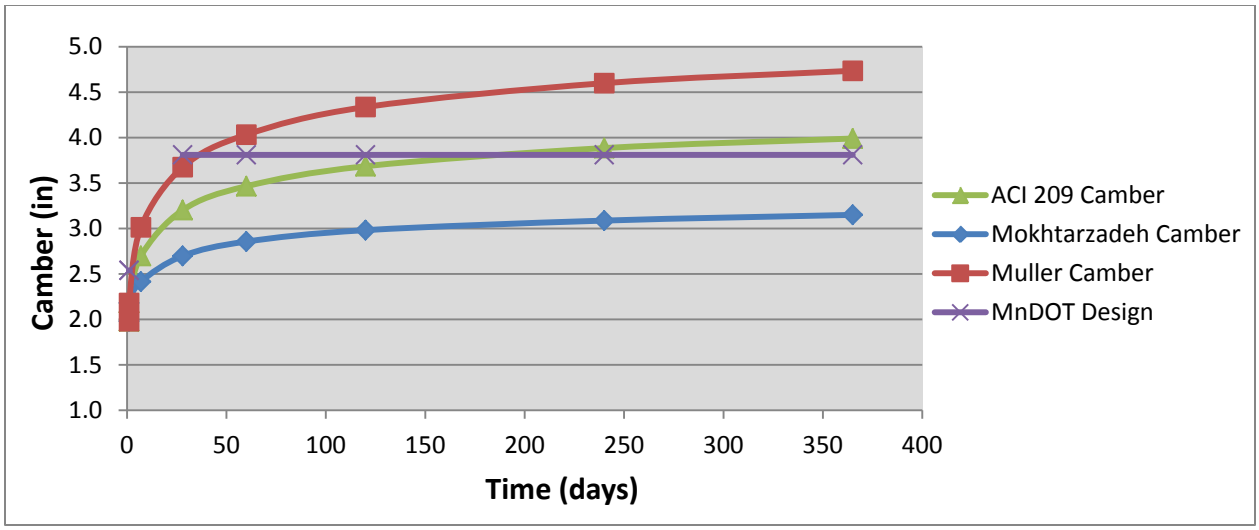

Figure 8-7. 120' 81M camber predictions with differing creep and shrinkage models

These results produced a camber range of approximately ±20% as a lower and upper bound, indicating that the choice of creep and shrinkage model has a significant effect on the camber predictions. Additionally, because the rest of the parameters were consistent with the "best prediction" values, this suggests that the camber range could be even larger if conditions changed. However, the Muller and Mokhtarzadeh variation creep and shrinkage models were found to be quite extreme bounds, and it is unlikely that camber variability of this magnitude would be expected. .

8.5 Multiplier Recommendations and Evaluation

As described in Section 8.2, each girder in this study was designed using the current MnDOT design procedure for release camber and an improved design procedure for release camber based on the observations from the material tests and thermal effects results, described in Chapter 5 and APPENDIX B. The recommended changes associated with the improved design procedure account for the major sources of the observed discrepancy between the measured and design release cambers, as discussed in Chapter 6. The improved design procedure for release camber consists of making the following changes to the camber calculations, which are discussed in further detail in Sections 6.4 and 9.3.1:

1. Replacing the ACI 363 equation for the concrete modulus of elasticity, used by MnDOT, with the Pauw (ACI 318-08, AASHTO LRFD 2010) equation.
2. Increasing the release concrete strength by 15% over the design strength.
3. Decreasing the strand stress at release by 3%, from $0.75*f_{pu}$ to $0.72*f_{pu}$, to account for thermal prestress losses and strand relaxation (unless changes are made during tensioning at the plant to account for the thermal effects).

Using the current MnDOT and improved design procedures, two separate release and erection camber predictions were made for each modeled girder in the study. By comparing the "best prediction" modeling results to each release camber prediction, two different sets of time-dependent and single-value multipliers were created. The "MnDOT Time-Dependent"

multipliers, which accompany the current MnDOT release camber calculations, are referred to as TDMnDOT. The "Improved Time-Dependent" multipliers, which accompany the improved release camber calculations described above, are referred to as TDImpr. Finally, single-value multipliers were created to accompany each set in case it was desired to continue using just one multiplier. These single-value multipliers are called the "MnDOT Single-Value" (SVMnDOT) and "Improved Single-Value" (SVImpr) multipliers and were based on the fact that the average age at erection of the girders in the historical database was 90-120 days. This method is NOT recommended, however, as it does not account for the increase in camber over time. Table 8-3 shows each set of multiplier recommendations.

Table 8-3. Long-term (erection) camber prediction multiplier recommendations

Girder Age at Erection	MnDOT Time-Dependent Multipliers	Improved Time-Dependent Multipliers
0-60 days	1.25	1.65
61-180 days	1.40	1.85
181-365 days	1.50	2.00
366+ days	1.55	2.05

MnDOT Single-Value Multiplier: 1.35
Improved Single-Value Multiplier: 1.80

In order to evaluate the effectiveness of these four (total) sets of multipliers, they were applied to the erection camber historical girder database. In other words, for the erection camber predictions associated with the TDMnDOT and SVMnDOT multipliers, the erection cambers for the girders in the historical database were recalculated by simply applying these multipliers to the original MnDOT design release cambers, instead of the 1.80/1.85 or 1.5 multipliers previously used. For the erection camber predictions associated with the TDImpr and SVImpr multipliers, the erection cambers were recalculated for the same girders using the improved release camber predictions and by applying the "Improved Single-Value" and "Improved Time-Dependent" multipliers. Figure 8-8, Figure 8-9, Figure 8-10 and Figure 8-11 illustrate the recalculated erection cambers relative to the recorded erection cambers, represented as a percent. For comparison with Figure 8-1 and Figure 8-2, the erection camber results within each figure were separated by which multiplier (i.e., 1.5 or 1.80/1.85) was used in the original design, such that girders designed before the multiplier change by MnDOT in 2007 are shown separately.

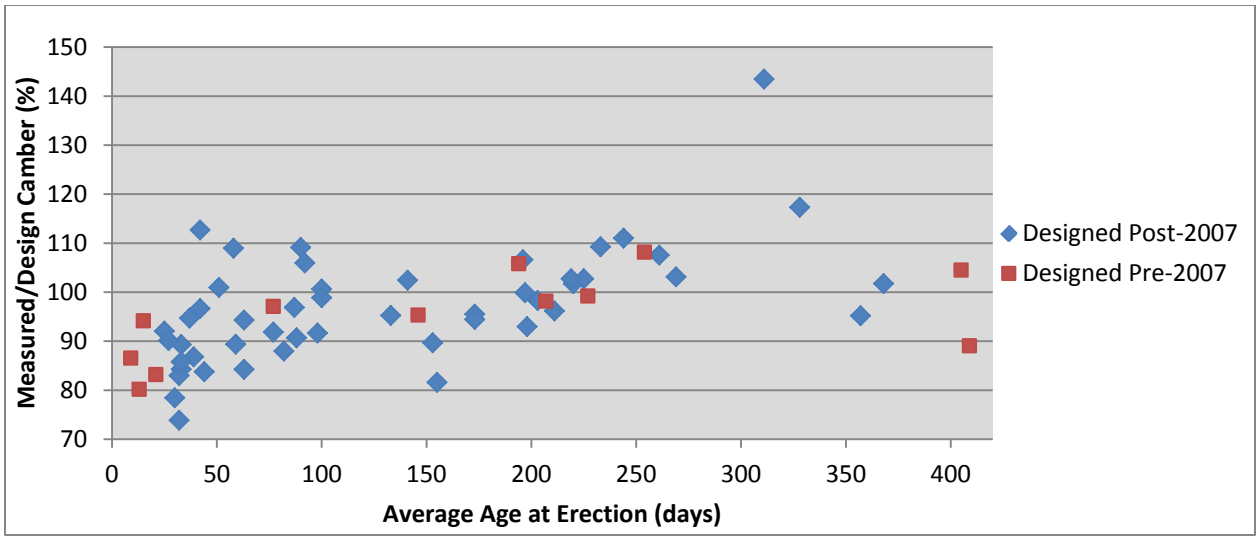

Figure 8-8. Measured/adjusted design erection cambers (MnDOT Single-Value)

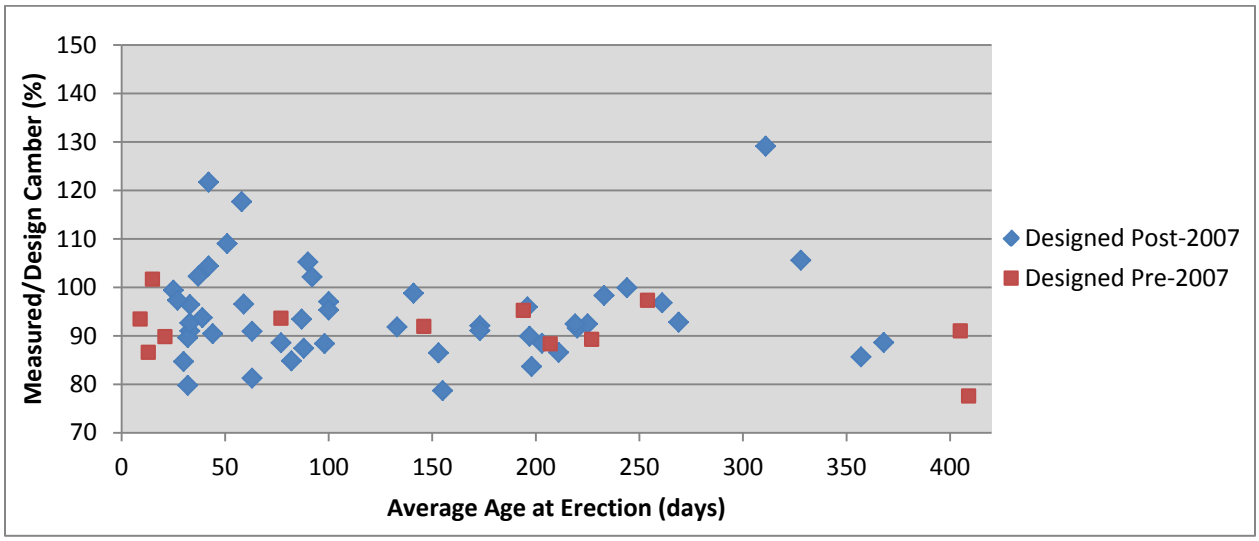

Figure 8-9. Measured/adjusted design erection cambers (MnDOT Time-Dependent)

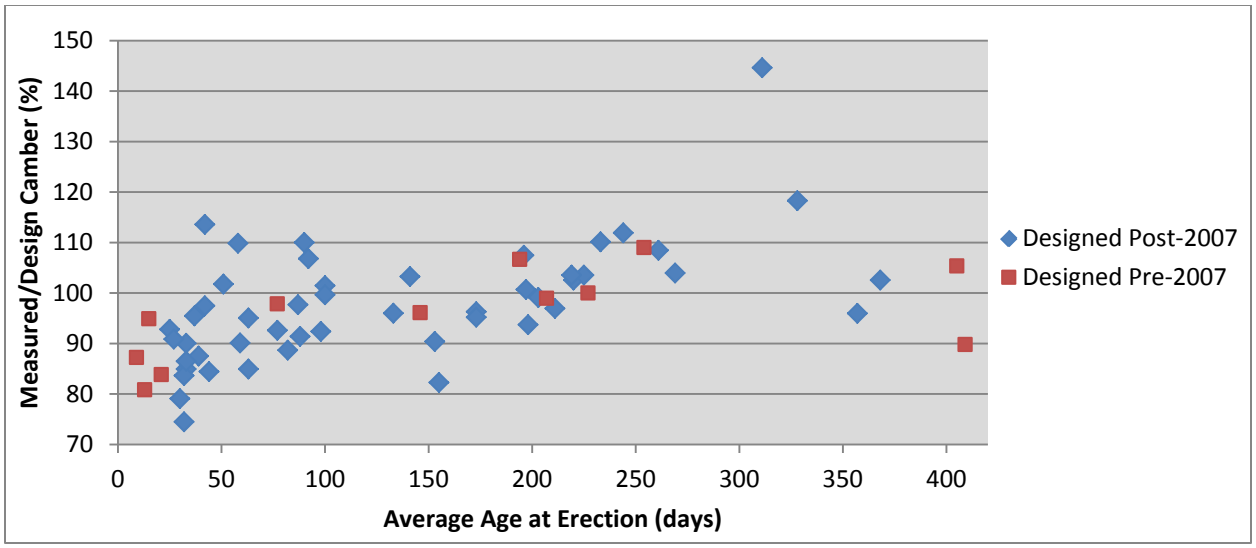

Figure 8-10. Measured/adjusted design erection cambers (Improved Single-Value)

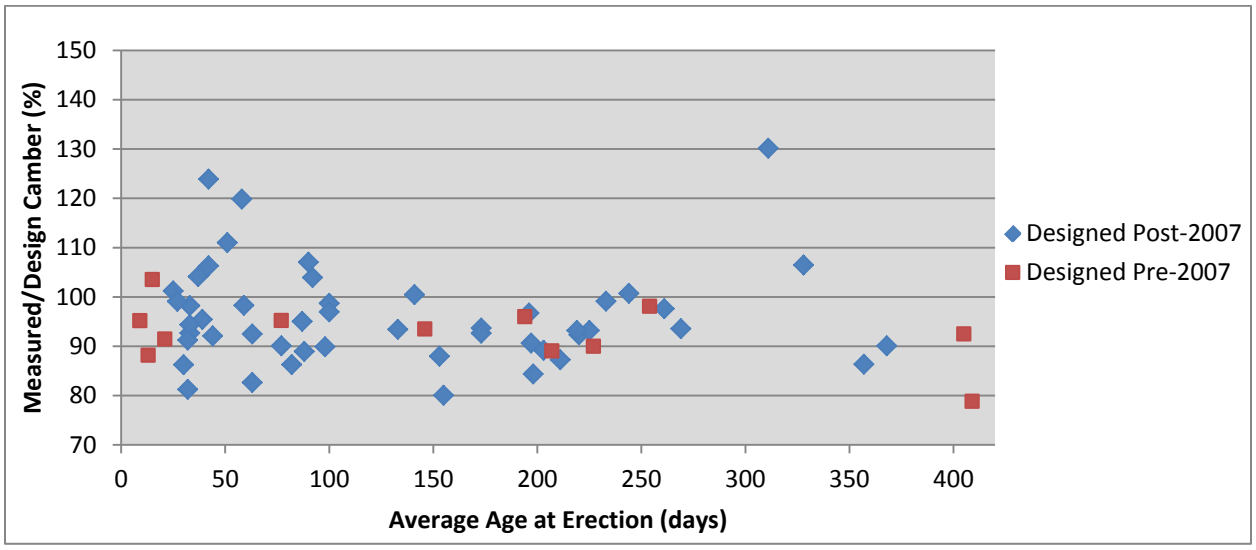

Figure 8-11. Measured/adjusted design erection cambers (Improved Time-Dependent)

These results represent significant improvement from the original erection camber results, shown in Figure 8-1 and Figure 8-2, and confirm that these four sets of multipliers would provide much more accurate long-term (erection) camber predictions. Each multiplier set (i.e., SVMnDOT, TDMnDOT, SVImpr, TDImpr) results in measured erection cambers that are, on average, 96.2%, 95.6%, 96.9% and 97.1% of the design values, respectively. These values are significant improvements from the 83.5% average measured vs. design value presented in Section 3.4.4. By examining Figure 8-9 and Figure 8-11, it is clear that the use of the time-dependent multipliers addresses the problem of low erection cambers for girders erected at early ages. Additionally, the range of camber results, or scatter, is also reduced, as only a few data points in Figure 8-9 and Figure 8-11 fall outside the ±20% range from the design erection camber. This was further examined using the coefficient of variation (COV). The COV for each set (i.e., SVMnDOT, TDMnDOT, SVImpr, TDImpr) is 3.22, 3.06, 3.22, and 3.07, respectively,

which illustrates that the time-dependent multipliers reduced the amount of expected scatter in the results. The single-value multipliers do not account for the increase in camber over time and resulted in slightly higher camber scatter. Table 8-4 summarizes these results.

Table 8-4. Summary of multiplier results

Release Camber Estimate	MnDOT		Improved	
Multiplier Set	Single-Value	Time-Dependent	Single-Value	Time-Dependent
Improves erection camber predictions?	Yes	Yes	Yes	Yes
Accounts for increase in camber over time?	No	Yes	No	Yes
Coincides with accurate release camber predictions?	No	No	Yes	Yes
Average % / COV	96.2 / 3.22	95.6 / 3.06	96.9 / 3.22	97.1 / 3.07

It is recommended that either the "MnDOT Time-Dependent" or "Improved Time-Dependent" multipliers be used for long-term (erection) camber prediction. However, given that the "Improved Time-Dependent" multipliers accompany the improved release camber predictions, the preferred method for camber prediction is the use of the improved release camber calculations and the "Improved Time-Dependent" multipliers. To further show the effectiveness of this camber prediction method, the measured erection camber values are plotted versus the nominal design values (in Figure 8-12) using the improved release camber calculations and the "Improved Time-Dependent" multipliers (the respective ages of the girders at erection were considered in the selection of the appropriate time-dependent multipliers used).

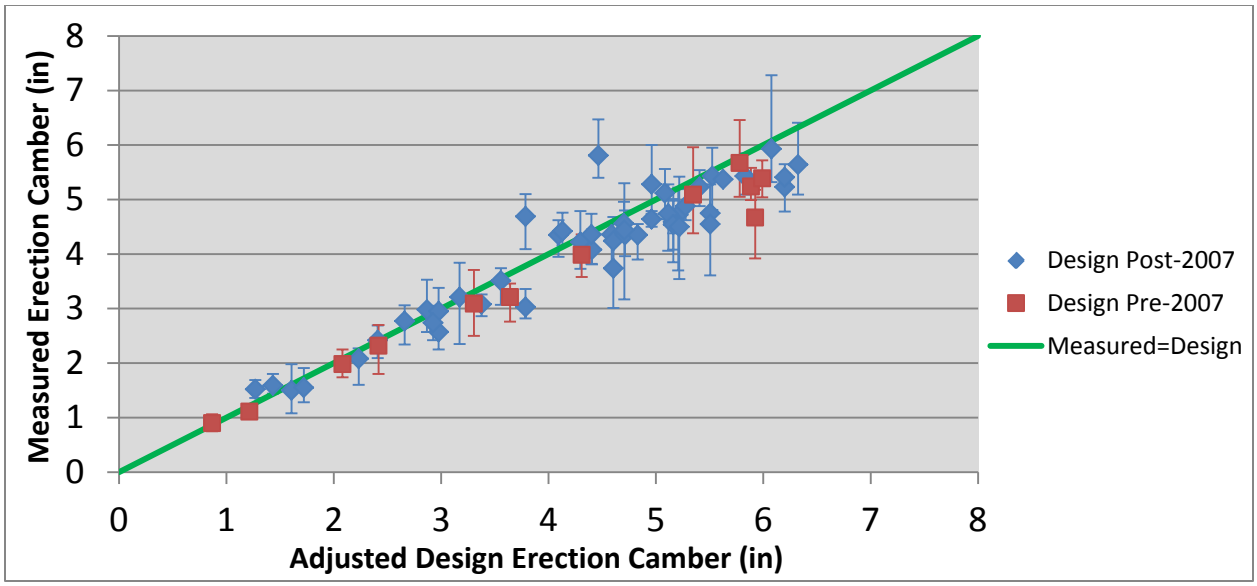

Figure 8-12. Measured vs. adjusted design erection cambers (Improved Time-Dependent)

These results show that the nominal differences between the measured and design erection camber values were greatly reduced using the improved release camber calculations and the "Improved Time-Dependent" multipliers, compared to the observed results shown in Figure 8-3. Further explanation regarding the validity and implementation of these recommended multipliers is given in Section 9.3.2.

Because a significant percent difference in camber between the measured and design values would be more of a problem for larger girders (with higher design cambers), it was necessary to investigate these nominal results further. It was desired to determine how many girders arrived at bridge sites with cambers that differed from the design value by more than 0.5 in, because it is possible to make up a smaller difference in camber with adjustments to the stool heights during bridge erection. From the results shown in Figure 8-3, it was found that of the 61 different girder designs (separated by erection camber design value), 38 had average camber values that differed from the design value by more than 0.5 in. However, using the results shown in Figure 8-12, this number was reduced to 16.

Furthermore, it was considered to be worse if the measured erection cambers were *higher* than the design values because of the more significant problems it can cause during bridge erection. In comparing the results from Figure 8-3 and Figure 8-12, it was found that there were only one and two cases, respectively, where the average erection cambers were *greater* than the design values by more than 0.5 in. It should be noted that the *total* number of girders in Figure 8-3 and Figure 8-12 with erection cambers that were greater than the design values by more than 0.5 in was 15 and 44, respectively, as is shown by the maximum "error" bounds. However, this discrepancy was largely due to one bridge in which it was known that the girder elevations were recorded on warm and sunny mid-August days. Additionally, the average age of the girders at erection was 45 days, which is getting close to the cut-off line between the 1.65 and 1.85 multiplier. If the 1.85 multiplier is used, only nine of the original 19 girders have cambers that are still greater than 0.5 in over the design value.

8.6 Camber Variability

For this study, it was important to not only provide a method for improved camber prediction, but also to investigate the potential range of camber variability. As can be seen in Figure 8-2, camber variability within girders of the same design can be very high. In order to evaluate the potential range of camber variability and examine the influence of each effect on that variability, each parameter in the prediction modeling setup (summarized in Table 8-2) was changed individually to either the "high camber" or "low camber" value (or both) from Table 8-2. Even though certain parameters have already been investigated earlier in this report (i.e., creep and shrinkage, length of cure, relative humidity and bunking), it was worthwhile to take another look at their influence as it pertains to potential camber variability. (Note: Length of cure was not examined in this analysis because it involved more complicated changes involving concrete strength and elastic modulus and strand stress.) For the following analysis, the 120 ft 81M girder was modeled for one year and the effect of changing each parameter was evaluated at release (if applicable) and after one year. Table 8-5 contains the results of the analysis.

Table 8-5. Influence of various effects on camber variability

Altered Parameter	Original "Best Prediction" Value	Altered Value	Effect on camber at release	Effect on camber after one year
f'ci (psi)	8625	9375	-3.03%[1]	-2.63%[1]
RH	73%	85%	N/A	-4.21%
RH	73%	55%	N/A	+6.05%
Thermal Losses	2.5% stress loss	5% stress loss	-4.04%	-3.95%
Relaxation	2 days	6 days	-0.51%	-0.26%
Bunking	L/24	L/30	N/A	-1.05%
Bunking	L/24	L/16	N/A	+2.89%
Solar Radiation	5% camber increase	10% camber increase	N/A	+4.76%

[1]Percent difference determined as ((altered camber-best prediction camber)/best prediction camber)*100

These results show how the camber variability ranges for the "short" and "long" girders, discussed in Section 8.4, were reached. The altered RH and bunking values for the "high camber" case had a more significant effect on camber than those for the "low camber" case, which is the cause of the greater high-end variability. Additionally, it was determined in Section 0, that the effect of bunking is more significant for the "long" girders, which is the cause of the greater camber variability observed for those girders.

These results also show that the influence of strand relaxation prior to release is minimal and that solar radiation, relative humidity and thermal losses are more major causes of camber variability. However, if the fabricators could use a temperature correction procedure that

properly accounts for thermal effects, then those effects would no longer significantly contribute to camber variability. (This is further discussed in Section 9.2.2 and APPENDIX B). Thus, it is reasonable to assume that the potential range of camber variability should not exceed ±15%, especially given that it is very unlikely that these extreme "low camber" and "high camber" effects would occur at the same time.

8.7 Conclusion

The modified camber calculation recommendations, detailed in Section 6.4, and the issues and investigated effects discussed in Chapter 7 (i.e., concrete creep and shrinkage, environmental effects, length of cure, bunking, etc.) were used to create PBEAM inputs and ensuing long-term (erection) camber predictions for girders of varying depth and length. From these results, four "sets" of multipliers (i.e., MnDOT Single-Value, MnDOT Time-Dependent, Improved Single-Value and Improved Time-Dependent) were determined by comparing the long-term (erection) camber predictions to the current MnDOT and improved release camber calculations. These multipliers were then verified using the historical erection camber data. It was found that all four sets greatly improved the erection camber prediction, on average, but only the Improved Time-Dependent multipliers accounted for the increase in camber over time AND coincided with more accurate release camber predictions. Thus, this multiplier set, or method, is recommended for future camber predictions by MnDOT.

The amount of camber variability that can be expected using these multipliers was also examined, and it was found that a camber range of approximately ±15% could be expected. It should be noted that the consequence of under-predicting camber may be worse than over-predicting camber; due to the adverse condition of having the girder protrude into the bridge deck profile at midspan. The specific causes for high camber are older girder ages at erection (i.e., exceeding 12-16 months), extreme amounts of bunking (overhangs of L/15 or more) and solar radiation. However, each one of these effects can be accounted for by adhering to the recommendations discussed in Sections 9.2 and 9.3. The time-dependent multipliers account for the increase in camber over time, the bunking recommendations limit the amount of girder overhang, and it was recommended that the survey shots be taken before the mid-afternoon to reduce the effect of solar radiation. Additionally, the average measured vs. design erection camber values for the recommended multiplier sets were 95.6% to 97.1%, indicating that the design erection cambers should still slightly over-predict the measured camber, on average.

CHAPTER 9. SUMMARY, CONCLUSIONS AND RECOMMENDATIONS

9.1 Summary

It was reported that the cambers at erection of prestressed concrete girders in Minnesota were often below their respective design values. On occasion, the erection cambers were so far below their design values that it resulted in construction delays and an increase in cost. This camber study sought to find the source of this problem and to provide an improved method for long-term (erection) camber prediction. Historical girder data was collected and analyzed, girders were instrumented for long-term observation, material tests were conducted and camber modeling was done in PBEAM in order to complete this objective.

The historical data was collected from fabricator records and bridge plans for 1067 girders produced between 2006 and 2010. Erection camber data was also collected for 768 of those 1067 girders. Fourteen girders of varying length and shape were instrumented at Plant A using a stretch-wire system in order to observe their long-term camber behavior. Concrete strength and elastic modulus material testing was conducted on multiple cylinder samples from both plants. Time-dependent camber modeling was conducted in PBEAM, which included program validation, a parametric study and camber predictions. Finally, four sets of long-term (erection) camber multipliers were created using the camber prediction modeling results.

For release camber, it was found that the most significant causes of the discrepancy between measured and predicted cambers were higher release concrete strengths and associated higher concrete elastic moduli, and thermal prestress losses. On average, among the 1067 historical girders, the measured release concrete strength was 15% higher than the specified design value. From the results of material testing, it was found that the Pauw (ACI 318-08, AASHTO LRFD 2010) equation for the concrete elastic modulus was a much better predictor than the ACI 363 equation used by MnDOT, which greatly under-predicted the E_c from the material tests. Finally, it was found that strand relaxation and concrete and ambient temperature effects that take place between strand pull, concrete-steel bond, and strand release, cause a reduction of prestress of 3%, on average.

For long-term (erection) camber, PBEAM was used to evaluate the effects of concrete creep and shrinkage, relative humidity, length of cure and bunking/storage conditions. Solar radiation was found to cause an increase in camber of up to 15% (based on experiential evidence). From the examined historical girders, weekend curing was found to cause a reduction in long-term camber of approximately 6%, on average, when compared to weekday-cured girders. However, it was also found that the effect of weekend curing was not as noticeable at release because the amount of strand stress loss was reduced by cooler concrete temperatures at bond and release. Because the remaining effects are time-dependent and because the girder age at erection is not known at the time of design, PBEAM was validated and then used to make long-term (erection) camber predictions for a range of girders that were designed to represent short- and long-span bounds for commonly-used MnDOT girder shapes. Using these predictions and the MnDOT and improved camber calculation methods, four sets of multipliers were created for long-term (erection) camber prediction.

PBEAM was also used to conduct a parametric study of time-dependent effects to determine the potential effects on camber variability. It was found that bunking caused a significant increase in camber, especially for girders with larger length-to-depth ratios. Because of the change in creep caused by the overhanging girder ends, the increase in camber was found

to be permanent (i.e., not elastically recoverable) and increase with time. As described in Section 0, the girders in the parametric study experienced a wide range of camber variability because the effect of bunking was highly dependent on the bunk locations and the length-to-depth ratio of the girders. For example, an 80 ft and 120 ft MN54 girder bunked at L/20 and L/10 from the girder ends, had camber increases ranging from 6% to 25% after one year, over the end-supported case. For longer girders with higher design cambers, this percent increase can mean a significant nominal increase in camber. For the 120 ft MN54 girder, the 25% increase after one year represents a nominal camber increase of 1.2 in over the end-supported case.

Ambient relative humidity and creep and shrinkage were also found to cause camber variability. For the girders used in the long-term camber modeling, a low and high relative humidity of 55% and 85%, respectively, caused a camber range of approximately 10% after one year of constant low or high relative humidity. The camber variability caused by changes in relative humidity is discussed further in Sections 7.5.2 and 8.6. Because no creep or shrinkage tests were conducted in this study, it was more difficult to quantify the potential range of camber variability caused by these effects. Based on the comparative analysis of creep and shrinkage models described in 7.2 and the long-term camber modeling results detailed in Section 8.4, it was found that camber could vary by as much ±20%, depending on the creep model used in the PBEAM analysis. However, further testing would be required to determine the camber variability caused directly by varying creep and shrinkage in different specimens.

Finally, because camber increases with time, girder age was a source of camber variability. If an average age at erection of 100 days is used, ages at erection of 30 and 365 days would result in camber differences of approximately ±10%. For longer girders with higher design cambers, the nominal difference in camber would be on the order of 0.5 in. The figures shown regarding the long-term (erection) camber modeling results in Section 8.4 provide good illustrations of the effect of girder age on camber variability.

Based on these results and conclusions, recommendations were made to improve the release and long-term (erection) camber predictions and reduce camber variability. These recommendations apply to both girder fabrication and the camber design calculation procedures, and are discussed in the following sections.

9.2 Girder Fabrication Recommendations

Major changes to the girder fabrication procedure at both Plants A and B could cause significant side-effects related to plant management, cost, efficiency and personnel. Fortunately, minor changes to the procedure that are easy to implement could significantly reduce the camber variability from girder to girder, pour to pour, and project to project. The recommendations for these changes in the girder fabrication procedure are described below:

9.2.1 Pouring Schedule and Management

1. A concerted effort should be made to pour all girders within a bridge project (or construction stage), that have the same design erection camber, in as short a time span as possible to minimize the difference in girder ages at the time of bridge erection.
2. Multiple-day pouring on the same precasting bed should be avoided. Differences in environmental and curing conditions that are present during multiple-day pours can cause significant changes to the strand stress at release and can lead to high camber variability.

3. The strands should be cut as soon as possible after uncovering the girders and stripping off the side-forms in order to avoid the adverse effects of significant concrete cooling and possible pre-release cracking.

9.2.2 Strand Tensioning and Temperature Corrections

1. A spreadsheet has been developed for both Plants A and B that uses the thermal effects analysis, discussed in APPENDIX B, to provide a temperature correction output based on a few important inputs that the fabricators provide. Because certain inputs are not known precisely prior to strand tensioning (e.g., concrete and ambient temperatures at concrete-steel bond), some reasonable approximations must be made and are appropriately taken into account in the spreadsheet. Different spreadsheets were created for each plant to cater to their unique strand tensioning procedures. Prior to implementation, it is recommended that a short field study be conducted to further quantify the effect of temperature and girder setting on strand stress.
2. For any other plant, the amount of pull force correction due to temperature effects should be based on the comparison of the strand temperature at the time of tensioning and some pre-determined standard temperature (i.e., 90-100 °F), which is assumed to be an average of the temperatures at strand pull and concrete-steel bond. This will still minimize the stress loss due to thermal effects but is less precise than using the developed spreadsheet and will not eliminate camber variability.
3. The free length of strand in the bed should NOT be covered. Covering the free length of strand almost always results in undesired additional thermal prestress losses.

9.2.3 Bunking/Storage Conditions

1. Girders of shapes 27M, 36M and MN45 should be placed on storage bunks with AT LEAST 2 feet and NO MORE THAN 6 feet of girder end overhang.
2. Girders of shapes MN54, MN63, 72M and 81M should be placed on storage bunks with AT LEAST 3 feet and NO MORE THAN 8 feet of girder end overhang.
3. EXCEPTION: If it is desired to intentionally increase the camber (possibly in rushed shipping situations), girders of shapes 27M, 36M and MN45 can be placed on storage bunks with up to 10 feet of overhang and girders of shapes MN54, MN63, 72M and 81M on storage bunks with up to 12 feet of overhang.
4. ALL girders within a bridge project that have the same design erection camber should be placed on storage bunks with girder overhangs that differ by NO MORE THAN 2 feet from one another.
5. ALL girders should be placed symmetrically on the storage bunks so that the amount of overhang on each end is roughly the same. This provides a symmetric girder profile, which is desired for creating a uniform bridge deck profile.

9.3 Camber Prediction Recommendations

Changes to the initial design camber calculations can be easily implemented with minimal effect on the overall design procedure. This study has shown that current camber design calculations do not accurately predict the release or erection cambers of girders produced at Plants A and B, which has caused significant problems at the bridge erection sites. However, the

following recommendations represent modifications to the current method for release and long-term (erection) camber prediction that should greatly improve the accuracy and consistency of camber predictions and should alleviate the problems during bridge erection.

9.3.1 Release Camber

As previously described in Section 6.4, the recommendations for modified camber calculations are as follows:

1. The concrete release strength used in the camber calculations should be the design concrete release strength, f'_{ci}, multiplied by a factor of 1.15. This modification accounts for the higher release strengths produced at the fabrication plants because of the need to exceed the design strength and efficiently turn over the precasting beds.
2. The Pauw (ACI 318-08, AASHTO LRFD 2010) equation for the concrete modulus of elasticity should replace the ACI 363 equation currently used by MnDOT in the camber calculations. This modification accounts for the stiffer concrete produced at the fabrication plants.
3. The stress in the strands at release should be reduced by 3%, from $0.75*f_{pu}$ to $0.72*f_{pu}$, in the camber calculations. This modification accounts for the stress loss due to strand relaxation and thermal effects. ***Note: This recommendation should be eliminated if the fabricators are allowed to use the provided spreadsheet for temperature corrections***

9.3.2 Long-Term (Erection) Camber

In current Minnesota bridge designs, a single "Total Initial Camber" is recorded on the bridge plans, which corresponds to the design erection camber before the application of external loads, such as the cast-in-place bridge deck. This erection camber value is simply equal to the design release camber, multiplied by the 1.5 multiplier, as discussed in Section 1.2. In this study, four different multiplier sets were created to improve the erection camber calculations based on the results of long-term camber prediction modeling. As described in Section 8.5, the multiplier set to be used depends on the release camber prediction method. The four proposed multiplier methods are: "MnDOT Single-Value", "MnDOT Time-Dependent", "Improved Single-Value", and "Improved Time-Dependent" multipliers. These four sets of multipliers are shown in Table 9-1.

Table 9-1. Long-term (erection) camber prediction multiplier recommendations

Girder Age at Erection	MnDOT Time-Dependent Multipliers	Improved Time-Dependent Multipliers
0-60 days	1.25	1.65
61-180 days	1.40	1.85
181-365 days	1.50	2.00
366+ days	1.55	2.05

MnDOT Single-Value Multiplier: 1.35
Improved Single-Value Multiplier: 1.80

As discussed in Section 8.5, it is recommended that either the "MnDOT Time-Dependent" or the "Improved Time-Dependent" multiplier methods be used for long-term (erection) camber prediction because they account for the increase in camber over time and the fact that girders are shipped at varying ages. However, if the recommendations for improved release camber predictions are implemented, then the "Improved Time-Dependent" multipliers must be used. The recommended approach is to use the improved release camber predictions accompanied by the use of the "Improved Time-Dependent" multipliers. This method is expected to provide the most accurate release AND erection camber predictions. As discussed in Sections 8.4 and 8.6, an erection camber variability of ±15% can be expected using this prediction method, as a result of variation in concrete strength, strand stress at release, relative humidity, bunking and solar radiation. It is also interesting to note that the "Improved Time-Dependent" multiplier for 61-180 days is 1.85, which closely matches the Martin (PCI) 1.80/1.85 multipliers. Because Martin based his multipliers on a girder age at erection of about 60 days (Martin 1977), this shows that the "Improved Time-Dependent" multipliers are on par with the original Martin assumptions, even though material properties and fabrication procedures have changed greatly since the 1970s.

The use of the "MnDOT Time-Dependent" or "Improved Time-Dependent" multipliers requires changes to be made to the reporting of the design erection camber on the bridge plans. The proposal for the implementation of these time-dependent multiplier methods is as follows:

1. The designer would report four separate design erection cambers on the bridge plans, each corresponding to the design camber at each time interval (0-60 days, 61-180 days, 181-365 days and 366+ days).
2. Prior to bridge erection, the contractor or bridge surveyor would determine which design erection camber value to use based on the estimated average age at erection of the girders in the bridge.

In this manner, the correct design erection camber could simply be determined by matching the estimated age of the girders at erection to the corresponding design erection camber value already printed on the bridge plans.

To provide an opportunity, prior to bridge erection, for girder camber to be compared to the design values, the predicted design camber at release could also be printed on the bridge

plans. Once the girders are fabricated and the strands are released, the measured on-bed release cambers could then be compared to the design values to estimate if the measured cambers at erection will differ from the design erection camber values.

Additionally, it is common for MnDOT to calculate a dead load deflection (i.e., the downward deflection due to the superimposed dead load of the bridge deck) and list it on the bridge plans. The dead load deflection is then subtracted from the predicted camber at erection to provide the "residual camber," which is the camber expected after completing construction of the bridge and before the addition of traffic live loads. The modulus of elasticity used for the girder concrete, E_c, in the calculation of dead load deflection is determined by using the ACI 363 equation with the design shipping strength, f'_c. However, as discussed previously in Section 5.2.4, the shipping strength is determined based on the strength needed to be within the stress limits at service and may not provide a good value for estimating E_c. There are numerous instances where the concrete strength at release may have controlled the mix design, resulting in much higher than anticipated strengths at shipping and service. It was found in Section 5.2.4 that the 28-day modulus could be conservatively approximated as 1.15 times the elastic modulus at release. Using this estimation for calculating E_c, the following modification to the calculation of the dead load deflection is recommended.

1. The ACI 363 equation currently used by MnDOT to estimate E_c should be replaced by the modulus of elasticity at release, E_{ci}, calculated based on the recommendations discussed in Section 9.3.1, multiplied by a factor of 1.15.

9.4 Camber Prediction Method Comparison

To further illustrate the implementation of the recommendations to the release camber calculations and the long-term (erection) camber multipliers, the current and recommended prediction methods were applied to a selected girder design from the historic database. The selected girder design was the 122 ft-4.75 in MN54 girder set from Bridge 73038, which was also represented in Set 1 of the instrumented girders. Important information regarding this girder design is shown below so that the results can be duplicated.

Girder Information:
Bridge Number: 73038
Girder Shape/Length: MN54 122 ft 4.75 in
Strand Type: 0.6 in dia. 270 ksi low-relaxation 7-wire strand
Straight Strand Pattern: 36 strands, 12 in each row spaced at 2 in on center
Draped Strand Pattern: 8 strands, 2 in each row spaced at 2 in on center

Dimensions and Material Properties:
L_{des} = 121 ft 1.75 in
w_c = 155 pcf
A_c = 749 in^2
I_c = 285690 in^4
A_s = 44x0.217 = 9.55 in^2
f'_{ci} = 7000 psi
f'_c = 9000 psi
E_{ps} = 28500 ksi
e_{mid} = 20.32 in
e_{end} = 13.04 in
e' = e_{mid} - e_{end} = 7.27 in
$x_{hold\text{-}down}$ = 48.45 ft

Table 9-2 shows the comparison of the current camber prediction method used by MnDOT to the recommended method, which utilizes all of the release camber recommendations from Section 9.3.1 and the Improved Time-Dependent Multipliers from Section 9.3.2.

Table 9-2. Comparison of current and recommended camber prediction methods

	Current Method	Recommended Method
E_{ci}	$1265\sqrt{f'_{ci}} + 1000 = 4347\ ksi$	$33{w_c}^{1.5}\sqrt{1.15f'_{ci}} = 5714\ ksi$
E_{cbmf}	$1265\sqrt{f'_c} + 1000 = 4795\ ksi$	$1.15E_{ci} = 6571\ ksi$
f_{pj}	$0.75 * 270 = 202.5\ ksi$	$0.72 * 270 = 194.4\ ksi$
Δf_{pES}	22.8 ksi	17.1 ksi
P_{re}	1715.6 k	1693.3 k
Δ_{ps}	6.85 in	5.14 in
Δ_{bm}	3.15 in	2.39 in
Release Camber	3.70 in	2.75 in
Erection Camber	1.5*Release Camber = 5.55 in	1.65*Release Camber = 4.54 in (0-60 days)
		1.85*Release Camber = 5.09 in (61-180 days)
		2.00*Release Camber = 5.50 in (181-365 days)
		2.05*Release Camber = 5.63 in (366+ days)

9.5 Additional Multiplier Option

The recommended long-term (erection) camber multipliers presented in Section 9.3.2 depend on the calculations used to predict the release camber (i.e., the "MnDOT multipliers" assume that no changes are made and the "Improved multipliers" assume that all of the recommended changes listed in Sections 6.4 and 9.3.1 are used). Therefore, if MnDOT chose to use just *some* of the recommended changes to the release camber calculations, a new set of multipliers would need to be created. Because it was expressed by MnDOT that making adjustments to the design procedure that are specific to camber was not desired, an additional multiplier option was created for the case where *only* the change in the expression used for

concrete elastic modulus (ACI 363 to Pauw/ACI 318/AASHTO LRFD) was used (Recommendation #2 from Section 9.3.1). Additionally, to be consistent with current MnDOT design procedures, a unit weight of concrete of 150 pcf was used to create these multipliers in place of the 155 pcf previously used in this study. The additional multipliers for this case are shown in Table 9-3.

Table 9-3. Additional long-term (erection) camber multiplier recommendations

Girder Age at Erection	Additional Time-Dependent Multipliers
0-60 days	1.45
61-180 days	1.60
181-365 days	1.75
366+ days	1.80

Additional Single-Value Multiplier: 1.55

The use of the additional multiplier option with the single-value multiplier and time-dependent multipliers resulted in measured erection cambers that were, on average, 96.0% and 93.2% of the design values, respectively. It should be noted that the preference of MnDOT to prevent situations where girders have erection cambers greater than 0.5 in over the design value was considered in producing the Additional Time-Dependent Multipliers. In other words, the multiplier values were rounded up to the nearest 0.05 number in order to slightly lower the average measured vs. design percentage and help prevent the problem of under-predicted erection camber.

9.6 Conclusion

The primary objective of this study was to investigate and determine the cause of low girder camber at both release and bridge erection, which was observed by MnDOT, and to create an improved method for camber prediction, through modified calculations (if necessary) and a new set of multipliers. The causes of low girder camber at release were found and discussed in Chapters 5 and 6, and recommendations were created for modification of the camber calculations, which were shown to provide improved camber predictions. The causes of low girder camber at the time of bridge erection were found and discussed in Chapters 7 and 8, and recommendations were made for the use of a new set of multipliers. Furthermore, girder fabrication recommendations were developed to reduce camber variability and are discussed in Section 9.2.

Based on the results of the implementation of these recommendations on the historical and instrumented girders, it was determined that the objective of the study had been achieved, and that the recommendations should be immediately put to use by MnDOT to improve their release and erection camber predictions.

REFERENCES

AASHTO (2010). *LRFD Bridge Design Specification, 5th Edition.* American Association of State Highway and Transportation Officials, Washington, DC.

ACI Committee 209 (2008). *ACI 209.2R-08 Guide for Modeling and Calculating Shrinkage and Creep in Hardened Concrete.* American Concrete Institute, Farmington Hills, MI.

ACI Committee 209 (1992). *ACI 209R-92 Prediction of Creep, Shrinkage, and Temperature Effects in Concrete Structures.* American Concrete Institute, Farmington Hills, MI.

ACI Committee 318 (2008). *ACI 318-08 Building Code Requirements for Structural Concrete and Commentary.* American Concrete Institute, Farmington Hills, MI.

ACI Committee 363 (2010). *ACI 363R-10 State-of-the-Art Report on High-Strength Concrete.* American Concrete Institute, Farmington Hills, MI.

Ahlborn, T.M., French, C.E., Shield, C.K. (2000). *High-Strength Concrete Prestressed Bridge Girders: Long Term and Flexural Behavior*. MnDOT Final Report 2000-32, Minnesota Department of Transportation, St. Paul, MN.

Ahmad, S.H., Shah, S.P. (1985). "Structural Properties of High Strength Concrete and its Implications for Precast Prestressed Concrete." *PCI Journal*, Vol. 30(6), 92-119.

Al-Omaishi, N., Tadros, M.K., Seguirant, S.J. (2009). "Elasticity Modulus, Shrinkage, and Creep of High-Strength Concrete as Adopted by AASHTO." *PCI Journal,* (Summer 2009), 44-63.

Barr, P.J., Angomas, F. (2010). "Differences between Calculated and Measured Long-Term Deflections in a Prestressed Concrete Girder Bridge." *Journal of Performance of Constructed Facilities*, Vol. 24(6), 603-609.

Barr, P.J., Stanton, J.F., Eberhard, M.O. (2005). "Effects of Temperature Variations on Precast, Prestressed Concrete Bridge Girders." *Journal of Bridge Engineering,* Vol. 10(2), 186-194.

Bažant, Z.P., Baweja, S. (1996). "Short Form of Creep and Shrinkage Prediction Model B3 for Structures of Medium Sensitivity." *Materials and Structures*, Vol. 29, 587-593.

Carrasquillo, R.L., Nilson, A.H., Slate, F.O. (1981). "Properties of High Strength Concrete Subject to Short-Term Loads." *ACI Journal*, Vol. 87(3), 171-178.

Comité Euro-International du Béton (CEB) and the Fédération International de la Précontrainte (FIP) (1990). *CEB-FIP Model Code 1990*, Final Draft.

Erkmen, B., Shield, C.K., French, C.E. (2008). *Self-Compacting Concrete (SCC) for Prestressed Bridge Girders*. MnDOT Final Report 2008-51, Minnesota Department of Transportation, St. Paul, MN.

Gardner, N.J., Lockman, M.J. (2001). “Design Provisions for Drying Shrinkage and Creep of Normal-Strength Concrete.” *ACI Materials Journal,* Vol. 98(2), 159-167.

Goel, R., Kumar, R., Paul, D.K. (2007). “Comparative Study of Various Creep and Shrinkage Prediction Models for Concrete.” *Journal of Materials in Civil Engineering,* Vol. 19(3), 249-260.

Jayaseelan, H., Russell, B.W. (2007). *Prestress Losses and the Estimation of Long-Term Deflections and Camber for Prestressed Concrete Bridges*. Oklahoma State University Final Report.

Martin, L.A. (1977). “A Rational Method for Estimating Camber and Deflection of Precast Prestressed Members.” *PCI Journal,* Vol. 22(1), 100-108.

Mazloom, M. (2008). “Estimating Long-Term Creep and Shrinkage of High-Strength Concrete.” *Cement and Concrete Composites*, Vol. 30, 316-326.

MnDOT (2009). *LRFD Bridge Design Manual.* MnDOT Bridge Office, Minnesota Department of Transportation, St. Paul, MN.

Mokhtarzadeh, A., French, C.E. (1998). *Mechanical Properties of High-Strength Concrete*. MnDOT Final Report 1998-11, Minnesota Department of Transportation, St. Paul, MN.

Muller, H.S., Hilsdorf, H.K. (1999). General Task Group 9, Comité Euro-International du Béton (CEB) and the Fédération International de la Précontrainte (FIP).

NS 3473 (1992). *Concrete Structures – Design Rules*, Norges Standardiseringsfund, Oslo, Norway.

Pauw, A. (1960). “Static Modulus of Elasticity of Concrete as Affected by Density.” *ACI Journal*, Vol. 32(6), 679-687.

PCI (2010). *PCI Design Handbook*: *Precast and Prestressed Concrete, 7th Edition.* Precast/Prestressed Concrete Institute, Chicago, IL.

PCI (1975). “Recommendations for Estimating Prestress Losses,” *PCI Committee on Prestress Losses, PCI Journal*, Vol. 20(4), 43-75.

Radain, T.A., Samman, T.A., Wafa, F.F. (1993). “Mechanical Properties of High-Strength Concrete.” *Proceedings of the Third International Symposium on Utilization of High-Strength Concrete*, Lillehammer, Norway, Vol. 2, 1209-1216.

Rosa M.A., Stanton, J.F., Eberhard, M.O. (2007). “Improving Predictions for Camber in Precast, Prestressed Concrete Bridge Girders.” *Concrete Bridge Conference*.

Saiidi, M.S., Shields, J., O'Connor, D., Hutchens, E. (1996). "Variation of Prestress Force in a Prestressed Concrete Bridge During the First 30 Months." *PCI Journal,* Vol. 41(5), 66-72.

Suttikan, C. (1978). *A Generalized Solution for Time-Dependent Response and Strength of Noncomposite and Composite Prestressed Concrete Beams*. University of Texas at Austin PhD Dissertation.

Tadros, M.K., Fawzy, F., Hanna, K.E. (2011). "Precast, Prestressed Girder Camber Variability." *PCI Journal,* (Winter 2011), 135-154.

Tomosawa, F., Noguchi, T. (1993). "Relationship Between Compressive Strength and Modulus of Elasticity of High-Strength Concrete." *Proceedings of the Third International Symposium on Utilization of High-Strength Concrete,* Lillehammer, Norway, Vol. 2, 1247-1254.

Woolf, D., French, C.E. (1998). *A Camber Study of MnDOT Prestressed Concrete I-Girders*. MnDOT Final Report 1998-08, Minnesota Department of Transportation, St. Paul, MN.

APPENDIX A. ADDITIONAL HISTORICAL GIRDER FIGURES

The following figures (A-1 to A-7) contain information regarding the effect of bed position on the camber at release. Each figure shows the normalized release camber (i.e., measured vs. design (with the measured f'_{ci}) release camber) of girders of the same design for a particular bridge from the historical database. These figures accompany the discussion and conclusions in Section 5.3.3. Also included are figures (A-7 to A-16) that contain information regarding the effect of length of cure on the camber at erection. Each figure shows the normalized erection camber (i.e., measured vs. original MnDOT design erection camber) of girders of the same design for a particular bridge from the historical database. These figures accompany the discussion and conclusions in Section 7.5.1.

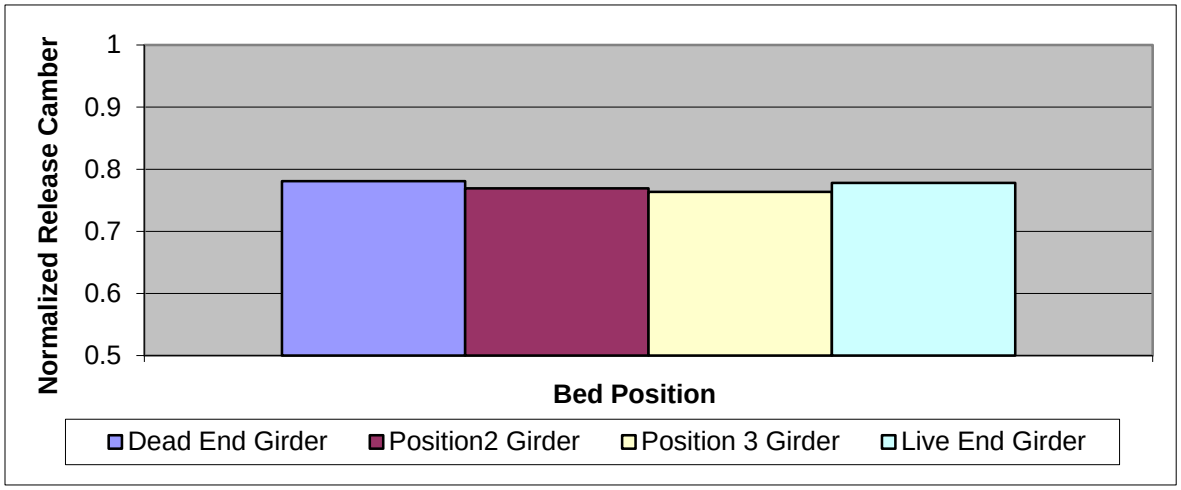

Figure A-1. Camber of girders in different bed positions for Br. 02051 (Plant A)

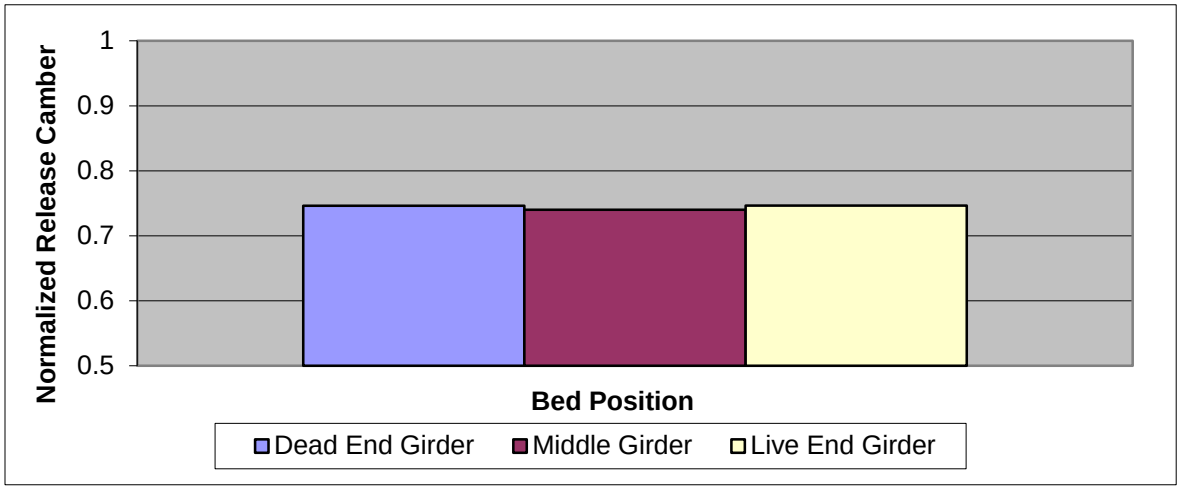

Figure A-2. Camber of girders in different bed positions for Br. 19561 (Plant A)

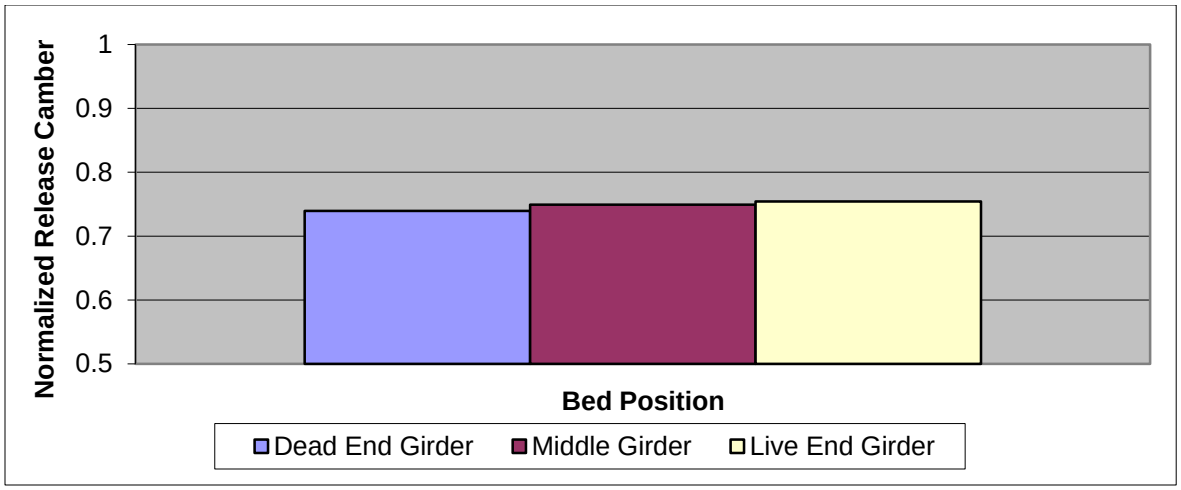

Figure A-3. Camber of girders in different bed positions for Br. 13809 (Plant A)

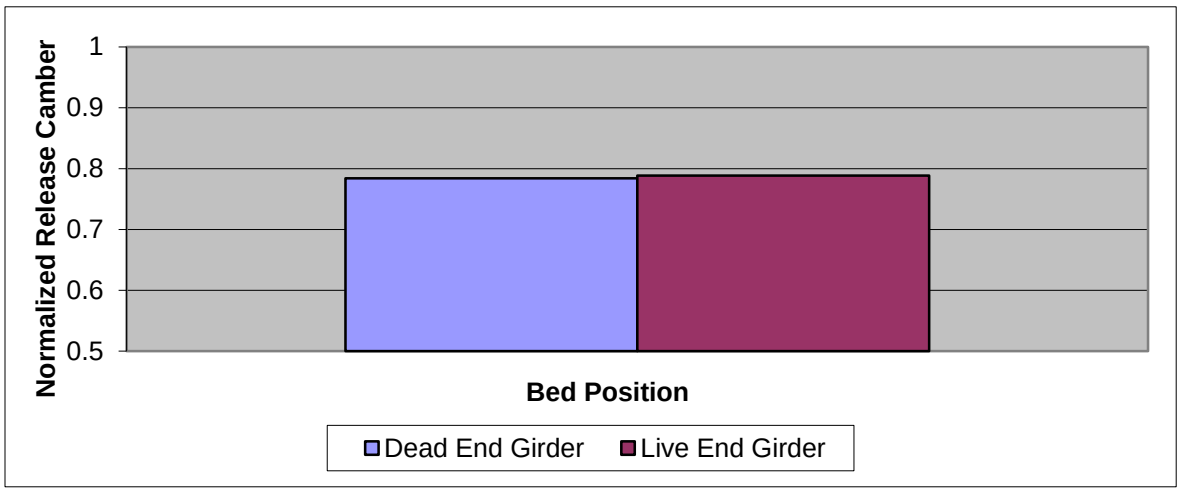

Figure A-4. Camber of girders in different bed positions for Br. 19850 (Plant A)

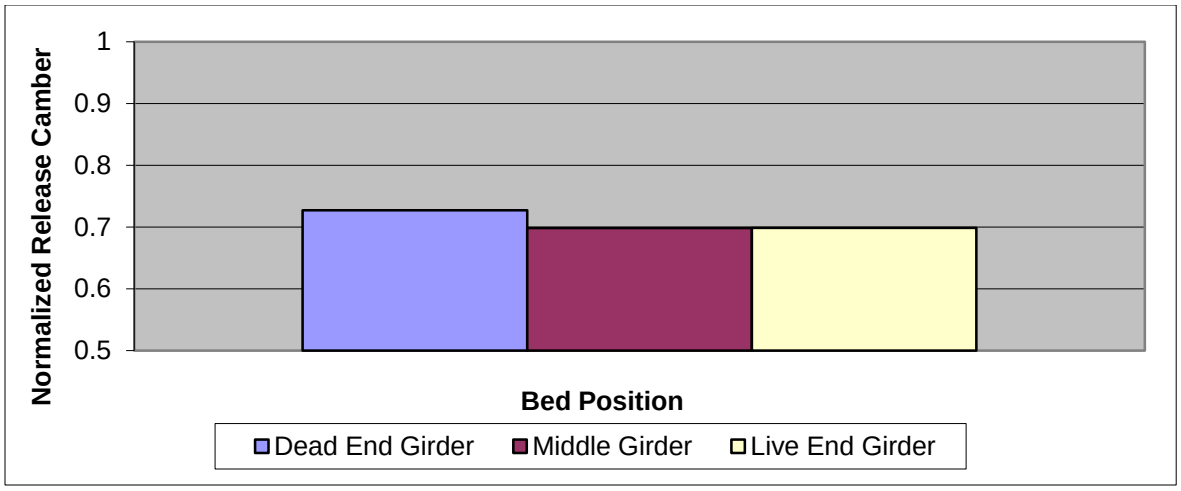

Figure A-5. Camber of girders in different bed positions for Br. 07581 (Plant A)

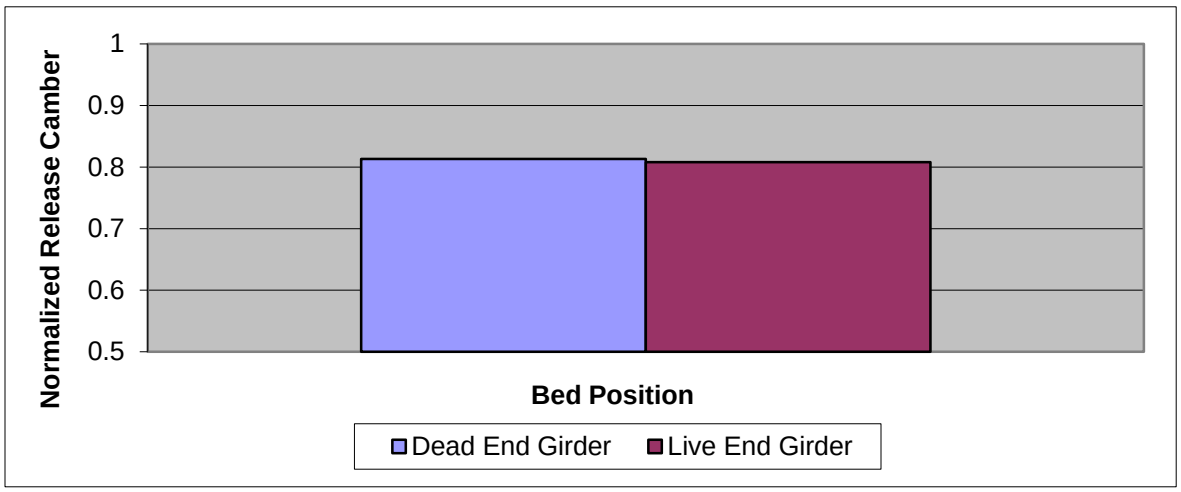

Figure A-6. Camber of girders in different bed positions for Br. 07581 (Plant A)

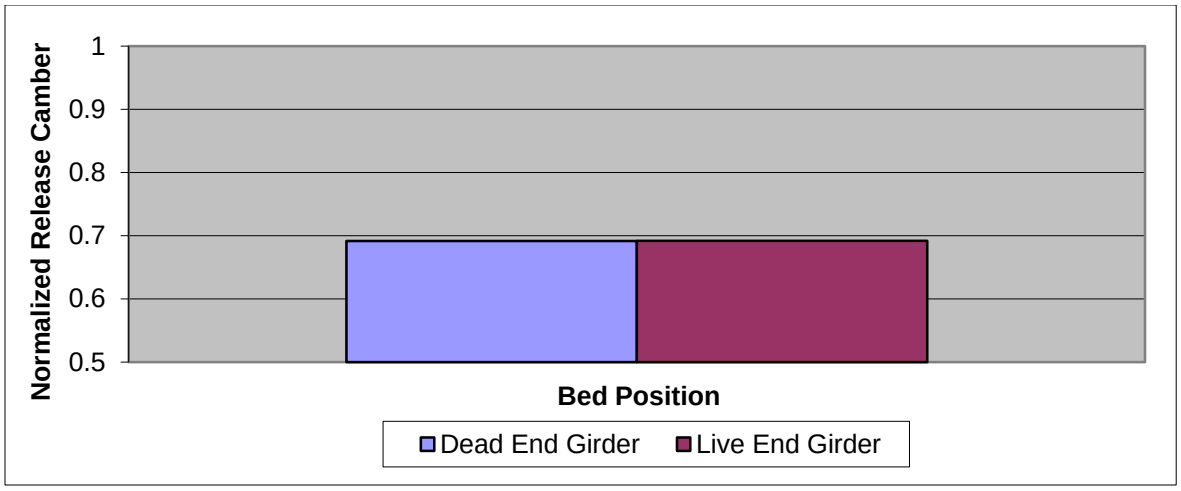

Figure A-7. Camber of girders in different bed positions for Br. 72013 (Plant A)

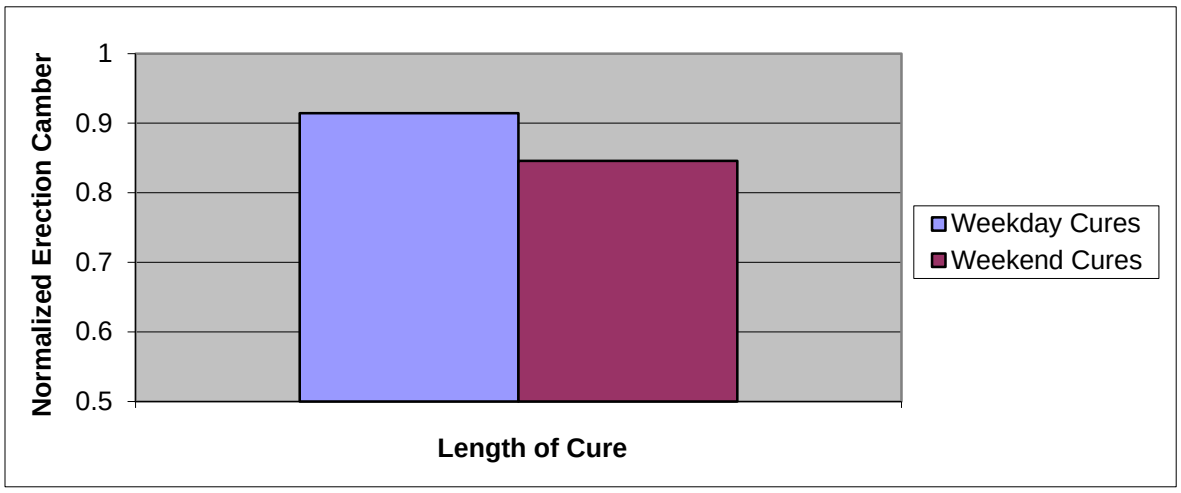

Figure A-8. Normalized camber of weekend vs. weekday cured girders for Br. 01531

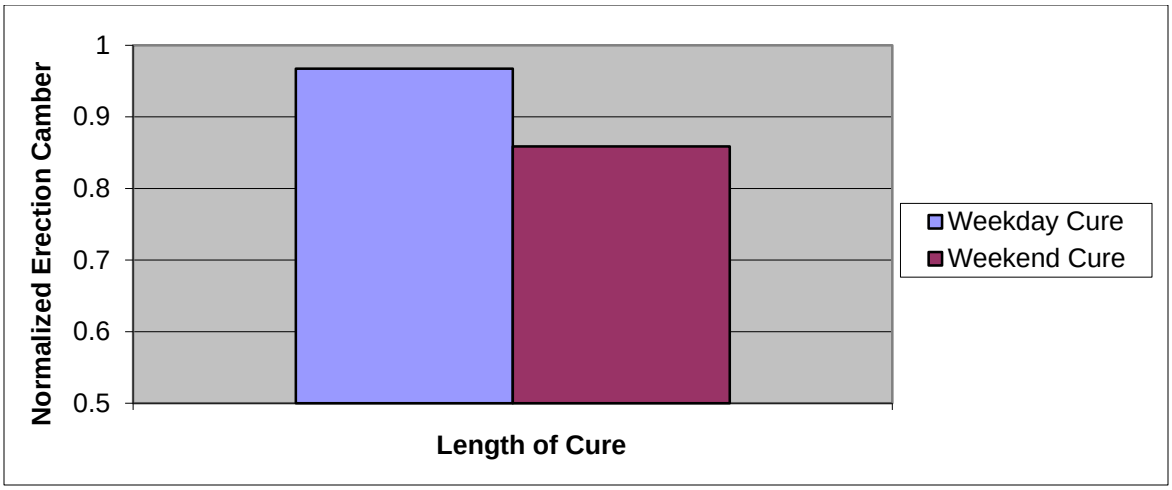

Figure A-9. Normalized camber of weekend vs. weekday cured girders for Br. 17532

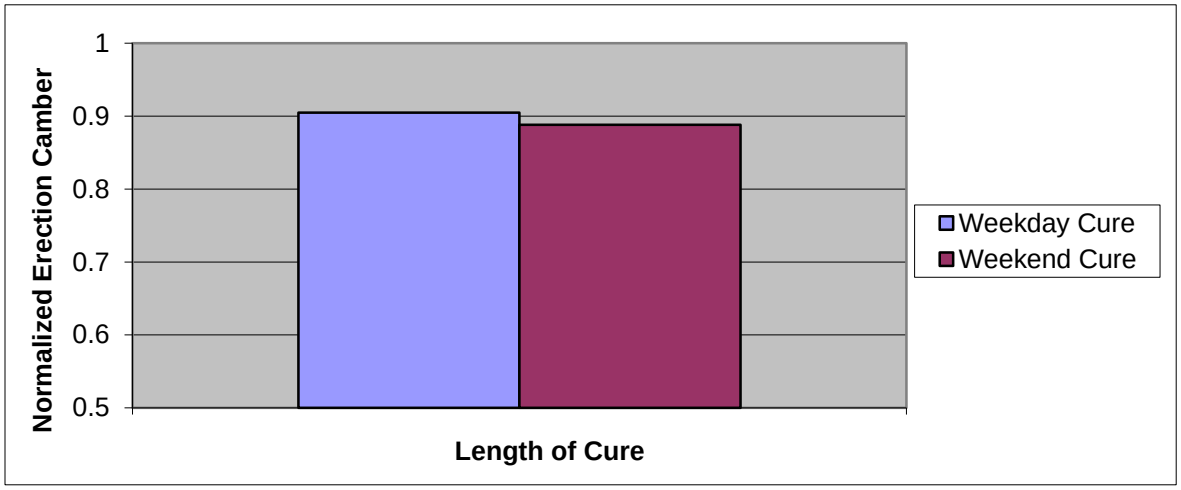

Figure A-10. Normalized camber of weekend vs. weekday cured girders for Br. 19561

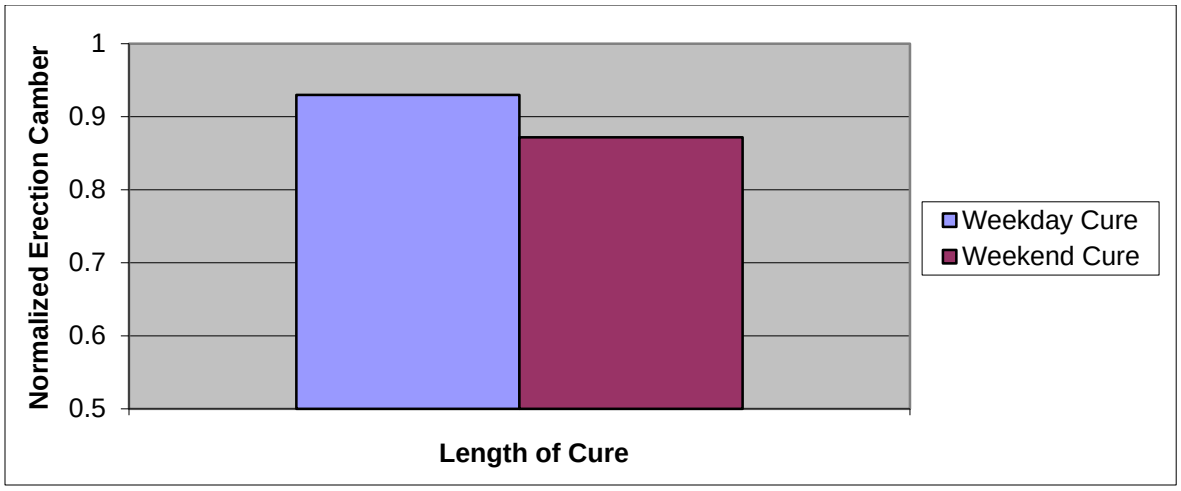

Figure A-11. Normalized camber of weekend vs. weekday cured girders for Br. 27R20,21

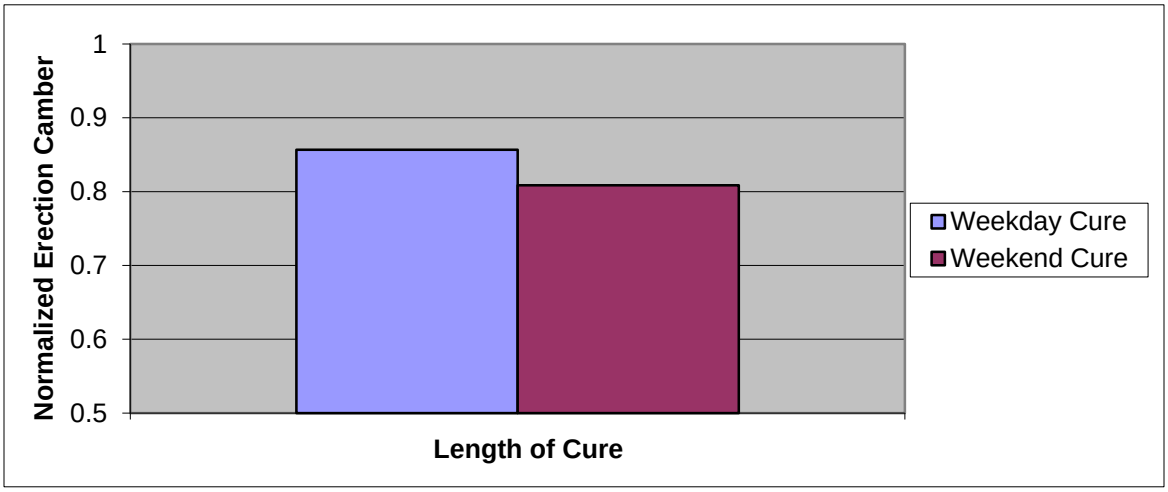

Figure A-12. Normalized camber of weekend vs. weekday cured girders for Br. 14549

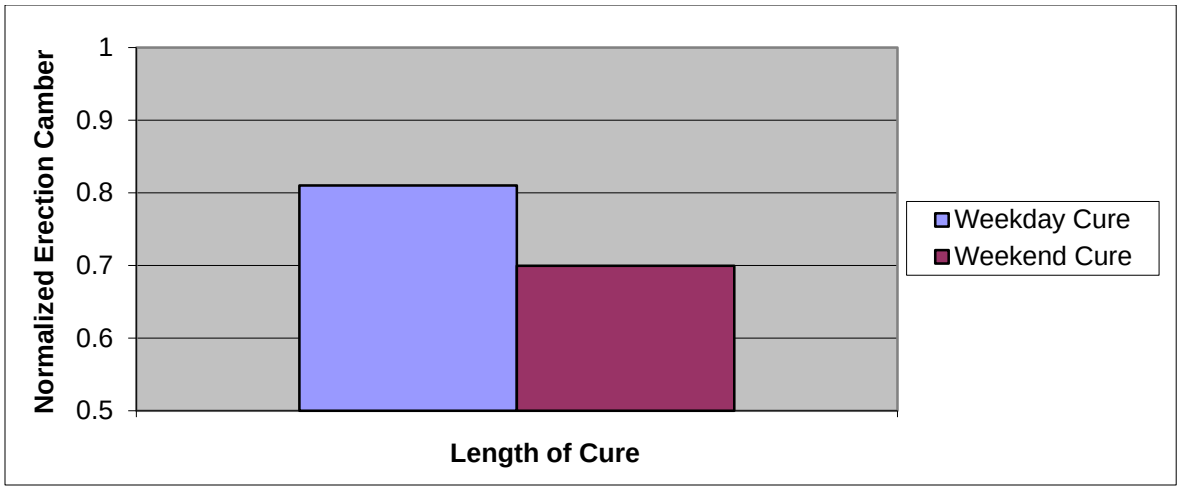

Figure A-13. Normalized camber of weekend vs. weekday cured girders for Br. 69844

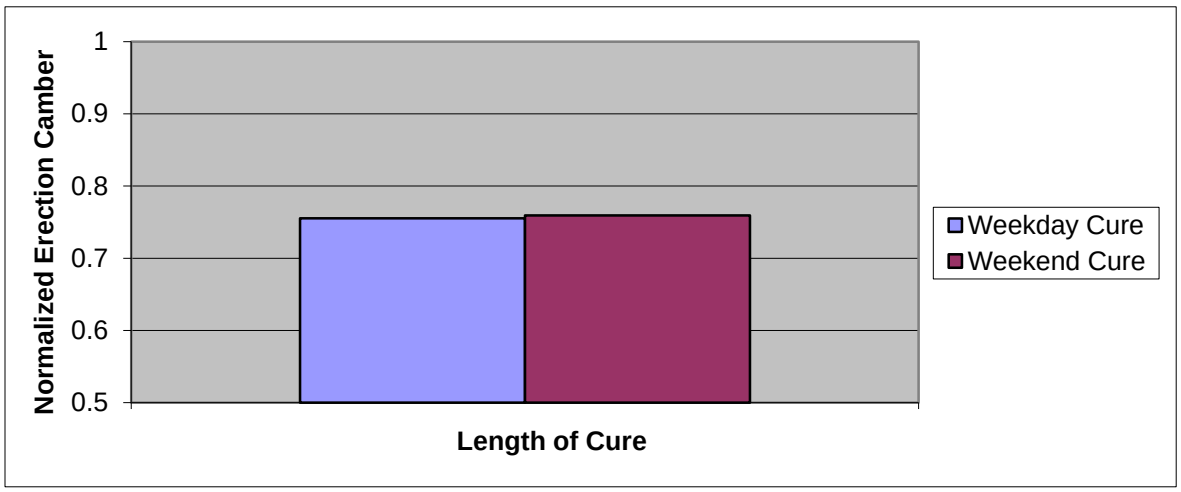

Figure A-14. Normalized camber of weekend vs. weekday cured girders for Br. 14816

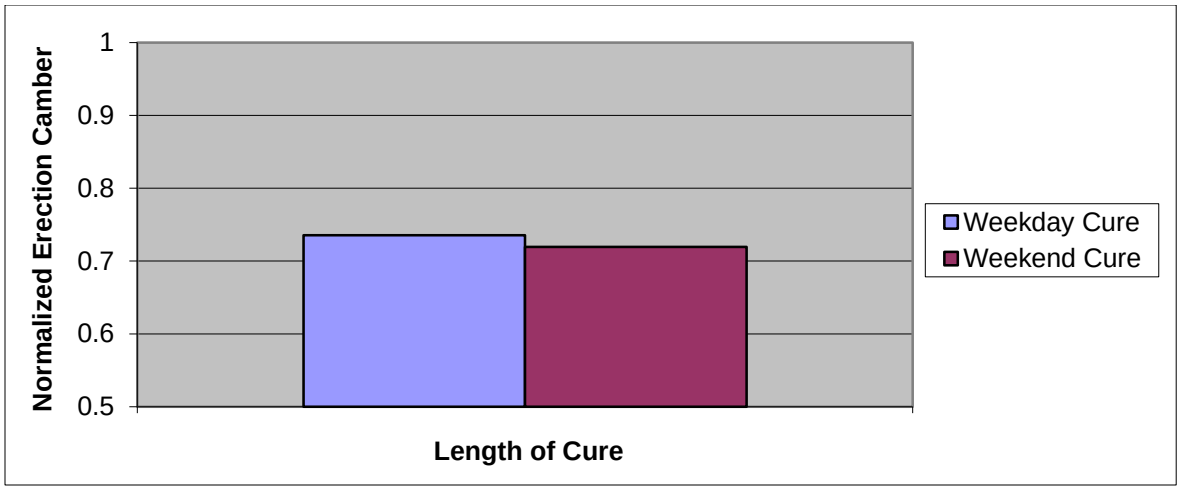

Figure A-15. Normalized camber of weekend vs. weekday cured girders for Br. 07581

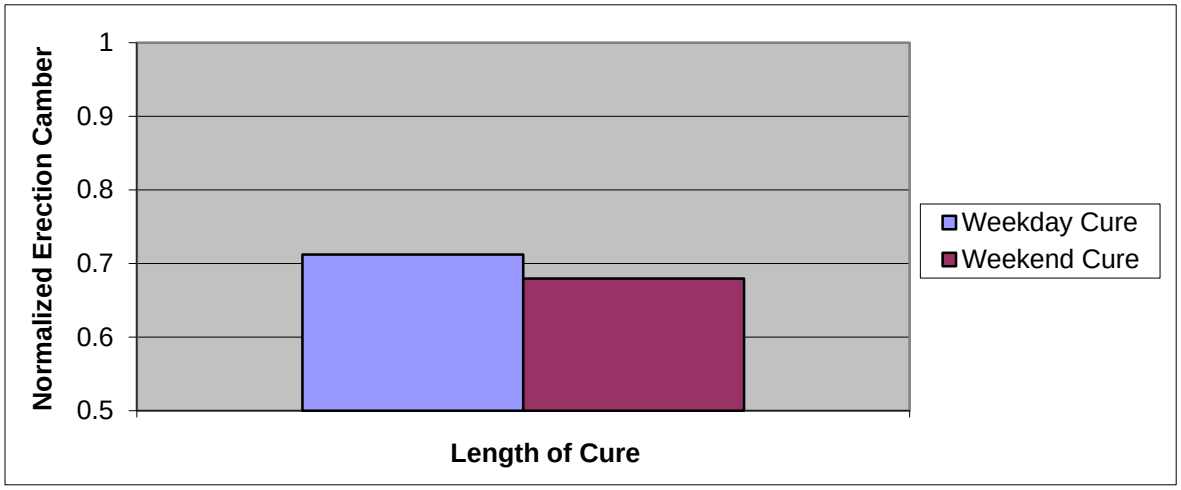

Figure A-16. Normalized camber of weekend vs. weekday cured girders for Br. 72013

APPENDIX B. THERMAL EFFECTS ANALYSIS

B.1 Introduction

During fabrication, the prestressing strands are anchored to the precasting bed to the abutments at each end. Because the precasting bed has a fixed length, the changes in the mechanical and thermal strains in the strand must sum to zero. As a consequence, the temperature changes along the length of strand in the bed will impact the amount of mechanical stress at the time of concrete-steel bonding and strand release. Between strand pull and concrete-steel bond, strands within the freshly cast concrete heat up as a result of the concrete heat of hydration while curing, and undergo a loss in mechanical strain to balance the increase in thermal strain. Additionally, any uncovered free length of strand on the bed must be taken into consideration when determining the effect of temperature on the strand stress, because the ambient air temperature at the time of concrete-steel bonding is likely to have changed since the strands were initially stressed. However, these changes in strand stress due to thermal effects prior to concrete-steel bond are partially recoverable, as long as the concrete temperature drops between bond and strand release.

Because the coefficients of thermal expansion of the steel and concrete differ, additional prestress changes occur as the system changes temperature between concrete-steel bond and strand release. Because the concrete temperature at strand release is typically lower than it is at the time of concrete-steel bond, this effect usually results in the recovery of prior prestress losses that occur between strand pull and concrete-steel bond. In other words, some of the stress loss that occurs prior to concrete-steel bond will be recovered due to the cooling of the concrete and strand during the curing process. Finally, after strand release, additional prestress changes occur as the system undergoes further thermal changes to match the ambient temperature. As such, a thermal datum point should be selected such that the desired level of prestress in the section can be referenced relative to that temperature (e.g., 70 ^{o}F).

Even though steps are taken by the precasters to account for strand temperature changes, as described in Section 3.2, the current temperature correction procedures only account for the differences in strand temperature at tensioning relative to the temperature assumed at concrete placement (i.e., the concrete mix temperature). These corrections do not take into account the effect of ambient temperature changes on the uncovered free length of strand in the bed or the effect of elevated temperatures on the strand within the concrete during curing as the bond between the strand and concrete develops.

B.2 Analysis

Barr et al. (2005) examined thermal effects in their study and developed a simple expression to calculate the stress loss in the strand between strand pull and concrete-steel bond, due to high fabrication temperatures. Erkmen et al. (2008) also examined the effect of high fabrication temperatures, but included an extensive analysis of the effect due to the cooling of the concrete and strand prior to strand release. Erkmen et al. (2008) did not, however, investigate the effect of varying ambient temperatures on the stress in the free length of strand. The following derivation represents the procedure used for the thermal effects analysis, which uses expressions from both Barr et al. (2005) and Erkmen et al. (2008). Also included in the derivation is the calculation of prestress losses due to elastic shortening, which is presented in Section 1.2.

The following conceptual assumptions were made for the thermal effects analysis conducted in the parametric study.

1. Bending stresses/strains due to thermal effects can be neglected.
2. Concrete coefficient of thermal expansion remains constant.
3. Concrete modulus of elasticity remains constant from time of bond to strand release.
4. No thermal gradient along the girders or through the girder depth.
5. No thermal gradient along the free length of strand.
6. The ambient temperature between concrete-steel bond and strand release remains constant. In other words, once bond is achieved, any stress changes in the free length of strand due to thermal effects are assumed to have a negligible effect on the prestress in the girder(s).

Between concrete-steel bond and strand release, there are certain effects that could influence the stress in the strands but are difficult to quantify. There is friction present between the girder and the precasting bed and side-forms that could provide additional restraint as the girder cools. Additionally, the drape hold-downs are anchored to the precasting bed, and further resist girder shortening as it cools. It has been observed (by Ahlborn et al. (2000) and in this study) that this effect can cause pre-release cracking and that pre-release cracks tend to occur at the location of the hold-downs. Thus, it is recommended that the amount of time between the tarp removal and strand release be minimized to avoid this undesirable effect, caused by the restraint provided by the hold-downs that prevent girder shortening as it cools. For the following derivation, the possible effects of restraint due to friction and the hold-downs were ignored.

Notation

L_{bed}	Total length of precasting bed
$L_{in(i)}$	Length of strand inside the girders (covered) at step i
$L_{out(i)}$	Free (uncovered) length of strand at step i
ΔL_{in}	Change in length for the strands in the girders
ΔL_{out}	Change in length for the free strands
ΔL_g	Change in length for the girders
α_s	Coefficient of thermal expansion for strands
α_c	Coefficient of thermal expansion for concrete
A_s	Total area of prestressing strands
E_s	Modulus of elasticity of prestressing strands
A_c	Gross cross-sectional area of concrete girder section
E_c	Modulus of elasticity of concrete
I_c	Gross moment of inertia of concrete girder section
e_{mid}	Strand eccentricity at midspan
M_{sw}	Self-weight moment of girder
T_{ai}	Ambient (outside strand) temperature at step i
T_{ci}	Concrete (inside strand) temperature at step i
f_{pull}	Initial (pull) strand stress
f_{si}	Strand stress at step i
Δf_{si}	Strand stress change at step i

Δf_{net}	Total strand stress change
f_{final}	Final strand stress
P_{si}	Total strand force at step *i*
P_{ci}	Concrete reaction force at step *i*

Step 0: Initial Strand Pull

$$f_{pull} = f_{s0} \quad \textbf{(B-1)}$$

$$P_{s0} = f_{s0} A_s \quad \textbf{(B-2)}$$

Step 1: Concrete-Steel Bond

Between strand pull and concrete steel bond, the stress loss caused by thermal effects is due to the temperature changes for the strand inside the curing concrete and ambient temperature changes for the free (uncovered) length of strand. As such, the amount of thermal prestress loss depends on the proportion of strand inside the concrete. The following equation is similar to the one derived by Barr et al. (2005).

$$\Delta f_{s1} = -\frac{\alpha_s E_s}{L_{bed}}\left\{(T_{a1} - T_{a0})L_{out(0)} + (T_{c1} - T_{a0})L_{in(0)}\right\} \quad \textbf{(B-3)}$$

$$P_{s1} = (f_{s0} + \Delta f_{s1})A_s \quad \textbf{(B-4)}$$

Step 2a: Just Before Strand Release

Between concrete-steel bond and strand release, the change in strand stress is caused by the change in temperature inside the concrete and the fact that the steel and concrete have different coefficients of thermal expansion (ambient temperature changes on the free length of strand and other force restraints due to friction or hold-downs are ignored). Strain compatibility can be used to solve for the change in stress in the strands during this stage. The free-body diagram shown in Figure B-1 gives the force transfer between the steel and concrete between bond and release, simplified as a resultant force on each end. This figure was used to derive the following equations (B-5 to B-9). The figure and equations are similar to those developed by Erkmen et al. (2008).

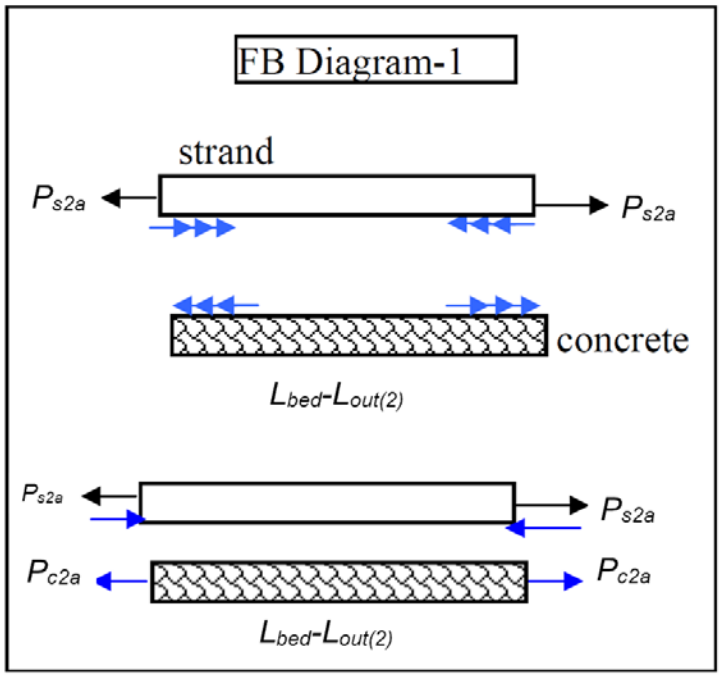

Figure B-1. Free-body diagram of forces present just before strand release

Change in length for the strands in the concrete (from step 1 to step 2a):

$$(L_{bed} - L_{out(2)}) - (L_{bed} - L_{out(1)}) = (T_{c2} - T_{c1})\alpha_s(L_{bed} - L_{out(1)}) - \frac{P_{c2a}}{A_s E_s}(L_{bed} - L_{out(2)}) + \frac{P_{s2a} - P_{s1}}{A_s E_s}(L_{bed} - L_{out(1)}) \quad \textbf{(B-5)}$$

$$(L_{out(1)} - L_{out(2)}) = (T_{c2} - T_{c1})\alpha_s(L_{bed} - L_{out(1)}) - \frac{P_{c2a}}{A_s E_s}(L_{bed} - L_{out(2)}) + \frac{P_{s2a} - P_{s1}}{A_s E_s}(L_{bed} - L_{out(1)}) \quad \textbf{(B-6)}$$

Change in length for the concrete (from step 1 to step 2a):

$$(L_{bed} - L_{out(2)}) - (L_{bed} - L_{out(1)}) = (T_{c2} - T_{c1})\alpha_c(L_{bed} - L_{out(1)}) + \frac{P_{c2a}}{A_c E_c}(L_{bed} - L_{out(2)}) \quad \textbf{(B-7)}$$

$$(L_{out(1)} - L_{out(2)}) = (T_{c2} - T_{c1})\alpha_c(L_{bed} - L_{out(1)}) + \frac{P_{c2a}}{A_c E_c}(L_{bed} - L_{out(2)}) \quad \textbf{(B-8)}$$

Change in length for the free length of strands (from step 1 to step 2a):

$$(L_{out(2)} - L_{out(1)}) = \frac{P_{s2a} - P_{s1}}{A_s E_s}(L_{out(1)}) \quad \textbf{(B-9)}$$

There are three equations (B-6, B-8 and B-9) and three unknowns ($L_{out(2)}$, P_{s2a} and P_{c2a}). Thus, the three unknowns can be found. The following equations show the solution for P_{s2a} and P_{c2a} and the resulting stress change at Step 2a.

$$P_{s2a} = P_{s1} + \frac{(L_{out(1)} - L_{bed})(T_{c2} - T_{c1})A_s E_s(\propto_s A_s E_s + \propto_c A_c E_c)}{A_s E_s L_{bed} + A_c E_c L_{out(1)}} \quad \textbf{(B-10)}$$

$$P_{c2a} = \frac{A_s E_s A_c E_c (T_{c2} - T_{c1})(\propto_s L_{out(1)} - \propto_c L_{bed})}{A_s E_s \left((T_{c2} - T_{c1}) \propto_s L_{out(1)} + L_{bed}\right) + A_c E_c \left((T_{c2} - T_{c1}) \propto_c L_{out(1)} + L_{out(1)}\right)} \quad \textbf{(B-11)}$$

$$\Delta f_{s2a} = \frac{(P_{s2a} - P_{c2a}) - P_{s1}}{A_s} \quad \textbf{(B-12)}$$

Step 2b: Just After Strand Release (Elastic Shortening)

At strand release, elastic shortening causes a further loss in strand stress. The expression used by MnDOT for calculating elastic shortening losses, given in Section 1.2, was used in this analysis.

$$\Delta f_{s2b(ES)} = -\frac{\left(A_s f_{s2a}(I_c + (e_{mid})^2 A_c)\right) - e_{mid} A_c M_{sw}}{\left(A_s(I_c + (e_{mid})^2 A_c)\right) + \frac{I_c A_c E_c}{E_s}} \quad \textbf{(B-13)}$$

$$P_{s2b} = \left(f_{s2a} + \Delta f_{s2b(ES)}\right) A_s \quad \textbf{(B-14)}$$

Step 3: Additional Girder Cooling

After strand release, the free length of strand no longer needs to be considered. The strand stress change is due to the change in temperature within the girder between strand release and some reference temperature, and the fact that the steel and concrete have different coefficients of thermal expansion. Strain compatibility can be used to find the change in stress in the strands for this stage. The free-body diagram shown in Figure B-2 gives the force equilibrium between the steel and concrete during additional girder cooling, simplified as a resultant force on each end, and was used to derive the following equations (B-15 and B-16). The figure and equations are similar to those developed by Erkmen et al. (2008).

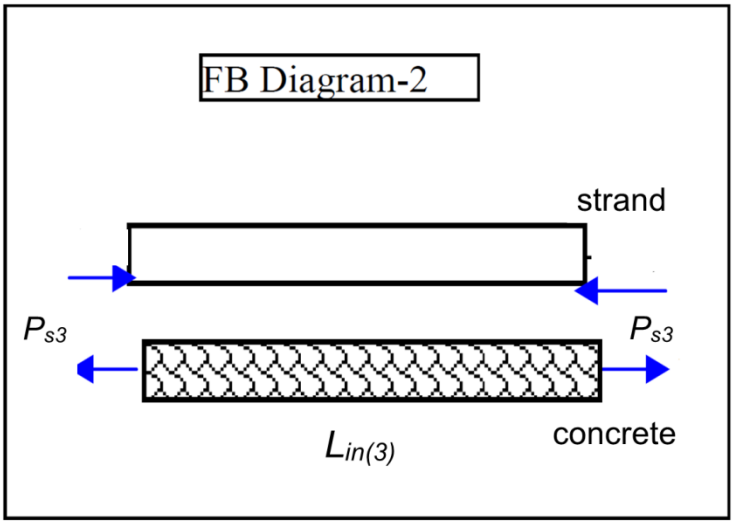

Figure B-2. Free-body diagram of forces present during additional girder cooling

Change in length for the strands (in the concrete):

$$\left(L_{in(3)} - L_{in(2)}\right) = (T_{c3} - T_{c2})\alpha_s\left(L_{in(2)}\right) - \frac{P_{s3}}{A_s E_s}(L_{in(3)}) \quad \textbf{(B-15)}$$

Change in length for the concrete:

$$\left(L_{in(3)} - L_{in(2)}\right) = (T_{c3} - T_{c2})\alpha_c\left(L_{in(2)}\right) + \frac{P_{s3}}{A_c E_c}(L_{in(3)}) \quad \textbf{(B-16)}$$

There are two equations (B-15 and B-16) and two unknowns ($L_{in(3)}$ and P_{s3}). Thus, the two unknowns can be found. The following equations show the solution for P_{s3} and the resulting stress change at Step 3.

$$P_{s3} = P_{s2b} - \frac{A_s E_s A_c E_c (T_{c3} - T_{c2})(\propto_s - \propto_c)}{A_s E_s\left((T_{c3} - T_{c2}) \propto_s + 1\right) + A_c E_c\left((T_{c3} - T_{c2}) \propto_c + 1\right)} \quad \textbf{(B-17)}$$

$$\Delta f_{s3} = \frac{P_{s3} - P_{s2b}}{A_s} \quad \textbf{(B-18)}$$

Results

The total net change in strand stress is the sum of the stress changes at each of the previous steps and the final strand stress is the initial pull stress plus the total net stress change.

$$\Delta f_{net} = \Delta f_{s1} + \Delta f_{s2a} + \Delta f_{s2b(ES)} + \Delta f_{s3} \quad \textbf{(B-19)}$$

$$f_{final} = f_{pull} + \Delta f_{net} \quad \textbf{(B-20)}$$

B.3 Parametric Study

A parametric study was conducted using the thermal effects analysis in order to investigate the changes in prestress (and release camber) due to the variation of total strand area, girder size, amount of free length of strand and concrete and ambient temperatures. The results of the study were based on the following assumptions, unless otherwise stated:

- A 129 ft-9 in (39.55 m) MN54 girder (A_c = 749 in^2, w_c = 155 pcf) with 50 0.6 in (15.2 mm) diameter 270 ksi low relaxation strands (A_s = 50x0.217 in^2) was used.
- Strands were pulled to an initial stress of 202.5 ksi (i.e., 0.75f_{pu}).
- To take into account the temperature corrections used at the precasting plants, the initial strand stress was raised or lowered by 1% for each 10 °F difference in temperature between the ambient conditions at strand pull and the assumed concrete mix temperature, which was the typical procedure used. For the parametric study, the concrete mix temperature was assumed to be 70 °F (21 °C).
- The length of the bed and the amount of free length of strand were taken to be 365 ft (111.3 m) and 62 ft (18.9 m), respectively, which were average values for the 1067 girders in the historical database.
- The coefficients of thermal expansion were 6.8 με/°F (12 με/°C) for the prestressing strand and 5.8 με/°F (10.4 με/°C) for the concrete.
- The elastic modulus of the prestressing strand was 28,500 ksi.
- The elastic modulus of the concrete was 4464 ksi.
- The temperature in the concrete at the time of concrete-steel bond and strand release were assumed to be 140 °F (60 °C) and 97 °F (36 °C), respectively. These concrete temperature values were consistent with those used by Barr et al. (2005) and Erkmen et al. (2008), respectively, and with observations from thermal curing data obtained from the precasting plants, discussed in Section 7.5.1. It should be noted that the time at which concrete-steel bond occurred was assumed to be 6-10 hours after concrete pouring, which was consistent with the assumption made by Barr et al. (2005).
- The ambient temperature at strand pull and concrete-steel bond was taken as 70 °F (21 °C).

The procedure outlined in the previous section was used in the study. Because it was of most interest to investigate these effects on release camber, only the thermal prestress losses that occurred between strand pull and strand release were used. The changes in prestress that occurred after strand release due to additional girder cooling were ignored. In the following tables, TL_1 represents the stress loss between strand pull and concrete-steel bond (i.e., $(P_{s1}-P_{s0})/A_s$) and TL_2 represents the stress loss between bond and strand release (i.e., $((P_{s2a}-P_{c2a})-P_{s1})/A_s$). It should be noted that TL_2 will usually be positive (stress gain) due to the cooling of the concrete and strands. The corresponding loss in camber due to the total thermal prestress losses was calculated by reducing the prestress force at release by the appropriate amount in the calculations for camber, including prestress losses due to elastic shortening, as described in Section 1.2.

B.3.1 Effect of Total Strand Area

The thermal prestress losses that occur between stand pull and concrete-steel bond, TL_1, are a function of temperature change and the strand length within the girders and outside the girders (free length of strand). Thus, the total strand area does not affect this initial stress loss. However, the stress losses that occur from bond to strand release, TL_2, are a function of total strand area, concrete area and moment of inertia, the elastic modulus and coefficient of thermal expansion of the concrete and strand, and temperature changes. The relationship between strand area and TL_2 is nonlinear and the magnitude of TL_2 decreases as the strand area increases. Table B- shows the results of the calculated prestress and camber losses. The total amount of thermal losses ranges from 4.65% (10 strands) to 3.81% (60 strands) and the total amount of camber loss ranges from 8.50% to 6.97%.

Table B-1. Effect of total strand area on thermal camber losses

# strands	A_s (in^2)	A_s/A_c*100	TL_1 (ksi)	TL_2 (ksi)	TL_1+TL_2 (ksi)	Prestress change (%)	Camber change (%)
10	2.17	0.290	-11.07	1.65	-9.42	-4.65[1]	-8.50[2]
20	4.34	0.579	-11.07	2.11	-8.96	-4.42	-8.08
30	6.51	0.869	-11.07	2.50	-8.57	-4.23	-7.74
40	8.68	1.159	-11.07	2.83	-8.25	-4.07	-7.44
50	10.85	1.449	-11.07	3.11	-7.96	-3.93	-7.19
60	13.02	1.738	-11.07	3.35	-7.72	-3.81	-6.97

[1]Percent change determined as (prestress change/initial strand stress)*100
[2]Percent change determined as the change in release camber associated with the use of the final strand stress in place of 202.5 ksi, in the camber calculations described in Section 1.2

B.3.2 Effect of Girder Size

To isolate the effect of girder size on thermal losses, 40 prestressing strands (A_s = 8.68 in^2) was used in each case. The girder shapes included in the study were the ones used by MnDOT. The stress losses that occur between strand pull and concrete-steel bond are independent of A_c, and thus, are the same for each case. However, the losses that occur between the time of bond and strand release are affected by a change in A_c. The relationship between girder size and TL_2 is nonlinear and the magnitude of TL_2 increases with girder size (A_c). Table B- shows the results of the calculated prestress and camber losses. The total amount of thermal losses ranges from 3.83% (for A_c = 516 in^2) to 4.14% (for A_c = 840 in^2) and the total amount of camber loss ranges from 7.01% to 7.56%.

Table B-2. Effect of girder size on thermal camber losses

Girder Shape	A_c (in^2)	A_s (in^2)	A_s/A_c*100	TL_1 (ksi)	TL_2 (ksi)	TL_1+TL_2 (ksi)	Prestress change (%)	Camber change (%)
27M	516	8.68	1.68	-11.07	3.31	-7.76	-3.83[1]	-7.01[2]
36M	570	8.68	1.52	-11.07	3.17	-7.90	-3.90	-7.13
MN45	690	8.68	1.26	-11.07	2.93	-8.14	-4.02	-7.35
MN54	749	8.68	1.16	-11.07	2.83	-8.25	-4.07	-7.44
72M	786	8.68	1.10	-11.07	2.77	-8.30	-4.10	-7.49
MN63	807	8.68	1.08	-11.07	2.74	-8.33	-4.11	-7.52
81M	840	8.68	1.03	-11.07	2.69	-8.38	-4.14	-7.56

[1]Percent change determined as (prestress change/initial strand stress)*100
[2]Percent change determined as the change in release camber associated with the use of the final strand stress in place of 202.5 ksi, in the camber calculations described in Section 1.2

B.3.3 Effect of Concrete Curing Temperature Variations

Because a concrete bond temperature of 140 °F (60 °C) and a release temperature of 97°F (36 °C) were only rough estimates, it was necessary to examine the effect of varying these temperatures. The temperature of the concrete at the time of bond can vary due to the type of curing (steam-cured vs. heat (heat-of-hydration)) and due to the time at which bond is formed. The temperature of the concrete at release can vary due to the ambient temperature, the length of cure, and the time elapsed between when the side-forms are removed and the strands are cut. Temperature variations of ±10 °C for both concrete temperatures were used in this study. The relationship between these temperature variations and prestress losses is nonlinear and the amount of prestress loss increases as the temperatures increase. Table B- shows the results of the calculated prestress and camber losses.

Table B-3. Effect of concrete curing temperatures on thermal camber losses

Temp at Bond (°F)	Temp at Release (°F)	TL_1 (ksi)	TL_2 (ksi)	TL_1+TL_2 (ksi)	Prestress change (%)	Camber change (%)
140	77	-11.07	4.53	-6.54	-3.23[1]	-5.91[2]
140	97	-11.07	3.11	-7.96	-3.93	-7.19
140	113	-11.07	1.94	-9.13	-4.51	-8.24
122	97	-8.23	1.81	-6.42	-3.17	-5.79
140	97	-11.07	3.11	-7.96	-3.93	-7.19
158	97	-13.91	4.40	-9.51	-4.70	-8.58

[1]Percent change determined as (prestress change/initial strand stress)*100
[2]Percent change determined as the change in release camber associated with the use of the final strand stress in place of 202.5 ksi, in the camber calculations described in Section 1.2

B.3.4 Effect of Free Length of Strand and Ambient Temperature Variations

Because the amount of free length in the bed for any given pour and the ambient temperatures present during a pouring season were so variable and because the ambient temperature affects the stress in the strands, variations in these parameters were combined in the analysis. The parameters varied in the study were the amount of free length of strand in the bed, the ambient air temperature at the time of strand pull, and the ambient air temperature at the time of concrete-steel bond. A minimum, average and maximum free (uncovered) length of strand was found by examining the historical girder data. These values were taken as 6 ft (1.83 m), 62 ft (18.9 m) and 260 ft (79.2 m), respectively. The ambient air temperatures used at both the time of strand pull and concrete-steel bond were 70 °F (21 °C), 36 °F (2.2 °C) and 104 °F (40 °C). These temperatures represented a realistic average value and lower and upper bounds for possible ambient temperatures experienced in a pouring season. As mentioned above, in order to take into account the temperature corrections used at the precasting plants, the initial strand stress was raised or lowered by 1% for each 10 °F difference in temperature between the ambient conditions at strand pull and the assumed concrete mix temperature, where the concrete mix temperature was assumed to be 70 °F (21 °C). There are 27 separate cases in the parametric study, resulting from three possible values for the three varied parameters. Table B- shows the results of the calculated prestress and camber losses.

Table B-4. Effect of strand free length and ambient temperature variations on thermal camber losses

Case	Free Length (ft)	Air Temp at Pull (°F)	Initial Strand Stress (ksi)	Air Temp at Bond (°F)	TL_1 (ksi)	TL_2 (ksi)	$TL_1 + TL_2$ (ksi)	Final Strand Stress (ksi)	Prestress change (%)	Camber change (%)
1	62	70	202.5	70	-11.07	3.11	-7.96	194.54	-3.93[1]	-7.19[2]
2	62	70	202.5	104	-12.18	3.11	-9.07	193.43	-4.48	-8.18
3	62	70	202.5	36	-9.98	3.11	-6.87	195.63	-3.39	-6.20
4	6	70	202.5	70	-13.12	7.02	-6.10	196.40	-3.01	-5.51
5	6	70	202.5	104	-13.23	7.02	-6.21	196.29	-3.07	-5.60
6	6	70	202.5	36	-13.01	7.02	-5.99	196.51	-2.96	-5.41
7	260	70	202.5	70	-3.84	1.24	-2.60	199.90	-1.28	-2.35
8	260	70	202.5	104	-8.47	1.24	-7.23	195.27	-3.57	-6.52
9	260	70	202.5	36	0.74	1.24	1.98	204.48	+0.98	+1.78
10	62	36	210.6	70	-17.50	3.11	-14.39	196.21	-6.83	-5.68
11	62	36	210.6	104	-18.61	3.11	-15.50	195.10	-7.36	-6.68
12	62	36	210.6	36	-16.41	3.11	-13.30	197.30	-6.32	-4.70
13	6	36	210.6	70	-19.55	7.02	-12.53	198.07	-5.95	-4.00
14	6	36	210.6	104	-19.66	7.02	-12.64	197.96	-6.00	-4.10
15	6	36	210.6	36	-19.44	7.02	-12.42	198.18	-5.90	-3.91
16	260	36	210.6	70	-10.27	1.24	-9.03	201.57	-4.29	-0.84
17	260	36	210.6	104	-14.90	1.24	-13.66	196.95	-6.48	-5.01
18	260	36	210.6	36	-5.69	1.24	-4.45	206.15	-2.11	+3.28
19	62	104	194.4	70	-4.57	3.11	-1.46	192.94	-0.75	-8.63
20	62	104	194.4	104	-5.67	3.11	-2.56	191.84	-1.32	-9.62
21	62	104	194.4	36	-3.48	3.11	-0.37	194.03	-0.19	-7.65
22	6	104	194.4	70	-6.62	7.02	0.40	194.80	+0.21	-6.95
23	6	104	194.4	104	-6.73	7.02	0.29	194.69	+0.15	-7.05
24	6	104	194.4	36	-6.52	7.02	0.50	194.90	+0.26	-6.86
25	260	104	194.4	70	2.66	1.24	3.90	198.30	+2.01	-3.79
26	260	104	194.4	104	-1.97	1.24	-0.73	193.67	-0.38	-7.96
27	260	104	194.4	36	7.24	1.24	8.48	202.88	+4.36	+0.33

[1]Percent change determined as (prestress change/initial strand stress)*100

[2]Percent change determined as the change in release camber associated with the use of the final strand stress in place of 202.5 ksi, in the camber calculations described in Section 1.2

Comparing Cases 1, 2 and 3 to Cases 4 through 9, the results indicate that the prestress and camber loss is more significant for the case(s) where the *average* amount of free length of strand is uncovered, which is clearly the most common situation. This is due to the fact that the net stress loss is a two-step process. The amount of stress loss between strand pull and concrete-steel bond is maximized when the free length of strand goes to zero. However, the stress recovery that occurs between bond and strand release is also maximized when the free length of strand goes to zero. Thus, there is an amount of free length of strand that is not zero, which maximizes the total *net* stress loss. The amount of prestress and camber loss also increases with increased ambient air temperature at the time of bond, as can be seen by comparing Case 3 to Cases 1 and 2. This is because the warmer ambient temperatures cause the strand to experience a reduction in mechanical strain. Therefore, the "worst-case" scenario is when the average amount of free length of strand (approximately) is on the bed and the ambient air temperature when the bond is formed is very high, relative to the temperature when the strands were pulled. In the

parametric study, this case leads to decreases in release cambers of 6-10%. Finally, the average reduction in strand prestress is approximately 5.5 ksi, (about 2.7% of the initial pull stress and 2.0% of f_{pu}), and the average reduction in camber is approximately 5.0% considering the 27 cases shown.

B.4 Example Problem

The following is an example problem created to illustrate the thermal effects analysis described in Section B.2 and used for the parametric study in Section B.3. In addition to the loss of prestress due to thermal effects between strand pull and strand release, the prestress loss due to elastic shortening and the change in prestress due to further concrete cooling are also included in the problem. In Section 7.5.1, it was discussed that the effect of weekend curing was not as significant at release because of cooler concrete temperatures at concrete-steel bond and strand release. To support this discussion and to illustrate the possible variation in thermal prestress losses, the basic assumptions (i.e., girder cross section, girder and bed lengths and material properties) used in the example problem are consistent with those used in that discussion. It should be noted that the change in prestress due to additional concrete cooling included in this example was not included in Section 7.5.1 (in that section only the immediate camber at release was considered).

The example problem consists of two 131 ft-6 in (40.1 m) MN63 girders with 42 0.6 in (15.2 mm) diameter strands, poured in a 357 ft (108.8 m) precasting bed. It should be noted that the small amount of strand located between the girders was always covered by the fabricators and was assumed to be included with the strand in the girders. For Plants A and B, the length of strand between the girders was typically approximately 40 in (1.02 m). The example problem consists of three cases: weekday and steam cured, weekend and steam cured, and weekend and heat (i.e., heat-of-hydration) cured. The inputs for the example problem that do not vary between each of these cases are shown below:

Example Problem Inputs

L_{bed}	357 ft	Total length of precasting bed
L_{in}	269.7 ft	Length of strand inside the girders (covered)
L_{out}	87.3 ft	Free (uncovered) length of strand
α_s	6.8 με/°F	Coefficient of thermal expansion for strands
α_c	5.8 με/°F	Coefficient of thermal expansion for concrete
A_s	42x0.217=9.11 in^2	Total area of prestressing strands
E_s	28500 ksi	Modulus of elasticity of prestressing strands
A_c	807 in^2	Gross cross-sectional area of concrete girder section
I_c	422570 in^4	Gross moment of inertia of concrete girder section
e_{mid}	24.66 in	Strand eccentricity at midspan
M_{sw}	22531.3 k-in	Self-weight moment due to girder (w_c = 155 pcf)
T_{a1}	70 °F (21 °C)	Ambient temperature at time of strand pull
T_{a2}	70 °F (21 °C)	Ambient temperature at time of concrete-steel bond
T_{c3}	70 °F (21 °C)	Concrete temperature after additional cooling
f_{pull}	202.5 ksi	Initial (pull) strand stress
f_{si}	N/A	Strand stress at step *i*
Δf_{si}	N/A	Strand stress change at step *i*
Δf_{net}	N/A	Total strand stress change
f_{final}	N/A	Final strand stress
P_{si}	N/A	Total strand force at step *i*
P_{ci}	N/A	Concrete reaction force at step *i*

Case 1: Weekday and Steam Cured

E_c	5515 ksi	Modulus of elasticity of concrete
T_{c1}	140 °F (60 °C)	Concrete temperature at time of concrete-steel bond
T_{c2}	97 °F (36 °C)	Concrete temperature at time of strand release

Step 1: Concrete-Steel Bond

$$\Delta f_{s1} = -\frac{\alpha_s E_s}{L_{bed}}\left\{(T_{a1} - T_{a0})L_{out(0)} + (T_{c1} - T_{a0})L_{in(0)}\right\} = -10.07\ ksi \quad \textbf{(B-21)}$$

$$P_{s1} = (f_{s0} + \Delta f_{s1})A_s = 1753.7\ kips\ (k) \quad \textbf{(B-22)}$$

Step 2a: Just Before Strand Release

$$P_{s2a} = P_{s1} + \frac{(L_{out(1)} - L_{bed})(T_{c2} - T_{c1})A_s E_s(\propto_s A_s E_s + \propto_c A_c E_c)}{A_s E_s L_{bed} + A_c E_c L_{out(1)}} = 1926.3\ k \quad \textbf{(B-23)}$$

$$P_{c2a} = \frac{A_s E_s A_c E_c (T_{c2} - T_{c1})(\propto_s L_{out(1)} - \propto_c L_{bed})}{A_s E_s \left((T_{c2} - T_{c1}) \propto_s L_{out(1)} + L_{bed}\right) + A_c E_c \left((T_{c2} - T_{c1}) \propto_c L_{out(1)} + L_{out(1)}\right)} = 153.7\ k \quad \textbf{(B-24)}$$

$$\Delta f_{s2a} = \frac{(P_{s2a} - P_{c2a}) - P_{s1}}{A_s} = 2.07\ ksi \quad \textbf{(B-25)}$$

Step 2b: Just After Strand Release (Elastic Shortening)

$$\Delta f_{s2b(ES)} = -\frac{\left(A_s f_{s2a}(I_c + (e_{mid})^2 A_c)\right) - e_{mid} A_c M_{sw}}{\left(A_s (I_c + (e_{mid})^2 A_c)\right) + \frac{I_c A_c E_c}{E_s}} = -15.75\ ksi \quad \textbf{(B-26)}$$

$$P_{s2b} = \left(f_{s2a} + \Delta f_{s2b(ES)}\right) A_s = 1629.1\ k \quad \textbf{(B-27)}$$

Step 3: Additional Girder Cooling

$$P_{s3} = P_{s2b} - \frac{A_s E_s A_c E_c (T_{c3} - T_{c2})(\propto_s - \propto_c)}{A_s E_s \left((T_{c3} - T_{c2}) \propto_s + 1\right) + A_c E_c \left((T_{c3} - T_{c2}) \propto_c + 1\right)} = 1635.0\ k \quad \textbf{(B-28)}$$

$$\Delta f_{s3} = \frac{P_{s3} - P_{s2b}}{A_s} = 0.65\ ksi \quad \textbf{(B-29)}$$

Results

$$\Delta f_{net} = \Delta f_{s1} + \Delta f_{s2a} + \Delta f_{s2b(ES)} + \Delta f_{s3} = -23.1\ ksi \quad \textbf{(B-30)}$$

$$f_{final} = f_{pull} + \Delta f_{net} = 179.4\ ksi \quad \textbf{(B-31)}$$

Case 2: Weekend and Steam Cured

E_c	5974 ksi	Modulus of elasticity of concrete
T_{c1}	140 °F (60 °C)	Concrete temperature at time of concrete-steel bond
T_{c2}	70 °F (21 °C)	Concrete temperature at time of strand release

(Note: A value of 97 °F (36 °C) was used for T_{c2} of the "weekend 1" girder from Section 7.5.1)

Step 1: Concrete-Steel Bond

$$\Delta f_{s1} = -\frac{\alpha_s E_s}{L_{bed}}\left\{(T_{a1} - T_{a0}) L_{out(0)} + (T_{c1} - T_{a0}) L_{in(0)}\right\} = -10.07\ ksi \quad \textbf{(B-32)}$$

$$P_{s1} = (f_{s0} + \Delta f_{s1})A_s = 1753.7\ kips\ (k) \quad \textbf{(B-33)}$$

Step 2a: Just Before Strand Release

$$P_{s2a} = P_{s1} + \frac{(L_{out(1)} - L_{bed})(T_{c2} - T_{c1})A_s E_s(\propto_s A_s E_s + \propto_c A_c E_c)}{A_s E_s L_{bed} + A_c E_c L_{out(1)}} = 2037.0\ k \quad \textbf{(B-34)}$$

$$P_{c2a} = \frac{A_s E_s A_c E_c (T_{c2} - T_{c1})(\propto_s L_{out(1)} - \propto_c L_{bed})}{A_s E_s \left((T_{c2} - T_{c1}) \propto_s L_{out(1)} + L_{bed}\right) + A_c E_c \left((T_{c2} - T_{c1}) \propto_c L_{out(1)} + L_{out(1)}\right)} = 253.5\ k \quad \textbf{(B-35)}$$

$$\Delta f_{s2a} = \frac{(P_{s2a} - P_{c2a}) - P_{s1}}{A_s} = 3.27\ ksi \quad \textbf{(B-36)}$$

Step 2b: Just After Strand Release (Elastic Shortening)

$$\Delta f_{s2b(ES)} = -\frac{\left(A_s f_{s2a}(I_c + (e_{mid})^2 A_c)\right) - e_{mid} A_c M_{sw}}{\left(A_s(I_c + (e_{mid})^2 A_c)\right) + \frac{I_c A_c E_c}{E_s}} = -14.79\ ksi \quad \textbf{(B-37)}$$

$$P_{s2b} = \left(f_{s2a} + \Delta f_{s2b(ES)}\right)A_s = 1648.8\ k \quad \textbf{(B-38)}$$

Step 3: Additional Girder Cooling

$$P_{s3} = P_{s2b} - \frac{A_s E_s A_c E_c (T_{c3} - T_{c2})(\propto_s - \propto_c)}{A_s E_s\left((T_{c3} - T_{c2}) \propto_s + 1\right) + A_c E_c\left((T_{c3} - T_{c2}) \propto_c + 1\right)} = 1648.8\ k \quad \textbf{(B-39)}$$

$$\Delta f_{s3} = \frac{P_{s3} - P_{s2b}}{A_s} = 0.0\ ksi \quad \textbf{(B-40)}$$

Results

$$\Delta f_{net} = \Delta f_{s1} + \Delta f_{s2a} + \Delta f_{s2b(ES)} + \Delta f_{s3} = -21.6\ ksi \quad \textbf{(B-41)}$$

$$f_{final} = f_{pull} + \Delta f_{net} = 180.9\ ksi \quad \textbf{(B-42)}$$

Case 3: Weekend and Heat (Heat-of-Hydration) Cured

E_c	5974 ksi	Modulus of elasticity of concrete
T_{c1}	122 °F (50 °C)	Concrete temperature at time of concrete-steel bond
T_{c2}	70 °F (21 °C)	Concrete temperature at time of strand release

Step 1: Concrete-Steel Bond

$$\Delta f_{s1} = -\frac{\alpha_s E_s}{L_{bed}}\{(T_{a1} - T_{a0})L_{out(0)} + (T_{c1} - T_{a0})L_{in(0)}\} = -7.49\ ksi \quad \textbf{(B-43)}$$

$$P_{s1} = (f_{s0} + \Delta f_{s1})A_s = 1777.2\ kips\ (k) \quad \textbf{(B-44)}$$

Step 2a: Just Before Strand Release

$$P_{s2a} = P_{s1} + \frac{(L_{out(1)} - L_{bed})(T_{c2} - T_{c1})A_s E_s(\propto_s A_s E_s + \propto_c A_c E_c)}{A_s E_s L_{bed} + A_c E_c L_{out(1)}} = 1987.9\ k \quad \textbf{(B-45)}$$

$$P_{c2a} = \frac{A_s E_s A_c E_c (T_{c2} - T_{c1})(\propto_s L_{out(1)} - \propto_c L_{bed})}{A_s E_s\left((T_{c2} - T_{c1}) \propto_s L_{out(1)} + L_{bed}\right) + A_c E_c\left((T_{c2} - T_{c1}) \propto_c L_{out(1)} + L_{out(1)}\right)} = 188.5\ k \quad \textbf{(B-46)}$$

$$\Delta f_{s2a} = \frac{(P_{s2a} - P_{c2a}) - P_{s1}}{A_s} = 2.43\ ksi \quad \textbf{(B-47)}$$

Step 2b: Just After Strand Release (Elastic Shortening)

$$\Delta f_{s2b(ES)} = -\frac{\left(A_s f_{s2a}(I_c + (e_{mid})^2 A_c)\right) - e_{mid} A_c M_{sw}}{\left(A_s(I_c + (e_{mid})^2 A_c)\right) + \frac{I_c A_c E_c}{E_s}} = -14.97\ ksi \quad \textbf{(B-48)}$$

$$P_{s2b} = \left(f_{s2a} + \Delta f_{s2b(ES)}\right)A_s = 1663.0 \quad \textbf{(B-49)}$$

Step 3: Additional Girder Cooling

$$P_{s3} = P_{s2b} - \frac{A_s E_s A_c E_c (T_{c3} - T_{c2})(\propto_s - \propto_c)}{A_s E_s\left((T_{c3} - T_{c2}) \propto_s + 1\right) + A_c E_c\left((T_{c3} - T_{c2}) \propto_c + 1\right)} = 1663.0\ k \quad \textbf{(B-50)}$$

$$\Delta f_{s3} = \frac{P_{s3} - P_{s2b}}{A_s} = 0.0\ ksi \quad \textbf{(B-51)}$$

Results

$$\Delta f_{net} = \Delta f_{s1} + \Delta f_{s2a} + \Delta f_{s2b(ES)} + \Delta f_{s3} = -20.0\ ksi \quad \textbf{(B-52)}$$

$$f_{final} = f_{pull} + \Delta f_{net} = 182.5\ ksi \quad \textbf{(B-53)}$$

For this example problem, the total prestress loss due to thermal effects for each of the three cases was 7.35, 6.81 and 5.06 ksi, respectively, which are approximately 3.6%, 3.4% and 2.5% of the initial pull stress, respectively. The total prestress loss due to thermal effects and elastic shortening for each of the three cases was 23.1, 21.6 and 20.0 ksi, respectively, which are approximately 11.4%, 10.7% and 9.88% of the initial pull stress, respectively. These results show that the amount of thermal prestress loss was reduced because of cooler concrete temperatures at both concrete-steel bond and strand release. Additionally, the results show that the amount of thermal prestress loss was more sensitive to changes in the concrete temperature at bond than at strand release, which was also reported in Table B-.

B.5 Temperature Correction Spreadsheet for Fabricators

Because the temperature correction procedures used by the fabricators and recommended by MnDOT do not adequately take into account the prestress losses due to thermal effects, a spreadsheet was created for both precasting plants that outputs a temperature correction based on the thermal effects analysis. The temperature correction is calculated such that an increase (or decrease) in pull force is required so that the stress in the strands at a standard reference temperature after strand release and additional concrete cooling (Step 3 in Section B.2) matches the strand stress that would be achieved with the design pull force and no thermal stress losses. It should be noted that prestress losses due to elastic shortening are not accounted for in the spreadsheet because they are already calculated in design and should not alter the required pull stress. Separate spreadsheets were created for Plant A and Plant B associated with their respective tensioning procedures, which require the fabricators to insert a few simple inputs. Because some temperatures are clearly not known explicitly at the time of strand pull, certain assumptions were made in the spreadsheets. These assumptions are detailed below:

- The concrete temperature at the time of concrete-steel bond was approximated as 140 °F (60 °C) for steam cures and 122 °F (50 °C) for heat (heat-of-hydration) cures. These values were determined from examining the thermal curing data obtained from the precasting plants and shown in Section 7.5.1.
- The ambient temperature at the time of concrete-steel bond and the concrete temperature after additional cooling were both assumed to be the average daily ambient temperature leading up to the pour. This value would be input by the fabricators.

- The girder temperature at the time of strand release depends on the length of cure and the amount of time the girders are exposed before strand cutting. Because the fabricators do not necessarily know at the time of strand pull whether or not the cure will be over a weekday or weekend, the concrete temperature at strand release was assumed to be the average of the concrete temperature at concrete-steel bond and the average daily ambient temperature input by the fabricators.
- The standard reference temperature at which the strand stress in the girders should match the stress that would be achieved with the design pull force and no thermal stress losses was assumed to be 70 °F (21 °C). This reference temperature could be changed to accommodate the weather conditions at a particular precasting plant at any given time.

Finally, the spreadsheets calculate a maximum allowable pull force ($0.80*f_{pu}*A_s$) as specified in the ACI 318-08 code provisions and the AASHTO LRFD 2010 Bridge Design Specification. If the spreadsheets calculate a required increase in pull force that exceeds this value, it outputs the maximum allowable pull force as that associated with the required temperature correction. As previously mentioned in Sections 6.4 and 9.2.2, it is recommended that a short field study be conducted prior to implementation of the spreadsheet, in order to further quantify the effect of temperature and girder setting on strand stress.

B.6 Modified Thermal Effects Analysis and Sources of Potential Variation in the Results

After steel-concrete bond occurs, not only does the free length of strand act as a restraint to shortening of the girders due to cooling, there are a number of other possible restraints including the friction between the girders and the precasting bed and side-forms, and the drape hold-downs that are anchored to the bed. These additional restraints were ignored in the derivation in Section B.2. In this modified derivation, it is assumed that once the steel bonds to the concrete, the restraint effects that occur in the bed have a temporary effect on the girder and are completely recoverable (unless they cause prerelease cracking which is ignored in this derivation). In other words, in this modified derivation, all of the temporary restraints (including the restraint of the free length of strand after bond) are ignored.

If the free length of strand is ignored after concrete-steel bond, Step 2a of the derivation in Section B.2 must be changed. Because the free length of strand is not present after strand release, the following modified Step 2a is analogous to Step 3, where the only effect considered was the change in strand stress due to additional girder cooling. It should be noted that the other steps of the derivation in Section B.2 remain the same.

Step 2a: Just Before Strand Release (Modified)

The strand stress change is due to the change in temperature within the girder between concrete-steel bond and strand release, and the fact that the steel and concrete have different coefficients of thermal expansion. Strain compatibility can be used to find the change in stress in the strands for this stage. The free-body diagram shown in Figure B- gives the force equilibrium between the steel and concrete between bond and release, simplified as a resultant force on each end, and was used to derive the following equations (B-54 and B-55).

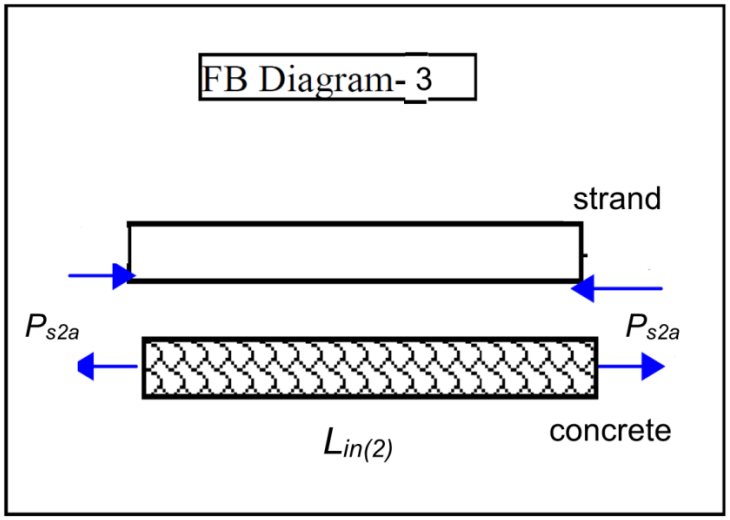

Figure B-3. Free-body diagram of forces present between bond and release

Change in length for the strands (in the concrete):

$$\left(L_{in(2)} - L_{in(1)}\right) = (T_{c2} - T_{c1})\alpha_s\left(L_{in(1)}\right) - \frac{P_{s2a}}{A_s E_s}(L_{in(2)}) \qquad \textbf{(B-54)}$$

Change in length for the concrete:

$$\left(L_{in(2)} - L_{in(1)}\right) = (T_{c2} - T_{c1})\alpha_c\left(L_{in(1)}\right) + \frac{P_{s2a}}{A_c E_c}(L_{in(2)}) \qquad \textbf{(B-55)}$$

There are two equations (B-54 and B-55) and two unknowns ($L_{in(2)}$ and P_{s2a}). Thus, the two unknowns can be found. The following equations show the solution for P_{s2a} and the resulting stress change at Step 2a.

$$P_{s2a} = P_{s1} - \frac{A_s E_s A_c E_c (T_{c2} - T_{c1})(\propto_s - \propto_c)}{A_s E_s\left((T_{c2} - T_{c1}) \propto_s + 1\right) + A_c E_c\left((T_{c2} - T_{c1}) \propto_c + 1\right)} \qquad \textbf{(B-56)}$$

$$\Delta f_{s3} = \frac{P_{s2a} - P_{s1}}{A_s} \qquad \textbf{(B-57)}$$

To determine the effect of ignoring the free length of strand between bond and release on the thermal prestress losses that could be expected, the parametric study discussed in Sections 5.3.1 and B.3.4 was re-evaluated using the modified derivation. Because the free length of strand is ignored, the thermal stress change at Step 2a (modified) depends only on the temperature change between bond and release, and the differing coefficients of thermal expansion of the strand and concrete. Using the same assumptions (i.e., section and material properties and ambient and concrete temperatures), it was found that the thermal prestress change between bond and release (i.e., TL_2) was +1.00 ksi for all 27 cases in the parametric study. This was because the concrete temperatures assumed at bond and strand release (140 °F (60 °C) and 97 °F (36 °C), respectively) were the same for all 27 cases. It should be noted that for some cases in the parametric study, this result was significantly different than the stress

change between bond and release found using the original derivation from Section B.2 (shown in Table B-). The resulting average total thermal stress loss (i.e., TL_1+TL_2), using the modified derivation, was approximately 8.3 ksi (about 4.1% of the initial pull stress and 3.1% of f_{pu}). The implication of this result is that the average strand stress loss due to thermal and strand relaxation effects would be approximately 4% (not 3% as reported in Chapters 5 and 6).

Another source of potential variation in the results is the assumed coefficient of thermal expansion for concrete. This parameter has been reported to range between 4.1 and 7.3 με/°F (7.4 and 13 με/°C). Using the upper and lower bound values within that range in place of the 5.8 με/°F (10.4 με/°C) value assumed in the parametric study resulted in average total thermal stress losses of approximately 6.4 ksi and 10.0 ksi, respectively, instead of the 8.3 ksi loss described above. This difference in total thermal stress loss is on the same order of magnitude as the difference due to ignoring the free length of strand after concrete-steel bond. Finally, Barr et al. (2005) found that there can be significant thermal stress loss due to the presence of thermal gradients (discussed in Section 2.6), which was also ignored in the thermal effects analysis derivation.

APPENDIX C. MATERIAL TESTING EQUIPMENT CALIBRATION

A compressometer was used to determine the concrete modulus of elasticity. The compressometer was made of two aluminum yokes connected by a mounting bracket. The bottom yoke was fixed while the top yoke was hinged at the top of the mounting bracket. Opposite the mounting bracket, the linear variable differential transformer (LVDT) was fixed to the top yoke and rested on the bottom yoke. This LVDT measured twice the linear displacement in the specimen while the cylinder was compressed. Figure C-1 shows the material testing equipment from two different angles.

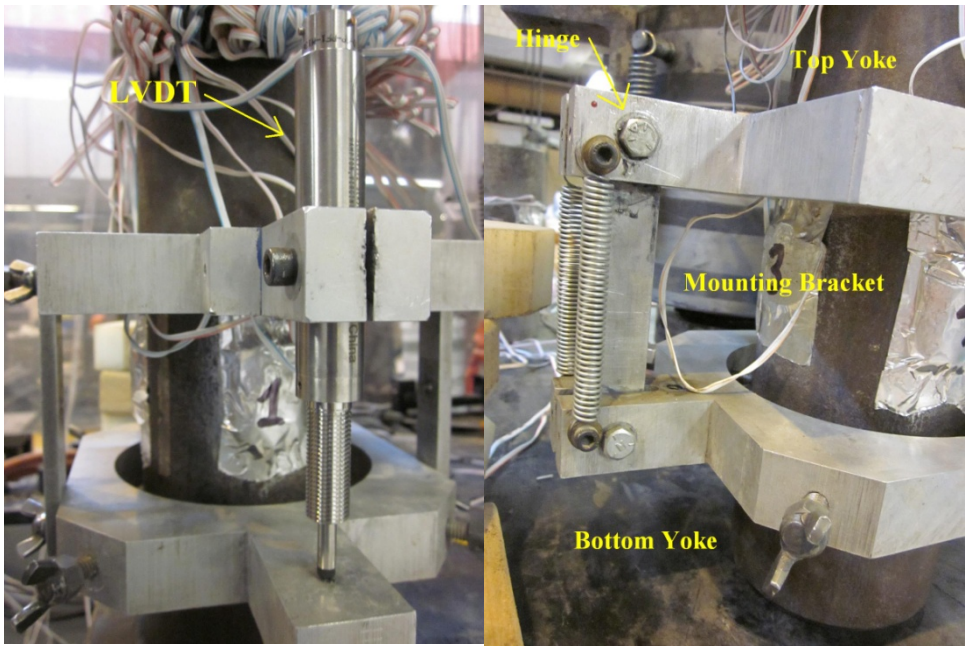

Figure C-1. Material testing equipment (compressometer and LVDT)

The material testing equipment was calibrated before conducting the compression and elastic modulus tests on the concrete cylinders. The LVDT was calibrated using a precision micrometer. Once the LVDT was calibrated and yielding accurate displacement results, aluminum and steel reference cylinders with known elastic moduli were tested. Rosette strain gauges were applied to the reference cylinders to compare to the results obtained from the LVDT. Initially, the compressometer and LVDT were yielding results that were about 8-10% higher than the strain gauge results. This was attributed to friction in the compressometer hinge. After the hinge was greased and loosened slightly to allow for near-frictionless movement, the compressometer and LVDT yielded results that were approximately 0-5% higher than the strain gauge results. There were still possible sources of error in both the LVDT and strain gauge readings due to equipment imperfections or human error. However, because the compressometer and LVDT were yielding acceptable results for the aluminum and steel modulus of elasticity, when compared to the known values, it was determined that the compressometer and LVDT could produce accurate results for concrete cylinder testing.

APPENDIX D. PBEAM INPUT DESCRIPTION

D.1 Introduction

The program PBEAM, developed by Suttikan (1978), was used to model the time-dependent response of all of the girders considered in the parametric study. The program utilizes a finite element technique, where any cross section can be analyzed. The effects of variation of strength and stiffness with time, creep and shrinkage of concrete, relaxation of prestressing steel, varying support conditions and nonlinear stress-strain material relations can all be considered.

PBEAM was chosen for the time-dependent analysis because its input format is well suited for girders and because of its flexibility with the input of material properties. Before any analysis was done, a very simple beam was modeled in order to validate the accuracy of the stresses, strains and deflections in the program. Additionally, each time-dependent parameter was modeled individually in order to validate the accuracy of the inputs and the equations used.

D.2 Cross Section and Loading Age

The cross section of each girder was divided into rectangular regions with elemental divisions through the depth. The total depth and the total cross-sectional area were kept consistent with the actual girder dimensions. However, the moment of inertia and the centroid of the concrete sections were not identical to the real values, but were kept to within 1.0% or less. This was more difficult to accomplish for the MN shapes, because of the unique curvature of their cross section. For these shapes, the moment of inertia in PBEAM was lower than the actual value by as much as 1.0%. Each row of prestressing strands was also modeled as a rectangular region, located at the centroid of the row. However, the small amount of mild steel that was located in the top flange of most the girders in this study was not modeled in PBEAM.

The loading age (time of release) of each girder was determined from the fabricator records and input in PBEAM to reflect the curing time of each girder. The girders were then modeled from the time of release to the time of bridge erection at various intervals.

D.3 Material Properties

The prestressing strand was assumed to be 0.6 in diameter 270 ksi low-relaxation strand, with a cross-sectional area of 0.2227 in^2, a self-weight of 0.2805 lb/in^3, and an elastic modulus of 28,500 ksi, which are all manufacturer-provided average values. The stress-strain curve for the strand was assumed to be linear (elastic) up to yielding, with a nonlinear strain hardening branch post-yield. However, it should be noted that for this analysis, the prestressing strand never went past yielding.

PBEAM has an input option for the stress-strain curve of the concrete, in which the curve is generated based on a few input points on the curve; namely f''_c (peak stress), ε_0 (strain at peak stress), $0.5f''_c$, ε_{50c} (strain at $0.5f''_c$) and E_c (28-day elastic modulus). The concrete was assumed to be unconfined and have a self-weight of 155 lb/ft^3, which was consistent with the material tests and the value used by MnDOT for reinforced concrete. The release and 28-day strengths for each girder modeled were obtained from the fabricator records and the elastic modulus was determined using the Pauw (1960) equation, which is recommended by ACI318-08 and AASHTO LRFD 2010. This equation was used because it most accurately predicted the elastic modulus of the samples taken from both plants, as discussed in Section 5.2.4.

D.4 Concrete Aging

Concrete gains strength over time due to further hydration of the cement. PBEAM is able to take into account the effect of concrete aging through built-in strength-age curves, which match those proposed by the ACI 209 Committee (1992). These curves are given as:

$$f'_t = f_{28}(t/(a + bt)) \quad \textbf{(D-1)}$$

$$\varepsilon'_t = \varepsilon_{28}\sqrt{(t/(a + bt))} \quad \textbf{(D-2)}$$

where f'_t, f_{28}, ε'_t and ε_{28} are concrete strengths and corresponding strains at age t and 28 days. However, to ensure that PBEAM uses the appropriate concrete modulus of elasticity at release and other time intervals, the constants *a* and *b* were determined by fitting the measured concrete elastic modulus data, instead of the measured concrete strength data. Using Hooke's law, the modulus-age curve is given as:

$$E'_t = E_{28}\sqrt{(t/(a + bt))} \quad \textbf{(D-3)}$$

where E'_t and E_{28} are concrete moduli at the age t and 28 days. The constants *a* and *b* are functions of cement type and method of curing but have recommended values (by ACI 209) in the absence of experimental data. For steam curing and Type III cement, ACI 209 recommends using 0.70 and 0.98 for *a* and *b*, respectively. For steam curing and Type I cement, ACI 209 recommends using 1.00 and 0.95 for *a* and *b*, respectively (ACI 209R-92). However, Mokhtarzadeh et al. (1998) recommended using different values for *a* and *b*, based on extensive material testing on concrete obtained from Plant A, that examined both steam and moist curing and different cement admixtures. Because experimental data was available for this analysis, a nonlinear least square fit was used to obtain values for *a* and *b*. The constants *a* and *b* were found separately for Plants A and B because different cement types were used at each plant. Based on this analysis, values for *a* and *b* were selected that appropriately matched the data collected from both plants. The results of this analysis can be found in Section 5.2.5.

D.5 Elastic Modulus and Aging in PBEAM

The concrete stress-strain curve in PBEAM is generated using the 28-day strength and elastic modulus and the input aging coefficients to determine the strength and elastic modulus at any time. PBEAM also internally calculates an initial tangent modulus, E_{ci}, given as:

$$E_{ci} = E_c(1 + (\frac{f'_c}{E_c\varepsilon_0} - 1)^2) \quad \textbf{(D-4)}$$

Depending on the stresses and strains in the member at any given time, PBEAM uses a value for the elastic modulus that is somewhere between E'_t and E_{ci}. At 28 days, the elastic

modulus used by PBEAM is usually about the average of E_{28} and E_{ci}. Thus, even though E_c is input into the program as the 28-day modulus, the actual modulus that PBEAM appears to calculate at 28 days will exceed E_c. Therefore, a simple algorithm was developed to calculate the appropriate input E_c to give the desired release and 28-day modulus in PBEAM. The algorithm can best be described as the following two-step process:

1. Calculate the 28-day modulus that gives the desired release modulus based on the chosen aging coefficients.
2. Calculate the input E_c that yields this previously-calculated 28-day modulus in PBEAM.

It should be noted that this process essentially depends entirely on the release modulus and the aging coefficients. However, this is intentional, given that these are the values known most accurately based on the results of the material testing discussed in Section 5.2.3. Additionally, the 28-day f'_c was not always accurately known due to the fact that the fabricators, at times, did not test the 28-day cylinders to failure. In these cases, approximations were made based on tests taken to failure with concrete of similar mix design.

D.6 Creep and Shrinkage

PBEAM uses built-in expressions for creep and shrinkage which match the form of those recommended by the ACI 209 Committee (1992). These expressions are given as:

$$(\varepsilon_{sh})_t = \frac{t}{f+t}(\varepsilon_{sh})_u \gamma_{sh} \quad \textbf{(D-5)}$$

$$v_t = \frac{t^{\varphi}}{d+t^{\varphi}} v_u \gamma_{cr} \quad \textbf{(D-6)}$$

where

$(\varepsilon_{sh})_t$ = shrinkage strain at time t
f = constant; 55 (given by ACI 209)
$(\varepsilon_{sh})_u$ = ultimate shrinkage strain; 780×10^{-6} in/in (given by ACI 209)
v_t = creep coefficient at time t (ratio of creep strain to initial elastic strain)
φ = constant; 0.6 (given by ACI 209)
d = constant; 10 (given by ACI 209)
v_u = ultimate creep coefficient; 2.35 (given by ACI 209)
γ_{sh} and γ_{cr} : Represent the product of applicable correction factors for conditions other than the standard conditions defined by ACI 209 (i.e., volume-surface ratio (V/S) of 1.5 in, 1-3 days steam cured, 40% ambient relative humidity, etc.)

Various creep and shrinkage models were examined for use in this study and are discussed in Section 7.2.1. However, because it is cumbersome and less precise to input these curves as a few data points, a nonlinear least square fit was used to obtain the appropriate input constants for the curves using the ACI 209 expressions. Thus, only the constants needed to be

altered to represent and input each creep and shrinkage model. The results of this analysis are discussed in Section 7.2.3.

D.7 Strand Relaxation

Strand relaxation begins as soon as the strands are tensioned and anchored in place. However, PBEAM incorrectly assumes that the steel relaxation begins at the time of strand release. Thus, the program does not take into account the amount of relaxation that occurs between strand pull and strand release. The expression for calculating the magnitude of relaxation over time was recommended by the PCI Committee on Prestress Losses (1975) and is given as:

$$(f_{st})_{i+1} = (f_{st})_i + (f_{st})_i \frac{\log(24t_{i+1}) - \log(24t_i)}{C_2}\left(\frac{(f_{st})_i}{C_1} - C_3\right) \quad if \quad \frac{(f_{st})_i}{f_{sy}} \geq C_4 \qquad \textbf{(D-7)}$$

where

f_{st} = steel stress at any time t (days) after strand pull
f_{sy} = specified yield strength of steel strand
f_{pu} = specified ultimate strength of steel strand
C_1 = $f_{sy} = 0.90 f_{pu}$
C_2 = 45
C_3 = 0.55
C_4 = 0.6

for low-relaxation strands (PCI 1975)

From this expression, the amount of relaxation that occurs between strand pull and strand release can be calculated and then subtracted from the initial pull force. However, the input coefficients still need to be modified because PBEAM still assumes that relaxation begins at the time of strand release. It should be noted that only C_2 and C_3 can be appropriately modified.

Using the fabricator records, it was found that the amount of time between strand pull and strand release varied from ~1 to 6 days. Thus, different relaxation stress losses and C_2 and C_3 coefficients were determined for times between pull and release of 1, 2, 3, 4, 5 and 6 days. Because this analysis was only concerned with the camber from release to erection, the relaxation coefficients (C_2 and C_3) were adjusted so that the total relaxation was about the same at approximately one year, for each case. In other words, the difference in relaxation losses computed using the modified coefficients and using equation D-7 was less than 1.0 ksi at any given time within one year. Table D-1 gives the results of this analysis, assuming an initial pull force of $0.75 * f_{pu}$, which is specified by the AASHTO LRFD 2010 Bridge Design Specification and typically used at both plants. The stress losses are subject to change depending on the actual pull force used in any given case.

Table D-1. Adjusted strand relaxation coefficients

Time between pull and release	1 Day	2 Days	3 Days	4 Days	5 Days	6 Days
Stress loss (ksi)	1.76	2.13	2.35	2.50	2.62	2.71
C_2	100	120	140	160	180	200
C_3	0.45	0.41	0.37	0.33	0.29	0.25

D.8 Support/Bunking Conditions

At both Plants A and B, fabricators store their girders on bunks while they are waiting to be shipped to the bridge site. The bunks are typically made out of concrete or cinder block with wood planks placed on top to provide some cushion for the girder. The bunks are typically located anywhere from 1 to 20 ft (0.3 to 6.1 m) in from the ends of the girder and there is no regulation for this distance.

Due to the significant weight of the overhanging ends of the girders, the cantilevered effect causes the girder to experience an instantaneous elastic increase in camber. This cantilever effect also alters how the creep develops throughout the beam and creates a non-recoverable increase in camber over time. When a girder is brought to the bridge site and supported at its ends, the camber is reduced by the elastic effect of bunking. However, the camber at erection will be higher than if the girder had been supported on its ends in storage due to the time dependent increase in camber due to bunking.

The effect of bunking was analyzed in detail with an example, prior to conducting a parametric study (discussed in Section 0), to ensure the accuracy of the modeling results. To begin, the support conditions in PBEAM were such that a support must be placed at a nodal zone (i.e., border between two elements). Therefore, the number of elemental divisions along the length had to be adjusted for each instrumented girder to accurately model the location of the bunks. In the preliminary study, one of the instrumented girders was modeled with supports located at the end of the beam and at L/16.

To validate the accuracy of the results, the method of superposition was used for the two deflections involved (upward deflection due to prestress and downward deflection due to self-weight). First, the girder was modeled with prestress only (no self-weight). In this case, the location of the supports should not matter. Then, the girder was modeled with self-weight only (no prestress). In this case, the deflections for the two support locations can be determined from linear elastic analysis. Table D-2 shows the deflection results (in inches) of the analysis:

Table D-2. Deflection validation in PBEAM

Analysis	PBEAM			Linear Elastic
Support Condition	Ends	Bunks at L/16	% Diff	% Diff
Prestress Only	2.46	2.46	0	0
Self-Weight Only	-0.967	-0.677	42.8	42.5
Total Deflection (in)	1.49	1.78	19.4	19.3

The results show that PBEAM gives accurate results for the deflection of girders supported at any location.

Given the above results, the long-term effect of bunking conditions could be examined to investigate the non-recoverable increase in camber over time. The same instrumented girder was modeled for 100 days with supports at the end of the beam and at L/16. Figure D- shows that the camber increases more for the case of bunked supports relative to the end supported case, due to the effect of creep.

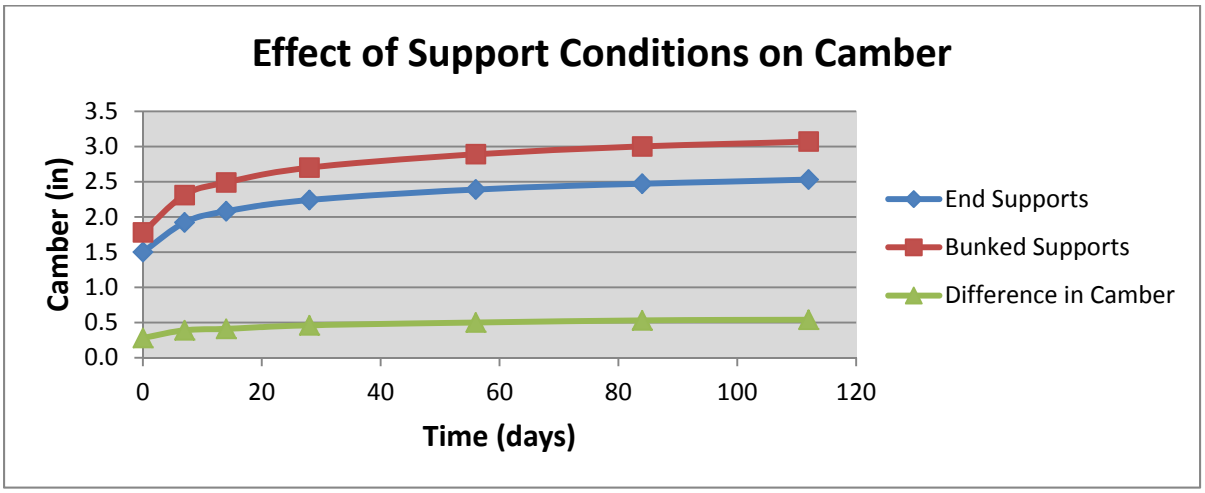

Figure D-1. Effect of support conditions on camber over time

When the girder is placed on end supports at the bridge site, the camber will decrease by the linear elastic difference at release and will be higher than if the beam had been stored on end supports.

D.9 Sample PBEAM Input

The following sample PBEAM input corresponds to the “best prediction” long-term camber modeling of a 120 ft 81M girder, as used in Chapter 8.

```
Predict 120' 81M
Prest/concrete beam(81M, L=120'=1440")
START    1aging-yes,creep-yes,shrink-yes,relax-yes,no deck
   12                                          1         1    1
         4   10    4   23         3
    7    7       1.0    365.00
      1.00      7.00     28.00     60.00    120.00    240.00    365.00
      1.00      7.00     28.00     60.00    120.00    240.00    365.00
    5   20           1.000e+00 1.000e+00 1.000e+10 1.000e+10
    2
    1         1    1    1    1  8.97e-02
 1.000e+01 1.000e-05 2.241e-04-4.500e-03
      0.28      0.99
     1.450      0.70
      0.60      10.0      1.00    -0.000
-410.0e-06      55.0
    2    1    2         1         0.2805
 1.000e+02 1.000e-04 6.530e-02-6.530e-02
 2.430e+05     120.0      0.41      0.60
    1               -1050 -525-6450
                     -220 -255-1000
    2    9    1          0 2250 2450 2500 2550 2600 2620 2650 2650
                         0   80  100  110  120  150  175  250  650
   24         1440.0
    9
         1    8    1                 0.1      1.00      1.00
                26.0       7.5    -36.29       0.0
         1    4    1                 0.1      1.00      1.00
                19.0       2.5    -31.29       0.0
         1   20    1                 0.1      1.00      1.00
                 6.0      62.5     1.210       0.0
         1    4    1                 0.1      1.00      1.00
                17.0       2.5     33.71       0.0
         1    8    1                 0.1      1.00      1.00
                30.0       6.0     37.96       0.0
         2    1    1                 0.0      1.00      1.00
                3.712      0.6    -38.04 6.845e-03
         2    1    1                 0.0      1.00      1.00
                3.712      0.6    -36.04 6.845e-03
         2    1    1                 0.0      1.00      1.00
                3.712      0.6    -34.04 6.845e-03
         2    1    4                 0.0      1.00      1.00
 0.000e+00 2.969e-00 6.000e-01     34.96 6.845e-03
     576.0 2.969e-00 6.000e-01    -34.04 6.845e-03
     864.0 2.969e-00 6.000e-01    -34.04 6.845e-03
    1440.0 2.969e-00 6.000e-01     34.96 6.845e-03
         2
      60.0          -1.000e+30-1.000e+30
    1380.0                    -1.000e+30
CEASE
```

APPENDIX E. FABRICATION DATA FOR INSTRUMENTED GIRDERS

The following tables provide the complete fabrication, thermal and camber records of the instrumented girders. This data was used for the thermal effects analysis and revised release camber predictions (discussed in Section 6.3.2), the PBEAM long-term modeling (discussed in Chapter 8) and the review of the Tadros et al. (2011) method (discussed in APPENDIX H).

Table E-1. Girder design section properties and dimensions

Girder Description	Full Length (ft)	Design Length (ft)	Hold-down location (ft)	# straight strands	# draped strands	I_g (in^4)	A_g (in^2)	y (in)	V/S (in)	e_{end} (in)	e_{mid} (in)	w_{sw} (k/ft)
73037 122' MN54 #1-2	122.4	122.15	49	34	8	285690	749	24.68	3.67	12.78	20.39	0.806
73038 122' MN54 #1-2	122.4	122.15	48.5	36	8	285690	749	24.68	3.67	13.04	20.32	0.806
73038 93' MN54 #1-3	92.76	91.5	37.2	24	4	285690	749	24.68	3.67	14.68	20.97	0.806
27B58 119' MN45 #1-3	119.25	118	47.6	36	10	179000	690	20.63	3.7	9.24	15.98	0.743
73044 131'6" MN63 #1-4	131.5	130.25	52.75	36	6	422570	807	28.8	3.63	17.09	24.66	0.869

Table E-2. Design and measured strand pull forces and concrete strengths

Girder Description	Design pull force (lb)	Straights pull force (lb)	Drapes pull force (lb)	Design f'_{ci} (psi)	Design f'_c (psi)	Measured f'_{ci} (psi)	Measured f'_c (psi)
73037 122' MN54 #1-2	44500	44500	41500	6700	7500	9450[1]	11270[1]
73038 122' MN54 #1-2	44500	45000	42000	7000	9000	8000	11190
73038 93' MN54 #1-3	44500	46000	33000	6000	6500	8150	11700
27B58 119' MN45 #1	44500	45500	41500	7400	8100	7125	10700
27B58 119' MN45 #2-3	44500	45500	41500	7400	8100	8300	10700
73044 131'6" MN63 #1-2	44540	45430	38750	7000	9000	7600	10750
73044 131'6" MN63 #3-4	44540	45430	39000	7000	9000	8620	10500

[1]All measured concrete strengths represent average values for the recorded strengths of each girder set.

Table E-3. Parameter values related to thermal and relaxation prestress losses

Girder Description	Length of cure (days)	Time between pull and release (days)	Bed Length (ft)	Free Length of Strand (ft)	Ambient Temp at Pull (°F)	Concrete Temp at Bond (°F)	Ambient Temp at Bond (°F)	Concrete Temp at Release (°F)
73037 122' MN54 #1-2	3.9	5	387	135.6	93	122[1]	60[1]	70[2]
73038 122' MN54 #1-2	0.9	6	386	134.6	93	125	60	97
73038 93' MN54 #1-3	0.9	3	387	98.7	59	126	50	97
27B58 119' MN45 #1	1.7	2	386	261.8	60	140	40	97
27B58 119' MN45 #2-3	0.8	3	261.8	18.3	50	140	32	97
73044 131'6" MN63 #1-2	0.9	1	357	87.3	55	146	32	97
73044 131'6" MN63 #3-4	2.8	4	357	87.3	55	140	30	70

[1]All assumed temperatures at bond were those at approximately 6-10 hours after the concrete pour.
[2]Concrete temperatures at release were approximated for weekday and weekend cures.

Table E-4. Design and measured cambers and related information

Girder Description	Design Release Camber	Design Erection Camber	Measured Release Camber	Measured Lift/Set Camber	Measured Erection Camber	Amount of Bunking (ft)	Age at Erection (days)
73037 122’ MN54 #1	3.5”	5.25”	--[1]	--	5.02”	5.5	202
73037 122’ MN54 #2	3.5”	5.25”	2.52”	--	4.80”	4.5	202
73038 122’ MN54 #1	3.67”	5.5”	2.80”	3.01”	5.47”	4	193
73038 122’ MN54 #2	3.67”	5.5”	2.60”	2.85”	5.23”	4	193
73038 93’ MN54 #1	1.75”	2.625”	1.34”	1.44”	2.51”	5.75	167
73038 93’ MN54 #2	1.75”	2.625”	1.14”	1.24”	2.32”	6.25	167
73038 93’ MN54 #3	1.75”	2.625”	1.18”	1.32”	2.39”	6	167
27B58 119’ MN45 #1	4.08”	6.125”	3.44”	3.60”	7.28”	4.75	272
27B58 119’ MN45 #2	4.08”	6.125”	2.54”	2.89”	6.0”	4.5	271
27B58 119’ MN45 #3	4.08”	6.125”	2.34”	2.46”	5.96”	5	271
73044 131’6” MN63 #1	3.33”	5”	2.09”	2.17”	4.62”	5	270
73044 131’6” MN63 #2	3.33”	5”	1.91”	2.15”	4.5”	5.25	270
73044 131’6” MN63 #3	3.33”	5”	1.93”	2.13”	4.61”	5	267
73044 131’6” MN63 #4	3.33”	5”	1.94”	2.17”	4.56”	5.75	267

[1]Denotes camber values that were not recorded

APPENDIX F. ADDITIONAL PBEAM MODELING RESULTS

The following figures (F-1 to F-9) contain information regarding the PBEAM validation modeling results that were conducted using the instrumented girders (F-1 to F-5) and selected historical girders (F-6 to F-9), which accompany the discussion and conclusions in Section 7.4. The measured cambers for the girders and the PBEAM output cambers using various creep and shrinkage models are included in these figures. Also included in this appendix are figures (F-10 to F-18) that contain information regarding the long-term camber at erection prediction modeling results (conducted in PBEAM) that accompany the discussion and conclusions in Section 8.4.

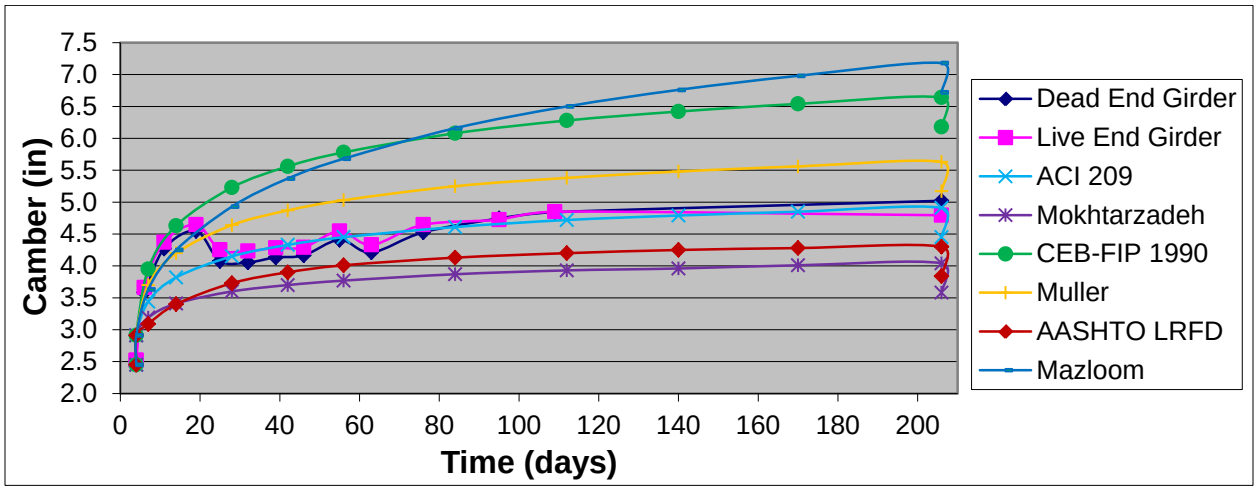

Figure F-1. Long-term camber comparison for Br. 73037 122' MN54 (weekend cure) girders

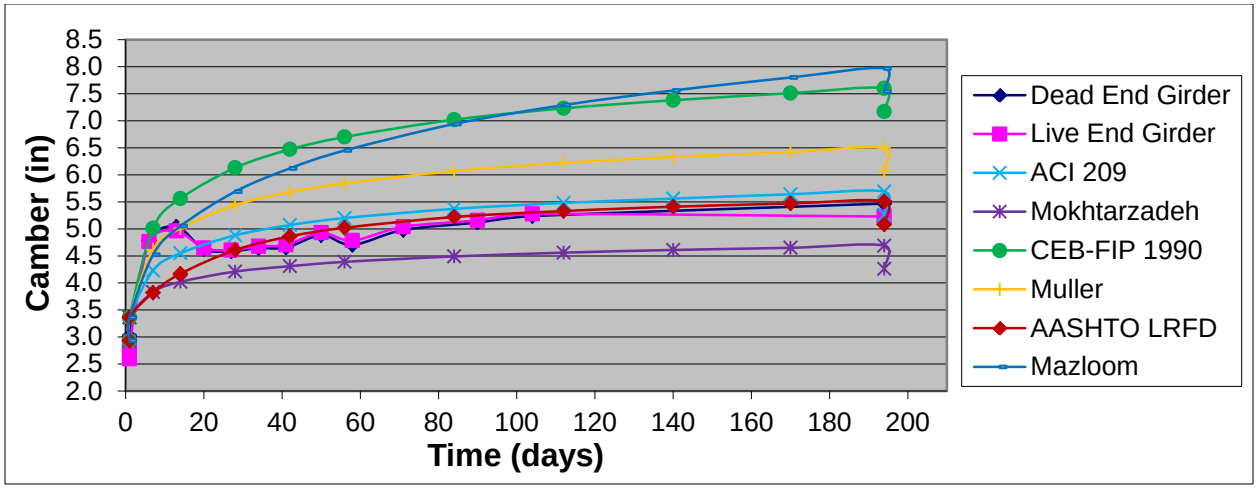

Figure F-2. Long-term camber comparison for Br. 73038 122' MN54 (weekday cure) girders

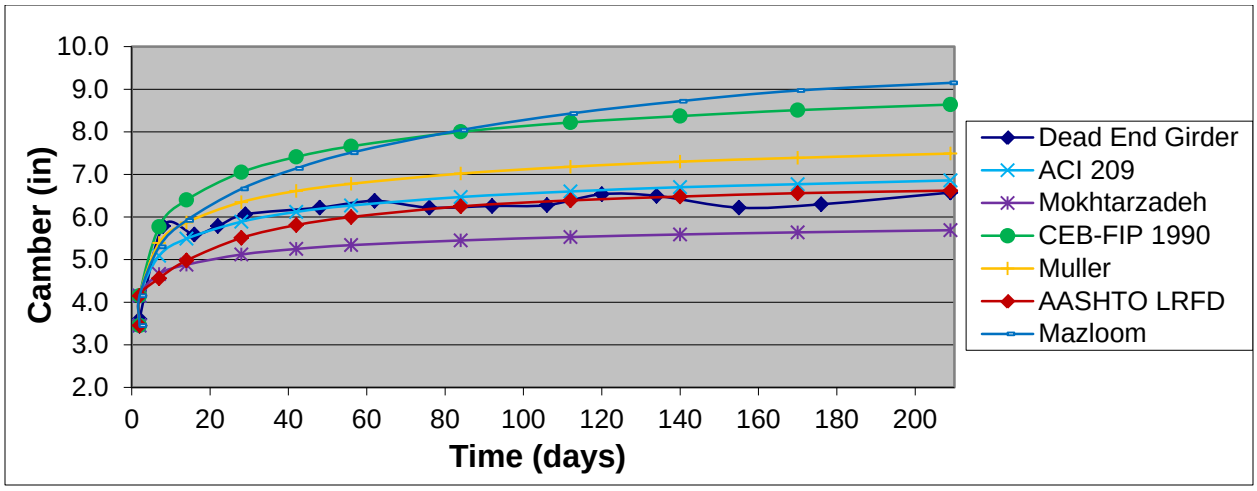

Figure F-3. Long-term camber comparison for Br. 27B58 119' MN45 (2-day cure) girders

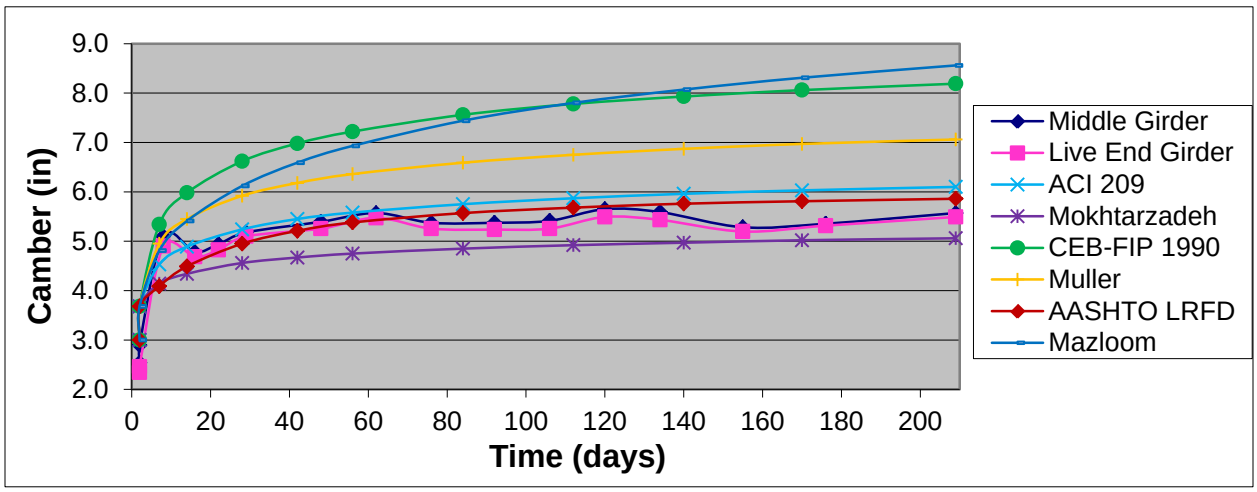

Figure F-4. Long-term camber comparison for Br. 27B58 119' MN45 (1-day cure) girders

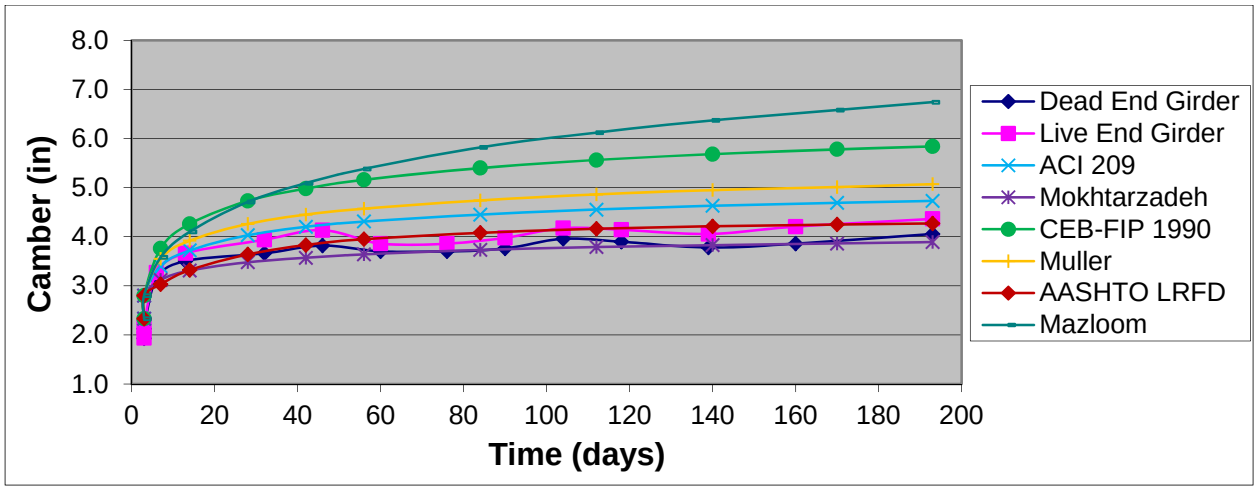

Figure F-5. Long-term camber comparison for Br. 73044 131’ 6” MN63 (weekend cure) girders

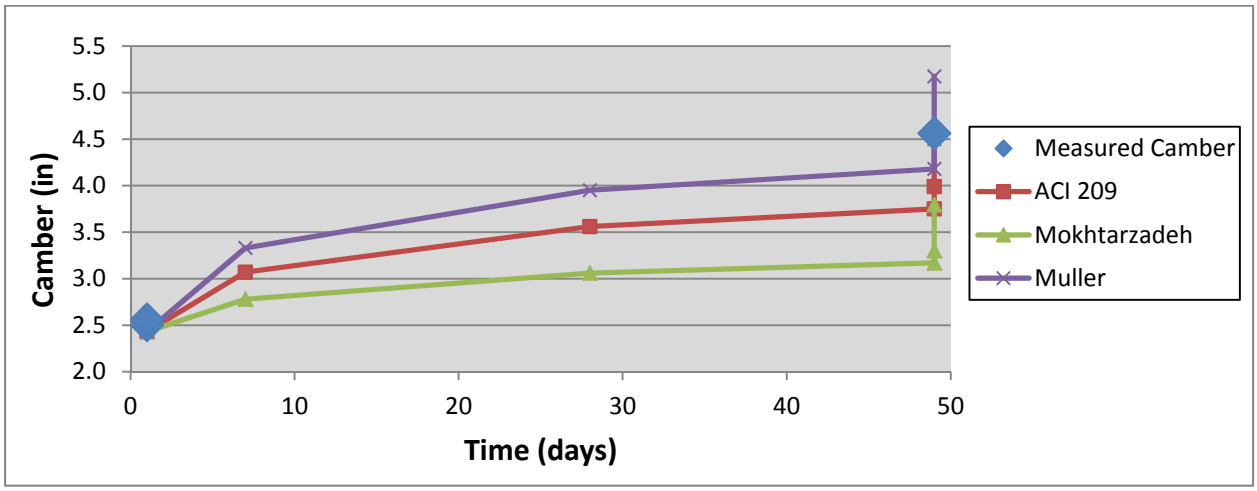

Figure F-6. Camber comparison for Br. 25025 72’ 6.5” 27M girder

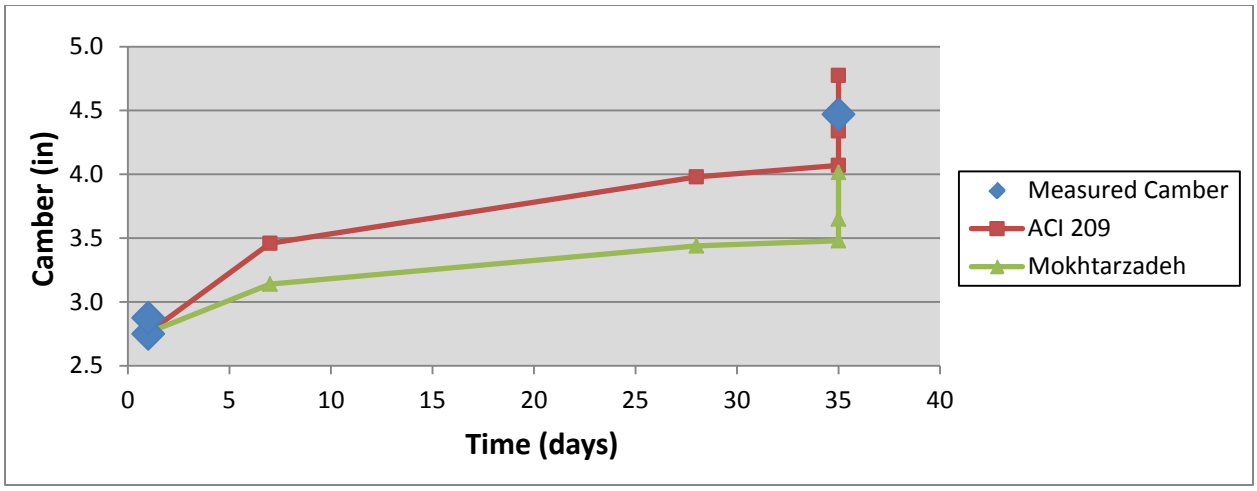

Figure F-7. Camber comparison for Br. 17532 93' 36M girder

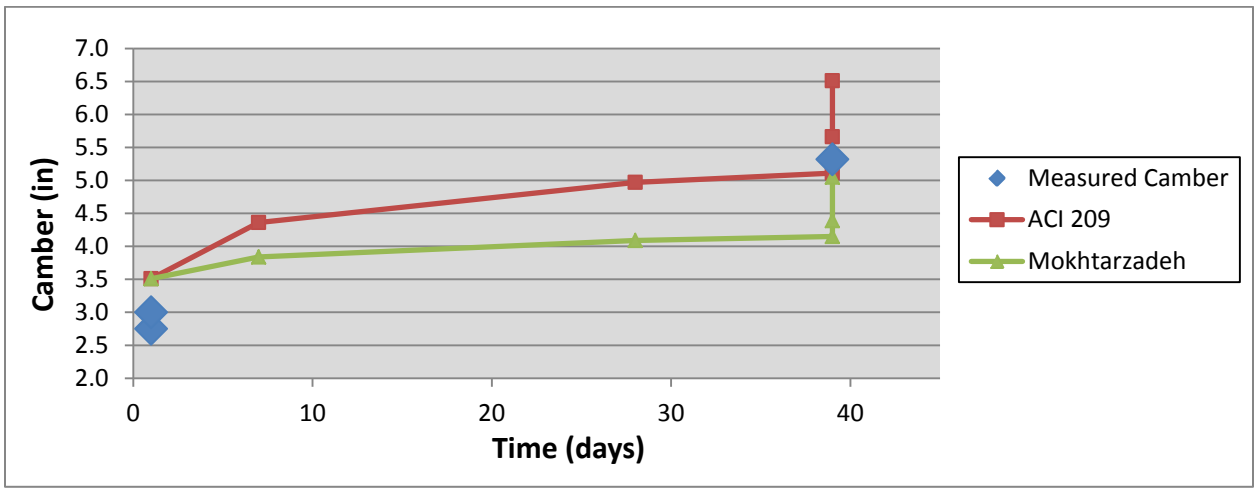

Figure F-8. Camber comparison for Br. 27302 145' 6" MN63 girder

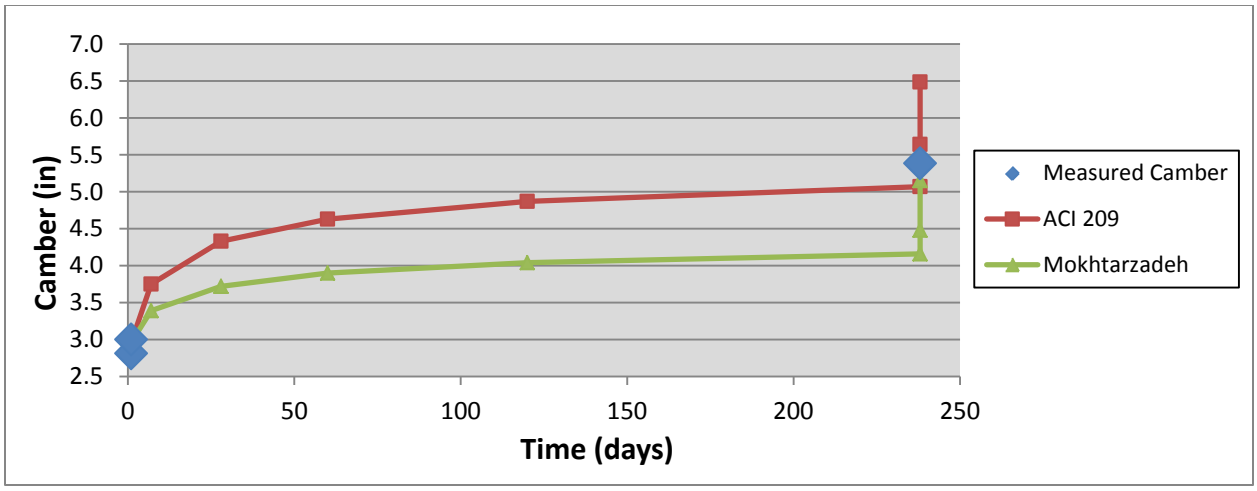

Figure F-9. Camber comparison for Br. 07581 139' 9" 72M girder

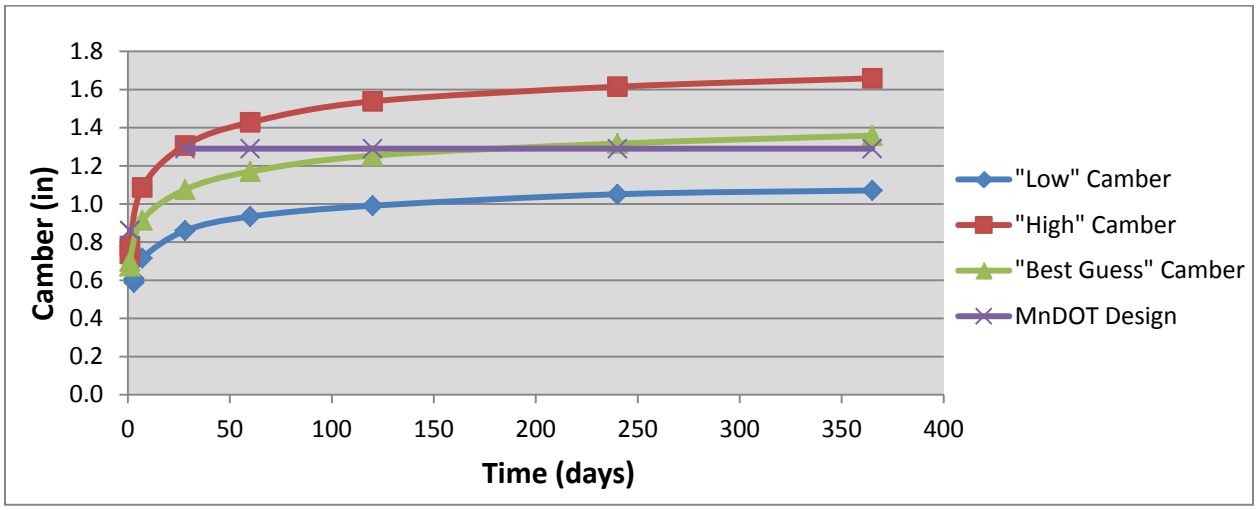

Figure F-10. Long-term (erection) camber predictions for 40' 27M girder

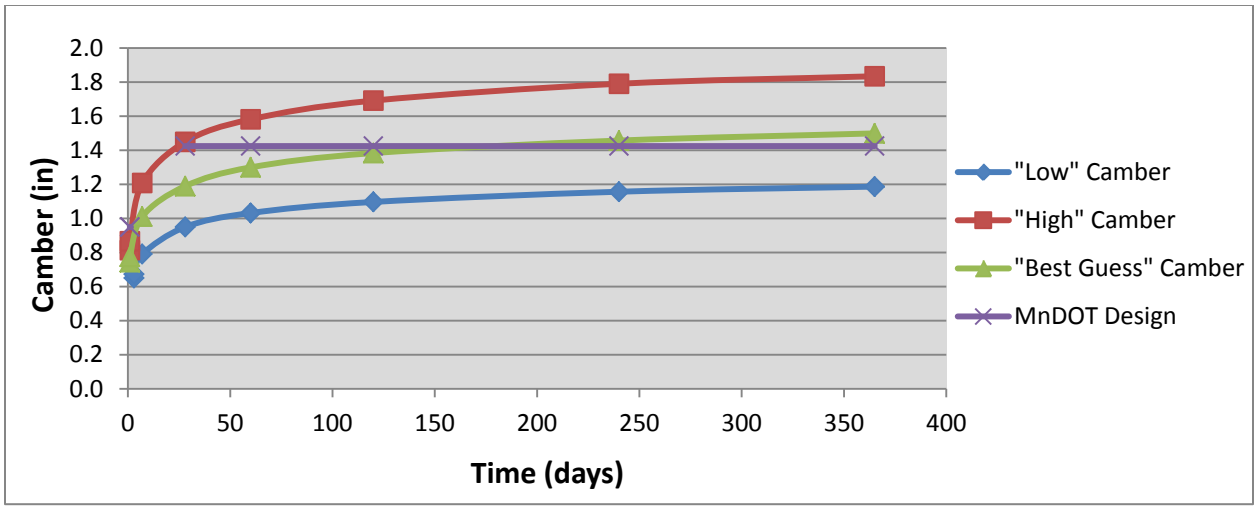

Figure F-11. Long-term (erection) camber predictions for 50' 36M girder

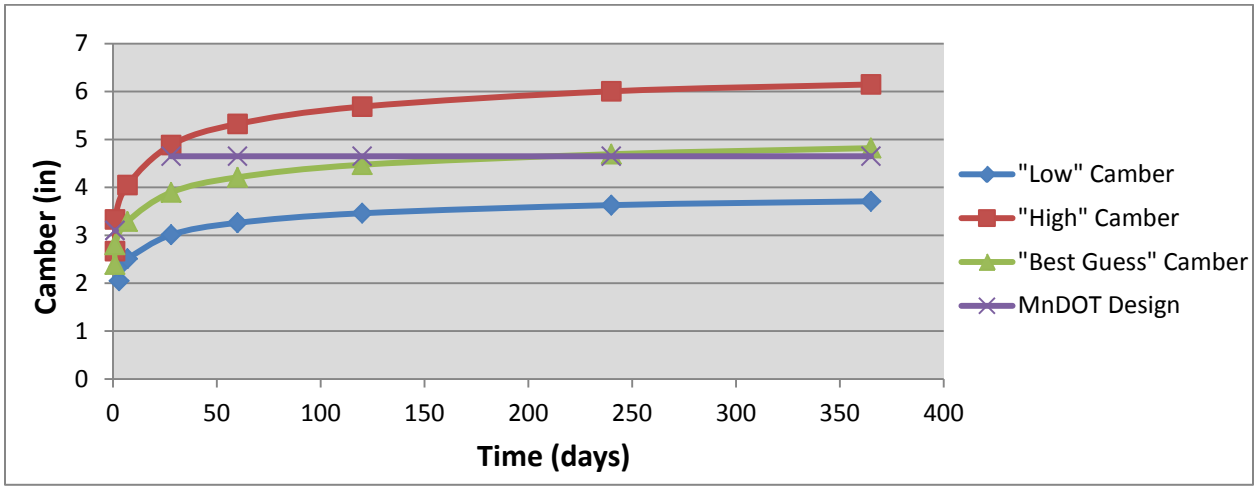

Figure F-12. Long-term (erection) camber predictions for 95' 36M girder

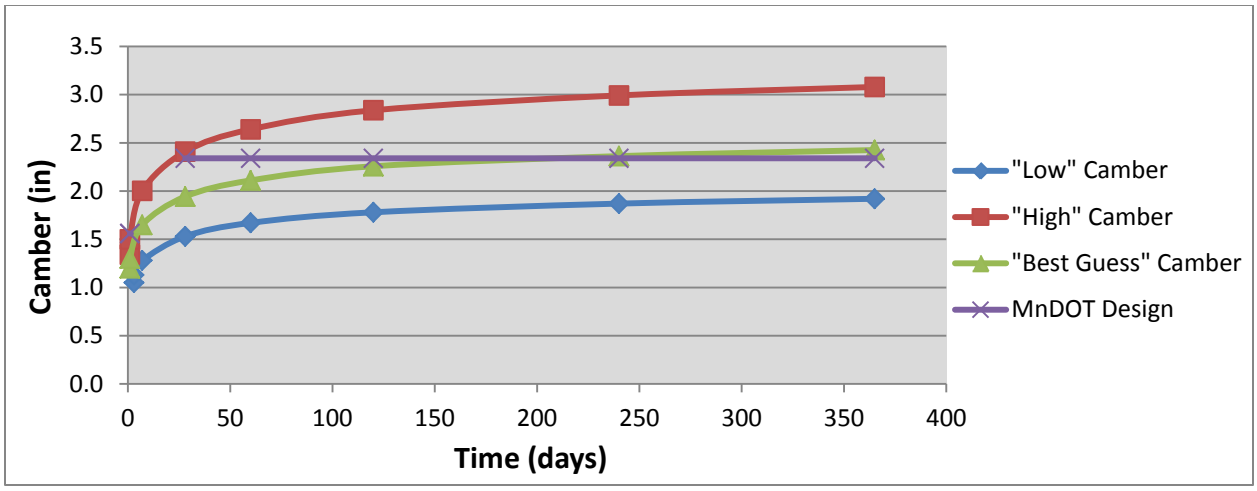

Figure F-13. Long-term (erection) camber predictions for 75' MN45 girder

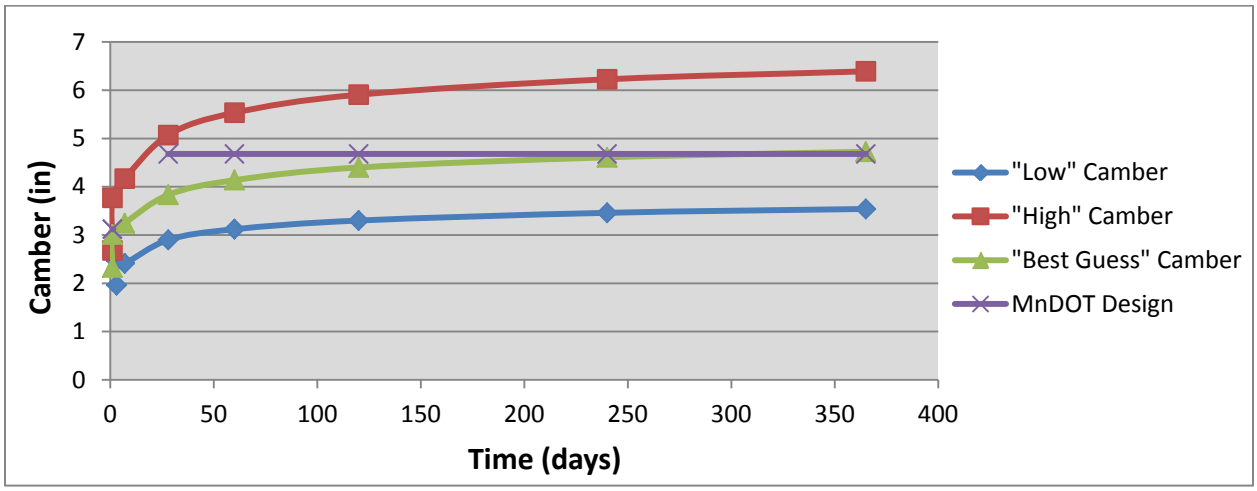

Figure F-14. Long-term (erection) camber predictions for 120' MN45 girder

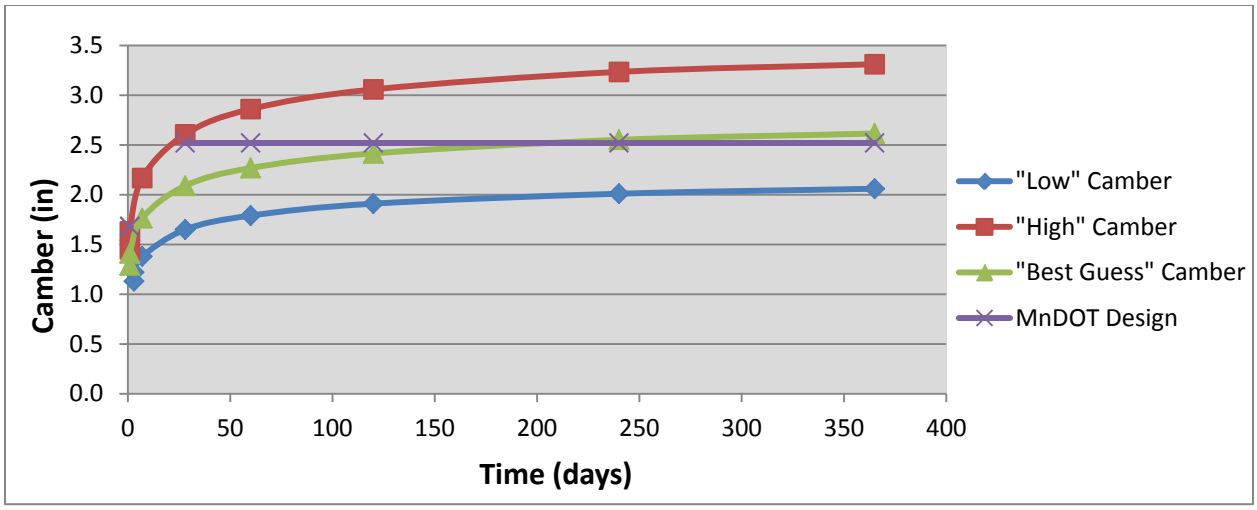

Figure F-15. Long-term (erection) camber predictions for 85' MN54 girder

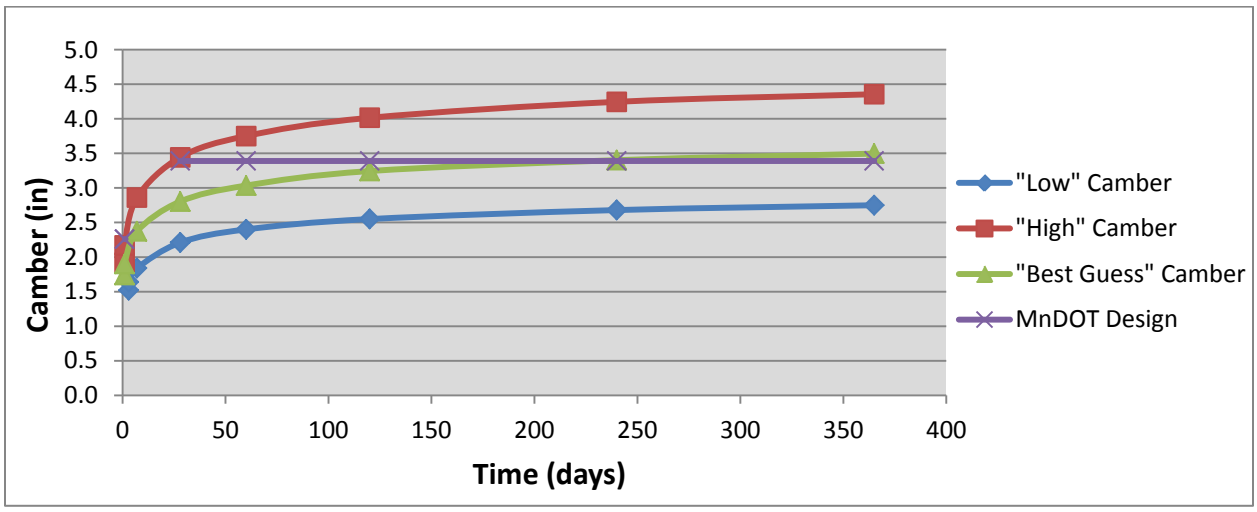

Figure F-16. Long-term (erection) camber predictions for 100' MN63 girder

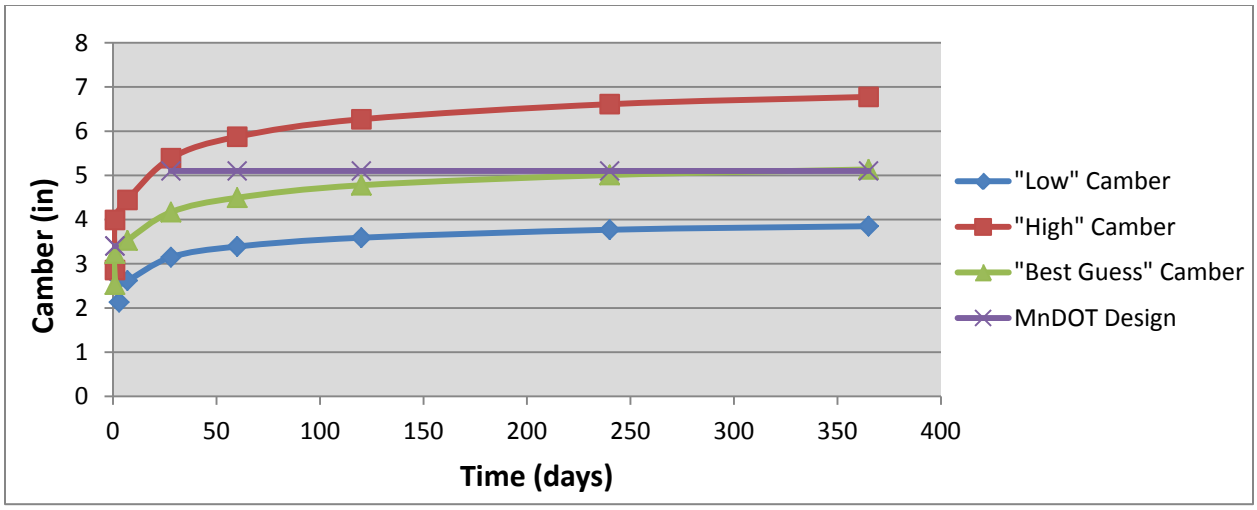

Figure F-17. Long-term (erection) camber predictions for 145' MN63 girder

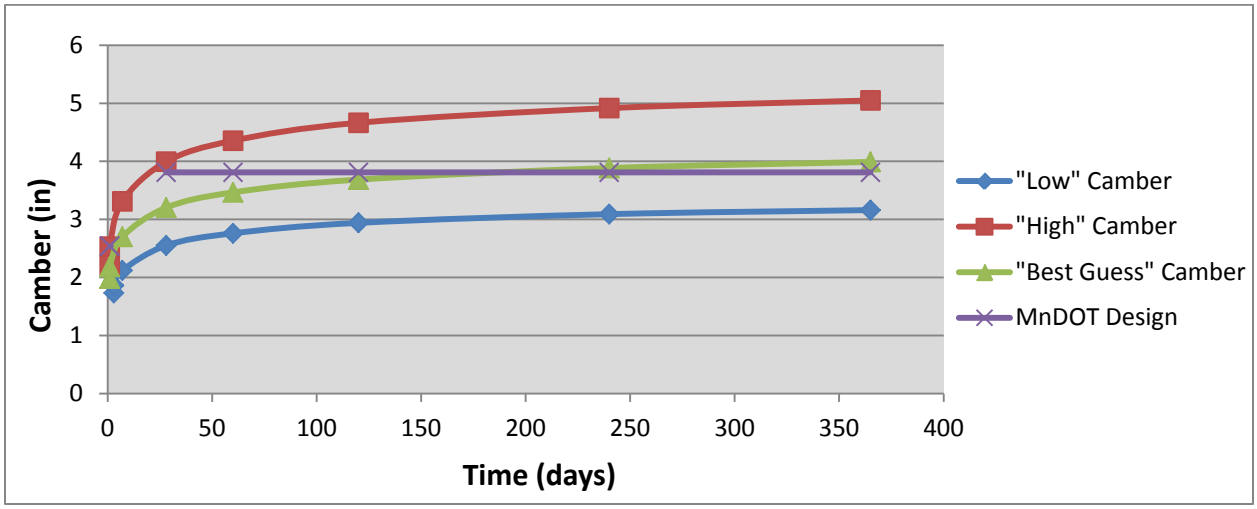

Figure F-18. Long-term (erection) camber predictions for 120' 81M girder

APPENDIX G. CREEP AND SHRINKAGE INPUTS

As part of the PBEAM model validation (discussed in Section 7.4), the chosen creep and shrinkage models (i.e., ACI 209, Mokhtarzadeh variation, CEB-FIP 1990, Muller, AASHTO LRFD and Mazloom) were modeled separately to investigate which model most closely followed the actual behavior of the girders. However, because PBEAM assumes the ACI 209 form of the creep coefficient and shrinkage strain expressions, a nonlinear least square fit analysis was conducted to convert the CEB-FIP 1990 and Muller models into PBEAM-ready inputs by using the following general form of the ACI 209 expressions. (The AASHTO LRFD and Mazloom models take the general form of the ACI 209 expressions, with different, but easy-to-calculate input coefficients).

Shrinkage strain:

$$(\varepsilon_{sh})_t = \frac{t}{f + t}\Phi \qquad \textbf{(G-1)}$$

Creep coefficient:

$$v_t = \frac{t^{\Psi}}{d + t^{\Psi}}\Omega \qquad \textbf{(G-2)}$$

The CEB-FIP 1990 and Muller models were plotted for 500 days, which was selected as a reasonable upper bound for the age of a girder at bridge erection. The creep and shrinkage inputs for each model used in Phase 1 of the PBEAM model validation are given in Table G-1.

Table G-1. Creep and shrinkage inputs for Phase 1 of the PBEAM validation

Girder Set	Model	Creep coefficient Ω	Creep coefficient d	Creep coefficient ψ	Shrinkage coefficient Φ (x10^{-6})	Shrinkage coefficient f
73037 122’ MN54 #1-2	ACI 209	1.403	10	0.6	395	55
	Mokhtarzadeh	0.782	10	0.6	268	65
	CEB-FIP	1.977	9.27	0.56	153	108
	Muller	1.452	8.83	0.57	318	38
	AASHTO	0.753	23.2	1	225	23.2
	Mazloom	4.548	26.5	0.6	252	12.6
73038 122’ MN54 #1-2	ACI 209	1.414	10	0.6	395	55
	Mokhtarzadeh	0.788	10	0.6	268	65
	CEB-FIP	2.563	9.27	0.56	156	108
	Muller	1.889	8.83	0.57	318	39
	AASHTO	1.030	29	1	261	29
	Mazloom	4.323	26.5	0.6	252	12.6
73038 93’ MN54 #1-3	ACI 209	1.414	10	0.6	395	55
	Mokhtarzadeh	0.788	10	0.6	268	65
	CEB-FIP	2.505	9.27	0.56	138	108
	Muller	1.817	8.83	0.57	317	37
	AASHTO	1.013	28.4	1	257	28.4
	Mazloom	4.363	26.5	0.6	252	12.6
27B58 119’ MN45 #1	ACI 209	1.411	10	0.6	394	55
	Mokhtarzadeh	0.786	10	0.6	267	65
	CEB-FIP	2.306	9.27	0.56	172	108
	Muller	1.726	8.83	0.57	319	41
	AASHTO	1.042	32.2	1	286	32.2
	Mazloom	4.057	26.5	0.6	249	12.6
27B58 119’ MN45 #2-3	ACI 209	1.411	10	0.6	394	55
	Mokhtarzadeh	0.786	10	0.6	267	65
	CEB-FIP	2.618	9.27	0.56	172	108
	Muller	1.959	8.83	0.57	319	41
	AASHTO	0.997	27.8	1	252	27.8
	Mazloom	4.403	26.5	0.6	249	12.6
73044 131’6” MN63 #1-2	ACI 209	1.418	10	0.6	397	55
	Mokhtarzadeh	0.791	10	0.6	270	65
	CEB-FIP	2.623	9.27	0.56	172	108
	Muller	1.962	8.83	0.57	322	41
	AASHTO	1.078	30.6	1	273	30.6
	Mazloom	4.213	26.5	0.6	255	12.6
73044 131’6” MN63 #3-4	ACI 209	1.418	10	0.6	397	55
	Mokhtarzadeh	0.791	10	0.6	270	65
	CEB-FIP	2.175	9.27	0.56	181	108
	Muller	1.643	8.83	0.57	323	42
	AASHTO	0.847	26.5	1	244	26.5
	Mazloom	4.391	26.5	0.6	255	12.6

APPENDIX H. REVIEW OF TADROS ET AL. 2011 METHOD

Tadros et al. (2011) proposed a method for camber prediction that was published in the PCI Journal (described in Section 2.4). The proposed method uses the conventional elastic camber equations to predict the camber at release, but includes an adjustment for the change in downward self-weight deflection due to the location of the storage bunks once the girder is removed from the precasting bed. To estimate the camber at erection, the proposed method incorporates the AASHTO LRFD 2007 detailed method for prestress losses, an aging factor of 0.7 for prestress loss and the calculation of a creep coefficient (multiplier) based on various factors (i.e., volume-to-surface ratio, relative humidity, f'_{ci}, loading age and age at erection). To predict the release camber, the proposed method uses the AASHTO LRFD 2007 equation for concrete modulus of elasticity and transformed section properties, which implicitly account for the effects of elastic shortening. The relevant equations from Tadros et al. (2011) method for predicting camber are shown below:

Camber at release

Upward deflection due to prestressing:

$$\Delta_{ps} = \frac{P_i}{E_{ci} I_t}\left(\frac{e_{mid} {L_{des}}^2}{8} - \frac{(e_{mid} - e_{end}) {x_{hold}}^2}{6}\right) \quad \textbf{(H-1)}$$

Downward deflection due to self-weight:

$$\Delta_{sw} = \frac{5 * w_{sw} {L_{des}}^4}{384 * E_{ci} I_t} \quad \textbf{(H-2)}$$

Total camber at release:

$$\Delta_{release} = \Delta_{ps} - \Delta_{sw} \quad \textbf{(H-3)}$$

Camber after placement on storage bunks

Downward deflection due to self-weight and girder end overhangs:

$$\Delta_{sw\_bunked} = \frac{5 * {L_{des}}^4}{48 * E_{ci} I_t}(0.1 M_{e1} + M_c + 0.1 M_{e2}) \quad \textbf{(H-4)}$$

$$M_c = \frac{w_{sw} {L_c}^2}{8} - M_{e1} \quad \textbf{(H-5)}$$

$$M_{e1} = \frac{w_{sw} {L_{e1}}^2}{2} \; (similar\ for\ right\ support) \quad \textbf{(H-6)}$$

Total after placement on storage bunks:

$$\Delta_{bunked} = \Delta_{ps} - \Delta_{sw\_bunked} \quad \textbf{(H-7)}$$

Camber at Erection

Creep coefficient:

$$\psi(t,t_i) = (1.9)(1.45 - 0.13v/s)(1.56 - 0.008RH)(\frac{5}{1+f'_{ci}})(\frac{t}{61-4f'_{ci}+t})t_i^{-.118} \quad \textbf{(H-8)}$$

Elastic deflection due to long-term prestress loss:

$$\Delta_{el\_loss} = \Delta_{ps}(\Delta f_{lt}/f_i) \quad \textbf{(H-9)}$$

Multiplier for initial prestress plus self-weight:

$$\phi_{ips} = 1 + \psi(t,t_i) \quad \textbf{(H-10)}$$

Multiplier for the prestress loss:

$$\phi_{pl} = 1 + 0.7\psi(t,t_i) \quad \textbf{(H-11)}$$

Total camber at erection:

$$\Delta_{erection} = \Delta_{bunked}\phi_{ips} - \Delta_{el\_loss}\phi_{pl} \quad \textbf{(H-12)}$$

where:

- P_i: Total pull force in prestressing strands
- I_t: Transformed section moment of inertia
- E_{ci}: Concrete modulus of elasticity at release (AASHTO LRFD 2007)
- e_{mid}: Strand eccentricity at midspan from centroid of transformed section
- e_{end}: Strand eccentricity at girder end from centroid of transformed section
- w_{sw}: Concrete self-weight
- L_{des}: Girder design length
- x_{hold}: Distance from girder end to hold-down point for draped strands
- M_c: Midspan moment
- M_{e1}: Moment at left support, negative if overhang exists
- M_{e2}: Moment at right support, negative if overhang exists
- L_c: Girder length between bunked supports
- L_{e1}: Girder overhang length at left support (similar for right support)
- v/s: Volume-to-surface ratio
- RH: Relative humidity
- f'_{ci}: Concrete strength at release
- t_i: Loading age (age of girder at strand release)
- t: Age of girder at bridge erection
- f_i: Initial pull stress in each strand
- Δf_{lt}: Long-term prestress loss calculated by AASHTO LRFD 2007 detailed method

In order for this method to function as a predictive design method, the specific information (i.e., length of overhanging girder ends, loading age, age at erection, etc.), that is not known at the time of design, must be approximated. However, this method could also be

evaluated using the obtained girder data in the historical database for this study. Because all of the necessary information for this method was known for the instrumented girders, they were used to evaluate the Tadros et al. (2011) method in both a predictive design and post-fabrication check manner. The measured and recorded information for these girders (given in APPENDIX E) was used for the post-fabrication check and the original MnDOT design values were used for the predictive evaluation. The following values were used for the parameters not normally defined at the time of design, which are consistent with those used in the camber prediction modeling in Chapter 8.

t_i: 1 day
t: 120 days
L_{e1}: L/24
RH: 70%

Table H-1 contains the transformed properties for each instrumented girder set using the value of 'n' calculated with the design E_{ci}.

Table H-1. Transformed section properties for instrumented girders

Girder Description	n	I_t (in^4)	A_t (in^2)	y_t (in)	$e_{end,t}$ (in)	$e_{mid,t}$ (in)
73037 122' MN54 #1-2	5.47	301752	789.7	23.63	11.72	19.34
73038 122' MN54 #1-2	5.35	301930	790.5	23.61	11.98	19.25
73038 93' MN54 #1-3	5.78	297974	778.0	23.90	13.90	20.18
27B58 119' MN45 #1-3	5.20	189096	731.9	19.71	8.32	15.06
73044 131'6" MN63 #1-4	5.35	445541	846.6	27.65	15.93	23.50

Table H-2 and Table H-3 show the results of the Tadros et al. (2011) method for each instrumented girder as if used in predictive design and as a post-fabrication check, respectively.

Table H-2. Camber results of Tadros et al. (2011) method in predictive design

Girder Description	Δ_{ps}	Δ_{sw}	$\Delta_{release}$	Δ_{sw_bunked}	Δ_{bunked}	$\Psi(t,t_i)$	Δ_{el_loss}	$\Delta_{erection}$
73037 122’ MN54 #1-2	5.48[1]	2.48[1]	3.00[1]	1.99[1]	3.49[1]	0.93	0.56[1]	5.83[1]
73038 122’ MN54 #1-2	5.62	2.43	3.19	1.94	3.68	0.91	0.57	6.07
73038 93’ MN54 #1-3	2.37	0.87	1.51	0.69	1.68	1.01	0.23	2.98
27B58 119’ MN45 #1-3	6.65	3.13	3.52	2.30	4.35	0.87	0.67	7.05
73044 131’6” MN63 #1-4	5.19	2.37	2.82	2.04	3.15	0.91	0.50	5.19

[1]Values shown are in inches and calculated based on the method described above

Table H-3. Camber results of Tadros et al. (2011) method as a post-fabrication check

Girder Description	Δ_{ps}	Δ_{sw}	$\Delta_{release}$	Δ_{sw_bunked}	Δ_{bunked}	$\Psi(t,t_i)$	Δ_{el_loss}	$\Delta_{erection}$
73037 122’ MN54 #1	4.71[1]	2.11[1]	2.60[1]	1.69[1]	3.03[1]	0.66	0.35[1]	4.52[1]
73037 122’ MN54 #2	4.71	2.11	2.60	1.69	3.02	0.66	0.35	4.51
73038 122’ MN54 #1	5.30	2.28	3.02	1.83	3.47	0.88	0.51	5.71
73038 122’ MN54 #2	5.30	2.28	3.02	1.83	3.47	0.88	0.51	5.71
73038 93’ MN54 #1	2.06	0.75	1.32	0.60	1.47	0.85	0.16	2.46
73038 93’ MN54 #2	2.06	0.75	1.32	0.60	1.47	0.85	0.16	2.46
73038 93’ MN54 #3	2.06	0.75	1.32	0.60	1.47	0.85	0.16	2.46
27B58 119’ MN45 #1	6.76	3.18	3.58	2.34	4.42	0.93	0.74	7.31
27B58 119’ MN45 #2	6.33	2.96	3.37	2.18	4.15	0.90	0.63	6.86
27B58 119’ MN45 #3	6.33	2.96	3.37	2.18	4.15	0.90	0.63	6.86
73044 131’6” MN63 #1	5.00	2.28	2.72	1.97	3.04	0.96	0.49	5.13
73044 131’6” MN63 #2	5.00	2.28	2.72	1.97	3.04	0.96	0.49	5.13
73044 131’6” MN63 #3	4.73	2.15	2.58	1.85	2.88	0.76	0.38	4.48
73044 131’6” MN63 #4	4.73	2.15	2.58	1.85	2.88	0.76	0.38	4.48

[1]Values shown are in inches and calculated based on the method described above

Table H-4 shows the results of each analysis compared to the measured cambers for each instrumented girder. These results indicate that, for most cases, the camber values calculated using the Tadros et al. (2011) method in predictive design were higher than those calculated

using the method as a post-fabrication check. Because the measured quantities were used for the post-fabrication check, those results also more closely matched the measured camber values at release, bunking and erection. However, the accuracy of these results varied. For the release camber, the post-fabrication check estimated cambers consistently overestimated the measured values. But, for the erection camber, the estimated cambers overestimated the measured values for weekday-cured girders and underestimated the measured values for weekend-cured girders. This is likely due to the fact that the creep coefficient is sensitive to changes in loading age and concrete strength at release.

Table H-4. Camber comparison for Tadros et al. (2011) method to measured values

Girder Description	$\Delta_{release}$ (in)			Δ_{bunked} (in)			$\Delta_{erection}$ (in)		
	Measured	Tadros design	Tadros check	Measured	Tadros design	Tadros check	Measured	Tadros design	Tadros check
73037 122’ MN54 #1	--	3.00	2.60	3.03	3.49	3.03	5.02	5.83	4.52
73037 122’ MN54 #2	2.52	3.00	2.60	2.95	3.49	3.02	4.80	5.83	4.51
73038 122’ MN54 #1	2.80	3.19	3.02	3.54	3.68	3.47	5.47	6.07	5.71
73038 122’ MN54 #2	2.60	3.19	3.02	3.58	3.68	3.47	5.23	6.07	5.71
73038 93’ MN54 #1	1.34	1.51	1.32	1.61	1.68	1.47	2.51	2.98	2.46
73038 93’ MN54 #2	1.14	1.51	1.32	1.44	1.68	1.47	2.32	2.98	2.46
73038 93’ MN54 #3	1.18	1.51	1.32	1.50	1.68	1.47	2.39	2.98	2.46
27B58 119’ MN45 #1	3.44	3.52	3.58	--	4.35	4.42	7.28	7.05	7.31
27B58 119’ MN45 #2	2.54	3.52	3.37	--	4.35	4.15	6.00	7.05	6.86
27B58 119’ MN45 #3	2.34	3.52	3.37	--	4.35	4.15	5.96	7.05	6.86
73044 131’6” MN63 #1	2.09	2.82	2.72	--	3.15	3.04	4.62	5.19	5.13
73044 131’6” MN63 #2	1.91	2.82	2.72	--	3.15	3.04	4.50	5.19	5.13
73044 131’6” MN63 #3	1.93	2.82	2.58	--	3.15	2.88	4.61	5.19	4.48
73044 131’6” MN63 #4	1.94	2.82	2.58	--	3.15	2.88	4.56	5.19	4.48

As previously mentioned, for the Tadros et al. (2011) method to be used in design, the parameters not known at the time of design must be approximated. Because the camber prediction method proposed to MnDOT in this study (discussed in Section 9.3) recommends adjustments to certain parameters and uses multipliers to estimate erection camber, these two methods were compared and validated against the measured cambers for the instrumented

girders. The following assumptions were used for the approximated parameters in both camber prediction methods:

f'_{ci}: Design f'_{ci} multiplied by a factor of 1.15
E_{ci}: Calculated using the Pauw (ACI318-08, AASHTO LRFD 2010) equation
f_i: $0.72*f_{pu}$ = 194.4 ksi
t_i: 0.75 days
L_{e1}: L/24
RH: 73%
t: 120 days (Tadros); 1.85 multiplier (O'Neill, 2-6 months recommendation)
t: 270 days (Tadros); 2.00 multiplier (O'Neill, 6-12 months recommendation)

Table H-5 shows the predicted cambers at release and erection for the Tadros et al. (2011) and O'Neill prediction methods, compared to the measured cambers for the instrumented girders.

Table H-5. Camber comparison for Tadros et al. (2011) and O'Neill prediction methods

Girder Description	$\Delta_{release}$ (in)			$\Delta_{erection}$ (in)		
	Measured[1]	O'Neill	Tadros	Measured[2]	O'Neill	Tadros
73037 122' MN54 #1	--[3]	2.58	2.62	5.02	5.16	5.23
73037 122' MN54 #2	2.52	2.58	2.62	4.80	5.16	5.23
73038 122' MN54 #1	2.80	2.75	2.80	5.47	5.50	5.45
73038 122' MN54 #2	2.60	2.75	2.80	5.23	5.50	5.45
73038 93' MN54 #1	1.34	1.31	1.33	2.51	2.43	2.56
73038 93' MN54 #2	1.14	1.31	1.33	2.32	2.43	2.56
73038 93' MN54 #3	1.18	1.31	1.33	2.39	2.43	2.56
27B58 119' MN45 #1	3.44	3.02	3.08	7.28	6.04	6.32
27B58 119' MN45 #2	2.54	3.02	3.08	6.00	6.04	6.32
27B58 119' MN45 #3	2.34	3.02	3.08	5.96	6.04	6.32
73044 131'6" MN63 #1	2.09	2.42	2.46	4.62	4.84	4.64
73044 131'6" MN63 #2	1.91	2.42	2.46	4.50	4.84	4.64
73044 131'6" MN63 #3	1.93	2.42	2.46	4.61	4.84	4.64
73044 131'6" MN63 #4	1.94	2.42	2.46	4.56	4.84	4.64

[1]Measured on-bed release cambers.
[2]The age of the girders at erection is given in APPENDIX E. This information was used to determine the multiplier and erection age (t) for the O'Neill and Tadros methods, respectively.
[3]Denotes camber values that were not recorded.

These results show that the Tadros et al. (2011) and the O'Neill camber prediction methods yielded very similar estimations for the camber at release, which was expected as the two methods are equivalent at this stage (i.e., O'Neill method uses gross section properties and elastic shortening losses, Tadros method uses transformed section properties which implicitly account for the effects of elastic shortening). The results also show that the two methods yielded fairly similar estimations for the camber at erection. Both prediction methods gave erection camber estimates that were close to the measured values for the instrumented girders. In fact, the average absolute percent difference between the camber at erection predictions and the measured values were 4.8% for both the O'Neill and Tadros methods. Therefore, according to these results, either method could be used as an effective camber prediction method, although the O'Neill method may be simpler to implement in practice.